Active metal oxides and polymer hybrids as biomaterials

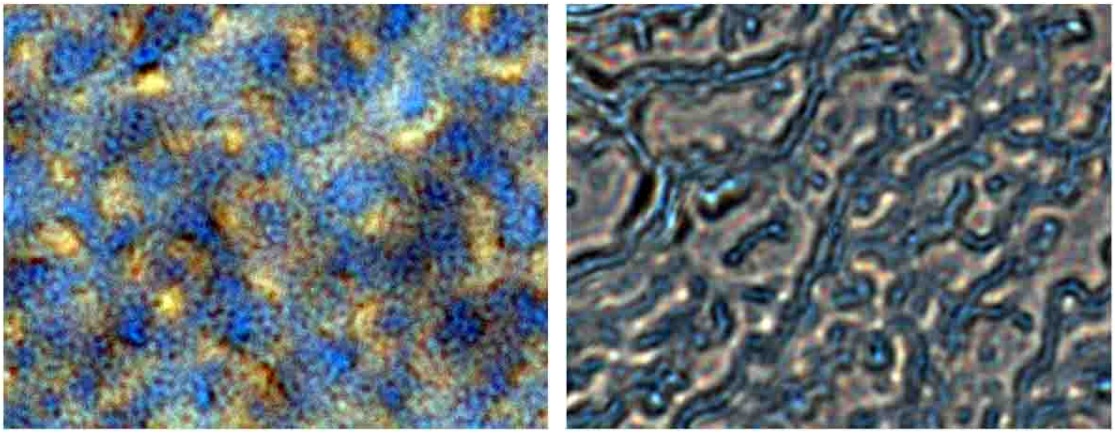

by

John D. Jarrell

ScB, Brown University, 1988

MSc, Brown University, 1991

Submitted in partial fulfillment of the requirements for the degree of Doctor of Philosophy in

the Division of Biology and Medicine

and the Division of Engineering at Brown University

Providence, Rhode Island.

May 2008

This dissertation by John D. Jarrell is accepted in its present form

by the Division of Biology and Medicine

and the Division of Engineering as satisfying the

dissertation requirement for the degree of Doctor of Philosophy.

Date _____ _____

Jeffrey R Morgan, Ph.D., Advisor

Recommended to the Graduate Council

Date _____ _____

Edith Mathiowitz, Ph.D., Reader

Date _____ _____

Anubhav Tripathi, Ph.D., Reader

Date _____ _____

Diane Hoffman-Kim, Ph.D., Reader

Date _____ _____

William Lee, Ph.D., External Reader

Approved by the Graduate Council

Date _____ _____

Sheila Bonde, Dean of the Graduate School

Vita

John D. Jarrell, Sr. was born in Upland, Pa, on October 4, 1965, to Joan B. and Eugene F. Jarrell, II. He spent his childhood among the woods and streams of Rose Valley, Pa. In 1984 he graduated from Strath Haven High School as a Varsity letterman in Track & Field and was recruited to Brown University for the javelin throw.

He studied Materials Science and Engineering at Brown University, obtaining the Bachelor's of Science degree in 1988 and Master's of Science degree in 1991. He worked his way through school, performing engineering failure analysis for Avery Technical Services (Barrington, RI). While a graduate student, John married his friend Krista A. Sullivan of Branford, CT. They had their first child, John David Jarrell, Jr. in 1990.

John operated an analytical laboratory at Thielsch Engineering (Cranston, RI) for two years before starting his own consulting firm, Materials Science Associates, in April of 1993. He was awarded a Professional Engineering license in Mechanical Engineering by the State of Rhode Island in 1996. In 1998, he began renovations on a historic ten bedroom Victorian home with stable, carriage house and guest house.

After eleven years of private practice, and his eighth child with Krista, John returned to Brown University to pursue a Doctorate of Philosophy in Biomedical Engineering. During his free time, he enjoys his family, the Scriptures, hymn singing, the study of athletics, weight lifting, skateboarding, the outdoors and his addiction to "useful" information.

Preface

Traditionally, biomaterials were selected on the basis of inertness within the body from materials developed primarily for Industry and Aerospace. Here we seek to explore biologically active metal oxides and polymer hybrids, which participate in a dynamic exchange with living cells and tissues. We look at the use of metal oxides to modulate cellular activity and as integrative controlled delivery devices. New classes of materials which can be activated by external photon irradiation are presented as an option for influencing implant integration, controlled delivery and providing the possibility of *in situ* activation and disinfection.

Acknowledgements

I would like to thank Clyde Briant and my advisor Jeffrey Morgan for offering me the opportunity to return to graduate studies and participate in an exciting new joint-venture with the Department of Veteran's Affairs. Special thanks go to Roy Aaron and Deborah Ciambor, co-directors of the VA Center for Restorative and Regenerative Medicine, for their inspiration and commitment to advancing the needs of veterans, through this project.

I am thankful to my thesis committee members, Edith Mathiowitz, Anubhav Tripathi, Diane Hoffman-Kim and William Lee for their time, counsel, encouragement and enthusiasm for my research and studies. I am grateful for the assistance of Roxanne Burrill for help with animal studies, Bryan Laulicht for FT-IR data and assistance with x-ray experiments and Takahiro Hiroi for gathering near and mid IR reflectance data. Special thanks to Evan Werlin for his persistent, friendly and reliable assistance.

Finally, I give thanks to my children (John David Jr., Elizabeth Anna, Stephen Philip, David Andrew, Ebed Yazziah, Nethaneel Charis, Joanna Krista & little Michael Eugene) and especially my dear wife, Krista, for their willingness to endure and sacrifice very many things to help me fulfill a long-held dream, now come true. May they all enjoy the benefits of my labors.

Dedication

I dedicate this dissertation to my father, for his loving and kind service to my mother and his lifelong support and patience.

בְּרֵאשִׁית בָּרָא אֱלֹהִים אֵת הַשָּׁמַיִם וְאֵת הָאָרֶץ׃

ἐν ἀρχῇ ἦν ὁ λόγος, καὶ ὁ λόγος ἦν πρὸς τὸν θεόν, καὶ θεὸς ἦν ὁ λόγος.

IN DEO SPERAMUS

Contents

List of Tables

List of Figures

Chapter 1

Introduction

1.1 Background and significance

The skin is the body's first line of defense against outside assaults, such as dehydration and pathogenic microbes. The keratinocytes of the epidermis layer form a vapor barrier and provide abrasive protection, while mechanical strength is derived mostly from the fibroblast-deposited collagen matrix of the underlying dermis layer. Chronic breaches in the skin from non-healing wounds, percutaneous devices and burns are an especially challenging medical problem. In the United States, approximately 8 million people suffer from non-healing wounds, including 6.5 million with pressure ulcers, 915,000 with venous ulcers and 900,000 with diabetic ulcers, which result in 55,000 amputations per year [1-3]. Percutaneous devices, such as catheters, are known for poor tissue integration, chronic inflammation and infection [4-7]. Figure 1.1 presents four visual examples of chronic dermal breaching situations. Innovative biomaterial solutions are needed to address the complex issues of wound healing involved with these devices, which include managing inflammation, bacterial infection, scar reduction, and wound closure.

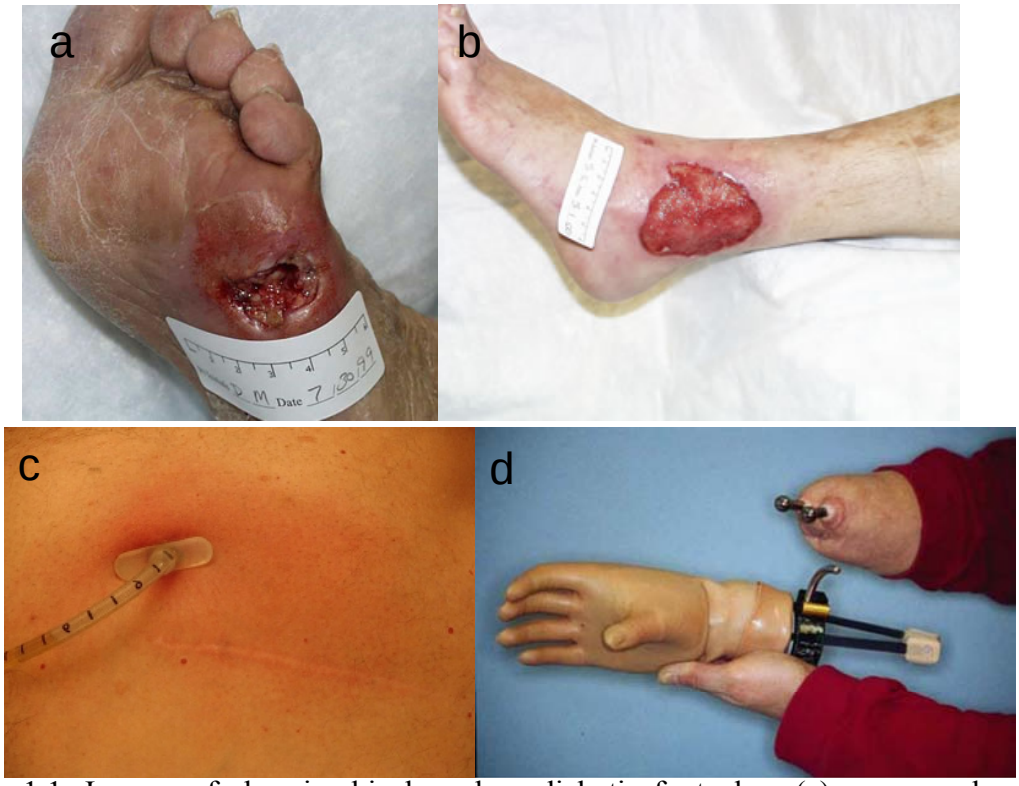

Figure 1.1: Images of chronic skin breaches, diabetic foot ulcer (a), venous ulcer (b), percutaneous endoscopic gastrostomy (PEG) tube (c), osseointegrated percutaneous prosthetic (d); www.unchealthcare.org/site/woundmanagement/nonhealingwounds 12-27-2007; http://insidesurgery.com/media/1/20061024-peg2.jpg 1-19-2008; Ref [4].

1.2 Percutaneous devices

Percutaneous devices (PD) are particularly problematic because of low soft tissue integration, resulting in the high incidence of infection and epithelial down growth, all of which are exacerbated by stresses on the device [5,6]. While in medicine, PD catheters and titanium abutments of various types are widely used; in nature there exists only one permanent PD, the tusk of the babyrussa pig from South-East Asia. This tusk is in fact a tooth which avoids the oral cavity and grows through the dermal and epidermal layers of the face. Feathers, hooves, finger nails and hair, while seeming to penetrate the skin, are merely keratinized appendages of the epidermal layer [7]. Male deer possess temporary percutaneous antlers that are shed yearly. The percutaneous aspect of antlers have been

characterized and used to model transcutaneous devices [8]. In nature, there are differences in surface texture between percutaneous and exposed portions of the antler. In the field of medicine, implants composed of silicone rubber and Dacron as well as pure and alloyed titanium are in common use. There has been good success with implants of various biomaterials; however, we have been hindered from adequately investigating the variables that influence and control soft tissue sealing around PDs.

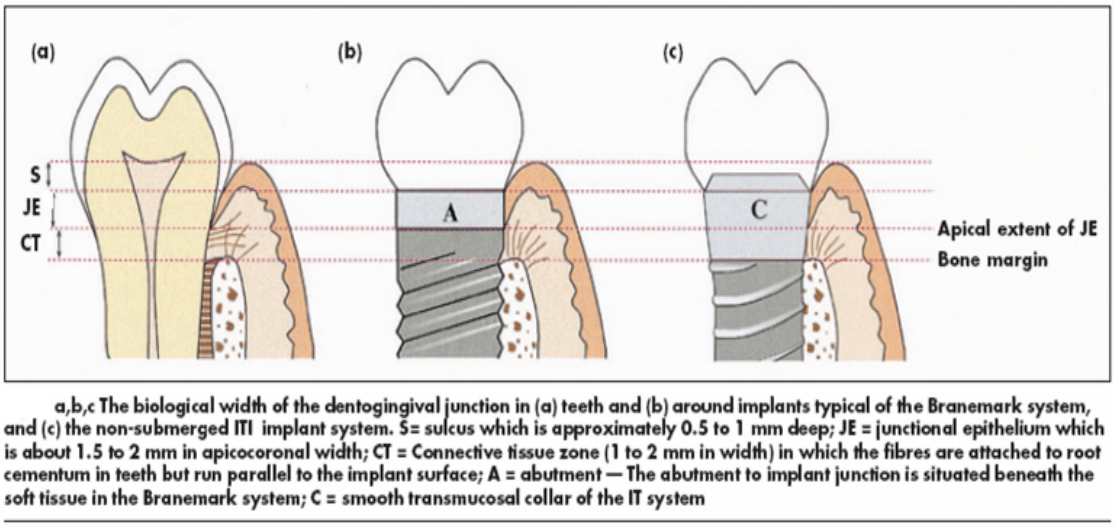

a,b,c The biological width of the dentogingival junction in (a) teeth and (b) around implants typical of the Branemark system, and (c) the non-submerged ITI implant system. S= sulcus which is approximately 0.5 to 1 mm deep; JE = junctional epithelium which is about 1.5 to 2 mm in apicocoronal width; CT = Connective tissue zone (1 to 2 mm in width) in which the fibres are attached to root cementum in teeth but run parallel to the implant surface; A = abutment — The abutment to implant junction is situated beneath the soft tissue in the Branemark system; C = smooth transmucosal collar of the IT system

Figure 1.2: Illustration of teeth and implants: Dr. Richard Palmer. British Dental Journal 1999;187(4): 183-188.

One analog to the percutaneous problems is seen in the most successful application of an osseointegrated trans-epithelial device, the titanium dental implant. While the implant is well tolerated, the attachment of epidermis and dermis (present in the natural tooth) is lost. The perpendicular bundles of collagen fibers that are normally inserted into the cementum layer are replaced by additional fibers running parallel to the implant [9,10] Figure 1.2 presents a summary of the problem induced by the altered soft tissue function at the implant interface. A functional soft tissue seals develops instead of cellular attachment. In the tooth, parallel bundles of collagen fibers insert perpendicularly into

spaces within both the cementum layer and the bone for anchorage. The histology section presented in Figure 1.3 shows these Sharpey's fibers forming the transition between bone and ligament adjacent to a tooth.

With PD catheters, generally constructed of silicon rubber, no real integration takes place. Figure 1.4 presents histology of percutaneous silicone catheter. To help overcome this, Dacron and other meshes are incorporated to encourage tissue ingrowth. This however, is accompanied by chronic and active inflammatory responses in both the granulation tissue above the scar and in the dermal layer [11]. Varying degrees of epithelial down growth and epithelial nonadherance to the Dacron is also observed. This is in contrast to the more stable interface formed at the interface between epidermis and the babyrussa tusk or to a lesser degree, between titanium implants and epidermis.

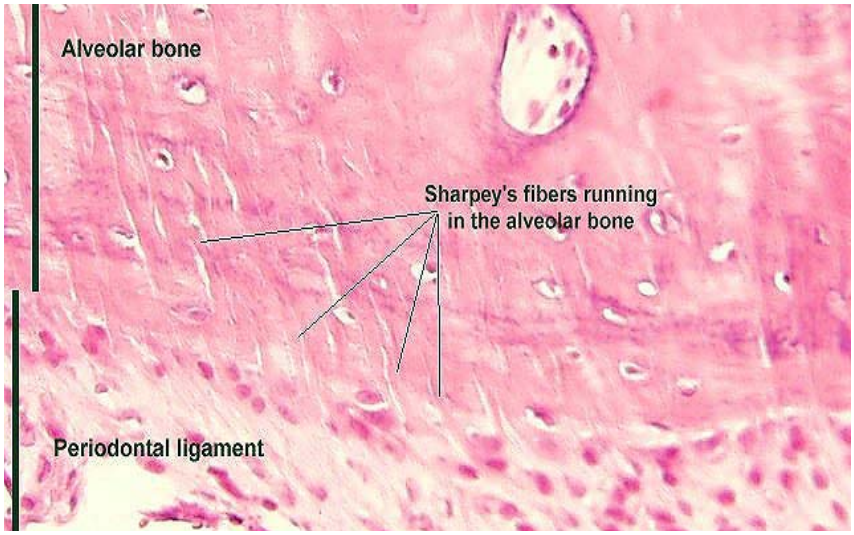

Figure 1.3: Histology section showing Sharpey's fibers forming the transition between bone and ligament adjacent to a tooth. http://neuromedia.neurobio.ucla.edu/campbell/toothandgingiva/wp_images/159_sharpeys_bone.jpg 01-18-2008.

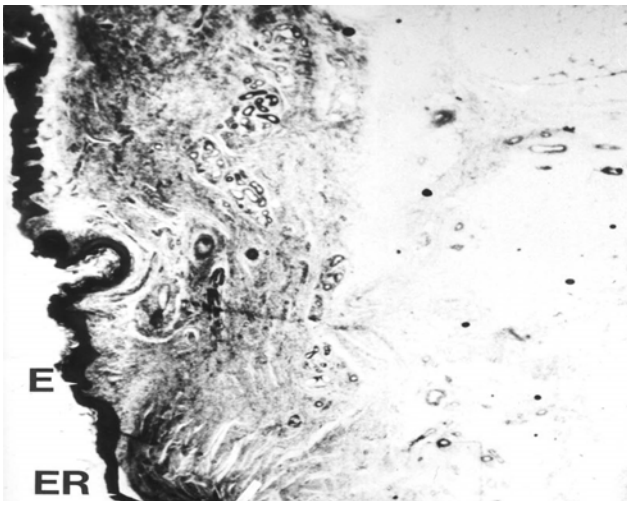

Figure 1.4: Micrograph of CAPD catheter showing epithelial down growth (arrow) along the catheter surface. Sawed section, Giemsa staining, bar, 500 um. Epidermis (E), epithelial regenerate (ER) contacting the implant (I) and covering the scar. From Knabe C, Große-Siestrup C, Gross U. Histologic evaluation of a natural permanent percutaneous structure and clinical percutaneous devices. Biomaterials 1999;20:503-510.

1.3 Titanium oxide layer

Since the discovery of osseointegration by PI Branemark, titanium implants have been successfully used in a variety of dental and medical applications including tooth implants, facial reconstructions and recently percutaneous bone anchors prostheses attachment [12]. Titanium has been found to be superior to previously used stainless steels and chromium cobalt alloys for implantation. The presence of a naturally occurring TiO_2 passivation film [13] and subsequent biological modification during implantation [14] is generally regarded as responsible for the inhibition of inflammation, and good bio-integration achieved with both bone and soft tissues [15-18].

The surfaces of most metals, with the exception of gold, readily form a thin oxide layer when exposed to oxygen containing environments. In corrosion resistant materials, this oxide layer is relatively stable, continuous and tenacious providing a barrier to

further metal oxidation [18]. It is the chromium oxide layer that is responsible for the corrosion resistance of stainless steels and other high chromium alloys. With titanium and its alloys, it is the continuous titania film that provides this protection. For titanium, oxygen is present in sufficient quantities in air and most biological environments to continuously replenish the surface oxide if disrupted. This oxide layer is often thought of as being inert. This is true only in a relative sense. Exposure of titanium to different environments drives reactions at various rates that affect the exact composition and condition of the oxide layer. It has been shown that in each location of biological implantation dynamic processes occur between the titanium oxide layer and the biological tissue [19-22]. There are specific surface changes that occur which are governed by the contact environment, whether cortical bone, marrow or soft tissue. Biological contact with titanium brings about an increased thickness of an amorphous structured oxide layer and an incorporation of elements from the surrounding tissue such as calcium, phosphorous and sulfur, until a steady-state condition is reached, often years later [19-25]. An artist's representation of transitional regions between a bulk titanium metal implant and native tissue is presented in Figure 1.5.

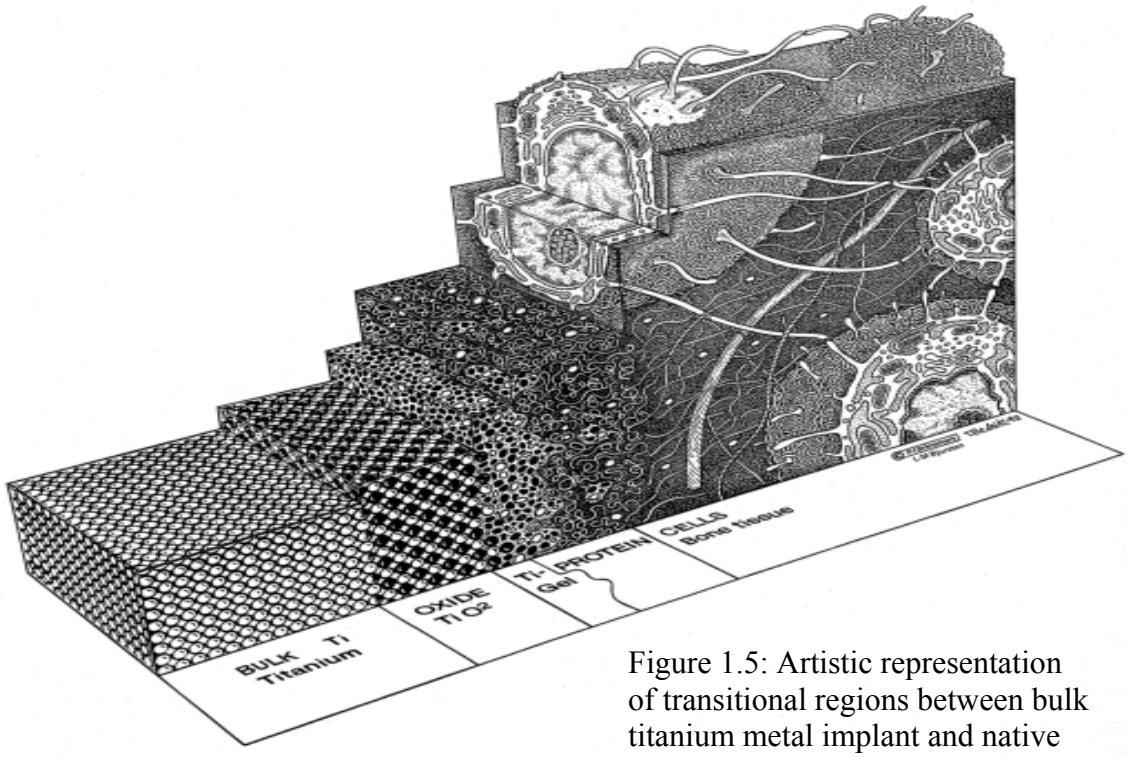

Figure 1.5: Artistic representation of transitional regions between bulk titanium metal implant and native tissue (Bjursten L-M [19]).

A titanium gel layer forms where the oxide coating contacts the biological tissue or media. It is this region that is believed to be responsible for deactivation of inflammatory cells. It also acts as a sink for reducing reactive oxygen species with the net affect of reducing the foreign body reaction [26-28]. The actions taking place at the gel layer are summarized in Figure 1.6.

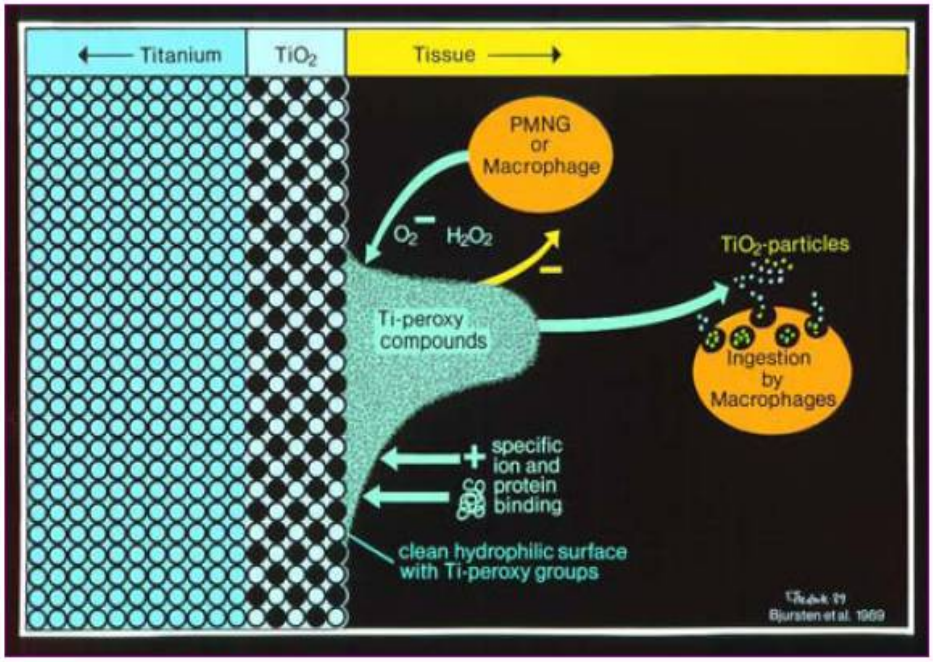

Figure 1.6: Summary of actions taking place at implant Ti gel layer, were deactivation of inflammatory cells, reduction of reactive species and reduction of foreign body reaction occurs [4].

1.4 Surface property modifications and biological response

While titanium has good biocompatibility, modifications of surface properties have been studied in an attempt to better understand and improve biological response to implant materials. These modifications can be characterized as surface texture modifications, alteration of surface chemistry and crystalline structure. Many surface treatments change a combination of these properties. Alterations to surface chemistries vary from complete coating with organics and inorganics to surface alloyed coatings using various plasma based methods. These influence cellular adhesion during centrifugation [29]. Combined thermal and chemical modifications of titanium using heat, peroxide and butanol treatments influence protein binding and cell attachment [30,31].

Cellular response to surface textures created by sandblasting, plasma-spray and polishing are dependent on cell line [32]. Cell morphology, orientation, proliferation and adhesion of human gingival epithelial cells have been found to be very dependent on the surface texture of titanium, (improving with smoother surfaces), while maxillar osteoblast-like cells were not affected to the same degree. Introducing nano verses micro scale grain features through specialized processing also strongly influences tissue, cell and bacterial responses [33,34]. For oesteoblasts, adhesion may be similar for very different materials if the surface topography is controlled [35]. Generally going from highly polished surfaces to gradually increasing roughness slightly increases osteoblast-like cell adhesion, proliferation and differentiation [36]. High surface roughness from 60 grit sandblasting, however can slow proliferation, encourage morphologic differentiation and upregulate cytokine expression of MG63 osteoblast-like cells [37]. Osteoblasts also release cytokines differently when exposed to pure titanium verses alloy and rough surfaces compared to smooth [38]. Varying the uniform spacing of micro features on silicone from 400 nm to 4000 nm demonstrated that adhesion of human corneal epithelial cells improved with the smallest spacing [39]. Percutaneous implants with micro-features perpendicular to the skin encourage epithelium down growth compared to smooth or parallel features [40]. Combination studies comparing porous and plane surfaces of both titanium and P-doped silicon, indicated that soft tissue response to texture was similar for both materials [41].

Cellular responses to chemistry and crystallinity have also been explored. For oesteoblasts, adhesion may be similar for very different materials if the surface topography is controlled. Mirror polished samples of Ti-6Al-4V and stainless steel

showed similar trypsin responsive adhesion as polystyrene and glass slides. Osteoblast cell proliferation was roughly twice as high on the glass and autoclaved stainless steel compared to polystyrene and autoclaved titanium alloy [35]. For sol-gel deposited hydroxyapatite coated titanium, osteoblast-like cell attachment, proliferation, expression of alkaline phosphatase and osteocalcin increased with increased levels of heat treatment induced coating crystallinity [42]. In summary, differences in cellular responses to texture, chemistry and crystallinity indicate that implant surface properties should be specialized for each tissue interface.

1.5 Influence of soluble metals and ceramic particles

Biomaterial implantation is associated with release of metallic ions and compounds that are detectible within cells, surrounding tissues and systematically. Various metal ions of Be, Cr, Ni and Mo preferentially accumulated within different subcellular fractions of fibroblasts such as the plasma membrane and cytosol lipid droplets, where they are involved in related cellular alterations to morphology and metabolism [43]. The cytotoxic dose response to various metallic ions and salts in solution has been established for osteoblasts, fibroblasts and keratinocytes [44,45]. In general, cells begin to show morphological changes with mildly toxic concentrations of metal ions and a rounded appearance with toxic concentrations. Metals that are toxic at low concentrations (0.1 mM) include Mn, V, Cu, Fe, at medium concentrations (1 mM) Ta, Co, Ni, Al, and at high concentrations (over 5 mM) Mg, Mo, Na, Cr. Fibroblasts maintained basal cell survival at concentrations of nickel that induced mild toxicity in keratinocytes [46]. The

toxicity of particles from implantable ceramics appears to be more dependent on total volume of particles and shape than on chemistry and particle size [47].

1.6 Limitations of metal samples

Earlier biological work on metal oxide surfaces has been hindered by the limitations imposed by using solid metal samples. Metal disks are opaque while typical cell culture techniques use transparent materials for easy observation using biological microscopes. These samples are usually produced by standard melt metallurgy or powder metallurgy technique. For practical purposes, wrought samples are generally limited to those compositions commercially available. Powder metallurgy techniques allow investigators to mix custom compositions, but require compaction and sintering steps to form solid samples. Size, opaqueness and handling still hinder the adaptation of powder metallurgy samples to small format, rapid assay platforms. Currently there is a need for rapidly producing metal oxide surfaces of controlled and variable chemistry, texture, structure and crystallinity, in a format conducive to rapid biological screening, to increase understanding of which properties dominate cellular responses important for implant integration. The sol-gel method of producing metal oxides from metal-organic precursors is a good candidate for meeting these requirements [48-54].

1.7 Metal-organic derived biomaterials

Sol-gel has been defined as a method for preparing specialty metal oxide glasses and ceramics by hydrolyzing a chemical precursor or mixture of chemical precursors that pass sequentially through a solution state and a gel state before being dehydrated to a glass or

ceramic. The use of this method for creating fine powders, thin films, fibers and microspheres has expanded greatly since the 1980's. Metal alkoxides are a successful means of producing sol-gels with a wide variety of chemistries. Metal alkoxide sol-gels can be considered derivatives of alcohols, where the hydroxyl hydrogen is replaced by a metal atom. The characteristics of an alkoxide are governed by the particular metal used and the size and shape of the alkyl groups [48]. Representations of two titanium alkoxide structures are presented in Figure 1.7.

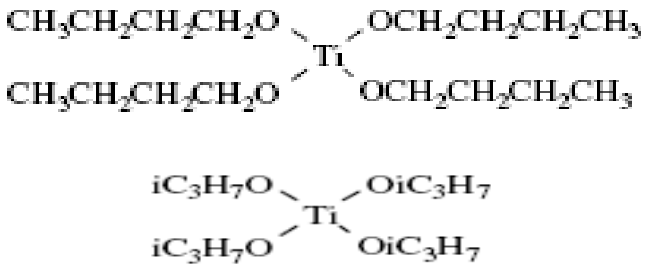

Figure 1.7: Chemical structure of titanium n-butoxide (top), showing central Ti atom tethering four butyl groups. Bottom structure is for titanium isopropoxide, based on four isopropyl molecules. (Source, Gelest, Inc.)

The sol-gel process involves two major reactions, hydrolysis and condensation. In the first, the alkoxide is hydrolyzed by a water molecule:

Monomer Formation (Partial Hydrolysis)

$$M(OR)_n + H_2O \text{ ----------} \rightarrow (RO)_{n-1}MOH + ROH$$

e.g. for Ti n-butoxide $Ti(OC_4H_9)_4 + H_2O$ ---------$\rightarrow (C_4H_9O)_3TiOH + C_4H_9OH$

The second reaction occurs when hydrolyzed molecules react to form a metal oxygen metal matrix:

Sol Formation (Polycondensation)

$$2\ (RO)_{n-1}MOH \text{ ---------}\rightarrow (RO)_{n-1}M\text{-}O\text{-}M(OR)_{n-2}OH + ROH$$

M in the equations stands for metal atom and R for the alkyl group. Additional hydrolysis promotes polymerization and cross-linking, leading to a 3-dimensional matrix (gel formation). These reactions cause the formation of a metal oxide matrix and alcohol. The rate of hydrolysis can be slowed by diluting the alkoxide in other solvents, thus limiting the rate of exposure to atmospheric moisture. The structure of several useful solvents is presented below in Figure 1.8.

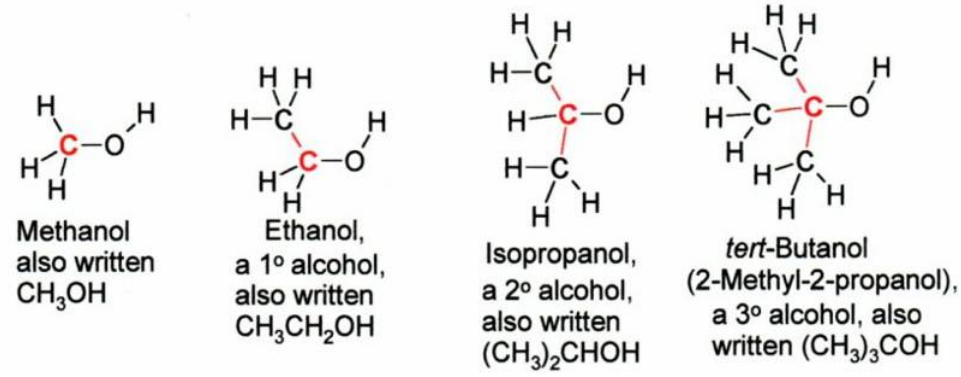

Figure 1.8: Chemical structure of first, second and third degree alcohols useful for diluting alkoxides [Source, http://en.wikipedia.org/wiki/Alcohol].

The combination of alkoxides and solvents produce distinct smooth, micro and nano textures as seen in the composite SEM Figure 1.9. These features are also a product of the method and perimeters of application, whether spin coating or some form of dip coating is used [42,48,49,50].

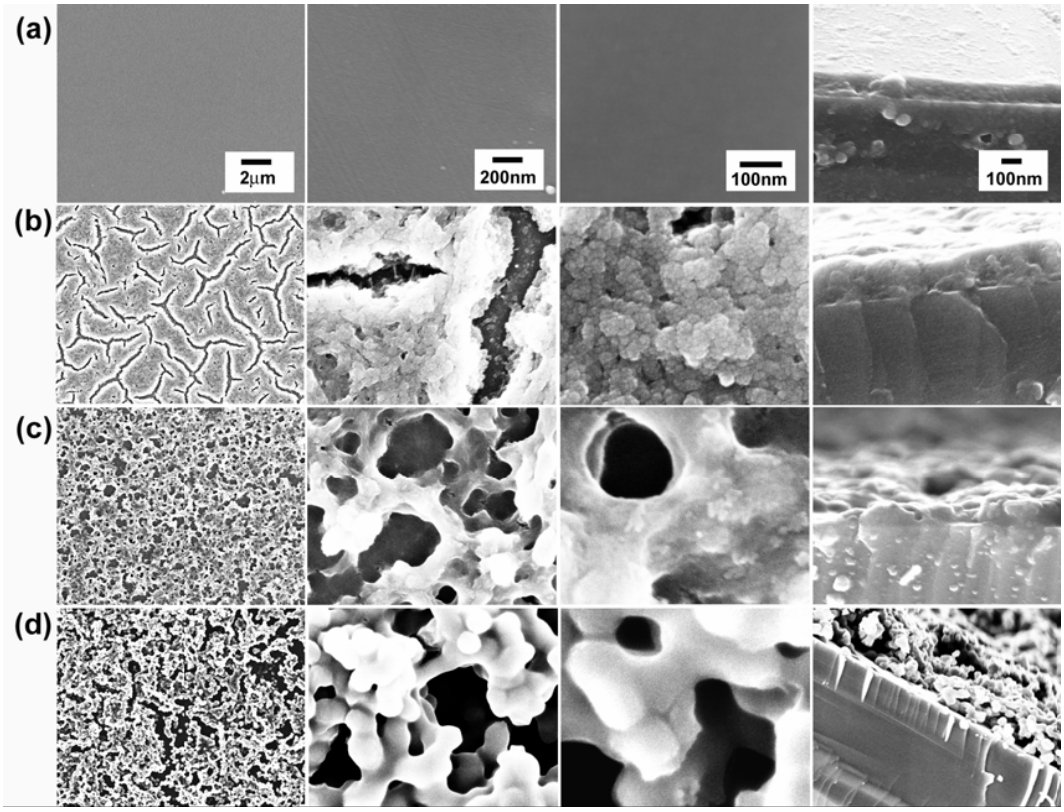

Figure 1.9: Scanning electron micrographs of thin films (1 layer) derived from different solutions of titanium alkoxides and solvents with different magnifications of top-view and cross-sectional images. (a): titanium n-butoxide in toluene. (b): titanium isopropoxide in toluene. (c): titanium isopropoxide in isopropanol. (d): titanium isopropoxide in n-propanol. (Tai Hee Eun, Ph.D. Thesis, Brown University, 2006 [49])

Post deposition heat treatment of sol-gels facilitates the transformation of an amorphous metal oxide matrix to varying levels of crystallinity. We have accomplished this with heat treatments in air for a variety of chemistries resulting in a range of grain sizes and crystallinity. The variation of grain size as a function of heat treatment temperature is presented in Figure 1.10. Presented in Figure 1.11 are sequential XRD plots from pure titanium n-butoxide derived spin coatings from five different 3 hour heat

treatments in air, indicating transition from amorphous to increasing crystallinity beginning at 450 °C.

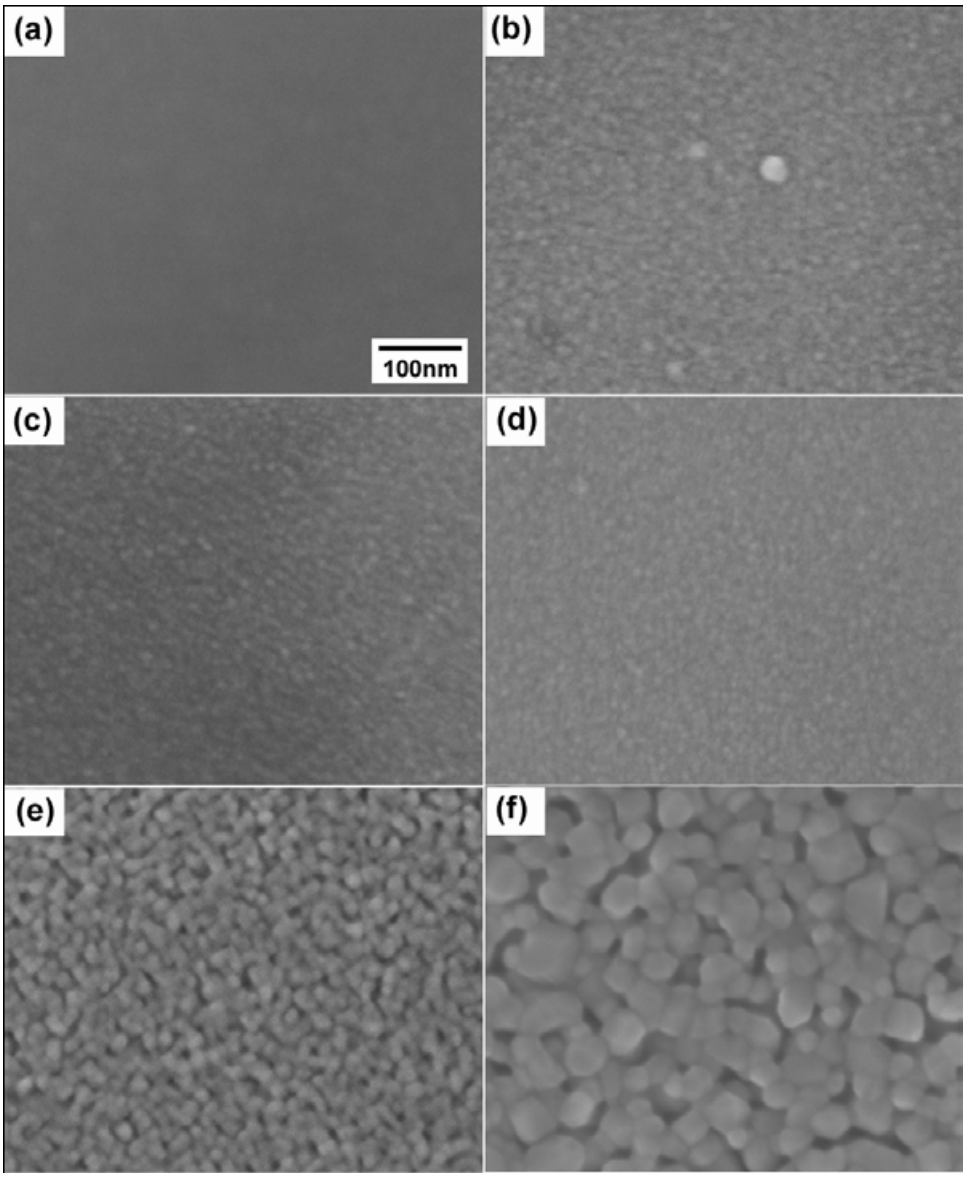

Figure 1.10: SEM micrographs of 1-layered films derived from titanium n-butoxide in toluene with a range of temperature of annealing for 3 hours: (a) room temp., (b) 300 °C, (c) 400 °C, (d) 450 °C, (e) 600 °C and (f) 900 °C (Eun TH [49]).

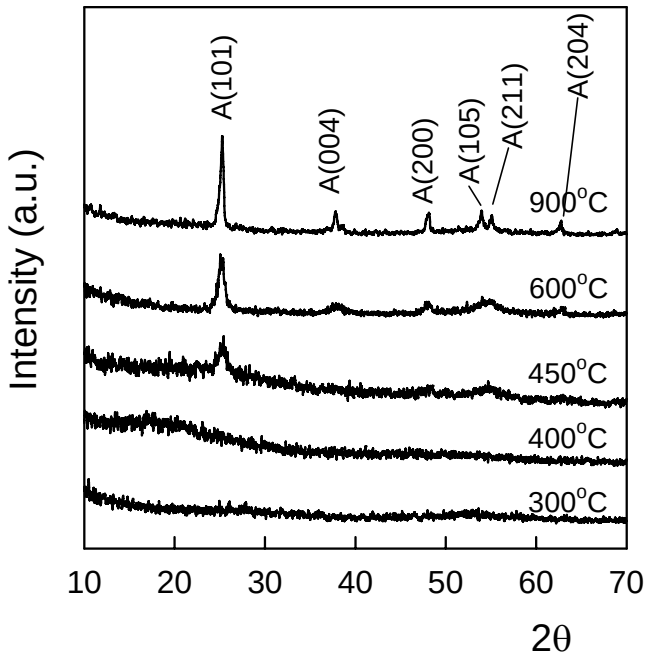

Figure 1.11: Sequential XRD plots from pure titanium n-butoxide derived spin coatings from five different 3 hour heat treatments in air, indicating transition from amorphous to crystallinity beginning at 450 °C (Eun TH [49]).

Metal-organic formulation is a versatile technology, rapidly finding its way into biomedical research and applications [42,48,51,52,53]. Sol-gels have recently been applied directly to large format culture dishes for bioassay [54], but a coating method and format for high throughput biological assays is needed.

1.8 Photocatalysis

With a unique combination of chemical, optical, electrical and biological properties, titanium dioxide has found its way into many high technology applications. It is the naturally occurring oxide passivation layer present on the surface of titanium medical implants that is responsible for biocompatibility and bone integration of everything from dental implants to total joint replacements. This is primarily due to the oxide's ability to reduce inflammation and adapt to surrounding biological tissues. As a photocatalyst, titanium dioxide has been applied to the light activated decomposition of organic pollutants in water, air and the production of antimicrobial surfaces, as well as the manufacture of antifogging mirrors, self cleaning windows and paints [55,56]. Photocatalysts were proposed and used for the generation of hydrogen gas from water and sun light back in 1972 [57] and research continues in using titanium dioxide for the direct production of hydrogen gas in hopes of powering a new hydrogen economy. When titanium dioxide is exposed to ultraviolet (UV) light, electrons in the outermost portion of the valance band are excited to the next energy level in the conductance band. The electron orbits responsible for this band gap are such that electron (-) and hole (+) pairs tend to remain separated and available to catalyze reactions at the oxide interface [58]. Most notably, oxygen absorbed on the oxide surface accepts an electron from the conductance band, forming superoxide, while absorbed water molecules donate an electron to fill the valence hole and produce the potent hydroxyl radical and hydrogen. These radicals are short-lived, but capable of converting organic matter, even drug resistant bacteria like MRSA [59,60], into carbon dioxide, water and trace minerals. Titanium dioxide has been the best candidate for organic degradation because it is both

stable over long periods of time and the redox potential for water and hydroxyl radical couple (-2.8 V) lies within the bandgap domain [55]. This ability to produce and carry separated electron charges has been enhanced by the addition of light capturing dyes and utilized in the manufacture of inexpensive photovoltaic devices to compete with silicon-based semiconductors.

While inexpensive to produce and modify, titanium dioxide has several limitations which have hindered more widespread use. First of all, the normal band gap of this semiconducting material is 3.2 eV, for the anatase crystalline phase, which means that photon utilization is limited to UVA (< 400 nm) and higher energy photons. These wavelengths of light are mostly absorbed by the earth's atmosphere and readily stopped by household glass windows and superficial layers of human skin. In addition to being a low portion of the total solar radiation spectrum reaching the earth's surface, UVB and UVA light can be damaging to biological cells causing mutagenesis through DNA cross-linking in the form of bipyrimidine and cyclobutane pyrimidine dimers [61,62]. The epidermal layer of human skin is efficient at blocking these rays; but most body tissues are relatively transparent to longer red and infrared wavelengths which have also been found to be therapeutic for wound healing [63,64]. A photocatalyst that responded to these longer wavelengths could allow medical implants close to the skin surface to be periodically disinfected with light. Extensive work has been performed to create visible-light responsive photocatalysts, mostly consisting of doping titanium oxide with nitrogen and other transitional metals [65,66] or more recently reported, by addition of secondary quantum sized phases like Au and or CdS [67]. This has extended the effective photocatalytic wavelength cutoff from approximately 400 nm to 525 nm and doubled the

catalytic response to UV light. There is a trade-off however to introducing energy states within the normal band gap, visible light is generally less effective compared to UV light for the production of reactive oxygen species with these materials. The second limitation with titanium dioxide based devices is the low quantum efficiency of electrons produced per absorbed photon, which has moved from 0.1% with the original Fujishima and Honda device to 10% with the dye-sensitized Graetzel cell. The more expensive silicon wafer materials used in everything from integrated circuitry to photovoltaic devices and x-ray detectors enable external quantum efficiencies of 80-90% for near-infrared light and hundreds to thousands of electrons per photon for ionizing x-ray irradiation.

What is needed for both energy production and environmental applications is a new class of materials which inexpensively combines the broad spectrum responsiveness and quantum efficiencies of silicon semiconductors with the economy, ease of manufacture and catalytic properties present with commercial titanium dioxide photocatalyst [68]. In our laboratory, we have developed metal oxide-polymer hybrids derived from metal-organic precursors, which address both the performance and the economic realities necessary to drive larger commercial use of photocatalytic materials.

The last twenty-five years has seen the rapid increase in the formation of multi component metal oxides and co-formation of metal oxides with polymers using sol-gel wet chemistry methods [48]. This involves the use of liquid precursors to make metal oxides either alone or mixed with elastomers or plastics and solvents to form coatings, particles, fibers or bulk materials [42,48,50-52,54]. These techniques offer great flexibility of composition, ease of coating application and low temperature processing when compared to plasma spray, sputter coating and chemical vapor deposition (CVD).

The nearly limitless compositional possibilities available with this versatile technology presents it's own problems; that is, choosing the best composition for a given application. The compositional options require the development of higher through-put methods for screening these materials for specific applications. To help deal with this challenge, we borrowed techniques common to pharmaceutical drug discovery and developed a new high throughput platform by directly coating the bottom of polystyrene and polypropylene multi-well cell culture microplates with these mixed metal oxides and hybrids [69]. This microplate platform has made possible the rapid exploration of novel polymer-coordinated metal oxide materials for biological and drug eluting applications [70]. The use of transparent to translucent thin films on multi-well cell culture microplates means that standard biological assays may be used to screen cellular bioresponses to these materials. This platform has also made possible the development of new methods for rapidly characterizing photocatalytic decomposition of organic matter using monochromatic light from a standard laboratory optical photo spectrometer. This arrangement solves two problems by allowing easy selection of monochromatic pulse-flashed irradiation wavelengths from 190 nm to 1000 nm and the simultaneous screening of as many as twenty-four coating compositions and controls with four replicates in a single microplate. The plate reader functions as both the illumination source and subsequent determiner of photocatalytic clearance using dynamic or endpoint optical density measurements of analytical reagents for photocatalysis like methylene blue (MB) [71] or general turbidity to monitor bacterial growth rates [72,73].

Using this platform and assay methods can aid in the discovery of unique hybrid compositions useful for combining the bioactive properties of metal oxides with the

flexibility of biocompatible polymers like silicones and polyurethanes. Broad spectrum photocatalytic materials make it possible to create biocompatible soft tissue and orthopedic devices, like simple catheters or hip and knee joints that can be disinfected by light or x-rays after implantation. While incidence of infection in bone implants is low at about 1%, re-infection rates are as high as 30 and can be catastrophic to the patient [74-76]. Similarly, photocatalyst responsive to red and near-infrared light could make possible the prophylactic treatment of indwelling Foley, gastronomy, peritoneal dialysis and venous catheters, all of which are subject to high rates of infection [77].

1.9 References

[1] Claxton MJ, Armstrong DG, Boulton AJ. Healing the diabetic wound and keeping it healed: modalities for the early 21st century. Curr Diab Rep 2002; 2: 510–518.

[2] Greenhalgh D. Wound healing and diabetes mellitus. Clin Plast Surg 2003; 30:37–45.

[3] Moulik PK, Mtonga R, Gill GV. Amputation and mortality in new-onset diabetic foot ulcers stratified by etiology. Diabetes Care 2003; 26: 491–44.

[4] Branemark R. Osseointegration. Walter Reed Army Medical Center and Department of Veterans Affairs, Amputee Healthcare & Prosthetics Workshop, Nov. 17 - 18, 2003.

[5] von Recum, AF. Applications and failure modes of percutaneous devices: A review. J Biomed Mater Res 1984;18:323-336.

[6] Hall CW, Cox PA, McFarland SR. Some factors that influence prolonged interfacial continuity. J Biomed Mater Res 1984;18:383-393.

[7] Große-Siestrup C, Affeld K. Design criteria for percutaneous devices. J Biomed Mater Res 1984;18:357-382.

[8] Pendegrass CJ, Goodship AE, Price JS, Blunn GW. Nature's answer to breaching the skin barrier: an innovative development for amputees. J Anat 2006;209:59–67.

[9] Palmer R. Teeth and implants. British Dental Journal 1999;187:183-188.

[10] Sison S. Implant maintenance and the dental hygienist. Access 2003;May-June:1-11.

[11] Knabe C, Große-Siestrup C, Gross U. Histologic evaluation of a natural permanent percutaneous structure and clinical percutaneous devices. Biomaterials 1999;20:503-510.

[12] Branemark R, Branemark P-I, Rydevik B, Myers R. Osseointegration in skeletal reconstruction and rehabilitation: A review. JRRD March/April 2001;38(2):175-181.

[13] Massaro C, Rotolo P, Riccardis R. DE, Milella E. Comparative investigation of surface properties of commercial titanium dental implants. Part I: Chemical composition. J Mater Sci: Mater Med 2002;13:535-548.

[14] Kasemo B, Lausmaa J. Material-tissue interfaces: the role of surface properties and processes. Environ Health Perspect 1994;102(Suppl 5):41-55.

[15] Cuckler JM, Mitchell J, Baker DG, Ducheyne P, Imonitie V, Schumacher HR. A comparison of the biocompatibility of polymethyl methacrylate debris with and without titanium debris: A comparison of two *in vivo* models. In: St. John, KR, editor. Particular debris from medical implants. ASTM STP 1144. Philadelphia: ASTM; 1992. p118–126.

[16] Eriksson A, Thomsen P. *Ex vivo* analysis of leukocyte hydrogen peroxide production using a bi-plate model in mice. J Cell Physiol 1996;166:138–143.

[17] Thomsen P, Bjursten L, Ericson L. Implants in the abdominal wall of the rat. Scand J Plast Reconstr Surg 1986;20:173–182.

[18] Jacobs JJ, Cilbert JL, Urban RM. Current concepts review-corrosion of metal orthopaedic implants. J Bone Joint Surg 1998;80:268-282.

[19] Bjursten L-M. The bone-implant interface in osseointegration. In: Rydevik B, Branemark P-I, Skalak R, editors. International Workship on Osseointegration in Skeletal Reconstruction and Joint Replacement. The Institute for Applied Biotechnology, Goeborg, Sweden, 1991:25-31.

[20] Puleo DA, Nanci A. Understanding and controlling the bone-implant interface. Biomaterials 1999;20:2311-2321.

[21] Brunski JB, Puleo DA, Nanci A. Review article: Biomaterials and biomechanics of oral and maxillofacial implants: Current status and future developments. International Journal of Oral & Maxillofacial Implants 2000;15(1):15-46.

[22] Sundgren JE, Bodo P, Lundstrom I. Auger electron spectroscopic studies of the interface between human tissue and implants of titanium and stainless steel. J Colloid Interface Sci 1986;110:9-20.

[23] Effah E, Bianco P, Ducheyne P. Crystal structure of the surface oxide layer on titanium and its changes arising from immersion. J Biomed Mater Res 1995;29:73-80.

[24] Healy K, Ducheyne P. Hydration and preferential molecular adsorption on titanium *in vitro*. Biomaterials 1992;13:553-561.

[25] Li P, Ducheyne P. Quasi-biological apatite film induced by titanium in simulated body fluid. J Biomed Mater Res 1998;41:341-348.

[26] Suzuki R., Muyco J, McKittrick J, and Frangos JA. Reactive oxygen species inhibited by titanium oxide coatings. J Biomed Mater Res 2003;66A: 396–402.

[27] Suzuki R. and Frangos JA. Inhibition of Inflammatory Species by Titanium Surfaces. Clin Orthop 2000;372:280-289.

[28] Overgaard L, Danielsen N, Bjursten LM. Anti-inflammatory properties of titanium in the joint environment. An experimental study in rats. J Bone Joint Surg Br 1998;80-B:888–893.

[29] Sauberlich, S, Klee D, Richter E-J, Hocker H, Spiekermann H. Cell culture tests for assessing the tolerance of soft tissue to variously modified titanium surfaces. Clin Oral Impl Res 1999;10:379-393.

[30] MacDonal DE, Rapuano BE, Deo N, Stranick M, Somasundaran P, Boskey AL. Thermal and chemical modification of titanium-aluminum-vanadium implant materials: effects on surface properties, glycoprotein absorption, and MG63 cell attachment. Biomaterials 2004;25:3135-3146.

[31] Kern T, Yanf Y, Glover R, Ong JL. Effect of heat-treated titanium surfaces on protein absorption and osteroblast precursor cell initial attachment. Implant Dentistry 2005;14(1):70-76.

[32] Lauer G, Wiedmann-Al-Ahmad, Otten JE, Huber U, Schmelzeisen R, Schilli W. The titanium surface texture effects adherence and growth of human gingival keratinocytes and human maxillar osteoblast-like cells *in vitro*. Biomaterials 2001;22:2799-2809.

[33] Webster TJ, Ergun C, Doremus RH, Siegel RW, Bizios R. Enhanced functions of osteoblasts on nanophase ceramics. Biomaterials 2000;21:1803-1810.

[34] Colon G, Ward BC, Webster TJ. Increased osteoblast and decreased *Staphylococcus epidermidis* functions on nanophase ZnO and TiO_2. J Biomed Mater Res 2006;78A:595–604.

[35] Anselme K, Noel B, Hardouin P. Human osteoblast adhesion on titanium alloy, stainless steel, glass and plastic substrates with same surface topography. J Mater Sci: Mater Med 1999;10:815-819.

[36] Korovessis PG, Deligianni DD. Role of Surface roughness of titanium versus hydroxyapatite on human bone marrow cells response. J Spinal Disord & Techniques 2002;15(2):175-183.

[37] Kim HJ, Kim, HS, Kim MS, Lee EJ, Oh HG, Oh WM, Park SW, KimWJ, Lee GJ, Choi NG, Koh JT, Dinh DB, Hardin RR, Johnson K, Sylvia VL, Schmitz JP, Dean DD. Varying Ti-6Al-4V surface roughness induces different early morphologic and molecular responses in MG63 osteoblast-like cells. J Biomed Mater Res 2005;74A:366-373.

[38] Spyrou P, Papioannou S, Hampson G, Brady K, Palmer RM, McDonald F. Cytokine release by osteroblast-like cells cultured on implant discs of varying alloy compositions. Clin Oral Impl Res 2002;13:623-630.

[39] Karuri NW, Liliensiek S, Teixeira AI, Abrams G, Campbell S, Nealey PF, Murphy CJ. Biological length scale topography enhances cell-substratum adhesion of human corneal epithelial cells. J of Cell Science 2004;117:3153-3164.

[40] Walboomers XF, Jansen JA. Effect of microtexture surfaces on the performance of percutaneous devices. J Biomed Mater Res 2005;74A:381-387.

[41] Rosen A, Wallamn L, Danielsen N, Laurell T, Bjursten LM. Tissue reactions evoked by porous and plane surfaces made out of silicon and titanium. IEEE Transactions on Biomedical Engineering 2002;49(4):392-399.

[42] Kim H-W, Kim H-E, Salih V, Knowles JC. Sol-gel modified titanium with hydroxpapatite thin films and effect on osteoblast-like cell responses. Journal of Biomedical Materials Research 74(3):294-305.

[43] Messer RLW, Lucas LC. Localization of metallic ions within gingival fibroblasts subcellular fractions. J Biomed Mater Res 2002;59:466-472.

[44] Hallab NJ, Vermes C, Messina C, Roebuck KA, Glant TT, Jacobs JJ. Concentration and composition dependent effects of metal ions on human MG-63 osteoblasts. J Biomed Mater Res 2002;60A:420-433.

[45] Yamamoto A, Honma R, Sumita M. Cytotoxicity evaluation of 43 metal salts using murine fibroblasts and osteoblastic cells. J Biomed Mater Res 1998;39:331-340.

[46] Carroll S, Wood EJ. Exposure of Human Keratinocytes and Fibroblasts *In vitro* to nickel sulphate ions induces synthesis of stress proteins Hsp72 and Hsp 90. Acta Derm Venereol 2000;80:94-97.

[47] Yamamoto A, Honma R, Sumita M, Hanawa T. Cytotoxicity evaluation of ceramic particles of different sizes and shapes. J Biomed Mater Res 2004;68A:244-256.

[48] Metal-Organics for Materials, Polymers & Synthesis: A Survey of Properties and Chemistry, Arkles B, Larson G, editors. Gelest, Inc., Morrisville, PA, USA 2005.

[49] Hun TH. Microstructural evolutions and stress studies of titania films derived by “spin-deposition” methods. PhD Thesis, Brown University, Providence RI, USA 2006.

[50] Podbielska H., Ulatowska-Jarza, A. Sol-gel technology for biomedical engineering. Bull Pol Ac:Tech 2005;53(3):261-271.

[51] Advincula MC, Rahentulla FG, Advincula RC, Ada ET, Lemons JE, Bellis SL. Osteoblast adhesion and matrix mineralization on sol-gel derived titanium oxide. Biomaterials 2006;27:2201-2212.

[52] Piveteau L-D, Gasser B, Shlabach L. Evaluating mechanical adhesion of sol-gel titanium dioxide coatings containing calcium phosphate for metal implant application. Biomaterials 2000;21:2193-2201.

[53] Kang JS, Lee CL, Kim MS, Lee MS. New Routes to the preparation of silver-doped sol-gel films for a SERS study. Bull. Korean Chem Soc 2003;24(11):1599-1604.

[54] Nakazawa K, Lee S-W, Fukuda J, Yand D-H, Kunitake T. Hepatocyte spheroid formation on a titanium dioxide gel surface and hepatocyte long-term culture. J Mater Sci: Mater Med 2006;17:359-364.

[55] MR Hoffmann, ST Martin, W Choi, and DW Bahnemannt. Environmental Applications of Semiconductor Photocatalysis. Chemical Reviews, 1995, Vol. 95, No. 1, 69-91.

[56] Kazuhito Hashimoto, Hiroshi Irie, Akira Fujishima. TiO_2 Photocatalysis: A historical overview and future prospects. Japanese Journal of Applied Physics 2005;44(12):8269-8285.

[57] Akira Fujishima, Kenichi Honda. Electrochemical photolysis of water at a semiconductor electrode. Nature 1972;238:37-38.

[58] S Banerjee, J Gopal, P Muraleedharan, AK Tyagi, B Raj. Physics and chemistry of photocatalytic titanium dioxide: Visualization of bactericidal activity using atomic force microscopy. Current Science 2006;90(10):1378-1383.

[59] Y Sekiguchi, Y Yao, Y Ohko, K Tanaka, Te Ishido, A Fujishima, Y Kubota. Self-sterilizing catheters with titanium dioxide photocatalyst thin films for clean intermittent catheterization: Basis and study of clinical use. Inter J of Urology 2007;14:426–430.

[60] P-C Maness, S Smolinski, DM Blake, Z Huang, EJ Wolfrum, WA Jacoby. Bactericidal Activity of Photocatalytic TiO_2 Reaction: toward an Understanding of Its Killing Mechanism. Appl Envir Microbio 1999;65(9):4094–4098.

[61] UP Kappes, D Luo, M Potter, K Schulmeister, TM Rünger. Short- and long-wave UV light (UVB and UVA) induce similar mutations in human skin cells. Journal of Investigative Dermatology 2006;126:667–675.

[62] S Mouret, C Baudouin, M Charveron, A Favier, J Cadet, T Douki. Cyclobutane pyrimidine dimers are predominant DNA lesions in whole human skin exposed to UVA radiation. PNAS 2006;103:13765-70.

[63] Toyokawa H**,** Matsui Y**,** Uhara J**,** Tsuchiya H**,** Teshima S**,** Nakanishi H**,** Kwon AH**,** Azuma Y**,** Nagaoka T**,** Ogawa T**,** Kamiyama Y. Promotive effects of far-infrared ray on full-thickness skin wound healing in rats. Exp Biol Med 2003;228:724–729.

[64] Danno K, Noriko Mori N, Toda K, Kobayashi T, Utani A. Near-infrared irradiation stimulates cutaneous wound repair: laboratory experiments on possible mechanisms. Photodermatol Photoimmunol Photomed 2001;17:261–265.

[65] R Asahi, T Morikawa, T Ohwaki, K Aoki, Y Taga. Visible-light photocatalysis in nitrogen-doped titanium oxides. Science 2001;293:269-271.

[66] SI Shah, W Li, C-P Huang, O Jung, C Ni. Study of Nd3+, Pd2+, Pt4+, and Fe3+ dopant effect on photoreactivity of TiO_2 nanoparticles. PNAS 2002;99:6482–6486.

[67] Hiroaki Tada, Tomohiro Mitsui, Tomokazu Kiyonaga, Tomoki Akita, Koji Tanaka. All-solid-state Z-scheme in CdS–Au–TiO_2 three-component nanojunction system. Nature Materials Vol. 5 October 2006, 283-286.

[68] Nathan S Lewis, Daniel G Nocera. Powering the planet: Chemical challenges in solar energy utilization. PNAS 2006;103(43):15729–15735.

[69] JD Jarrell, TH. Eun, M. Samale, C Briant, B Sheldon, JR Morgan. Metal oxide coated cell culture arrays for rapid biological screening. J Biomed Mater Res 2007;83A (3):853-860.

[70] JD Jarrell, B Dolly, JR Morgan. Controlled release of vanadium from titanium oxide coatings for improved integration of soft tissue implants. (accepted March 27, 2008) J Biomed Mater Res A 2008.

[71] Andrew Mills, Jishun Wang. Photobleaching of methylene blue sensitised by TiO_2: an ambiguous system? Journal of Photochemistry and Photobiology A: Chemistry 127 (1999) 123–134.

[72] Bechert T, Steinrucke P, Guggenbichler J-P. A new method for screening anti-infective biomaterials. Nature Medicine 2000;6(8):1053-1056.

[73] Alt V, Bechert T, Steinrucke P, Wagener M, Seidel P, Dingeldein E, Domann E, Schnettler R. *In vitro* testing of antimicrobial activity of bone cement. Antimicrobial Agents and Chemotherapy 2004;48(11):4084-4088.

[74] AA Hofmann, TD Goldberg. Temporary reimplantation of TKA for two-stage revision. Techniques in Knee Surgery 2005;4(3):207-212.

[75] JG Hendriks, JR van Horn, HC van der Mei, HJ Busscher. Backgrounds of antibiotic-loaded bone cement and prosthesis-related infection. Biomaterials 2004;25(3):545-556.

[76] FS Haddad, SK Muirhead-Allwood, ARJ Manktelow, I Bacarese-Hamilton. Two-stage uncemented revision hip arthroplasty for infection. J Bone Joint Surg [Br] 2000;82B:689-94.

[77] JR Johnson, MA Kuskowski, TJ Wilt. Review: Systematic Review: Antimicrobial urinary catheters to prevent catheter-associated urinary tract infection in hospitalized patients. Ann Intern Med 2006;144(2):116-126.

Chapter 2

Metal oxide coated cell culture arrays for rapid biological screening

John D. Jarrell [1*], Tai H. Eun [2], Marcus Samale [2], Clyde Briant [2], Brian W. Sheldon[2], Jeffrey R. Morgan [1]

[1] Department of Molecular Pharmacology, Physiology, and Biotechnology, Brown University, Providence, RI, USA

[2] Division of Engineering, Brown University, Providence, RI, USA

Received 25 October 2006; revised 24 January 2007; accepted 6 April 2007
J Biomed Mater Res A 2007;83A(3):853-860

Abstract

The biointerface of metallic alloy implants is a spontaneously formed metal oxide layer. This study presents a novel method for creating titanium oxide xerogel coated microplates for high throughput biological screening that overcomes several limitations of using bulk metal samples to study oxides. Metal-organic precursors were used to evaluate the influence of Al, V, Ca and P doped smooth and textured titanium oxide xerogel coatings on the bioresponse of human fibroblasts to increase understanding of the soft tissue sealing around trans-epithelial devices. Coatings made of titanium n-butoxide were characteristically smooth, while those of titanium isopropoxide were micro and nano featured. Screening consisted of WST-1 proliferation assay, Calcein AM cell number and viability assay and a modified cell seeding efficiency and centrifugation adhesion assay. Small variations in initial attachment and centrifugation adhesion of human fibroblasts were observed among the coatings and comparable to tissue culture treated polystyrene. Proliferation and viability at 24 and 48 hours was reduced by the 10 and 20% vanadium additions. Metal oxide coated microplates are adaptable to the investigation of a wide range of metal-organic derived chemistries and the influence of oxide texture, level of oxide crystallinity and oxide grain size on the biological responses of cells.

Keywords: Titanium oxide, Fibroblast, Crystallinity, Surface modification, Cell viability, Sol-gel techniques

2.1 Introduction

Titanium implants have been successfully used in a variety of dental and medical applications including tooth implants, facial reconstructions and recently, osseointegrated percutaneous prostheses attachments [1]. The presence of a naturally occurring TiO_2 passivation film [2] and subsequent biological modification during implantation [3] is generally regarded as responsible for the inhibition of inflammation [4-6], and good bio-integration of titanium achieved with both bone and soft tissues. In each location of implantation, dynamic processes occur between the titanium oxide layer and the biological tissue, whether cortical bone, marrow or soft tissue. Biological contact generally results in an increased thickness of the oxide layer [7] and an incorporation of elements from the surrounding tissue such as calcium and phosphorous as is the case in bone marrow [8-10].

The bioresponse to surface roughness and chemistry is dependent on cell type. The introduction of micro and nano features strongly influences tissue cell and bacterial responses [11-13]. For oesteoblasts, adhesion is similar for very different materials if the surface topography is controlled [14]; proliferation, however, increases with increasing surface roughness [15]. Chemistries have been altered with organic and inorganic coatings or surface alloyed with plasma based methods. Some of these modifications have been shown to influence cellular adhesion during centrifugation [16]. Combined thermal and chemical modifications of titanium using heat, peroxide and butanol treatments can also influence protein binding and cell attachment [17-18].

Biological work on metal oxide surfaces has been hindered by the limitations associated with solid metal samples. Metal disks being opaque, generally available with limited chemistries and difficult to handle in large numbers and small sizes are not conducive to rapid biological screening in the microplate format. A better method to rapidly produce pure and alloyed metal oxide films to study the effect of oxide chemistry and oxide surface morphology, oxide crystallinity and oxide grain size on cellular response is needed.

Liquid, metal-organic precursors can be used to produce a wide variety of metal oxide thin films and coatings [19]. In particular, sol-gel methods have been widely studied to create glass and ceramic coatings and particles from solutions of metal-organic precursors. Because of the versatility of this technology, it is rapidly finding its way into biomedical research and applications [20-21]. Good results have been obtained with sol-gel coatings on titanium metal for implant applications with respect to coating adhesion and coating influence on bulk mechanical properties [22]. Sol-gels have recently been applied directly to large format culture dishes for bioassay [23], but have not been adapted to a high throughput platform.

This paper presents a method for rapidly creating transparent amorphous structured metal oxide coatings on the bottom of standard 96-well microplates with controllable chemistry and surface topography. The coatings were rapidly screened using high throughput assays to measure cell proliferation, viability, cell attachment and centrifugal adhesion. The method and platform explained in this paper was used to explore the influence of common titanium alloying elements, aluminum and vanadium and

biologically incorporated elements, calcium and phosphorus on the bioresponse of normal human fibroblast cells to metal oxide xerogels.

2.2 Materials and Methods

2.2.1 Solutions

To make stock solutions of titanium, one gram of titanium alkoxide was diluted in 10 ml of either toluene (for the n-butoxide form) or isopropanol (for the isopropoxide form). To make 10% and 20% aluminum solutions, 0.06 and 0.12 gm of aluminum isopropoxide was added to the toluene solution, while 0.07 and 0.14 gm was added to the isopropanol solution. To make 10% and 20% vanadium solutions, 0.1 and 0.2 gm of vanadium oxytripropoxide was added to the toluene solution, while 0.12 and 0.24 gm was added to the isopropanol solution. To make 10% calcium solutions, 69.4 mg of calcium nitrate hydrate was added to the toluene solution, while 83.1 mg was added to the isopropanol solution. To make 10% phosphorus solutions, 53.5 mg of triethyl phosphate was added to the toluene solution, while 64.1 mg was added to the isopropanol solution. The 10% calcium plus phosphorus solution had 10% of each precursor added. All of the metal-organic precursors were obtained through Aldrich Chemical (Allentown, PA).

2.2.2 Coating

Polystyrene 96-well tissue culture microplates (Corning Costar) were coated under a laminar flow hood. Using an eight-channel pipette, 30 μl of each solution was pipetted into each well of a column. After each filling, the plate was inverted and briefly shaken before applying solution to the next column of wells. Each column was coated with

different solution chemistries resulting in 8 different titania surfaces per plate. Four columns were left as uncoated culture treated polystyrene for comparison. A separate plate was used for each of the two solvent systems. The microplates were air-dried face up, under a laminar flow hood for 24 hours and subsequently heat treated in air on a hot plate (Dataplate, Barnstead/Thermolyte, Dubuque, IA) at 95 °C for one hour with the lids in place.

2.2.3 Surface Characterization

Scanning Electron Microscopy

A LEO 1530 Thermally-Assisted Field Emission (TFE) Scanning Electron Microscope (SEM) was used to establish surface morphology of the coatings. Samples were carbon sputter coated to overcome the inherent insulating properties of the metal oxide sol-gels. A working distance of 5 mm and accelerating voltage of 5.00 kV was used to collect electron images at various magnifications between 5,000 X and 300,000 X.

2.2.4 Cell Proliferation Assay

Human dermal fibroblasts were derived from neonatal foreskins, obtained at the Women & Infants Hospital of Rhode Island, Providence, RI, USA (approved by the Institutional Review Board and in adherence to Declaration of Helsinki Guidelines). Foreskins were trimmed with scissors to remove excess fatty tissue, rinsed repeatedly with sterile phosphate buffered saline (PBS), and diced into small fragments. The fragments were allowed to adhere to the bottom of a tissue culture plate in a humidified 10% CO_2 atmosphere, at 37 °C for 1 hour, and were covered with Dulbecco's Modified Eagle

Medium (DMEM) (Invitrogen Corporation, Carlsbad, CA) supplemented with 20% fetal bovine serum containing 100U of penicillin and 100μg of streptomycin per ml. Over a period of 14 days, fibroblasts migrated from the tissue fragments and formed a confluent layer on the culture plate. Fibroblasts were harvested with a 0.05% trypsin/0.53 mM EDTA solution and subcultured to near confluence in Human Fibroblast Medium (HFM) consisting of DMEM containing high glucose, L-glutamine, pyruvate and pyridoxine hydrochloride (Invitrogen Corporation, Carlsbad, CA) with additions of 10% fetal bovine serum and 1% penicillin-streptomycin. Cells were detached using 0.05% trypsin/0.53 mM EDTA for 3 minutes and re-suspended in serum containing medium. The cells were seeded onto 96 well microplates at a density of 5,000 cells per well in 100 μl of HFM.

To measure cell proliferation, the microplates were incubated at 37 °C with 10 % CO_2 for 48 hours, after which 10 μl of WST-1 (Roche Applied Science, Indianapolis, IN) was added into each well and incubated for 3 hours at 37 °C. The microplates were quantified using a microplate reader for absorbance at 440 nm (SPECTRAmax® PLUS 384 Microplate Spectrometer with SOFTmax PRO software, Molecular Devices Corporation, Sunnyvale, CA) and plotted. Five replicates with three cell-free controls were used for each coating type and the polystyrene plate bottom. Plates were also inspected under optical microscopy for cell spreading and morphology. Calibration curves were previously established for cell number versus optical density on polystyrene. Seeding density for the cell type was chosen within the linear portion of the calibration curve.

2.2.5 Cell Viability Assay

Human fibroblasts were seeded onto 96 well microplates at a density of 5,000 cells per well in 100 μl of HFM and incubated at 37 °C with 10 % CO_2. After 24 hours, cells were rinsed with 1X phosphate buffered saline with 100 mg of CaCl and 100 mg MgCl+6H_2O per liter added (complete PBS) (Invitrogen Corporation, Carlsbad, CA) and incubated in 100 μl of 1 μg/ml Calcein-AM (Molecular Probes, Inc., Eugene, OR) in complete PBS with 2 mM dextrose for 30 minutes at 22 °C.

Plates were read using a fluorescent microplate reader (SPECTRAmax® GEMINI XS Dual-Scanning Microplate Spectrofluorometer with SOFTmax PRO software, Molecular Devices Corporation, Sunnyvale, CA) set to 485 nm excitation, 535 nm emission. Five replicates with three cell-free controls were used for each coating type and the polystyrene plate bottom. Calibration curves were previously established for cell number versus fluorescence on polystyrene and used to select a seeding density within the linear portion of the calibration curve.

Cells were subsequently observed for cell spreading and morphology using optical and fluorescent microscopy.

2.2.6 Combined Cell Attachment and Cell Adhesion Assay

Initial cell attachment efficiency and cell adhesion were measured by modification of a previous method [24-25]. Normal human fibroblasts were grown in 500 cm^2 triple flasks to near-confluence using HFM. The cells were rinsed with complete PBS and incubated in 45 ml of 1 μg/ml calcein-AM in complete PBS with 2 mM dextrose for 30 minutes at 22 °C. Cells were detached using 0.05% trypsin and 0.53 mM EDTA for 3 minutes and re-suspended in serum containing medium. Cells were centrifuged at 500 rpm for 5

minutes and re-suspended in PBS dextrose, centrifuged again and re-suspended in PBS dextrose. The cells were then seeded onto microplates at a density of 10,000 cells per well and left to attach for one hour at 22 °C. Calibration curves were previously established for cell number versus fluorescence on polystyrene and used to a select seeding density within the linear portion of the calibration curve and to maximize signal to noise response of the plate reader.

Each well was completely filled with PBS-dextrose and the baseline fluorescence read (485 nm excitation, 535 nm emission). The wells were emptied by inversion to remove floating cells, refilled with PBS-dextrose and fluorescence read a second time. The microplate was covered with sealing tape (Corning Costar) and centrifuged upside down in a Centra-GP8R Refrigerated Centrifuge (Thermo Electron Corporation, Waltham, MA) using microplate buckets at 800 rpm for 5 minutes. The microplates were again inverted to empty and refilled with PBS-dextrose and read a third time in the plate reader. The first and second readings were compared to determine the fraction of cells that attached to the bottom of the microplate 1 hour after cell seeding. This corresponds to the one hour cell seeding efficiency. The post-centrifuge fluorescence (third) reading was compared to the pre-centrifuge (second) reading to determine the fraction of attached cells that remained adherent after exposure to normal forces from centrifugation. Together, these assays identify how readily cells attach to a surface (seeding efficiency) and quantify the strength of adhesion of the attached cells (adherent fraction). The rpm of the centrifuge was selected to remove approximately 50% of the cells from the tissue culture treated polystyrene. Five replicates with three cell-free controls were used for each coating type and the polystyrene microplate bottom.

2.3 Results

2.3.1 Surface Characterization

Polystyrene microplates coated with various sol-gel applied TiO_2 compositions were analyzed under the SEM to evaluate the surface appearance and morphology. Figure 2.1 presents SEM images from a MOC microplate array showing the surface texture of the isopropoxide based coatings in each of the eight tested compositions. Isopropoxide based coatings were generally textured with micro and nano sized features. Additions of calcium nitrate hydrate to the precursor caused the coatings to come out smooth with areas of micro-cracking`. Figure 2.2 presents SEM images from a MOC microplate array showing the surface texture of n-butoxide/toluene based coatings in each of the eight tested compositions. N-butoxide/toluene based coatings were generally smooth. Some crack-like appearances and stress relief features were dispersed throughout the coatings, especially away from the central region of the microplate wells.

2.3.2 Cell Proliferation Assay

To determine cell proliferation, the WST-1 colorimetric assay was used (Figure 2.3). Forty eight hours after seeding with cells, five replicates of each coating chemistry and type were tested for their ability to promote cell proliferation. The textured isopropanol based coatings are presented by the open diamonds and the toluene based coatings by closed squares. The polystyrene (PS) noncoated plate was used as a control to compare results from different plates. In general, the smooth surface of the titanium n-butoxide coatings showed slightly increased proliferation over the titanium isopropoxide coatings.

Most coatings showed proliferation results similar to the polystyrene plate bottom. However, there was a notable decrease in the reading from the 10% and 20 % vanadium samples.

2.3.3 Cell Viability Assay

Calcein AM was used to determine the number and viability of cells after 24 hours attachment (Figure 2.4). Cell viability, as measured by calcein fluorescence, was measured for five replicates of each coating chemistry and type. The textured isopropanol based coatings are presented by the open diamonds and the toluene based coatings by closed squares. The polystyrene (PS) noncoated plate was used as a control to compare results from different plates. A notable decrease in cell number was again indicated for the vanadium alloyed coatings. Under optical and fluorescent microscopy, cells were well spread on all coatings and uncoated polystyrene, except for those coatings containing 10% and 20% vanadium. Under those conditions, the cells were alive, but still rounded similar to the normal appearance of cells after one hour of attachment. Presented in Figure 2.5 are representative morphologies of normal human fibroblasts 24 hours after seeding onto titanium butoxide xerogel (A), xerogel with 20% vanadium (B) and tissue culture treated polystyrene (C). Images were taken using fluorescent microscopy of calcein loaded cells.

2.3.4 Initial Cell Attachment and Cell Adhesion Assay

To determine the efficiency of initial cell attachment (one hour after seeding) and cell adhesion under load, a modified centrifugation cell adhesion assay was used. The cell

attachment after one hour of seeding ranged from approximately 65% to 85% for the toluene based coatings as represented by the closed circles in Figure 2.6. Of these attached cells, approximately 45% to 65% of them remained adherent to the coatings after centrifugation as represented by the closed squares in Figure 2.6. Little variation was observed between the eight toluene based coatings and the tissue culture treated polystyrene, indicating that the coatings supported good initial cell attachment and good cell adhesion strength. For the isopropanol based coatings, approximately 70% to 85% of the cells attached one hour after seeding as represented by the open circles in Figure 2.7. Of these attached cells, approximately 40% to 55% of them remained adherent to the coatings after centrifugation as represented by the open squares in Figure 2.7. Surface chemistry mildly influenced initial attachment and adherence of cells. There appeared to be a slight preference of cell attachment to the smoother butoxide based coatings for most of the compositions.

2.4 Discussion

In this study we have developed a novel method for rapidly producing metal oxide coatings with varying chemical compositions and microtextures and testing the bioresponse of cells to these coatings. Solutions that were identical to those used here have also been used to produce sol gel films via spin coating [26]. With the methodology used in the current work (i.e., pipetting the solutions into a 96 well plate), the resulting coatings did not undergo the same sol-gel structural evolution. However, the chemical composition of both materials is expected to be very similar.

The methodology described here is very useful for studying biological responses to xerogel metal oxide surfaces. There are many possible metal oxide chemistries that can be explored with different liquid, metal-organic precursors. In addition to testing fully miscible chemistries, suspensions and emulsions can also be explored. Coatings derived from metal-organic precursors can also be used as a carrier for secondary therapeutic components.

The use of standard plastic microplates in this platform allows us to use various solvent systems, giving different surface morphologies. All of the films studied to date are amorphous. A general transformation from amorphous to crystalline titania coatings starts at approximately 450 °C in air [26]. While the use of glass or polyquartz microplates would enable these higher temperature heat treatments, these platforms add considerable expense for processing high volumes of sample compositions allowed by this method. Use of steam reduces the temperature necessary for oxide crystallization, making economical polypropylene microplates an option for the future. In particular, moist air heat treatments in the range of 60 °C to 80 °C also have the ability to induce oxide crystallinity [26-27] and are suitable for polystyrene culture plates.

There were several general observations with the chemical compositions and two microtextures evaluated. Fibroblast viability and proliferation were more controlled by the chemical composition of the coating than the very notable surface microtexture variation between the two solvent systems. The cell proliferation assay and cell viability and morphology assay used two different metabolic processes to produce the metabolites measured by the plate readers; however the plotted results were very similar. They both indicated that the effect of vanadium on cell proliferation and spreading was both

repeatable and significant. The phenomenon associated with vanadium alloyed titania is being further explored.

The coating of microplates has several limitations. Certain solvents, such as toluene, tend to attack the culture plate polystyrene. Immediate shaking after the introduction of the sol-gel solutions allowed the use of the toluene solvent without causing excessive distortion to the well bottoms. Full air drying before heat treatment was also required to prevent the toluene solvent from clouding the microplate lids. The toluene solvent coatings were, however, more uniform and adherent to the polystyrene. The isopropoxide coatings tended to exhibit higher degrees of residual stress relief cracking and adequate but poorer adhesion to the polystyrene. Some flaking of the isopropoxide based coatings was observed several days after testing was concluded. Other combinations of microplate materials, solvents and alkoxides bases may overcome these problems.

2.5 Conclusions

The technique for metal oxide film production presented in this paper allows for rapid production of varied titania and other mixed metal oxide coatings that may be applied to 96-well culture microplates for convenient and rapid biological assays. The butanol system generally produced smooth surfaces, while the isopropanol system produced surfaces with a micro-spongy texture.

This platform for producing and testing metal oxide coatings results in a high throughput assay, that overcomes several problems associated with commonly used metal disk samples. The coatings are transparent for easy inspection. The chemistry of the metal oxides can be rapidly changed compared to the difficulty of custom formulation

and sintering of powder metallurgy samples or the limited variations available with standard metal alloys. In addition, fully miscible sol-gel chemistries, suspensions and emulsions can also be explored.

Titanium and other metal oxide solutions can be used as carriers for secondary therapeutic drugs and chemistries. An additional benefit of being freed from using metal substrates is the ability to coat a wide variety of materials, including metals, ceramics, plastics, elastomers and rubbers, used for implantable devices. We have also applied these coatings to microplates that we first coated with PDMS, to mimic the coating of silicon rubber medical devices. Economical polypropylene microplates and expensive quartz microplates allow the exploration of the effects of oxide crystallinity and oxide grain growth that occurs during autoclave steam exposure and higher heat treatments in air (300 °C to 900 °C).

This method can be used for exploring the use of pure and modified titania or other metal oxide coatings on plastic and elastomeric based percutaneous devices to improve soft tissue integration. It is hoped that this platform can be further exploited to improve our understanding of how oxide chemistry, oxide surface morphology, oxide crystallinity and oxide grain size ultimately influence biointegration, especially of soft tissues.

Acknowledgements

This work was funded, in part, by VA Rehabilitation Research and Development Center for Restorative and Regenerative Medicine, Department of Veterans Affairs.

2.6 Figures

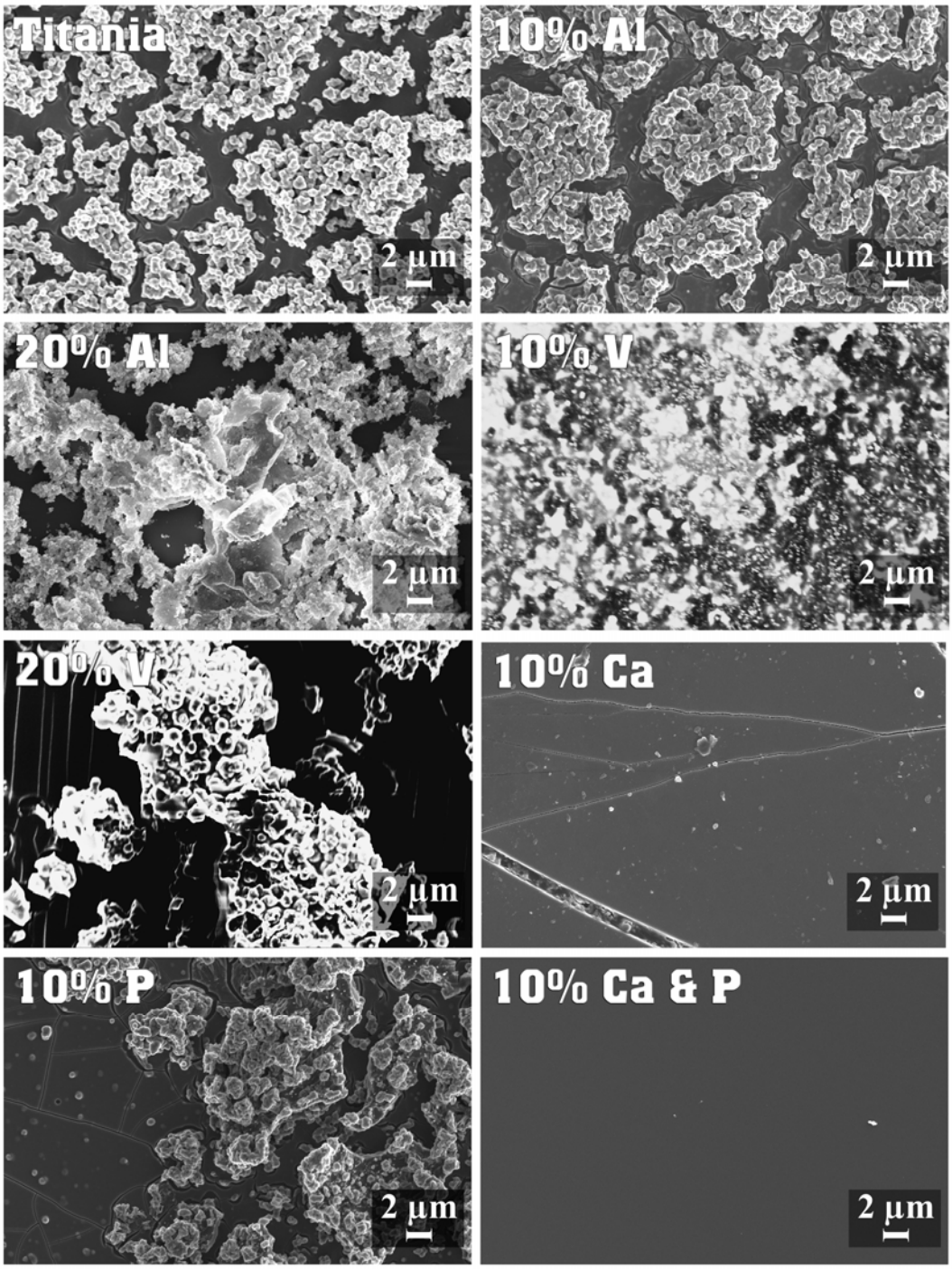

Figure 2.1: SEM images from MOC microplate array showing surface texture of isopropoxide base coating in each of the eight tested compositions. Isopropoxide based coatings were generally textured with micro and nano sized features. Coatings with calcium nitrate hydrate additions had a smooth appearance.

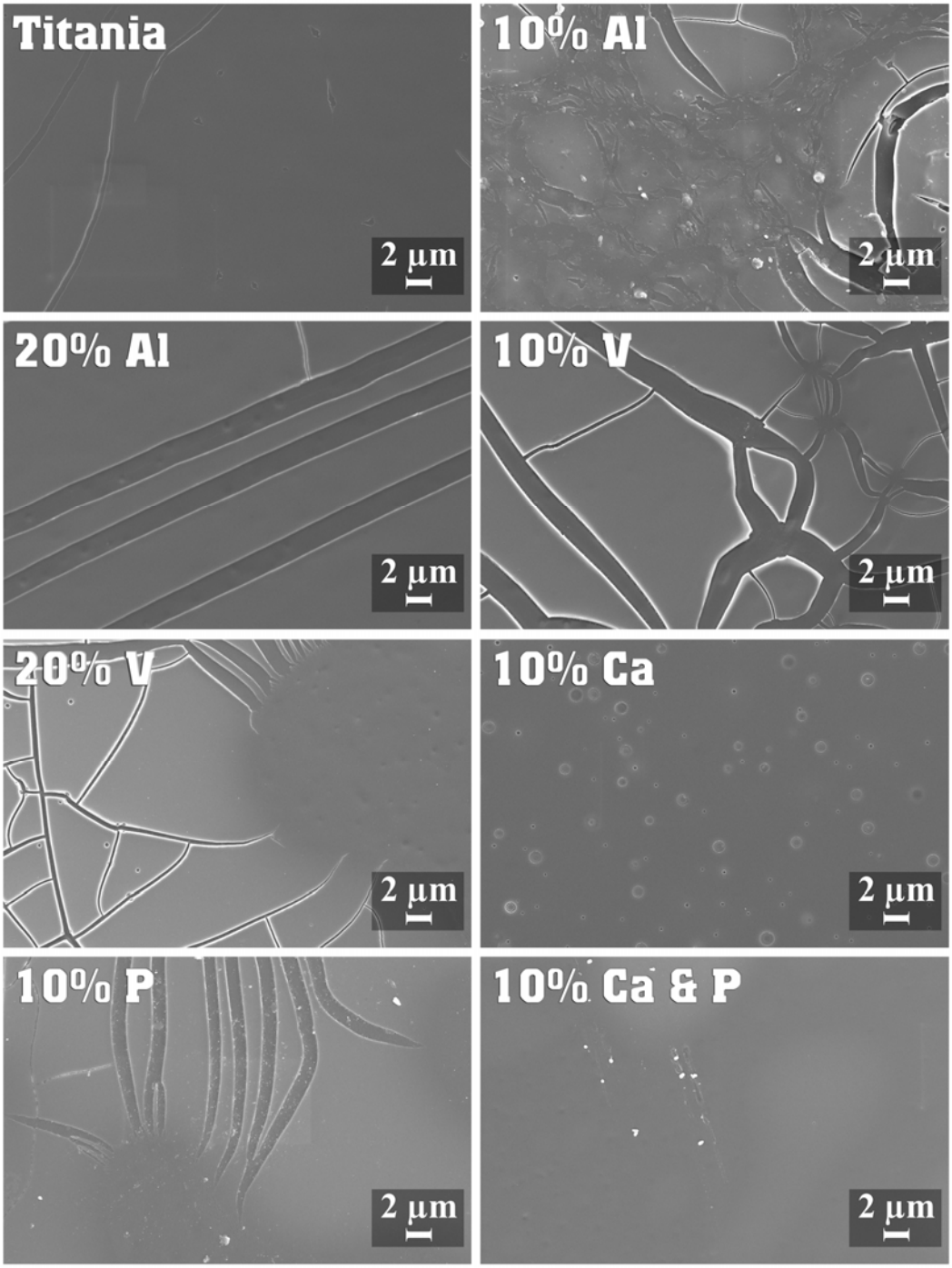

Figure 2.2: SEM images from MOC microplate array showing generally smooth surface texture of n-butoxide and toluene based coating with some micro-cracking in each of the eight tested compositions.

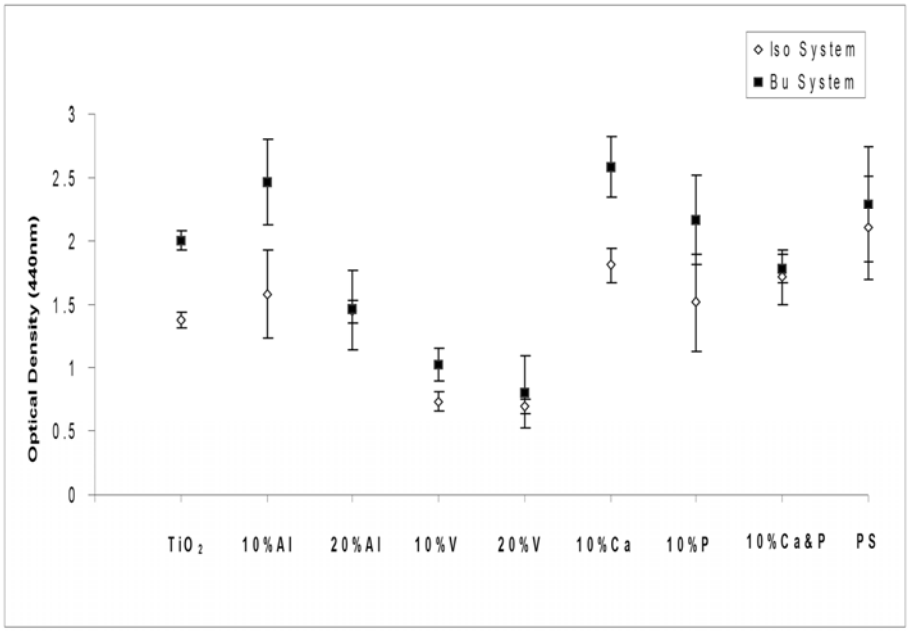

Figure 2.3: Results of 48 hour WST-1 cell proliferation assay with isopropoxide/isopropanol based coatings (Iso), butoxide/toluene based coatings (Bu) and uncoated tissue culture treated polystyrene (PS), indicating reduced proliferation with vanadium alloyed coatings.

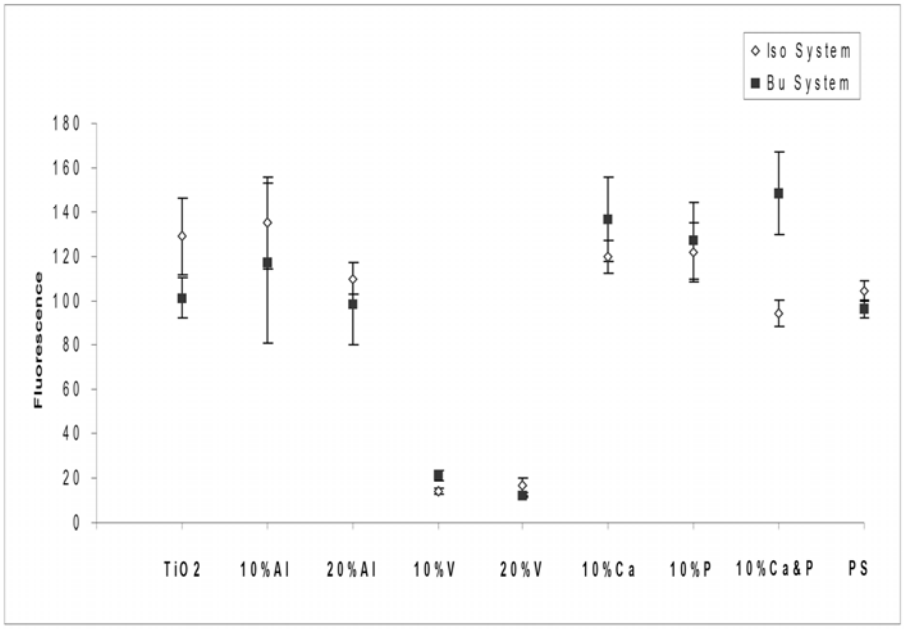

Figure 2.4: Relative fluorescence of cells on each isopropoxide/isopropanol based coating (Iso), butoxide/toluene based coating (Bu) and uncoated tissue culture treated polystyrene (PS) 24 hours after seeding, indicating reduced cell number and viability with vanadium alloyed coatings.

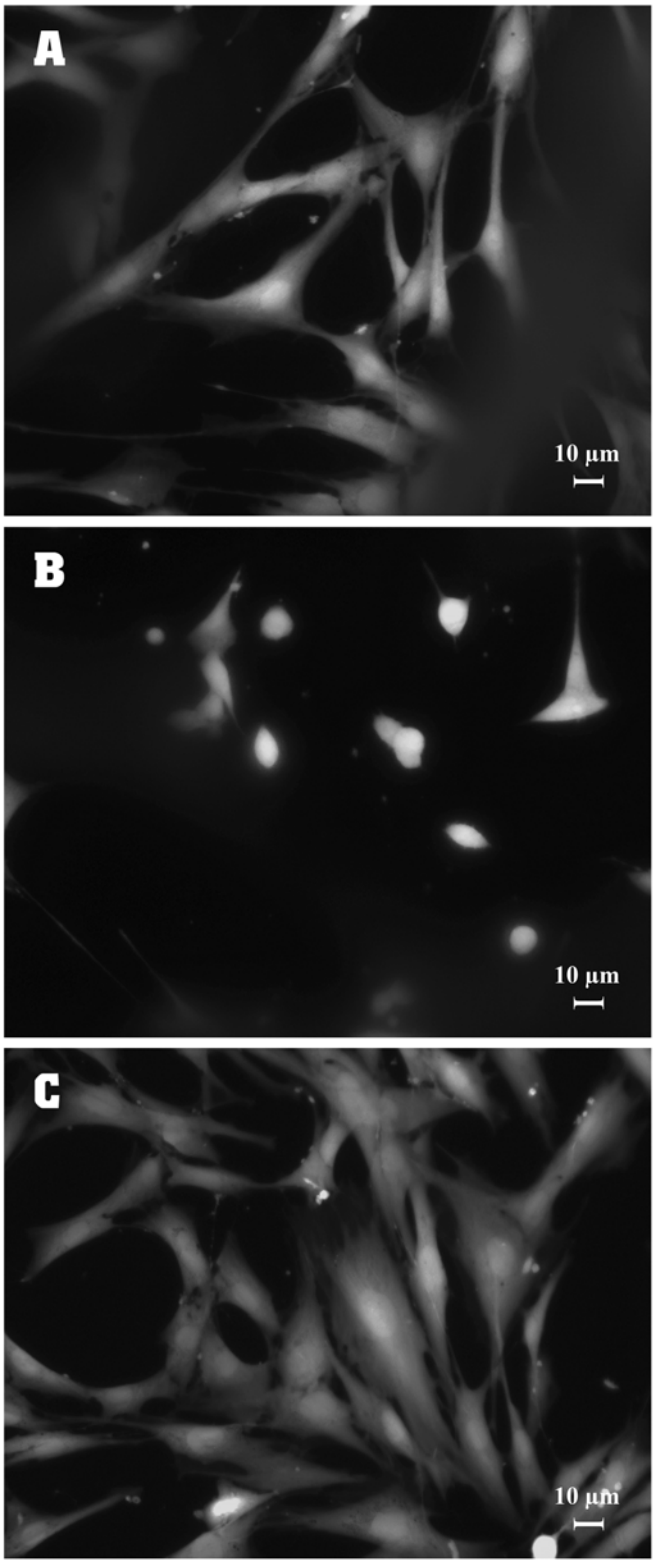

Figure 2.5: Morphologies of normal human fibroblasts 24 hours after seeding onto titanium butoxide xerogel (A), xerogel with 20% vanadium (B) and tissue culture treated polystyrene (C). Images were taken using fluorescent microscopy of calcein loaded cells.

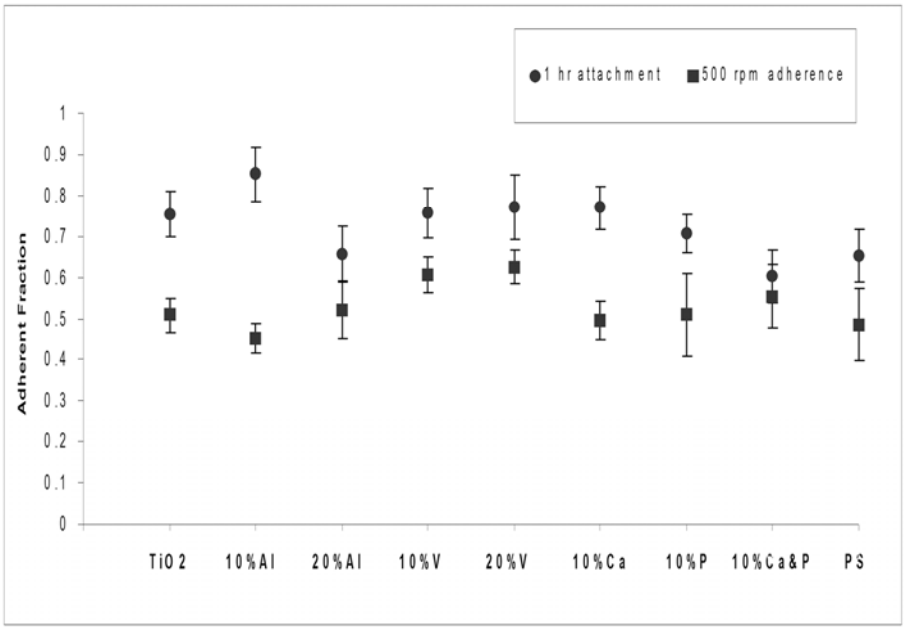

Figure 2.6: A graph indicating the fraction of cells attaching after one hour and those adhering after centrifugation is presented for all coating chemistries in a toluene solvent and uncoated tissue culture treated polystyrene (PS).

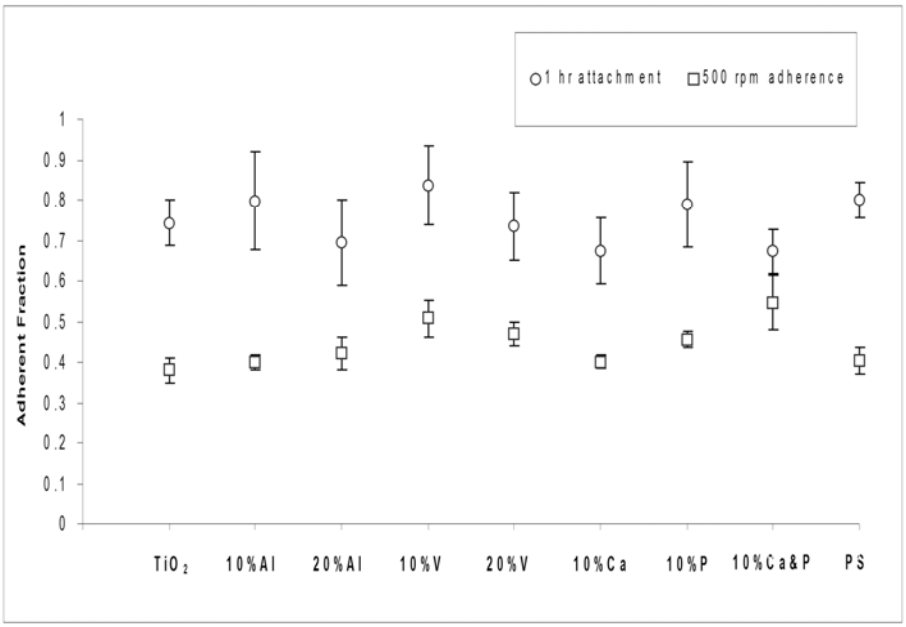

Figure 2.7: A graph indicating the fraction of cells attaching after one hour and those adhering after centrifugation is presented for all coating chemistries in an isopropanol solvent and uncoated tissue culture treated polystyrene (PS).

2.7 References

[1] Branemark R, Branemark P-I, Rydevik B, Myers R. Osseointegration in skeletal reconstruction and rehabilitation: A review. JRRD March/April 2001;3(2):175-181.

[2] Massaro C, Rotolo P, Riccardis R. DE, Milella E. Comparative investigation of surface properties of commercial titanium dental implants. Part I: Chemical composition. J Mater Sci: Mater Med 2002;13:535-548.

[3] Kasemo B, Lausmaa J. Material-tissue interfaces: the role of surface properties and processes. Environ Health Perspect 1994;102(Suppl 5):41-55.

[4] Suzuki R., Muyco J, McKittrick J, and Frangos JA. Reactive Oxygen Species Inhibited by Titanium Oxide Coatings. J Biomed Mater Res 2003;66A: 396–402.

[5] Suzuki R. and Frangos JA. Inhibition of Inflammatory Species by Titanium Surfaces. Clin Orthop 2000;372:280-289.

[6] Overgaard L, Danielsen N, Bjursten LM. Anti-inflammatory properties of titanium in the joint environment. An experimental study in rats. J Bone Joint Surg Br 1998;80-B:888–893

[7] Sundgren JE, Bodo P, Lundstrom I. Auger electron spectroscopic studies of the interface between human tissue and implants of titanium and stainless steel. J Colloid Interface Sci 1986;110:9-20.

[8] Effah E, Bianco P, Ducheyne P. Crystal structure of the surface oxide layer on titanium and its changes arising from immersion. J Biomed Mater Res 1995;29:73-80.

[9] Healy K, Ducheyne P. Hydration and preferential molecular adsorption on titanium *in vitro*. Biomaterials 1992;13:553-561.

[10] Li P, Ducheyne P. Quasi-biological apatite film induced by titanium in simulated body fluid. J Biomed Mater Res 1998;41:341-348.

[11] Lauer G, Wiedmann-Al-Ahmad, Otten JE, Huber U, Schmelzeisen R, Schilli W. The titanium surface texture effects adherence and growth of human gingival Keratinocytes and human maxillar osteoblast-like cells *in vitro*. Biomaterials 2001;22:2799-2809

[12] Webster TJ, Ergun C, Doremus RH, Siegel RW and Bizios R. Enhanced functions of osteoblasts on nanophase ceramics. Biomaterials 2000;21:1803-1810.

[13] Colon G, Ward BC, Webster TJ. Increased osteoblast and decreased *Staphylococcus epidermidis* functions on nanophase ZnO and TiO_2. J Biomed Mater Res 2006;78A:595–604.

[14] Anselme K, Noel B, Hardouin P. Human osteoblast adhesion on titanium alloy, stainless steel, glass and plastic substrates with same surface topography. J Mater Sci: Mater Med 1999;10:815-819.

[15] Korovessis P. G., Deligianni D. D. Role of Surface Roughness of Titanium Versus Hydroxyapatite on Human Bone Marrow Cells Response. J Spinal Disord & Techniques 2002;15(2):175-183.

[16] Sauberlich, S, Klee D, Richter E-J, Hocker H, Spiekermann H. Cell culture tests for assessing the tolerance of soft tissue to variously modified titanium surfaces. Clin Oral Impl Res 1999;10:379-393

[17] MacDonald DE, Rapuano BE, Deo N, Stranick M, Somasundaran P, Boskey AL. Thermal and chemical modification of titanium-aluminum-vanadium implant materials: effects on surface properties, glycoprotein absorption, and MG63 cell attachment. Biomaterials 2004;25:3135-3146.

[18] Kern T, Yanf Y, Glover R, Ong JL. Effect of Heat-Treated Titanium Surfaces on Protein Absorption and Osteoblast Precursor Cell Initial Attachment, Implant Dentistry 2005;14(1):70-76.

[19] Metal-Organics for Materials, Polymers & Synthesis: A Survey of Properties and Chemistry, Arkles B, Larson G, editors. Gelest, Inc., Morrisville, PA, USA 2005.

[20] Podbielska H., Ulatowska-Jarza, A. Sol-gel technology for biomedical engineering. Bull Pol Ac:Tech 2005;53(3):261-271.

[21] Kim H-W, Kim H-E, Salih V, Knowles JC. Sol-gel modified titanium with hydroxpapatite thin films and effect on osteoblast-like cell responses. Journal of Biomedical Materials Research 74(3):294-305.

[22] Piveteau L-D, Gasser B, Shlabach L. Evaluating mechanical adhesion of sol-gel titanium dioxide coatings containing calcium phosphate for metal implant application. Biomaterials 2000;21:2193-2201.

[23] Nakazawa K, Lee S-W, Fukuda J, Yand D-H, Kunitake T. Hepatocyte spheroid formation on a titanium dioxide gel surface and hepatocyte long-term culture. J Mater Sci: Mater Med 2006;17:359-364.

[24] Garcia AJ. A centrifuge cell adhesion assay for high-throughput screening of biomaterial surfaces. J Biomed Mater Res 2003;67A:328-333.

[25] Garcia AJ, Gallant ND. Stick and Grip, Measurement Systems and Quantitative Analyses of Integrin-Mediated Cell adhesion Strength. Cell Biochemistry and Biophysics 2003;39:61-76.

[26] Hun TH. Microstructural evolutions and stress studies of titania films derived by "spin-deposition" methods. PhD Thesis, Brown University, Providence RI, USA 2006, p. 70-95.

[27] Wang C-C, Ying JY. Sol-Gel Synthesis and Hydrothermal Processing of Anatase and Rutile Titania Nanocrystals. Chem Mater 1999;11:3113-3120.

Chapter 3

Controlled release of vanadium from titanium oxide coatings for improved integration of soft tissue implants

John D. Jarrell [1]*, Brandon Dolly [1], Jeffrey R. Morgan [1]

[1] Department of Molecular Pharmacology, Physiology, and Biotechnology, and the Center for Biomedical Engineering, Brown University, Providence, RI, USA

(Submitted 13 October, 2007; Accepted March 27, 2008, J Biomed Mater Res A)

Abstract

This study evaluates the potential of titanium oxide coatings for short-term delivery of vanadium for improved wound healing around implants. Titanium and vanadium oxides are bioactive agents that elicit different bioresponses in cells, ranging from implant integration and reduction of inflammation to modulation of cell proliferation and morphology. These oxides were combined in biomaterial coatings using metal-organic precursors and rapidly screened in cell culture microplates to establish how vanadium loading influences cell proliferation and morphology. Twenty-eight day elution studies indicated that there was a controlled release of vanadium from stable titanium oxide matrices. Elution profiles were mathematically modeled for vanadium loading of 20% to 1.25% up to a period of 28 days. Scanning electron microscopy and energy dispersive spectroscopy of the coatings indicated that the vanadium was present as a nano-scale dispersion and not segregated micron-scale islands. The study confirmed that the observed bioresponse of cells was modulated by the soluble release of vanadium into the surrounding medium. Controlled release of vanadium from titania coatings may be used to influence soft tissue integration of implants by modulating cell proliferation, attachment, inflammation and wound healing dynamics.

Keywords: Metal ion release, Titanium oxide, Fibroblast, Bioactivity, Sol-gel techniques

3.1 Introduction

Percutaneous devices completely traverse the skin, which is the body's first line of defense against infection and dehydration. These implants may be simple catheters to complex osseointegrated percutaneous prosthetic attachments. Chronic inflammation, high occurrences of infection and poor soft tissue integration are common among this whole class of devices. To overcome these problems, new combination devices need to be developed that enable short-term controlled delivery of bioactive components from stable matrices to improve initial healing, prevent bacterial colonization and down regulate the inflammatory response to encourage a stable soft tissue seal. Metal oxides form a thin tenacious layer covering the surface of most medical grade metal alloy implants. This layer is responsible for the corrosion resistance of these materials as well as their biointegrative properties. Once considered inert, these oxides have roles in biological processes from protein and cell attachment to regulation of inflammation and mimicry of polypeptide hormone [1,2]. Metal oxide matrices alone and in combination with polymers hold promise for simultaneously modulating soft tissue integration around implants and delivering a combination of bioactive and antimicrobial components.

Titanium has been used successfully for bone implants and trans-epithelia devices for many years. Applications include joint replacements, dental implants, suturing staples and, more recently, bone anchored prosthetics [3]. Titanium's widespread use started with the discovery of osseointegration by Ingvar Branemark, who pioneered the metal's use for implants. Osseointegration involves direct anchorage of bone around titanium (and some other materials), without the growth of fibrous tissue at the interface. Titanium also works well with soft tissue implants. An oxide surface layer spontaneously forms on

titanium, protecting the metal from corrosion [4] and helping to deactivate the inflammatory response [5]. The oxide layer possesses the ability to dynamically adjust composition by incorporation of biological calcium, phosphorus and sulfur, dependent on physiological environment, which promotes adjacent tissue formation [6-13]. The titanium oxide layer acts to reduce localized reactive oxygen species that are released as part of the host foreign body response [14,15]. The localization of leukocytes around titanium metal implants declines rapidly compared to other biocompatible implant materials like austenitic stainless steel [16].

Vanadium is a transitional metal that readily forms oxides and salt compounds. To look at vanadium compounds simply in terms of being a toxic metal is an over simplification of this unique, bioactive and water soluble oxide. Early work with vanadium compounds indicated that they mimicked insulin in a synergetic fashion, with systemic anti-diabetic effects [17-19]. Other studies indicated that several vanadium compounds increased proliferation at low doses, but inhibited cell growth and spreading at higher concentrations [20-23]. Oral ingestion of vanadium oxides dissolved in drinking water has improved wound strength [24], promoted rapid and orderly collagen deposition during skin wound healing [25], and improved tendon and ligament repair [26,27]. Similar effects have been reported with local bolus injections of vanadium oxides dissolved in saline into subcutaneous sponges [28]. Vanadium compounds have been shown to provide cytoprotective action and promote cell recovery from ischemic and reperfusion induced heart injury [29], when delivered by infusion of vanadium doped saline. In contrast to these prior methods of delivery, we propose local and even systemic

controlled delivery of vanadium from a non-eroding solid state device suitable for long-term implantation.

In an earlier work, we presented a method for rapidly creating and assaying the bioresponse of cells to pure and doped metal organic derived titanium oxide based coatings [30]. These coatings had advantages over solid metal and powder metallurgy derived samples because they were formed from liquid precursors, rapidly formulated, readily create coatings, easily handled and relatively transparent, making them conducive to investigation using previously established biological assays for microplates. This present study, used titanium based xerogels with smooth surfaces to investigate the delivery of vanadium and the influence of vanadium loading on the bioresponse of normal human fibroblasts.

3.2 Materials and Methods

3.2.1 Materials

To make stock solutions of titania, one ml of titanium n-butoxide was diluted in 10 ml of toluene. To test the influence of vanadium alloying, 20% vanadium solutions were made consisting of 0.2 ml of vanadium oxytripropoxide added to the titanium stock solution. These solutions were used to create eight serial dilutions with vanadium precursor concentrations ranging from 20% to 0.156%. Metal alkoxides were obtained from Sigma-Aldrich Chemical Company, Allentown, PA.

3.2.2 Preparation of titanium coatings

For the biological assays, metal-organic coated polystyrene 96-well tissue culture microplates (Corning Costar) were prepared under a fume hood. Using an eight-channel pipette, 25 μl of each solution was pipetted into each well of a microplate column. After each filling, the plate was inverted and briefly shaken before applying solution to the next column of wells. Each column was coated with different solution chemistries. Non-alloyed titanium oxide xerogel and non-coated cell culture treated polystyrene were used as controls in each plate. The microplates were air-dried face up, without lids, under a chemical hood for 12 to 24 hours. Subsequently, they were heat treated in air on a hot plate (Dataplate, Barnstead/Thermolyte, Dubuque, IA) at 95 °C for one hour with the lids in place.

For the short term elution study, metal-organic coated 12-well microplates were prepared using a total of 50 μl of solution per well. Each column contained 20, 10, 5 or 1.25 % vanadium in a titanium n-butoxide stock solution. The solutions were dispensed in two 25 μl doses per well with one minute of air-drying between doses. The microplates were air-dried face up, without lids, under a chemical hood for 12 to 24 hours. Subsequently, they were heat treated in air on a hot plate at 95 °C for one hour with the lids in place.

3.2.3 Scanning electron microscopy

A LEO 1530 Thermally-Assisted Field Emission (TFE) Scanning Electron Microscope (SEM) was used to establish surface morphology of the coatings. Samples were carbon sputter coated to overcome the inherent insulating properties of the metal oxide sol-gels.

A working distance of 3 to 5 mm and accelerating voltage of 5.00 kV was used to collect electron images at various magnifications between 200 X and 100,000 X.

3.2.4 Cell proliferation and cell viability assays

Human dermal fibroblasts were derived from neonatal foreskins, obtained at the Women & Infants Hospital of Rhode Island, Providence, RI, USA (approved by the Institutional Review Board and in adherence to Declaration of Helsinki Guidelines) as previously described [30]. Fibroblasts were harvested with a 0.05% trypsin/0.53 mM EDTA solution and subcultured to near confluence in Human Fibroblast Medium (HFM) consisting of DMEM containing high glucose, L-glutamine, pyruvate and pyridoxine hydrochloride (Invitrogen Corporation, Carlsbad, CA) with additions of 10% fetal bovine serum and 1% penicillin-streptomycin. Cells were detached using 0.05% trypsin/0.53 mM EDTA for 3 minutes and re-suspended in serum containing medium. The cells were seeded onto 96 well microplates at a density of 5,000 cells per well in 100 μl of HFM.

To measure cell proliferation, the microplates were incubated at 37 °C with 10 % CO_2 for 48 hours, after which 10 μl of WST-1 (Roche Applied Science, Indianapolis, IN) was added into each well and incubated for 3 hours at 37 °C. The optical density within each well, resulting from the cellular metabolism of the tetrazolium salt (WST-1), was quantified using a microplate reader for absorbance at 440 nm (SPECTRAmax® PLUS 384 Microplate Spectrometer with SOFTmax PRO software, Molecular Devices Corporation, Sunnyvale, CA) and plotted. Five replicates with three cell-free controls were used for each coating type and the polystyrene plate bottom. Plates were also inspected under optical microscopy for cell spreading and morphology. Calibration

curves were previously established for cell number versus optical density on polystyrene. Seeding density for the cell type was chosen within the linear portion of the calibration curve.

To measure cell number and viability, human fibroblasts were seeded onto 96 well microplates at a density of 5,000 cells per well in 100 μl of HFM and incubated at 37 °C with 10 % CO_2. After 24 hours, cells were rinsed with phosphate buffered saline with 100 mg of CaCl and 100 mg MgCl+6H_2O per liter added (complete PBS) (Invitrogen Corporation, Carlsbad, CA) and incubated in 100 μl of 1 μg/ml calcein-AM (Molecular Probes, Inc., Eugene, OR) in complete PBS with 2 mM dextrose for 30 minutes at 22 °C.

Plates were read using a fluorescent microplate reader (SPECTRAmax® GEMINI XS Dual-Scanning Microplate Spectrofluorometer with SOFTmax PRO software, Molecular Devices Corporation, Sunnyvale, CA) set to 485 nm excitation, 535 nm emission. Five replicates with three cell-free controls were used for each coating type and the polystyrene plate bottom. Calibration curves were previously established for cell number versus fluorescence on polystyrene and used to select a seeding density within the linear portion of the calibration curve. Cells were subsequently observed for cell spreading and morphology using optical and fluorescent microscopy.

3.2.5 Combined cell attachment and cell adhesion assay

To characterize the initial cell attachment (seeding efficiency) and cell adhesion, a modification of a previous reported method [31,32] was used. Normal human fibroblasts were grown in 500 cm^2 triple flasks to near-confluence using HFM. The cells were rinsed with complete PBS and incubated in 45 ml of 1 μg/ml calcein-AM in complete PBS with

2 mM dextrose for 30 minutes at 22 °C. Cells were detached using 0.05% trypsin and 0.53 mM EDTA for 3 minutes and re-suspended in serum containing medium. Cells were centrifuged at 500 rpm for 5 minutes and re-suspended in PBS dextrose, centrifuged again and re-suspended in PBS dextrose. The cells were then seeded onto microplates at a density of 10,000 cells per well and left to attach for one hour at 22 °C. Calibration curves were previously established for cell number versus fluorescence on polystyrene and used to select a seeding density within the linear portion of the calibration curve and to maximize the signal to noise response of the plate reader.

Each well was completely filled with PBS-dextrose and the baseline fluorescence read (485 nm excitation, 535 nm emission). The wells were emptied by inversion to remove floating cells and refilled with PBS-dextrose and fluorescence read, a second time. The microplate was covered with sealing tape (Corning Costar) and centrifuged upside down in a Centra-GP8R Refrigerated Centrifuge (Thermo Electron Corporation, Waltham, MA) using microplate buckets at 800 rpm for 5 minutes. The microplates were again inverted to empty and refilled with PBS-dextrose and read a third time. The first and second readings were compared to determine the fraction of cells that attached to the microplate 1 hour after seeding. This corresponds to the one hour cell seeding efficiency. The post-centrifuge fluorescence (third) reading was compared to the pre-centrifuge (second) reading to determine the fraction of attached cells that remained adherent after exposure to normal forces from centrifugation. Together, these assays identify how readily cells attach to a surface (seeding efficiency) and quantify the strength of adhesion (adherent fraction). The rpm of the centrifuge was selected to remove approximately 50%

of the cells from the tissue culture treated polystyrene. Five replicates with three cell-free controls were used for each coating type and the polystyrene microplate bottom.

3.2.6 Surface verses soluble assay

To determine whether surface or soluble factors were responsible for vanadium's influence on cell proliferation and morphology, a two part assay was performed. For the first part, 100 µl of HFM was added per microplate well and allowed to soak on coatings and PS controls for 24 hours at 37 °C with 10 % CO_2. 90 µl of this conditioned medium was subsequently transferred from each well to a new uncoated microplate. Human fibroblasts were added to this conditioned medium at a density of 5,000 cells per well in 10 µl of additional HFM, for a total of 100 µl of solution per well. The plate was incubated at 37 °C with 10 % CO_2. After 48 hours, 100 µl of medium solution was removed from eight replicate wells for each coating type (0.8 ml total) and stored in 15 ml centrifuge vials for elemental analysis. The cells in the microplates were rinsed with complete PBS and incubated in 100 µl of 1 µg/ml calcein-AM in complete PBS with 2 mM dextrose for 30 minutes at 22 °C. Plates were read using a fluorescent microplate set to 485 nm excitation, 535 nm emission. Five replicates with three cell-free controls were used for each coating type and the polystyrene plate bottom. Cells were subsequently observed for cell spreading and morphology using optical microscopy.

The second part of the assay was to seed 5,000 human fibroblasts per well in 100 µl of HFM onto the coated plates that were previously conditioned with culture medium. The plate was incubated at 37 °C with 10 % CO_2. After 48 hours, 0.8 ml of medium solution was removed from the wells of each coating type and stored in 15 ml centrifuge vials for

elemental analysis. The cells in the microplates were rinsed with complete PBS and incubated in 100 μl of 1 μg/ml calcein-AM in complete PBS with 2 mM dextrose for 30 minutes at 22 °C. Plates were read using a fluorescent microplate set to 485 nm excitation, 535 nm emission. Five replicates with three cell-free controls were used for each coating type and the polystyrene plate bottom. Cells were subsequently observed for cell spreading and morphology using optical microscopy. The results for the cells grown in conditioned medium on a new polystyrene microplate were compared with those grown in fresh medium on the coatings previously subject to medium conditioning.

Inductively Coupled Plasma (ICP) Spectrometry elemental analysis (performed by ESS Laboratory, Cranston, Rhode Island) was used to determine the concentration of vanadium that was eluted into the medium from each coating type at the 24 and 72 hour time points. 10 ml of deionized water was added to 0.8 ml of medium conditioned by each coating and run straight from the collection vials without digestion. Results were reported down to two times the detection limits of the equipment for both titanium (0.004 ppm) and vanadium (0.002 ppm). The results for vanadium were converted to units of micromolar in medium for comparison to earlier published work.

3.2.7 Short-term vanadium release

To better characterize the short-term delivery of vanadium from titanium xerogel matrices, metal-organic coated 12-well plates were prepared as described above and filled with 1 ml of PBS per well, covered with one or two layers of sealing tape (Corning Costar), and placed in a heated orbital shaker (ThermoForma Model 420, Marrietta, Ohio) set to 90 rpm and 37 °C. At each time point, (0.25, 1.3, 4, 7, 14 and 28 days), the

PBS was removed from each well and added to separate 15ml centrifuge vials and refilled with fresh PBS. To each vial was added 10 ml of triple deionized water to allow for ICP elemental analysis for vanadium and titanium. Four replicates of each coating were used. Pure titanium oxide and non-coated polystyrene were used for controls. The results for vanadium elution were reported as mg/L and converted to percentage of total initial vanadium in coatings and micrograms vanadium released per surface area. Results of the short-term elution study were plotted and trend lines fitted using SigmaPlot 8.0 (Systat Software Inc., San Jose, California, USA), which facilitated mathematical modeling of vanadium release as a function of time and initial vanadium concentration. After the elution study, the surfaces were inspected using SEM in conjunction with energy dispersive spectroscopy (EDS).

3.3 Results

In order to explore solid state release of vanadium, we created a series of vanadium loaded titanium oxide xerogel coatings and characterized the surface using scanning electron microscopy in conjunction with energy dispersive spectroscopy. This approach was followed by identifying the bioresponse of human fibroblasts to the same vanadium loaded coatings. The biological results were related to vanadium release in a short-term elution study. Finally a short-term controlled release study is presented with mathematical modeling of controlled release for loading levels between 1.25% and 20% vanadium to titanium precursor.

3.3.1 Surface characterization

To determine the surface appearance and morphology of the coatings, polystyrene microplates coated with various sol-gel applied TiO_2 compositions were analyzed under the SEM. Fig. 3.1 presents SEM images of representative coatings with 20% vanadium, 10% vanadium and pure titanium oxide xerogel. Images in the right column were taken at 10,000 X magnification, while those on the right were taken at 100,000 X. Coatings were tenacious and generally smooth. Some areas had collapsed micro and nano pores that left a smooth dimpled surface (Fig. 3.1, 20% V and 10%V). Others areas showed stress relief features and superficial micro-cracking (Fig. 3.1. Titania), especially away from the central region of the microplate wells.

3.3.2 Cell proliferation and viability on coatings

To quantify fibroblast proliferation 48 hours after cell seeding, a WST-1 colorimetric assay was used. Fig. 3.2 (top) presents a graph of the optical density as a function of vanadium concentration, for five replicates of each coating and polystyrene (PS). There were statistically significant differences (paired t-test) between the proliferation results of the non-doped and vanadium doped coatings (0.31, 0.62, 5, 10, 20%V ($p<0.001$); 1.25, 2.5%V, ($p<0.05$)), except for 0.15%V ($p= 0.06$). Initial additions of vanadium slightly increased cell proliferation until a threshold was reached. Cell proliferation dropped steeply with vanadium concentrations higher than 1.25% and leveled off for concentrations of 10% and 20%.

Calcein AM was used to determine the number and viability of cells 24 hours after seeding. Cell viability, as measured by calcein fluorescence, was recorded for five replicates of each coating chemistry (Fig. 3.2, bottom). There were statistically

significant differences (paired t-test) between viability results of the non-doped and all vanadium doped coatings (0.15, 0.31, 0.62, 1.25%V ($p<0.05$); 2.5, 5, 10, 20%V ($p<0.001$)). Cell number and viability was consistent for vanadium concentrations from 0% to 1.25%, but dropped off sharply for higher concentrations and leveled at 10% and 20%.

Fluorescent microscopy was used to observe cell morphology on the coatings (Fig. 3.3). Cells were well spread on uncoated polystyrene, titanium and the lower vanadium coatings (0% to 1.25%). At 5% vanadium cell morphology became slightly less spread, with cell rounding clearly observable on 10% and 20% coatings.

3.3.3 Cell attachment and cell adhesion

To determine the efficiency of initial cell attachment (one hour after seeding) and cell adhesion under load, a modified centrifugation cell adhesion assay was used to further define the bioresponse to vanadium containing coatings (Fig. 3.4). The cell attachment after one hour of seeding ranged from 66 to 90% for the coatings as represented by the circles in Fig. 3.4. Of these attached cells, 30 to 51% of them remained adherent to the coatings after centrifugation as represented by the squares in Fig. 3.4. Small additions of vanadium slightly improved initial attachment, while larger additions caused a slight decrease in attachment. Centrifugation adherence was less influenced by initial vanadium additions, but doping over 5 % caused a slight reduction in adherence. Little variation was observed between the lower concentration vanadium coatings and tissue culture treated polystyrene, indicating that these coatings supported good initial cell attachment and good cell adhesion strength.

3.3.4 Surfaces verses soluble effects

To determine if vanadium in the coatings mediates its biological effect by release from the titanium, culture medium was added to the coated microplate wells, incubated for 24 hours, removed and added to new polystyrene microplates (Fig. 3.5). Calcein loaded cells were added to this conditioned medium, allowed to attach for 24 hours and fluorescence measured. The level of vanadium in each of the conditioned medium samples was also determined by elemental analysis. The level of titanium in the medium was below the detection limit of the equipment for all the samples (0.002 ppm). Increasing concentration of vanadium in the coatings resulted in increased concentration of soluble vanadium in the conditioned medium samples. Similar to the results obtained in Fig. 3.2, low concentrations of vanadium improved cellular viability and number in the medium conditioned by coatings when compared to the control titanium coating without vanadium. As vanadium concentration increased in the conditioned medium, cell number also declined to levels below the titanium control. Fluorescence microscopy confirmed a decrease in cell number and spreading at the high vanadium concentrations. These results indicate that a significant part of the bioresponse to the coatings is due to the release of soluble vanadium and that these coatings are acting as a drug delivery device.

To determine if the original coatings that had been conditioned with medium were still bioactive and releasing vanadium, calcein loaded cells in fresh medium were added to the treated microplate, the cells allowed to attach and fluorescence determined after 24 hours (Fig. 3.6, top). The culture medium in these plates was removed after 24 hours of incubation and the level of released vanadium measured by elemental analysis (Fig. 3.6,

bottom). Coatings previously treated with medium continued to influence cell number and proliferation in a concentration dependent manner and the elemental analysis indicated that the coatings were still delivering vanadium into the growth medium. The coatings subject to 24 hour conditioning with medium continued to elute vanadium over the next 48 hours, but at a lower rate.

From the elemental analysis we compared the concentration of vanadium released into the medium from each coating after 24 hours and an additional 48 hours and plotted it as a function of initial vanadium loading (Fig. 3.7). There was a linear relationship between initial vanadium loading and release for all concentrations of vanadium between 20% and 0.156%, with an R^2 fit of 0.999 for the first 24 hours and 0.998 for the next 48 hour period.

3.3.5 Short-term release of vanadium

To characterize the short-term release of vanadium from titanium xerogel matrices, a 28 day elution study was performed (Fig. 3.8). Controlled release of vanadium occurred over 28 days for the four vanadium concentrations tested (20, 10, 5, 1.25%). The top plot of Fig. 3.8 presents the percentage of total vanadium loading released as a function of time, while the bottom plot gives the cumulative release rates per coating surface area. Increased loading with vanadium resulted in both a higher delivery rate and higher fraction of total vanadium delivery. These results are consistent with those typically found in drug delivery from non-erodible matrices. The concentration of titanium eluted in the medium was below the reporting limit (< 0.004 ppm).

3.3.6 Mathematical modeling of vanadium release

The short-term elution of vanadium from each of the four vanadium containing coatings was fitted with simple hyperbolic trend lines with R^2 values of 0.942 or better, for all four data sets after the form: $f(t,V) = \frac{a(V)t}{b(V)+t}$. The relationship between the initial vanadium concentration and the coefficient of the hyperbolic solution, a(*V*) and b(*V*), were fit to quadratic and cubic polynomial functions with perfect or near perfect R^2 fits.

The combined hyperbolic and polynomial functions for vanadium elution from doped titania xerogels are given below:

$$\mathrm{VE\%(t,V)} = \frac{(1.9265 + 0.2672V + 0.0117V^2)t}{6.7768 - 1.1195V + 0.1350V^2 - 0.0045V^3 + t}$$

$$\mathrm{VEa(t,V)} = \frac{(0.1833 - 0.0347V + 0.0314V^2)t}{6.7768 - 1.1195V + 0.1350V^2 - 0.0045V^3 + t}$$

Where VE%(t,V) is the cumulative total percentage of initial vanadium load eluted, while VEa(t,V) is the cumulative vanadium eluted per unit surface area ($\mu g/cm^2$), V is the solution percentage of vanadium tri isopropoxide oxide in titanium n-butoxide and *t* is time in days. These functions fit well the region between 0 and 28 days for all concentrations of vanadium between 1.25 to 20%. Future testing would be required to determine suitability of models for time points and vanadium concentrations outside of these limits.

3.3.7 Post-elution surface analysis

To observe the influence of vanadium elution on the surface topography of the coatings, SEM images were taken at the end of the study at 10,000 X and 100,000 X magnifications. There was no observable porosity in the coatings at the lower magnification and only the slightest perceivable roughing at the nano level in the high magnification images (data not shown) when compared to the coatings before elution. If the vanadium were present in micron-sized islands, then observable micron-scale porous features would be expected from vanadium leaching. This suggests that the vanadium was finely dispersed throughout the coatings at a submicron level. EDS elemental mapping of coatings before elution (data not shown), confirmed that vanadium dispersion was submicron in size.

3.4 Discussion

Many studies have investigated the influence of vanadium containing solutions on cellular function *in vitro* as well as on insulin mimicry and wound healing in animal models [17-22, 24-29]. This study however is a step toward the creation of solid vanadium eluting devices that provide controlled and selectable delivery from a non-erodible matrix. The selection of titanium oxide as the matrix material makes these coatings suitable to long-term or permanent implants, which possess the tissue integrative and anti-inflammatory properties inherent to titanium. Titanium oxides have been recently considered as matrices for the delivery of antimicrobial ions [33].

Cell proliferation data show that the concentration of vanadium in the coatings can be used to control the bioresponse of fibroblasts in a dose dependent way both in terms of

cell proliferation and in cell viability. The low concentration part of the curve shows that vanadium can stimulate the proliferation of cells even to levels beyond the proliferation seen for standard polystyrene plates. In contrast, as the concentration of vanadium in the coatings is increased, both cell proliferation and cell viability decline in a dose dependent manner (Fig. 3.2). Thus, depending on the concentration of vanadium in the coating chosen, it's possible to obtain a bioresponse where cell proliferation/viability is stimulated or inhibited. These data are similar to those where soluble vanadium was added to Swiss 3T3 fibroblast cells and it was shown that low doses stimulated proliferation and increasing doses inhibited proliferation (22). Depending on the application of the implant, vanadium containing coatings could be designed to elicit the desired bioresponse *in vivo*.

The general shape of the release profiles and modeling are typical of diffusion processes from nonerodible matrices. The release data indicate that vanadium is preferentially eluted from the stable titanium oxide matrices without the initial "burst" phase seen in biodegradable polymer devices. This is explained by the natural solubility of vanadium oxide in water compared to the insolubility of titanium oxide and the uniform, submicron mixing of elements indicated by SEM/EDS surface analysis. Avoiding bolus-like initial release can be advantageous for delivery of expensive agents or where the therapeutic window and desired dose response is narrow.

Solid state vanadium delivery from an implant presents an alternative to oral systemic delivery of vanadium compounds for the treatment of diabetes. Vanadium has shown early promise for the treatment of diabetes [34], but the high systemic doses required were both difficult to palate and the source of gastric disturbances. To avoid these and

other adverse side effects, transdermal routes of delivery have been investigated with less toxic, but orally unavailable forms, such as peroxovanadium compounds [35,36]. Vanadium eluting titanium oxide biomaterials may also avoid the oral route and allow for either systemic or localized delivery of insulin mimicking compounds to diabetic patients.

3.5 Conclusions

This study demonstrates that titania coatings doped with vanadium can function as a vanadium delivery device. Predictable vanadium delivery from a non-erodible titania matrix occurred for at least 28 days and the level of vanadium released was easily controlled by varying the concentration of vanadium in the coatings. Measuring the bioresponse to these coatings revealed that low doses of vanadium stimulated cell proliferation, whereas higher doses inhibited cell proliferation. These metal-organic matrices successfully delivered metal-based compounds that modulated human cellular responses in a fashion similar to drug delivery. This opens the door for the creation of hybrid materials that use mixed metal oxides to control cell attachment, proliferation, extracellular matrix formation and tissue ingrowth from integrated biomaterial systems. These systems can promote initial wound healing with transitional vanadium delivery from materials suitable for permanent implantation. This may be especially beneficial to applications involving diabetic patients and soft tissue healing or percutaneous devices.

Acknowledgements

Funded, in part, by VA Rehabilitation Research and Development Center for Restorative and Regenerative Medicine, Department of Veterans Affairs, Providence, Rhode Island.

3.6 Figures

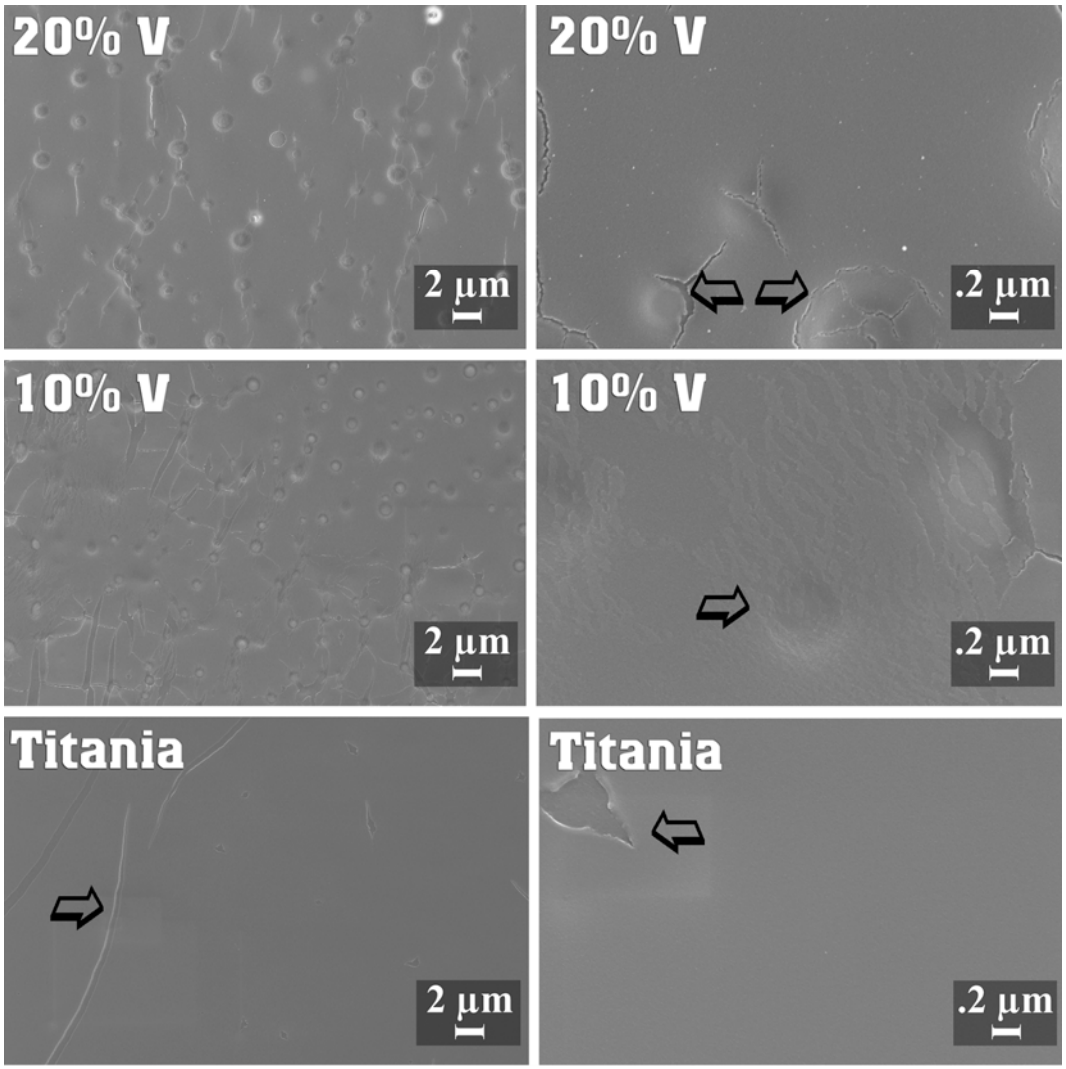

Fig. 3.1: Titanium coatings were generally smooth under scanning electron microscopy (SEM). Representative images of titanium n-butoxide xerogel coatings with 20%, 10% and 0% vanadium doping at medium and high magnifications. Arrows point to collapsed dimples and superficial stress relief features.

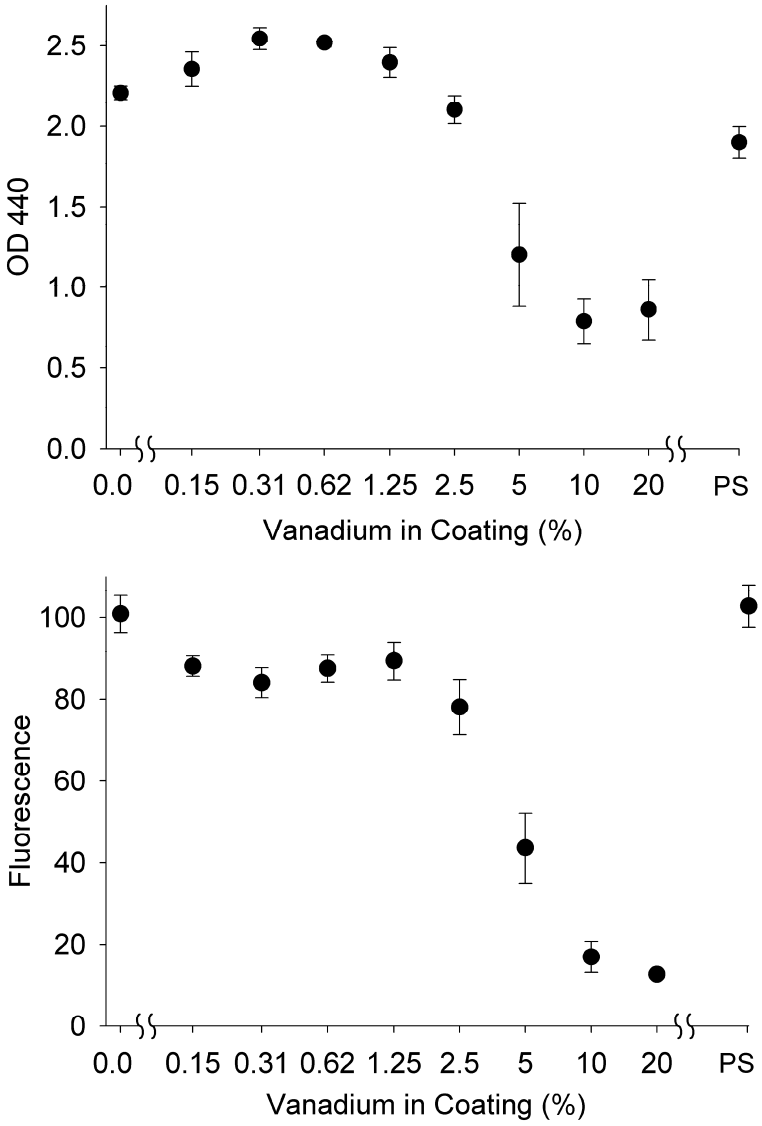

Fig. 3.2: Fibroblast proliferation (top) and viability (bottom) is influenced by vanadium loading. Top plot presents a graph of the optical density at 440 nm produced by WST-1 proliferation assay as a function of vanadium in coatings, 48 hours after seeding. Bottom plot presents cell viability as fluorescent calcein loading as a function of vanadium concentration in coatings, 24 hours after seeding.

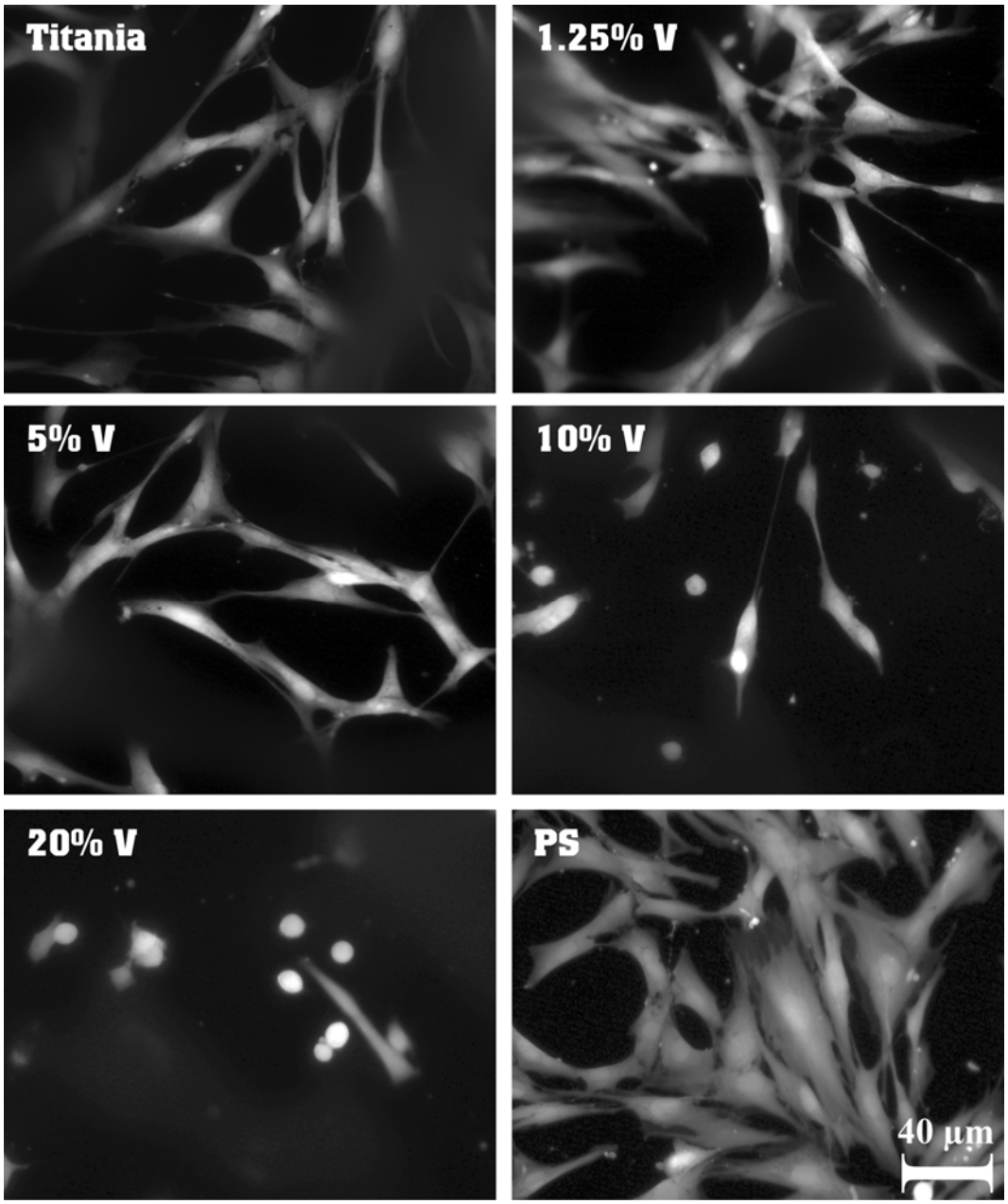

Fig. 3.3: Vanadium loading influences cell morphology and spreading. Representative fluorescent images of calcein loaded human fibroblasts 24 hours after seeding onto titanium n-butoxide xerogel (titania), xerogel with 1.25% vanadium (1.25% V), 5% vanadium (5% V), 10% vanadium (10% V), 20% vanadium (20% V) and tissue culture treated polystyrene (PS). Scale bar is 40 μm.

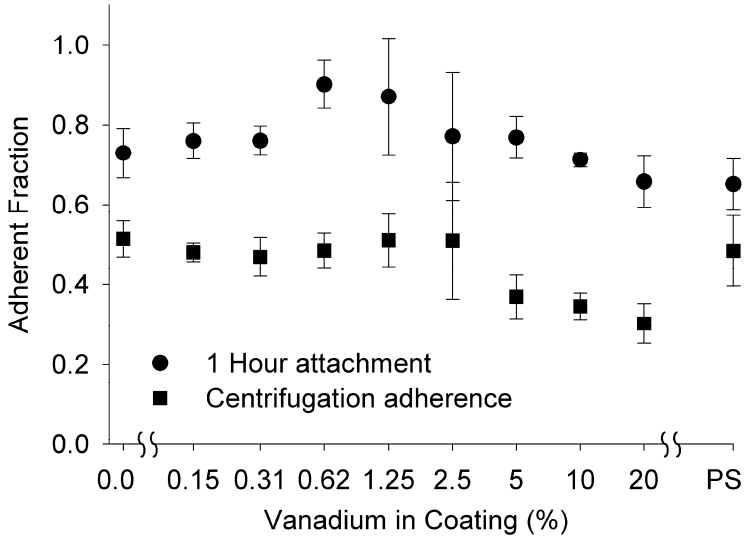

Fig. 3.4: Vanadium loading has a minor influence on initial cell attachment and adherence. The cell attachment of calcein loaded cells one hour after seeding ranged from 66 to 90% for the vanadium loaded coatings as represented by the circles. Of these attached cells, 30 to 51% of them remained adherent to the coatings after subsequent exposure to 800 rpm centrifugation as represented by the squares.

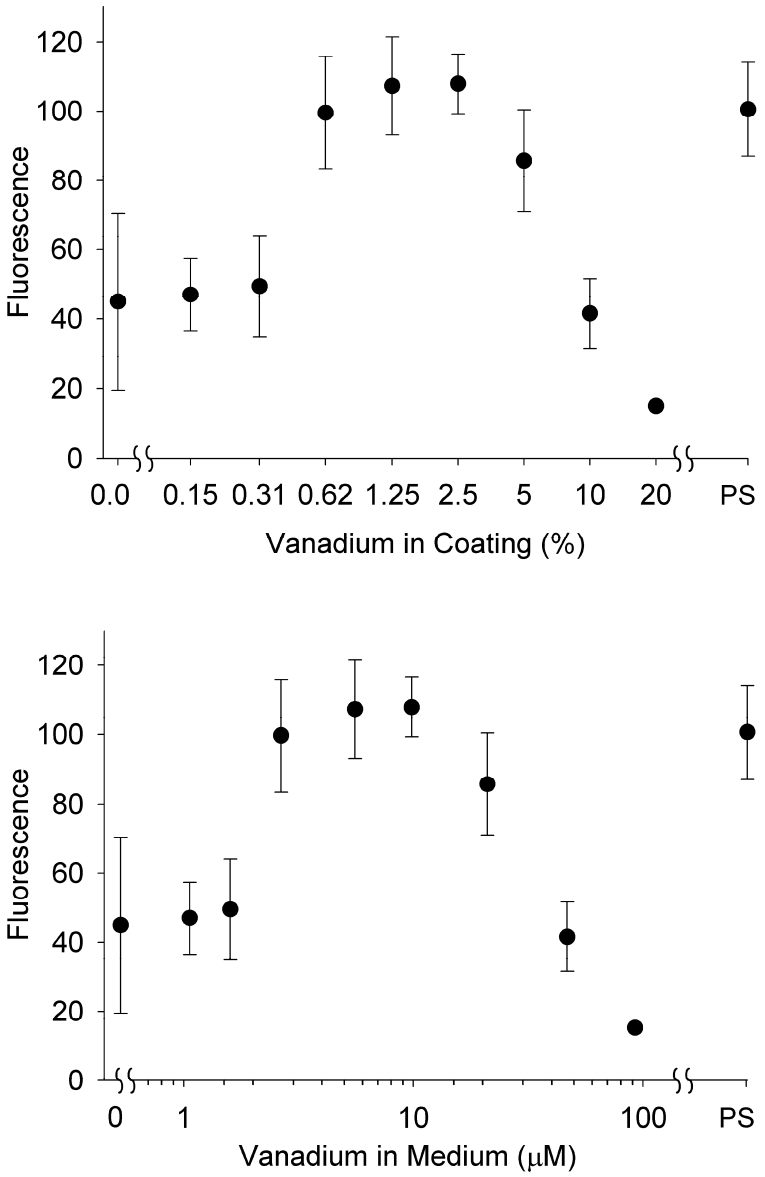

Fig. 3.5: Cell growth on new polystyrene plates in coating conditioned media was influenced by initial vanadium concentration. Fluorescence of calcein loaded cells grown on new PS plate (in coating conditioned media) as a function of initial vanadium loading is presented in the top plot. The dose response of cell growth was directly related to the vanadium concentration released into the media as determined by ICP elemental analysis (bottom). This indicated that proliferative and morphological changes of cells were mainly due to release of vanadium into the media and not surface bound vanadium.

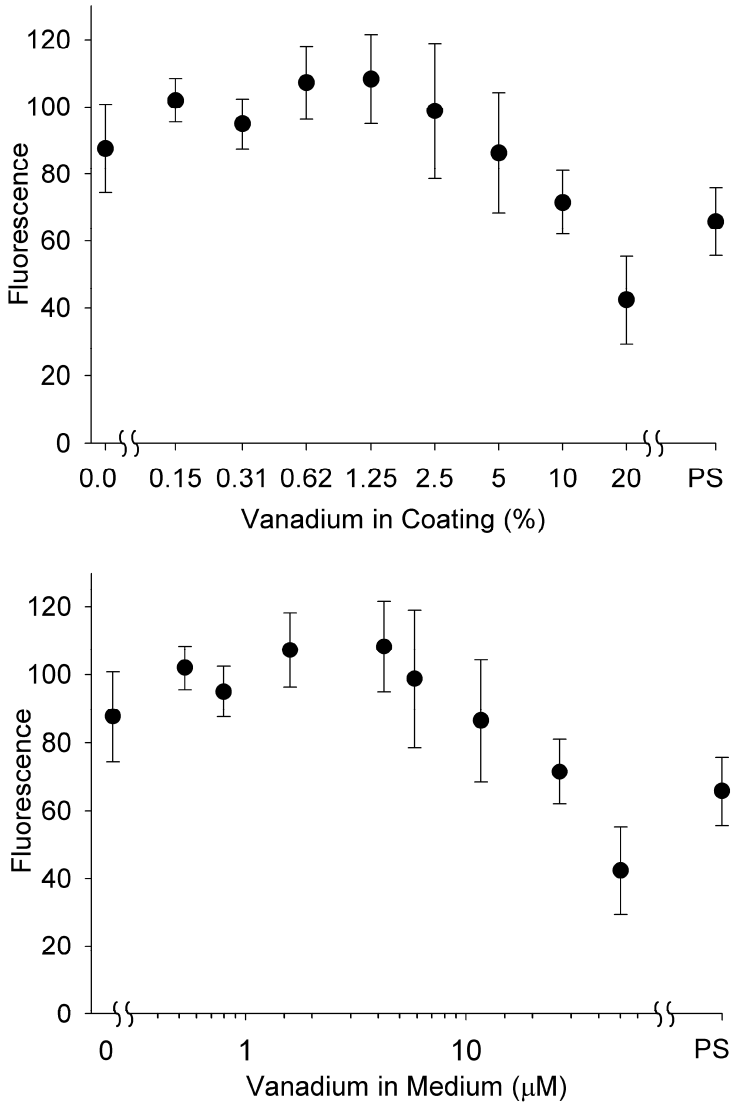

Fig. 3.6: Vanadium in coatings continues to influence cell growth after initial extraction by culture medium. Coatings previously used to condition medium continued to influence cell number and proliferation in a manner dependent on initial vanadium concentration (top). This continued to be directly related to the amount of vanadium delivered into the medium (bottom).

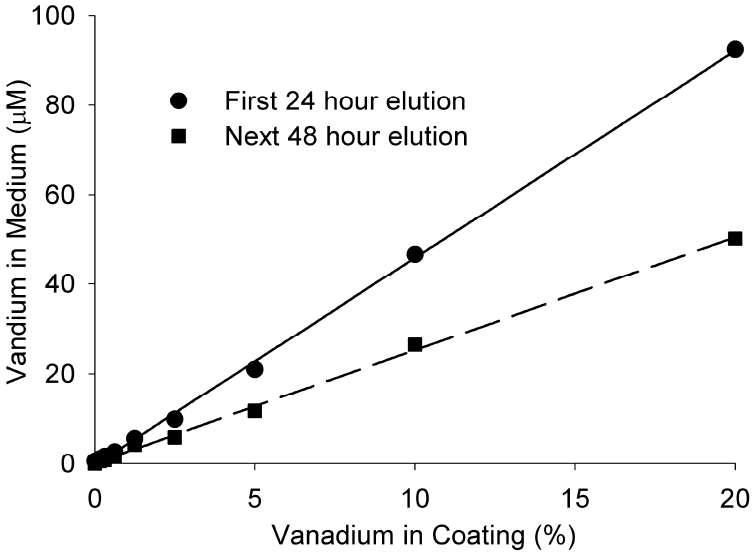

Fig. 3.7: There is a linear relationship between initial vanadium loading and vanadium release for all concentrations between 20% and 0.156%. The plots present the total vanadium eluted into the medium for each of the eight serial dilutions after 24 hours and after an additional 48 hours. These plots indicate a linear relationship ($R^2 > 0.99$) between coating loading and elution of vanadium for all the vanadium compositions tested during the first 72 hours.

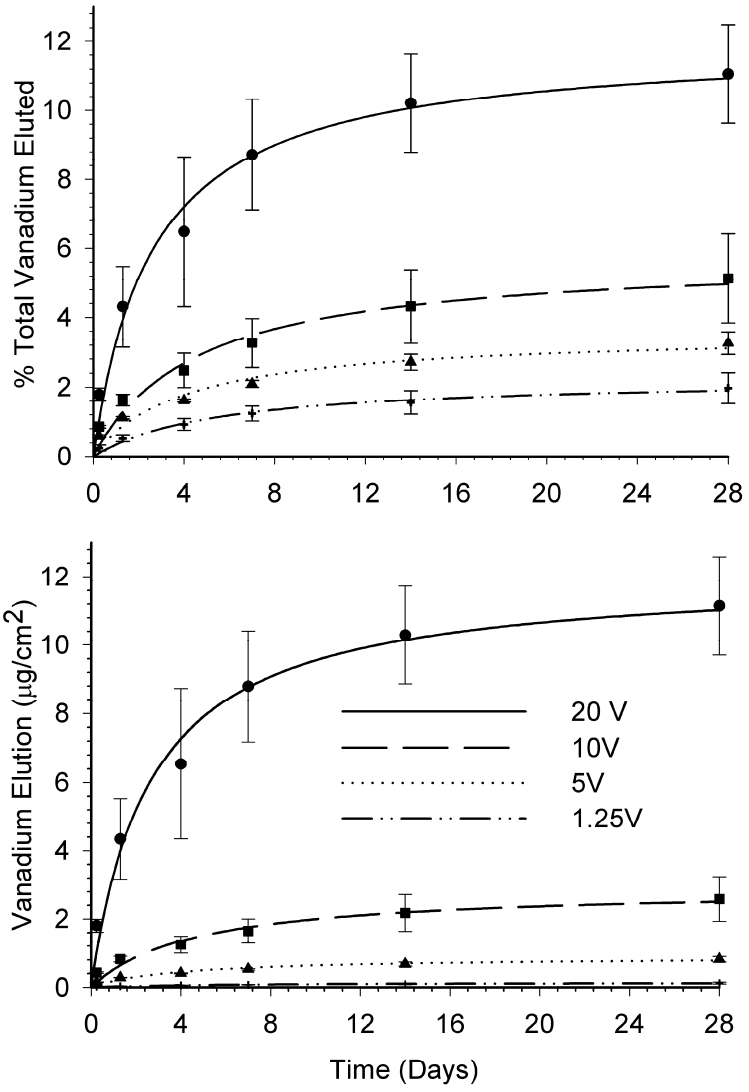

Fig. 3.8: Vanadium delivery for titanium based coatings is long term. The top plot presents the percentage of total vanadium loading released as a function of time, while the bottom plot gives the cumulative release rates per coating surface area over a period of 28 days for four different vanadium concentrations (20, 10, 5, 1.25%).

3.7 References

[1] Kasemo B, Gold J. Implant surfaces and interface processes. Adv Dent Res (13) June (1999) 8-20.

[2] Guo Z, Sadler PJ. Reviews: Metals in Medicine. Angew. Chem. Int. Ed. 38 (1999) 1512 – 1531.

[3] Branemark R, Branemark P-I, Rydevik B, Myers R. Osseointegration in skeletal reconstruction and rehabilitation: A review. JRRD March/April 2001;3(2):175-181.

[4] Jacobs JJ, Cilbert JL, Urban RM. Current concepts review. Corrosion of metal orthopaedic implants. J. Bone Joint Surg. Am. 80 (10) (1998) 1554.

[5] Overgaard L, Danielsen N, Bjursten LM. Anti-inflammatory properties of titanium in the joint environment. An experimental study in rats. J Bone Joint Surg Br 1998;80-B:888–893.

[6] Kasemo B**,** Lausmaa J. Material-tissue interfaces: the role of surface properties and processes. Environ Health Perspect 1994;102(Suppl 5):41-55.

[7] Bjursten LM. The bone-implant interface in osseointegration, in: B. Rydevik, P.I. Branemark, R. Skalak (Eds.), International Workshop on Osseointegration in Skeletal Reconstruction and Joint Replacement. The Institute for Applied Biotechnology, Goeborg, Sweden, 1991, pp. 25-31.

[8] Puleo DA, Nanci A. Understanding and controlling the bone-implant interface. Biomaterials 20 (23-24) (1999) 2311-2321.

[9] Brunski JB, Puleo DA, Nanci A. Biomaterials and biomechanics of oral and maxillofacial implants: current status and future developments. Int. J. Oral Maxillofac. Implants, 15 (1) (2000) 15-46.

[10] Sundgren JE, Bodo P, Lundstrom I. Auger electron spectroscopic studies of the interface between human tissue and implants of titanium and stainless steel. J. Colloid Interface Sci. 110 (1) (1986) 9-20.

[11] Effah EA, Bianco PD, Ducheyne P. Crystal structure of the surface oxide layer on titanium and its changes arising from immersion. J. Biomed. Mater. Res. 29 (1) (1995) 73-80.

[12] Healy KE, Ducheyne P. Hydration and preferential molecular adsorption on titanium *in vitro*. Biomaterials 13 (8) (1992) 553-561.

[13] Li P, Ducheyne P. Quasi-biological apatite film induced by titanium in simulated body fluid. J. Biomed. Mater. Res. 41 (3) (1998) 341-348.

[14] Suzuki R, Muyco J, McKittrick J, Frangos JA. Reactive oxygen species inhibited by titanium oxide coatings. J. Biomed. Mater. Res. 66 (2) (2003) 396–402.

[15] Suzuki R, Frangos JA. Inhibition of inflammatory species by titanium surfaces. Clin. Orthop. Relat. Res. 372 (2000) 280-289.

[16] Kraft CN, Hansis M, Aren S, Menger MD, Vollmar B. Striated muscle microvascular response to silver implants: A comparative *in vivo* study with titanium and stainless steel. J Biomed. Mater. Res. 49 (2) (2000) 192-199.

[17] Garcia-Vicente S, Yraola F, Marti L, Gonzalez-Munoz E, Garcia-Barrado MJ, Canto C, Abella A, Bour S, Artuch R, Sierra C, Brandi N, Carpene C, Moratinaos J, Camps M, Palacin M, Testar X, Guma A, Albericio F, Royo M, Mian A, Zorzano A. Oral insulin-mimetic compounds that act independently of insulin. Diabetes 56 (2) (2007) 486-493.

[18] Shechter Y. Insulin-mimetic effects of vanadate. Possible implications for future treatment of diabetes. Diabetes 39 (1) (1999) 1-5.

[19] Srivastava AK. Anti-diabetic and toxic effects of vanadium compounds. Mol. Cell. Biochem. 206 (1-2) (2000) 177-182.

[20] Yamamoto A, Honma R, Sumita M. Cytotoxicity evaluation of 43 metal salts using murine fibroblasts and osteoblastic cells. J. Biomed. Mater. Res. 39 (2) (1998) 331-340.

[21] Huang C, Zhang Z, Ding M, Li J, Ye J, Leonard SS, Shen HM, Butterworth L, Lu Y, Coasta M, Rojanasakul Y, Castranova V, Vallyathan V, Shi X. Vanadate Induces p53 transactivation through hydrogen peroxide and causes apoptosis. J. Biol. Chem. 275 (42) (2000) 32516-32522.

[22] Cortizo AM, Salice VC, Vescina CM, Etcheverry SB. Proliferative and morphological changes induced by vanadium compounds on Swiss 3T3 fibroblasts, BioMetals 10 (2) (1997) 127-133.

[23] Jarrell JD, Eun TH, Samale M, Briant C, Sheldon B, Morgan JR. Use of specialized metal oxide films for delivery of bioactive metal compounds. Orthopaedic Research Society 2007 Annual Meeting, February 2007;32:1590.

[24] Ehrlich HP, Keefer KA, Maish GO, Myers RL, Mackay DR. Vanadate ingestion increases the gain in wound breaking strength and leads to better organized collagen fibers in rats during healing. Plast. Reconstr. Surg. 107 (2) (2001) 471-477.

[25] Ehrlich HP, Keefer KA, Myers RL, Passaniti A. Vanadate and the absence of myofibroblasts in wound contraction. Arch. Surg. 134 (5) (1999) 494-501.

[26] Moyer KE, Saba AA, Hauck RM, Ehrlich HP. Systemic vanadate ingestion modulates rat tendon repair. Exp. Mol. Pathol. 75 (1) (2003) 80-88.

[27] Chen J, Iosifidis M, Zhu J, Tatarintsev I, Wang JH. Vanadate ingestion enhances the organization and collagen fibril diameter of rat healing medical collateral ligaments. Knee Surg. Sports Traumatol. Arthrosc. 14 (8) (2006) 750-755.

[28] Mackay DJ, Moyer KE, Saggers GC, Myers RL, Mackay DR, Ehrlich HP. Topical vanadate optimizes collagen organization within granulation tissue. Wound Repair Regen. 11 (3) (2003) 204-212.

[29] Takada Y, Hashimoto M, Kasahara J, Aihara K, Fukunaga K. Cytoprotective effect of sodium orthovanadate on ischemia/reperfusion-induced injury in the rat heart involves Akt activation and inhibition of fodrin breakdown and apoptosis. J. Pharmacol. Exp. Ther. 311 (3) (2004) 1249-1255.

[30] Jarrell JD, Eun TH, Samale M, Briant C, Sheldon B, Morgan JR. Metal oxide coated cell culture arrays for rapid biological screening. J. Biomed. Mater. Res. A 83A (3) (2007) 853-860.

[31] Garcia AJ. A centrifuge cell adhesion assay for high-throughput screening of biomaterial surfaces. J. Biomed. Mater. Res. 67A (1) (2003) 328-333.

[32] Garcia AJ, Gallant ND. Stick and grip: measurement systems and quantitative analyses of integrin-mediated cell adhesion strength. Cell. Biochem. and Biophys. 39 (1) (2003) 61-73.

[33] Ziegler G, Gollwitzer H, Heidenau F, Mittelmeir W, Stenzel F. Anti-infectious, biocompatible titanium coating for implants, and method for the production thereof. U.S. Patent Application Publication US 2006/0161256 A1, July 20, 2006.

[34] Thompson KH, Orvig C. Vanadium in diabetes: 100 years from phase 0 to phase I. J. Inorg. Biochem. 100 (12) (2006) 1925-1935.

[35] Brand RM, Duensing G, Hamel FG. Iontophoretic delivery of an insulin-mimetic peroxovanadium compound. Int. J. Pharm. 146 (1) (1997) 115-122.

[36] Brand RM, Hannah TL. A combination of iontophoresis and the chelating agent 1, 10 phenanthroline act synergistically as penetration enhancers. AAPS Pharmsci. 2 (4) (2000) E35.

Chapter 4

Biological response to polydimethylsiloxane coatings doped with titanium and vanadium for soft tissue contact, implantation and controlled delivery

John D. Jarrell *, Brandon Dolly, Jeffrey R. Morgan

Department of Molecular Pharmacology, Physiology, and Biotechnology, and the Center for Biomedical Engineering, Brown University, Providence, RI, USA

(Submitted 6 December, 2007; Manuscript: jbmt8288; Biomaterials)

Abstract

In this study, we used a high throughput platform to investigate the influence of metal-organic doping of polydimethylsiloxane (PDMS) coatings on cellular bioactivity and controlled release of vanadium compared to polymer free titania. Metal-organic derived titanium and or vanadium was doped into PDMS and used to form a coating on the bottom of cell culture microplates in the absence of added water, acids or bases. These hybrid coatings were rapidly screened to establish how titanium and vanadium concentration influences cell proliferation, adhesion and morphology. We demonstrate that titanium doping of PDMS can be used to improve cell proliferation and adhesion. Vanadium doping caused a biphasic dose response in cell proliferation. A twenty-eight day vanadium and titanium elution study indicated that titanium was not released. The presence of polydimethylsiloxane in coatings increased delivery rates of vanadium compared to titania coatings without polymer. Titanium doped polymers have potential for improving wound healing dynamics, soft tissue integration of medical implants and use as a controlled delivery device.

Keywords: Polydimethylsiloxane; Titanium oxide; Sol-gel techniques; Cell proliferation; Fibroblast; Metal ion release

4.1 Introduction

Polydimethylsiloxane (PDMS) has a long history of use in medical applications beginning with a bile duct repair by Lahey in 1946 [1], an artificial urethra in 1948 by DeNicola [2] and a hydrocephalus shunt constructed by Holter for his son in 1956 [3]. The wide applicability of PDMS to tissue contact is due to its generally low toxicity and biocompatibility, which was investigated in a publication by Rowe, Spence and Bass in 1948 [4] and continues to be extensively studied for general biomedical suitability and specific implant applications [5,6]. From the perspective of chemistry, the strength of the two oxygen and two carbon (methyl group) bonds per silicon atom, gives the material thermal stability up to 400 °C, allowing autoclave sterilization, and preventing chemical decomposition under most physiological conditions [7]. This inertness has a downside for some applications, PDMS tends to poorly facilitate protein and cell attachment, resulting in poor soft tissue integration, a lack of skin sealing around percutaneous devices and localized foreign body response with subcutaneous implants [8].

Titanium has also been recognized as material of choice for many implant applications, especially when contacting bone or to limit contact with nickel. More recently, it has been applied to osseointegrated trans-epithelial prosthetic fixation for dentistry and experimental limb attachment [9]. It is the presence of a spontaneous and self-regenerating passive oxide layer on titanium's surface that is primarily responsible for the corrosion resistance [10] and biointegrative properties of this metal [11, 12, 13]. Titanium oxide reduces local inflammatory responses [14,15], lowers the presence of local reactive oxygen species [16,17] and dynamically incorporates elements from surrounding tissues

after implantation [18,19]. Because of the properties of this (and other) refractory metal oxides, the problem of aseptic osseointegration of medical devices is all but solved.

Recently, liquid chemistry techniques (sol-gel) have been used to apply well adherent [20] pure and doped titanium oxide-based coatings to a variety of substrates for medical applications [21]. These may be left as low temperature formed xerogels or heat treated to induce various amorphous or crystalline microstructures [22,23] suitable for biological evaluation [24,25]. There has been a growing interest in the development of biomaterials which combine the properties of titanium oxides with silicon [26], silicates and organic derived polysiloxanes for both soft tissue and bone implants [27,28,29]. Hybridization of PDMS with single or mixed metal alkoxides has been promising for biomaterials, because of the ability to form silicon-oxygen-metal bonded matrices and thicker crack-free coatings than produced with metal oxides alone [30,31]. PDMS oligomers mix readily with alkoxide based metal-organics, which can be copolymerized by hydrolysis and polycondensation in the presence of water into bioactive apatite-forming bulk materials [32], elastic particles with nano-domain heterostructures [33] and blood compatible, low-adhesion coatings [34]. These materials may be used in the flexible as-formed condition or heat treated to remove organic components and induce porosity [35] or increase mechanical rigidity [36]. The use of metal oxide additions to polymers has been recognized in the development of bioadhesive properties for drug delivery [37] and is promising for modulating the adhesion of cells to PDMS.

Early work with vanadium oxide compounds indicated that they mimicke insulin in a synergetic fashion, with systemic anti-diabetic effects [38,39,40]. At low doses, vanadium compounds have been shown to increase proliferation of fibroblasts, but not

human osteoblasts [41] and inhibit fibroblast and osteoblast growth or viability and cell spreading at higher concentrations [42-45]. Animal models indicate that oral ingestion of vanadium oxides dissolved in drinking water and local bolus injections can promote rapid and orderly collagen deposition during skin wound healing [46,47], improve wound strength [48], improve tendon or ligament repair [49,50] and promote cell recovery after ischemic and reperfusion induced heart injury [51].

In this present study, we created binary and tertiary hybrid coatings formed from the co-hydrolysis and polycondensation (copolymerization) of various concentrations of titanium tetraisopropoxide and vanadium oxytriproxide in PDMS, diluted in mixed organic solvents without the addition of water, acids or bases. The almost limitless compositional options available with these binary and tertiary hybrid coatings required the development of higher through-put methods for screening these materials. To help deal with this challenge, we borrowed techniques common to pharmaceutical drug discovery and developed a new high throughput platform by directly coating the bottom of polystyrene and polypropylene multi well cell culture microplates with these mixed metal oxides and hybrids [52]. This microplate platform has made possible the rapid exploration of novel polymer-coordinated metal oxide materials for biological and drug eluting applications. In this paper, we show that titanium and vanadium oxides can be added to PDMS to influence cell proliferation and morphology, increase cell adhesion and create controlled delivery coatings. In contrast to prior methods for vanadium oxide delivery, we propose local controlled delivery of vanadium from metal oxides and hybridized polymer devices suitable for short-term delivery and long-term implantation.

4.2 Materials and Methods

4.2.1 Materials

To make titanium stock solutions 10 ml of titanium isopropoxide 99.999% (Sigma-Aldrich, St. Louis, MO) was added to 100 ml of isopropanol >=99.8% (Riedel-de Haën, Seelze, Germany) and mixed by brief shaking. Vanadium stock solution consisted of 10 ml of vanadium oxytripropoxide (Sigma-Aldrich) in 100 ml of isopropanol. A PDMS stock solution was made by adding 10 ml of Dow Corning MDX4-4159, 50% Medical Grade Dispersion into 100 ml of 70 % hexanes/30% isopropanol (vol/vol) and mixed by brief shaking at room temperature. This PDMS is supplied as a dispersion of 50% silicone in a co-solvent system of 70% Stoddard Solvent (mineral spirits) and 30% isopropanol. This amine functional polymer also incorporates reactive methoxy- groups that generally polymerizes in contact with moisture or added water to form thin coatings.

Stock solutions were allowed to age 15 minutes at room temperature and briefly shaken before use. These stock solutions were added together in a separate glass container using a pipette to make hybrid stock solutions of specific compositions and briefly shaken before use. Coating compositions were identified by vol % titanium isopropoxide precursor to polymer, excluding all volatile solvents. Stock solutions were mixed for 93.3%, 85.7% and 66.6% titanium-PDMS hybrids and were subsequently doped with vanadium solutions. Tertiary coatings are reported as vol % of vanadium solution per volume of titanium-PDMS hybrid solution. For example, coatings made for solutions consisting of equal volumes of vanadium and 66.6% titanium-PDMS hybrid stock solutions were designated as, “50 vol % vanadium oxypropoxide to 66.6% titanium isopropoxide-PDMS.”

4.2.2 Preparation of coatings

For the biological assays, metal-organic coated polystyrene 96-well tissue culture microplates (Corning Costar, Lowell, MA) were prepared under a fume hood. Using an eight-channel pipette, 20 µl of solution was pipetted into each well of a microplate column. After each filling, the plate was inverted and briefly shaken out to remove excess solution before filling the next column of wells. Each column was coated with different solution chemistries. Non-alloyed titanium oxide xerogel and non-coated cell culture treated polystyrene were used as controls in each plate. The microplates were air-dried face up, without lids, under a chemical hood for 12 to 24 hours. Subsequently, they were heat treated in air on a hot plate (Dataplate, Barnstead/Thermolyte, Dubuque, IA) at 95 °C for one hour with the lids in place.

For the short term elution study, metal-organic coated 12-well microplates were prepared using a total of 50 µl of solution per well for titanium isopropoxide xerogels. Because of the method of preparing tertiary solutions, 100µl was used for these coatings to ensure the total vanadium concentration was the same between xerogel and hybrid coatings designated by the same concentration. Each column contained 20, 10, 5 or 1.25 % vanadium in a titanium isopropoxide stock solution or hybrid stock solutions and non-coated polystyrene controls. The solutions were pipetted in multiple 25 µl doses with one minute of air-drying between doses to make uniform coatings with know total vanadium loading. The microplates were air-dried face up, without lids, under a chemical hood for 12 to 24 hours. Subsequently, they were heat treated in air on a hot plate at 95 °C for one hour with the lids in place.

4.2.3 Cell proliferation and cell viability assays

Human dermal fibroblasts were derived from neonatal foreskins, obtained at the Women & Infants Hospital of Rhode Island, Providence, RI, USA (approved by the Institutional Review Board). Foreskins were trimmed with scissors to remove excess fatty tissue, rinsed repeatedly with sterile phosphate buffered saline (PBS) (Invitrogen Corporation, Carlsbad, CA), and diced into small fragments. The fragments were allowed to adhere to the bottom of a tissue culture plate in a humidified 10% CO_2 atmosphere, at 37 °C for 1 hour, and were covered with Dulbecco's Modified Eagle Medium (DMEM) (Invitrogen Corporation) supplemented with 20% fetal bovine serum containing 100U of penicillin and 100μg of streptomycin per ml. Over a period of 14 days, fibroblasts migrated from the tissue fragments and formed a confluent layer on the culture plate. Fibroblasts were harvested with a 0.05% trypsin/0.53 mM EDTA solution and subcultured to near confluence in Human Fibroblast Medium (HFM) consisting of DMEM containing high glucose, L-glutamine, pyruvate and pyridoxine hydrochloride (Invitrogen Corporation) with additions of 10% fetal bovine serum and 1% penicillin-streptomycin. Cells were detached using 0.05% trypsin/0.53 mM EDTA for 3 minutes and re-suspended in serum containing medium. The cells were seeded onto 96 well microplates at a density of 5,000 cells per well in 100 μl of HFM.

To measure cell proliferation, the microplates were incubated at 37 °C with 10 % CO_2 for 48 hours, after which 10 μl of WST-1 (Roche Applied Science, Indianapolis, IN) was added into each well and incubated for 3 hours at 37 °C. The microplates were quantified using a microplate reader for absorbance at 440 nm (SPECTRAmax® PLUS 384

Microplate Spectrometer with SOFTmax PRO software, Molecular Devices Corporation, Sunnyvale, CA) and plotted. Five replicates with three cell-free controls were used for each coating type and the polystyrene plate bottom. Plates were also inspected under optical microscopy for cell spreading and morphology. Calibration curves were previously established for cell number versus optical density on polystyrene. Seeding density for the cell type was chosen within the linear portion of the calibration curve.

To measure cell number and viability, human fibroblasts were seeded onto 96 well microplates at a density of 5,000 cells per well in 100 μl of HFM and incubated at 37 °C with 10 % CO_2. After 24 hours, cells were rinsed with PBS with 100 mg of CaCl and 100 mg MgCl+6H_2O per liter added (complete PBS) (Invitrogen Corporation) and incubated in 100 μl of 1 μg/ml calcein-AM (Molecular Probes, Inc., Eugene, OR) in complete PBS with 2 mM dextrose for 30 minutes at 22 °C.

Plates were read using a fluorescent microplate reader (SPECTRAmax® GEMINI XS Dual-Scanning Microplate Spectrofluorometer with SOFTmax PRO software, Molecular Devices Corporation, Sunnyvale, CA) set to 485 nm excitation, 535 nm emission. Five replicates with three cell-free controls were used for each coating type and the polystyrene plate bottom. Calibration curves were previously established for cell number versus fluorescence on polystyrene and used to select a seeding density within the linear portion of the calibration curve. Cells were subsequently observed for cell spreading and morphology using optical and fluorescent microscopy.

4.2.4 Combined cell attachment and cell adhesion assay

To characterize cell attachment and adhesion of titanium doped PDMS, a modification of a previous reported method [53,54] was used. Normal human fibroblasts were grown in 500 cm^2 triple flasks to near-confluence using HFM. The cells were rinsed with complete PBS and incubated in 45 ml of 1 μg/ml calcein-AM in complete PBS with 2 mM dextrose for 30 minutes at 22 °C. Cells were detached using 0.05% trypsin and 0.53 mM EDTA for 3 minutes and re-suspended in serum containing medium. Cells were centrifuged at 500 rpm for 5 minutes and re-suspended in PBS dextrose, centrifuged again and re-suspended in PBS dextrose. The cells were then seeded onto microplates at a density of 10,000 cells per well and left to attach for one hour at 22 °C. Calibration curves were previously established for cell number versus fluorescence on polystyrene and used to select a seeding density within the linear portion of the calibration curve and to maximize the signal to noise response of the plate reader.

Each well was completely filled with PBS-dextrose and the baseline fluorescence read (485 nm excitation, 535 nm emission). The wells were emptied by inversion to remove floating cells and refilled with PBS-dextrose. The microplate was covered with sealing tape (Corning Costar) and centrifuged upside down in a Centra-GP8R Refrigerated Centrifuge (Thermo Electron Corporation, Waltham, MA) using microplate buckets at 500 rpm for 5 minutes. The microplates were again inverted to empty and refilled with PBS-dextrose and read again. The first and second readings were compared to determine the fraction of cells that attached to the microplate 1 hour after seeding and remained adherent after exposure to normal forces from centrifugation. This combined assay identifies how readily cells attach to a surface (seeding efficiency) and quantifies the strength of adhesion (adherent fraction). The rpm of the centrifuge was selected to

remove approximately 50% of the cells from the tissue culture treated polystyrene. Five replicates with three cell-free controls were used for each coating type and the polystyrene microplate bottom.

4.2.5 Short-term vanadium release

To characterize the short-term delivery of vanadium from titanium xerogels with or without PDMS, metal-organic coated 12-well plates were prepared as described above and filled with 1 ml of PBS per well, covered with one or two layers of sealing tape (Corning Costar), and placed in a heated orbital shaker (ThermoForma Model 420, Marrietta, Ohio) set to 90 rpm and 37 °C. At each time point, (0.25, 1.3, 4, 7, 14 and 28 days), the PBS was removed from each well and added to separate 15ml centrifuge vials and refilled with fresh PBS. To each vial was added 10 ml of triple deionized water to allow for ICP elemental analysis for vanadium and titanium. Four replicates of each coating were used. Pure titanium oxide and non-coated polystyrene were used for controls. The results for vanadium elution were reported as mg/L and converted to percentage of total initial vanadium in coatings and micrograms vanadium released per surface area. Results of the short-term elution study were plotted and trend lines fitted using SigmaPlot 8.0 (Systat Software Inc., San Jose, California, USA), which facilitated mathematical modeling of vanadium release as a function of time and initial vanadium concentration. After the elution study, the surfaces were inspected using scanning electron microscopy (SEM) in conjunction with energy dispersive spectroscopy (EDS).

4.2.6 Scanning electron microscopy

A LEO 1530 Thermally-Assisted Field Emission (TFE) Scanning Electron Microscope (SEM) was used to establish surface morphology of the coatings from the elution study. Samples were carbon sputter coated to overcome the inherent insulating properties of the coatings. A working distance of 3 to 5 mm and accelerating voltage of 5.00 kV was used to collect electron images at various magnifications between 200 X and 150,000 X.

4.3 Results and Discussion

4.3.1 Cell proliferation and viability on coatings

To quantify fibroblast proliferation 48 hours after cell seeding, a WST-1 colorimetric assay was used. Fig. 4.1 presents graphs of the optical density as a function of titanium (top) or vanadium (bottom) concentration in PDMS. Pure titanium oxide xerogel and cell culture treated polystyrene were used as controls. Proliferation of human fibroblasts on PDMS increases with small additions of titanium and continued to increase with large additions of titanium. Under optical microscopy, cells on pure PDMS were rounded, but began to spread out with increases in titanium concentration (not shown). Cell proliferation also increased on coatings with small additions of vanadium, but fell off rapidly with additions of vanadium over 11.2 % . Increases in proliferation as a function of vanadium concentration was not associated with increased cell spreading (not shown). Cells remained rounded and spherical for all vanadium-PDMS hybrids. As the composition of hybrid coating was changed from pure PDMS to pure titanium dioxide, unique optical microstructures arise, which made microscopic documentation of cell morphology difficult without fluorescent staining (Fig. 4.2).

Cell proliferation for tertiary combinations of vanadium, titanium and PDMS were also investigated and compared to binary vanadium and titanium coatings without PDMS. The proliferation of fibroblasts on coatings as a function of vanadium doping is graphed for 93.3% (Fig. 4.3, top right), 85.7% (Fig. 4.3, bottom left) and 66.6% (Fig. 4.3, bottom right) Ti-PDMS hybrids and compared to titanium oxide without PDMS (Fig. 4.3, top left). Vanadium doping of Ti-PDMS hybrids and titanium oxide coatings influenced human fibroblast proliferation in a biphasic manner. For all coatings, low doses of vanadium doping stimulated cell proliferation, whereas increasing vanadium steadily decreased cell proliferation in a dose dependent way. Cell proliferation was more affected by vanadium doping in 66.6% Ti-PDMS hybrids compared to 87.5% and 93.3 % hybrids or similarly doped titanium oxides without PDMS. Fibroblasts were well spread on uncoated cell culture polystyrene, titanium oxide, Ti-PDMS hybrids and the lower vanadium loaded coatings, but became morphologically rounded as proliferation dropped on hybrid coatings and PDMS-free coatings (not shown).

To quantify cell viability 24 hours after seeding, a fluorescent calcein uptake assay was used (Fig. 4.4). Fluorescence of live cells as a function of vanadium doping in titanium without PDMS also showed a biphasic dose response. Hybrid coatings became fluorescent when exposed to calcein AM loaded PBS and provided inconsistent results with the plate reader, making the assay unsuitable for these materials. However, the calcein loading revealed the differences cell morphology using fluorescent microscopy. Fibroblasts were well spread on uncoated cell culture polystyrene (Fig. 4.5, PS), titanium oxide, Ti-PDMS hybrids and the lower vanadium loaded coatings (Fig. 4.5, 1%V), but

became morphologically rounded on Ti-PDMS hybrids (Fig. 4.5, 3%V) with higher doses of vanadium loading, correlating with the drop in proliferation.

These data show that the concentration of titanium, vanadium and PDMS in the coatings can be used to control cell proliferation of fibroblasts in a dose dependent manner. The biphasic response of these data are similar to those found with soluble vanadium added to Swiss 3T3 fibroblast cells where it was shown that low doses stimulated proliferation and high doses inhibited proliferation [44]. Depending on the application of the implant, vanadium containing coatings could be designed to elicit the desired bioresponse *in vivo*.

4.3.2 Cell attachment and cell adhesion

To determine the efficiency of initial cell attachment and adhesion under load, a centrifugation cell adhesion assay was used to further define the influence of titanium doping of PDMS coatings (Fig. 4.6.). The total fraction of initially seeded cells after centrifugation ranged from 0.12 (12 %) for pure PDMS to 0.43 (43%) for pure titanium oxide xerogel. The adhesion of cells under these conditions increased rapidly with additions of more than 85 vol % titanium. In contrast, prior investigations indicated that vanadium doping of titanium oxide xerogels had little influence on either initial cell attachment or adhesion strength [45,52,55].

4.3.3 Short-term release of vanadium

To characterize the short-term release of vanadium from titanium oxide and Ti-PDMS hybrid matrices, a 28 day elution study was performed (Fig. 4.7.). The top plots present

the cumulative release (% initial loading) as a function of time for titanium oxide and 66.6% Ti-PDMS hybrid coatings, while the bottom plots give the cumulative release of vanadium per coating surface area for four different vanadium concentrations (20, 10, 5, 1.25%). Increased loading with vanadium resulted in both a higher release rate and higher fraction of total vanadium release for titanium coatings both with and without the addition of PDMS. The increase in release rates for higher vanadium loadings is consistent with results typically found in drug delivery from non-erodible matrices. More significant was that the addition of PDMS to titanium coatings increased the vanadium release rate and the fraction of total vanadium release by as much as 2000% for high vanadium loaded coatings. Hybrid coatings produced controlled elution over a period of 28 days which is a time period important to the soft tissue healing response [56-58]. The concentration of titanium eluted for all coatings was below the reporting limit (< 0.050 ppm) for ICP analysis, indicating that the titanium matrices were relatively insoluble and stable in PBS.

4.3.4 Mathematical modeling of vanadium release

The short-term elution of vanadium from each of the vanadium containing coatings was fitted with simple hyperbolic trend lines with R^2 values of 0.905 or better for titanium oxide without PDMS and 0.995 or better for Ti-PDMS hybrids, for all eight data sets after the form: $f(t,V) = \frac{a(V)t}{b(V)+t}$. The relationship between the initial vanadium concentration and the coefficient of the hyperbolic solution, a(V) and b(V), were fit to linear, quadratic or cubic polynomial functions with perfect or near perfect R^2 fits.

The combined hyperbolic and polynomial functions for vanadium elution from doped titania xerogels derived from titanium isopropoxide are given below:

$$\mathrm{VE\%(t,V)} = \frac{(1.3739 + 0.0633V)t}{6.9198 - 1.9643V + 0.2077V^2 - 0.0059V^3 + t}$$

$$\mathrm{VEa(t,V)} = \frac{(0.0794 + 0.0752V)t}{4.3859 - 0.5654V + 0.0290V^2 + t}$$

The combined hyperbolic and polynomial functions for vanadium elution from doped 66.6% titanium-PDMS hybrids are given below:

$$\mathrm{VE\%(t,V)} = \frac{(4.4504 + 2.5293V)t}{11.3755 - 0.6147V + 0.0143V^2 + t}$$

$$\mathrm{VEa(t,V)} = \frac{(0.0589 + 0.1954V + 0.1293V^2)t}{11.3755 - 0.6147V + 0.0143V^2 + t}$$

Where VE%(t,V) is the cumulative vanadium release (% of initial loading), while VEa(t,V) is the cumulative vanadium eluted per unit surface area ($\mu g/cm^2$), V is the solution percentage of vanadium oxytripropoxide oxide in titanium tetraisopropoxide and *t* is time in days. These functions fit well the region between 0 and 28 days for all concentrations of vanadium between 1.25 to 20%. Future testing would be required to determine the suitability of the models for time points and vanadium concentrations outside of these limits.

4.3.5 Surface characterization

To determine the influence of the elution study on the surface appearance and morphology of the vanadium doped Ti-PDMS hybrid coatings, SEM image analysis was used. Vanadium doped 66.6% titanium-PDMS hybrids showed evidence of preferential surface leaching after 28 day of elution into 37 °C PBS solutions (Fig. 4.8). Representative SEM images of 10% (Fig. 4.8, left column) and 5% (Fig. 4.8, right column) vanadium hybrids are given at low, medium and high magnifications. This suggests that there is a phase separation of the water soluble vanadium into 200 nm to 600 nm wide network structures during coating formation. This is in contrast to vanadium doped titanium xerogels without PDMS which do not show evidence of phase separation on this length scale [55].

Titanium oxide, being ceramic in nature, is mechanically brittle and poorly matches the physical properties of polymers used for soft tissue implants and tissue contacting applications like catheters and wound dressings. We selected a PDMS with reactive amine and methoxy functional groups that becomes hydrolyzed to yield hydroxy-functionality and can be polymerized onto surfaces capable of reacting with these groups, such as metals, metal oxides and functional plastics and elastomers [59]. This study is a step toward the creation of hybrid materials that can blend the bioactivity of titanium oxide with the flexible and inert properties of PDMS. Hybrids were also used to create solid-state vanadium eluting devices that provided controlled and predictable delivery of vanadium. The selection of titanium dioxide as a matrix material makes these coatings

suitable for use in long-term or permanent implants, which possess the tissue integrative and anti-inflammatory properties inherent to titanium.

4.4 Conclusions

This study demonstrates that doping PDMS with titanium and vanadium produces coatings that influence the proliferation and adhesion of human fibroblast cells. These hybrids also provided predictable vanadium delivery for at least 28 days, which could be controlled by varying the concentration of vanadium in the coatings. Measuring the bioresponse to these coatings revealed that low doses of vanadium stimulated cell proliferation, whereas higher doses inhibited cell proliferation. These metal-organic matrices successfully delivered metal-based compounds that modulated human cellular responses in a fashion similar to drug delivery. This opens the door for the creation of hybrid materials that use mixed metal oxides to control cell attachment, proliferation, extracellular matrix formation and tissue ingrowth from integrated biomaterial systems suitable for coating polymer and metal substrates.

Acknowledgements

This work was funded, in part, by the VA Rehabilitation Research and Development Center for Restorative and Regenerative Medicine, Department of Veterans Affairs, Providence, Rhode Island.

4.5 Figures

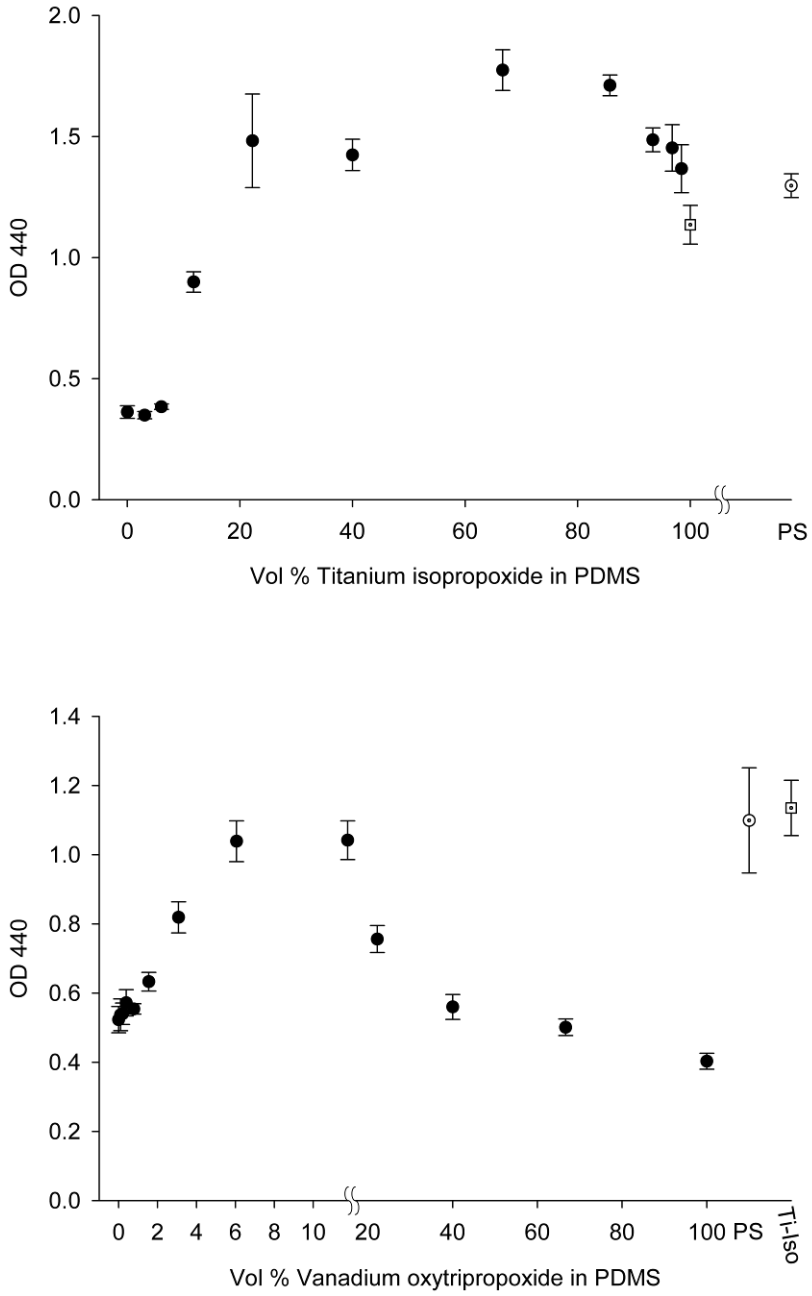

Figure 4.1: Proliferation of human fibroblasts on PDMS increases with small additions of titanium (top) and vanadium (bottom). Human fibroblasts were seeded on coatings incubated for 48 hours and cell proliferation was measured by the WST-1 assay. Cell proliferation continued to increase with large additions of titanium, but fell off rapidly with additions of vanadium over 11.2 %. Pure titanium oxide coatings (Ti-Iso, open squares) and cell culture treated polystyrene (PS, open circles) were used as controls.

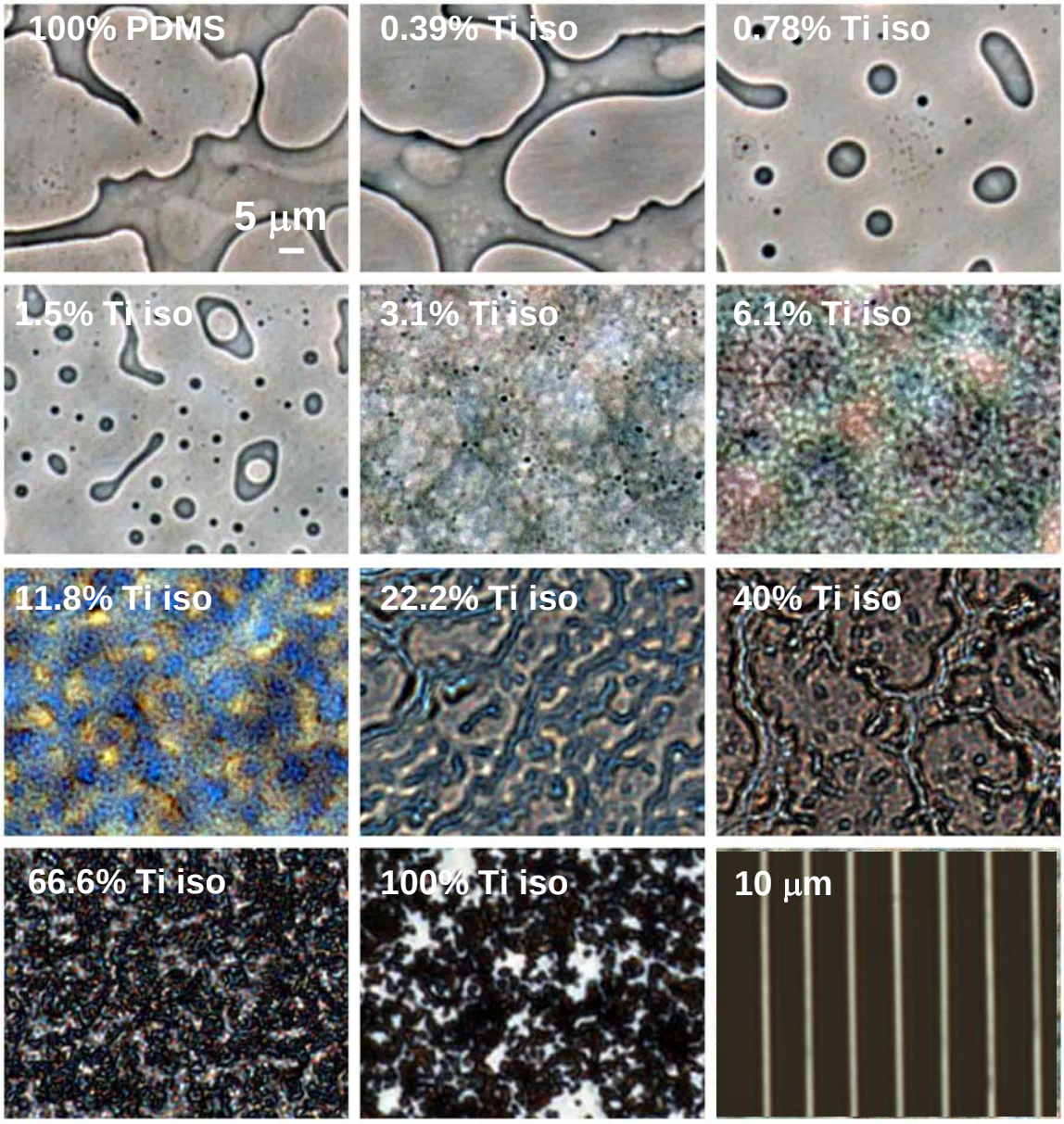

Figure 4.2: Coatings created from serial mixtures of titanium isopropoxide in PDMS form unique heterostructures as presented in the eleven brightfield optical microscopy images. Parallel scale lines in bottom right panel are 10 microns apart.

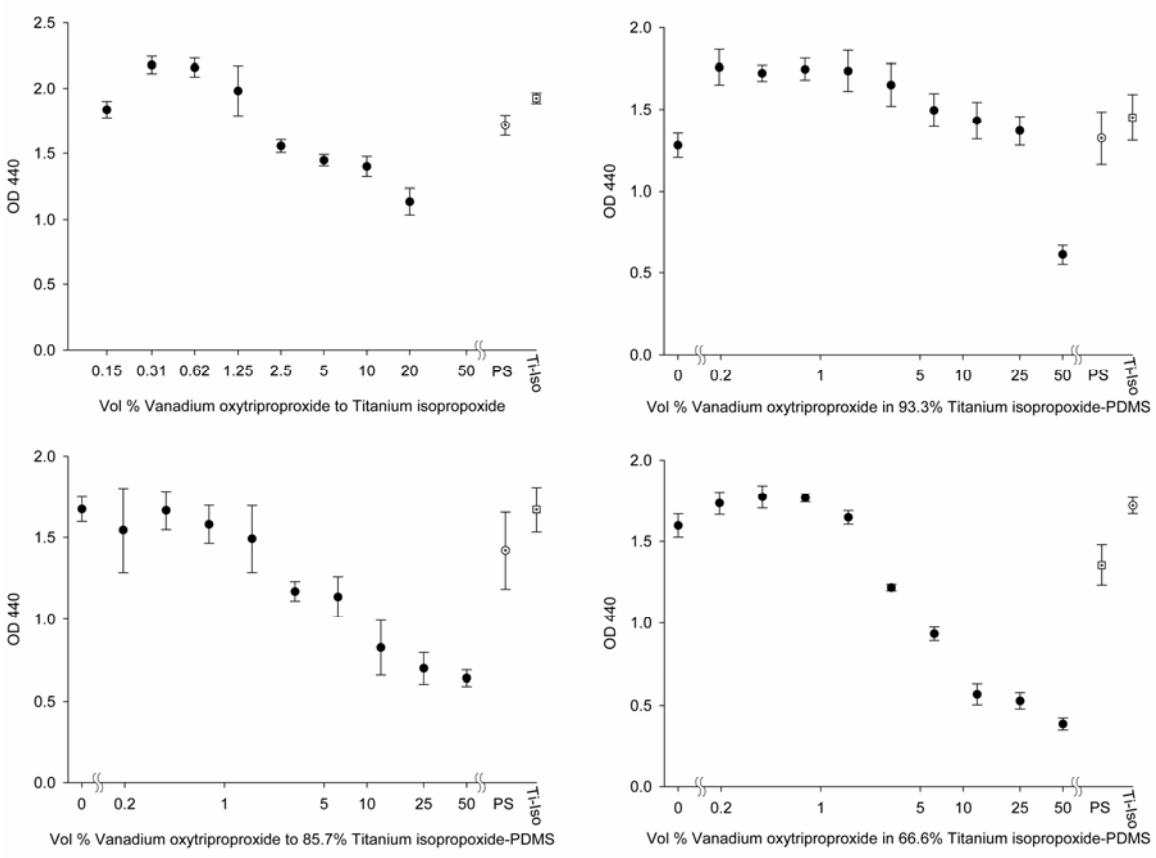

Figure 4.3: Vanadium doping of Ti-PDMS hybrids and titanium oxide coatings influences human fibroblast proliferation in a biphasic manner. Human fibroblasts were seeded on coatings incubated 48 hours and proliferation measured by the WST-1 assay. Low doses of vanadium doping stimulated proliferation, whereas higher doses inhibited cell proliferation. Cell proliferation was more sensitive to vanadium concentration on the 66.6 % Ti-PDMS hybrids (right bottom) compared to 87.5% (left bottom) or 93.3 % (top right) hybrids and similarly doped titanium xerogels without PDMS (top left). Pure titanium oxide coatings (Ti-Iso, open squares) and cell culture treated polystyrene (PS, open circles) were used as controls for each data set.

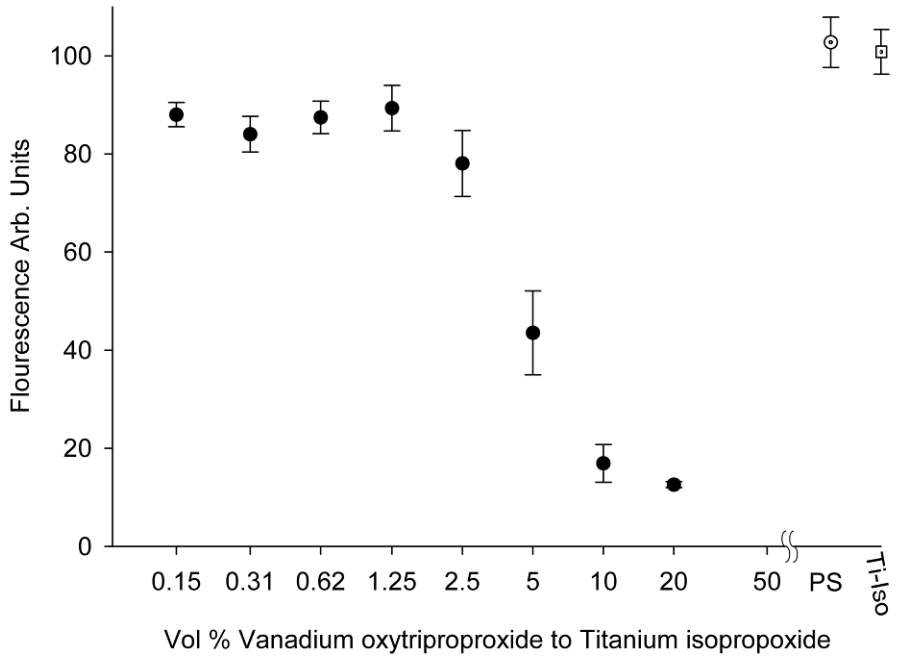

Figure 4.4: Fibroblast viability is influenced by vanadium loading. Plot presents fluorescent calcein loading as a function of vanadium concentration in titanium isopropoxide coatings, 24 hours after seeding.

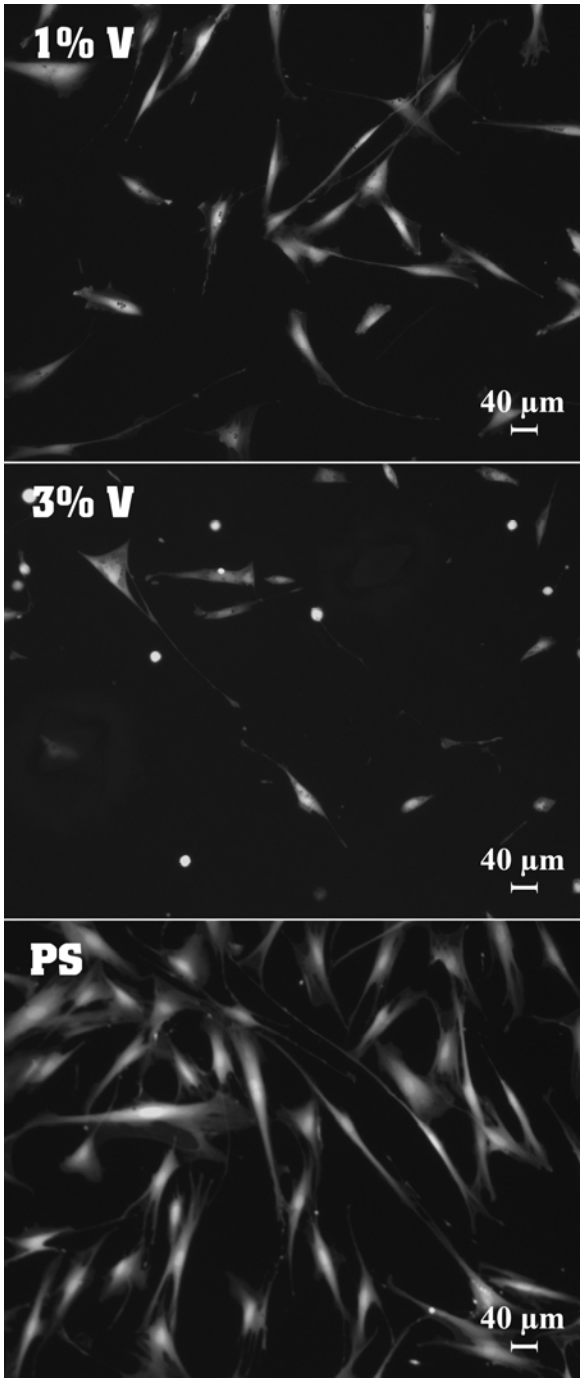

Figure 4.5: Vanadium concentration in 66.6% titanium-PDMS hybrids influences cell morphology and spreading. Representative fluorescent images of calcein loaded human fibroblasts 24 hours after seeding onto titanium isopropoxide-PDMS hybrid coatings with 1 % vanadium (1%V), 3% vanadium (3%V) and tissue culture treated polystyrene (PS). Fibroblasts were well spread on uncoated polystyrene (PS), titanium, Ti-PDMS hybrids and the lower vanadium loaded coatings (1%V), but became morphologically rounded as proliferation dropped (3%V).

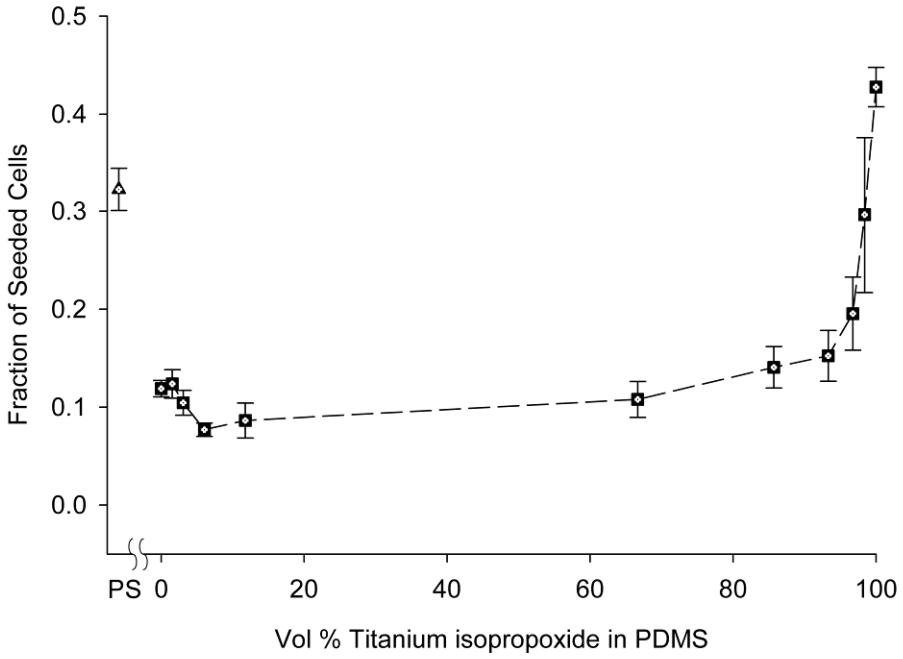

Figure 4.6: Titanium doping of PDMS (open squares) influences cell attachment and adhesion under centrifugation. Calcein loaded human fibroblasts were seeded onto coatings, allowed 1 hour to attach, and subjected to normal loads by inverted centrifugation at 500 rpm for 5 minutes. Fraction of remaining cells compared to initial seeding was determined by fluorescence and plotted as a function of titanium doping. Cell adhesion at one hour of attachment was maximal at high doses of titanium doping compared to cell culture polystyrene (PS).

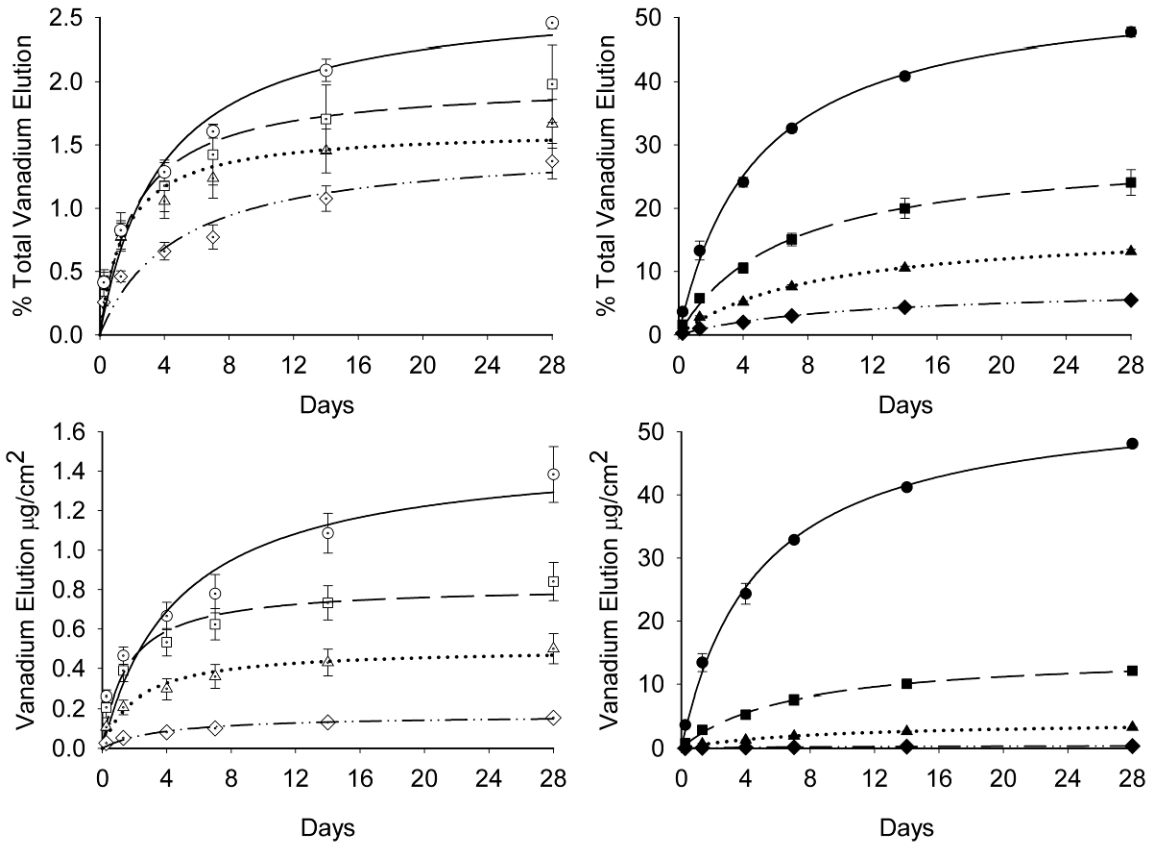

Figure 4.7: Addition of PDMS to titanium coatings increases the elution rate of vanadium. The top plots present the percentage of total vanadium loading released into PBS as a function of time for titanium oxide coatings without PDMS (left, open symbols) and Ti-PDMS hybrid coatings (right, closed symbols), while the bottom plots are the cumulative release rates per surface area over the same period for four different vanadium concentrations, 20% (circles), 10% (squares), 5% (triangles) and 1.25% (diamonds). Modeling curves of vanadium release are shown for 20% (——), 10% (– – –), 5% (·····) and 1.25% (–·–·) vanadium doping.

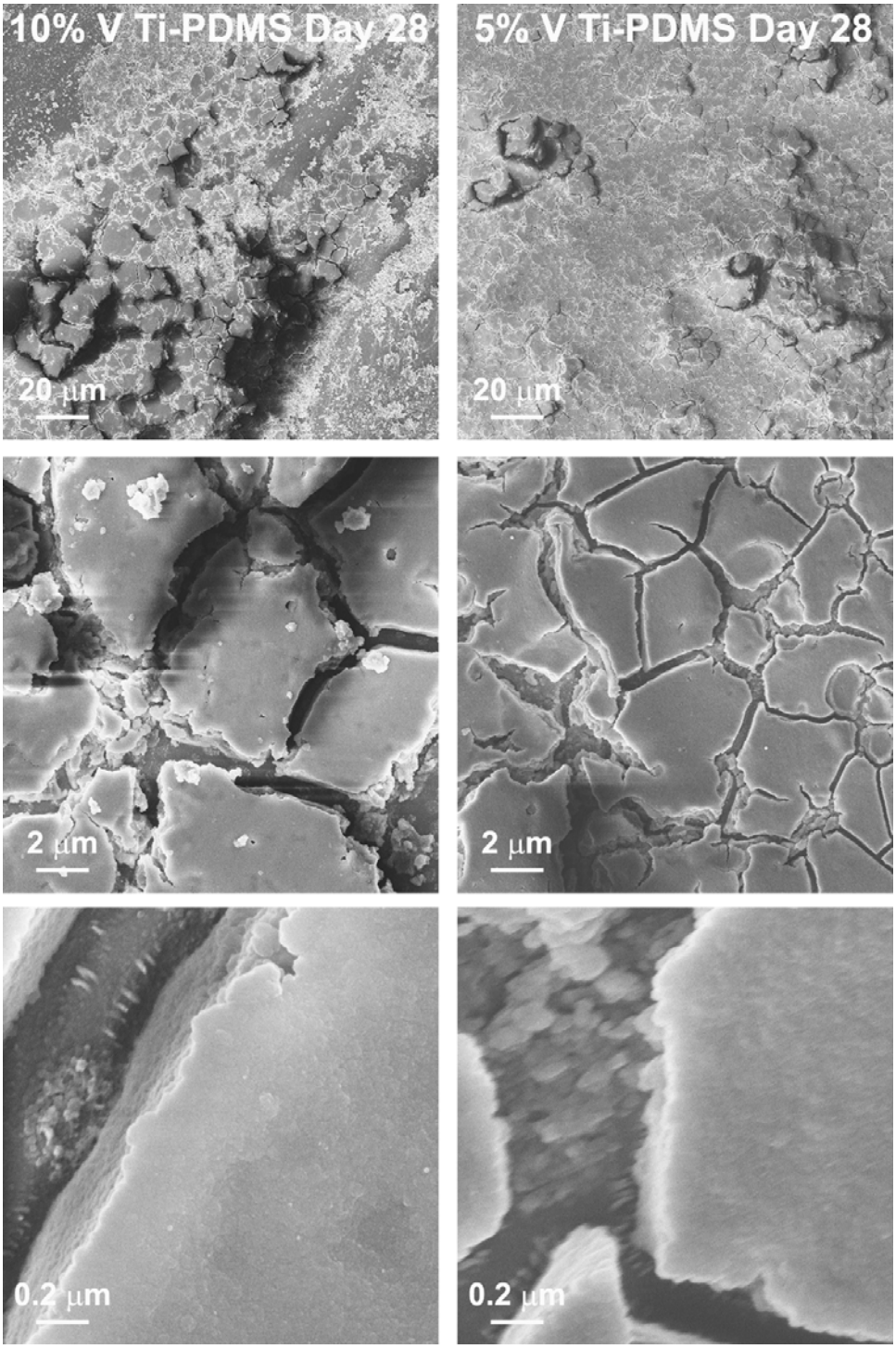

Figure 4.8: Vanadium doped 66.6% titanium-PDMS hybrids show evidence of preferential leaching after 28 day of elution into 37 °C PBS solutions. Representative SEM images of 10% (left column) and 5% (right column) vanadium in hybrids at low, medium and high magnifications.

4.6. Reference

1. Lahey FH. Comments made following the speech, “Results from using Vitallium tubes in biliary surgery,” read by Pearse HE before the American Surgical Association, Hot Springs, VA. Ann Surg 1946;124:1027.

2. DeNicola RR. Permanent artificial (silicone) urethra. J Urol 1950;63(1) :168-172.

3. LaFay H. A father’s last-chance invention saves his son. Reader’s Digest, January, 1957; 29-32.

4. Rowe VK. Spencer HC, Bass SL. Toxicological studies on certain commercial silicones and hydrolizable silane intermediates. J Indust Hyg Toxicol 1948;30:332.

5. Curtis J, Colas A. Medical applications of silicones, Biomaterials Science, 2nd Edition: An Introduction to Materials in Medicine. Elsevier, Inc., July 29, 2004;697-706.

6. Hron P. Hydrophilisation of silicone rubber for medical applications. Polym Int 2003;52:1531–1539.

7. Colas A, Curtis J. Silicone biomaterials: History and chemistry, Biomaterials Science, 2nd Edition: An Introduction to Materials in Medicine. Elsevier, Inc., July 29, 2004;80-86.

8. Abbasi F, Mirzadeh H, Katbab A-A. Modification of polysiloxane polymers for biomedical applications: A review. Polym Int 2001;50:1279-1287.

9. Branemark R, Branemark PI, Rydevik B, Myers RR. Osseointegration in skeletal reconstruction and rehabilitation: a review. J Rehabil Res Dev 2001;38(2):175-181.

10. Jacobs JJ, Cilbert JL, Urban RM. Current concepts review. Corrosion of metal orthopaedic implants. J Bone Joint Surg Am 1998;80(10):1554.

11. Brunski JB, D.Puleo DA, Nanci A. Biomaterials and biomechanics of oral and maxillofacial implants: current status and future developments. Int J Oral Maxillofac Implants 2000;15(1):15-46.

12. Sundgren JE, Bodo P, Lundstrom I. Auger electron spectroscopic studies of the interface between human tissue and implants of titanium and stainless steel. J Colloid Interface Sci1986;110(1):9-20.

13. Effah EA, Bianco PD, Ducheyne P. Crystal structure of the surface oxide layer on titanium and its changes arising from immersion. J Biomed Mater Res 1995;29(1):73-80.

14. Overgaard L, Danielsen N, Bjursten LM. Anti-inflammatory properties of titanium in the joint environment. An experimental study in rats. J Bone Joint Surg Br 1998;80(5):888-893.

15. Kraft CN, Hansis M, Aren S, Menger MD, Vollmar B. Striated muscle microvascular response to silver implants: A comparative *in vivo* study with titanium and stainless steel. J Biomed Mater Res 2000;49(2):192-199.

16. Suzuki R, Muyco J, McKittrick J, Frangos JA. Reactive oxygen species inhibited by titanium oxide coatings. J Biomed Mater Res 2003;66(2):396–402.

17. Suzuki R, Frangos JA. Inhibition of inflammatory species by titanium surfaces. Clin Orthop Relat Res 2000;372:280-289.

18. Healy KE, Ducheyne P. Hydration and preferential molecular adsorption on titanium *in vitro*. Biomaterials 1992;13(8):553-561.

19. Li P, Ducheyne P. Quasi-biological apatite film induced by titanium in simulated body fluid. J Biomed Mater Res 1998;41(3):341-348.

20. Piveteau L-D, Gasser B, Shlabach L. Evaluating mechanical adhesion of sol-gel titanium dioxide coatings containing calcium phosphate for metal implant application. Biomaterials 2000;21:2193-2201.

21. Podbielska H., Ulatowska-Jarza, A. Sol-gel technology for biomedical engineering. Bull Pol Ac:Tech 2005;53(3):261-271.

22. Wang C-C, Ying JY. Sol-gel synthesis and hydrothermal processing of anatase and rutile titania nanocrystals. Chem Mater 1999;11:3113-3120.

23. Hun TH. Microstructural evolutions and stress studies of titania films derived by “spin-deposition” methods. PhD Thesis, Brown University, Providence RI, USA 2006;70-95.

24. Areva S, Paldan H, Petola T, Narhi T, Jokenen M, Linden M. Use of sol-gel-derived titania coating for direct soft tissue attachment. J Biomed Mater Res 2004;70A:169-178.

25. Nakazawa K, Lee S-W, Fukuda J, Yand D-H, Kunitake T. Hepatocyte spheroid formation on a titanium dioxide gel surface and hepatocyte long-term culture. J Mater Sci: Mater Med 2006;17:359-364

26. Rosengren A, Wallman L, Danielsen N, Laurell T, Bjursten LM. Tissue reactions evoked by porous and plane surfaces made out of silicon and titanium. IEEE Transactions on biomedical Engineering, Vol 49, No. 4 April 2002; 392-399.

27. Meretoja VV, Tirri T, Ääritalo V, Walboomers XF, Jansen JA, Narhi T. Titania and titania-silica coatings for titanium: Comparison of ectopic bone formation within cell-seeded scaffolds. Tissue Engineering 2007;13(4):855-863.

28. Ääritalo V, Areva S, Jokinen M, Linden M, Peltola T. Sol-gel-derived TiO_2-SiO_2 implant coatings for direct tissue attachment. Part I: Design, Preparation and Characterization. J Mater Sci: Mater Med 2007;18(9):1863-1873.

29. Areva S, Ääritalo V, Tuusa S, Jokinen M, Linden M, Peltola T. Sol-gel-derived TiO_2-SiO_2 implant coatings for direct tissue attachment. Part II: Evaluation of cell response. J Mater Sci: Mater Med 2007;18(8):1633-1642.

30. Whang CM, Yeo CS, Kim YH. Preparation and characterization of sol-gel derived SiO_2-TiO_2-PDMS composite films. Bull Korean Chem Soc 2001;22(12):1366-1370.

31. Julian B, Gervais C, Cordoncillo E, Escribano P, Babonneau F, Sanchez C. Synthesis and characterization of transparent PDMS-metal-oxo based organic-inorganic nanocomposites. Chem Mater 2003;15;3026-3034.

32. Chen Q, Kamitakahara M, Miyata N, Kokubo T, Nakamura T. Preparation of bioactive PDMS-modified CaO-SiO_2-TiO_2 hybrids by sol-gel method. Journal of Sol-Gel Science and Technology 2000;19:101-105.

33. Nakade M, Kameyama K, Ogawa M. Synthesis and properties of titanium dioxide/polydimethylsiloxane hybrid particles. Journal of Materials Science 2004;39:4131-4137.

34. Yabuta T, Tsuru K, Hayakawa S, Osaka A. Synthesis of blood compatible PDMS-based organic-inorganic hybrid coatings. Journal of Sol-Gel Science and Technology 2004;31:273-276.

35. Nakade M, Ichihashi K, Ogawa M. Preparation of titania/PDMS hybrid films and the conversion to porous materials. Journal of Sol-Gel Science and Technology 2005;36:257-264.

36. Chen Q, Miyata N, Kokubo T, Nakamura T. Effect of heat treatment of bioactivity and mechanical properties of PDMS-modified CaO-SiO_2-TiO_2 hybrids via sol-gel process J Mater Sci: Mater Med 2001;12:515-522.

37. Jacobs JS, Mathiowitz E. Methods and compositions for enhancing the bioadhesive properties of polymers. U.S. Patent 6,123,965, Filed: August 18, 1998.

38. Garcia-Vicente S, Yraola F, Marti L, Gonzalez-Munoz E, Garcia-Barrado MJ, Canto C, Abella A, Bour S, Artuch R, Sierra C, Brandi N, Carpene C, Moratinaos J, Camps M, Palacin M, Testar X, Guma A, Albericio F, Royo M, Mian A, Zorzano A. Oral insulin-mimetic compounds that act independently of insulin. Diabetes 2007;56(2):486-493.

39. Shechter Y. Insulin-mimetic effects of vanadate. Possible implications for future treatment of diabetes. Diabetes 1999;39(1):1-5.

40. Srivastava AK. Anti-diabetic and toxic effects of vanadium compounds. Mol Cell Biochem 2006; 206(1-2):177-182.

41. Hallab NJ, Vermes C, Messina C, Roebuck KA, Glant TT, Jacobs JJ. Concentration and composition dependent effects of metal ions on human MG-63 osteoblasts. J Biomed Mater Res 2002;60:420-433.

42. Yamamoto A, Honma R, Sumita M. Cytotoxicity evaluation of 43 metal salts using murine fibroblasts and osteoblastic cells. J Biomed Mater Res 1998;39(2):331-340.

43. Huang C, Zhang Z, Ding M, Li J, Ye J, Leonard SS, Shen HM, Butterworth L, Lu Y, Coasta M, Rojanasakul Y, Castranova V, Vallyathan V, Shi X. Vanadate Induces p53 transactivation through hydrogen peroxide and causes apoptosis. J Biol Chem 2000;275(42):32516-32522.

44. Cortizo AM, Salice VC, Vescina CM, Etcheverry SB. Proliferative and morphological changes induced by vanadium compounds on Swiss 3T3 fibroblasts. BioMetals 1997;10(2):127-133.

45. Jarrell JD, Eun TH, Samale M, Briant C, Sheldon B, Morgan JR. Use of specialized metal oxide films for delivery of bioactive metal compounds. Orthopaedic Research Society Annual Meeting, February 2007;32:1590.

46. Ehrlich HP, Keefer KA, Myers RL, Passaniti A. Vanadate and the absence of myofibroblasts in wound contraction. Arch Surg 1999;134(5):494-501.

47. Mackay DJD, Moyer KE, Saggers GC, Myers RL, Mackay DR, Ehrlich HP. Topical vanadate optimizes collagen organization within granulation tissue. Wound Repair Regen 2003;11(3):204-212.

48. Ehrlich HP, Keefer KA, Maish GO, Myers RL, Mackay DR. Vanadate ingestion increases the gain in wound breaking strength and leads to better organized collagen fibers in rats during healing. Plast Reconstr Surg 2001;107(2):471-477.

49. Moyer KE, Saba AA, Hauck RM, Ehrlich HP. Systemic vanadate ingestion modulates rat tendon repair. Exp Mol Pathol 2003;75(1):80-88.

50. Chen J, Iosifidis M, Zhu J, Tatarintsev I, Wang JH. Vanadate ingestion enhances the organization and collagen fibril diameter of rat healing medical collateral ligaments. Knee Surg. Sports Traumatol. Arthrosc 2006;14(8):750-755.

51. Takada Y, Hashimoto M, Kasahara J, Aihara K, Fukunaga K. Cytoprotective effect of sodium orthovanadate on ischemia/reperfusion-induced injury in the rat heart involves Akt activation and inhibition of fodrin breakdown and apoptosis. J Pharmacol Exp Ther 2004;311(3):1249-1255.

52. Jarrell JD, Eun TH, Samale M, Briant C, Sheldon B, Morgan JR. Metal oxide coated cell culture arrays for rapid biological screening. J Biomed Mater Res A 2007;83A(3):853-860.

53. Garcia AJ. A centrifuge cell adhesion assay for high-throughput screening of biomaterial surfaces. J Biomed Mater Res 2003;67A(1):328-333.

54. Garcia AJ, Gallant ND. Stick and grip: measurement systems and quantitative analyses of integrin-mediated cell adhesion strength. Cell Biochem and Biophys 2003;39(1):61-73.

55. Jarrell JD, Dolly B, Morgan JR. Controlled release of vanadium from titanium oxide coatings for improved integration of soft tissue implants, (accepted March 27, 2008) J Biomed Mater Res A 2008.

56. Diegelma RF. Cellular and biochemical aspects of normal and abnormal wound healing: An overview. The Journal of Urology 1997;157(1):298-302.

57. Clark RA. Basics of cutaneous wound repair. J Dermatol Surg Oncol 1993;19:693–706.

58. Ross R. The fibroblast and wound repair. Biol Rev 1968;43:51–96.

59. Dow Corning MDX4-4159, 50% Medical Grade Dispersion, Frequently Asked Questions, Form 52-1039-01.

Chapter 5

Full spectrum photoactivated solid-state dispersions

John D Jarrell, Evan C Werlin, Bryan E. Laulicht, Jeffrey R Morgan

Department of Molecular Pharmacology, Physiology, and Biotechnology, and the Center for Biomedical Engineering, Brown University, Providence, RI, USA

(Submitted 14 January, 2008; Nature manuscript 2008-01-00416)

(Revised submission 29 March, 2008; Nature Materials manuscript)

5.1 Summary

TiO_2 is a well known photocatalyst with numerous applications including hydrogen production, photovoltaics, water/air purification and bacterial disinfection[1-5]. Semiconducting TiO_2 produces electron and hole pairs in response to ultraviolet radiation (UV) or when doped with certain metals, nitrogen, carbon or quantum-sized CdS phases, to visible light, but with minimal photoactivity beyond 500 nm[6-8]. A photoactive biomaterial, responsive to photons known to penetrate skin and soft tissues[9,10] could provide an opportunity for *in situ* activation and disinfection of medical implants and devices[11-14] without the damage to human cells associated with UV[15,16]. Here we show that the anhydrous reaction of metal-organic titanium with polydimethylsiloxane (silicone), two materials widely used in medical implants, produces an amorphous heterostructured coating with photoactive response to medical x-rays, UV, visible, and infrared light unlike anything previously reported[17]. Using a rapid screening platform, we've discovered a range of solid state dispersions with enhanced ability to block full spectrum photon transmission and remove methylene blue from solution using UV-visible and infrared irradiation. Visible light photocatalysis by these coatings is 12 times higher than standard Degussa P25 TiO_2. Our discovery is a significant step towards transdermal photoactive medical implants and improved efficiency for conventional photocatalytic applications.

5.2 Results and Discussion

TiO_2 degrades methylene blue (MB) dye solutions into a colorless form by surface absorption and both reduction and mineralization reactions from reactive oxygen species

generated during exposure to light with energy greater than 3.0 eV (400 nm) for rutile or 3.2 eV (388 nm) for the anatase crystalline phase[18,12]. Amorphous forms of TiO_2 are relatively non-photocatalytic, requiring either high thermal or hydro-thermal treatments to induce crystallinity[19]. Polydimethylsiloxane (PDMS) or "silicone", like titanium[20], has a long history of use in medical implantation as a hydrophobic and inert material[21].

We made a series of metal-organic derived hybrid coatings from solvent diluted mixtures of titanium isopropoxide (Ti-iso) and linear PDMS with active amino methoxy terminal groups or alternately with non-active silicone oil. These were evaluated for x-ray, UV, visible and infrared induced MB clearance using a high throughput assay previously described[22]. These coatings were previously evaluated for biological activity and compatibility with human cells[23].

Microplates coated with varying mixtures of Ti-iso and PDMS (Ti-PDMS) containing MB solution were irradiated with 161 flashes of monochromatic light (388-1000 nm). The levels of MB after irradiation were quantified as optical density at 664 nm ($OD664_{nm}$). There was a rapid onset of photoactivated MB removal with Ti-PDMS between 50% and 70%, for all tested wavelengths of UV, visible and infrared light (Fig. 5.1a). MB removal in response to red and infrared light increased dramatically for concentrations > 70% to 97.4%, after which MB clearance dropped sharply to nearly zero by 99.68%. In contrast to prior work with doped TiO_2, Ti-PDMS coatings in the >70% to ~97.4% range had higher activity with visible light compared to UV and maximum MB clearance between 720-1000 nm[7]. Coatings made with 75% Ti-iso in silicone oil (Ti-oil) showed a similar photoactive response, indicating that active terminal groups were not essential for broad spectrum photoactivity. Coatings made with a suspension of Degussa

Aerogel P25 TiO_2 photocatalyst showed no MB clearance under these test conditions, likely because of insensitivity to the low irradiation level provided by the flash source. Similar high photoactivity was demonstrated by Ti-PDMS coatings >50% Ti-iso, when exposed to full spectrum light from a 250 watt quartz halogen bulb with UV and IR filters (Fig. 5.1b). MB clearance with P25 coatings at 90 minutes was about equal to hybrids after only 10 minutes.

To confirm these results in a larger vessel, glass vials were coated and air dried at room temperature or heat treated in air to either 250 °C (1 hr) or 400 °C (2 hr). At 400 °C methyl groups decompose without fully crystallizing amorphous TiO_2. Vials were filled with MB which was stirred, while being illuminated by a 150 watt halogen fiber optic cool light source. Aliquots (100 μl) were removed over time and MB clearance measured. P25 coatings required 4 hr to clear 0.367 OD, while 75% Ti-PDMS required < 40 min and 94.7% Ti-PDMS < 20 min (Fig. 5.1c). This indicates better than a 6-fold and 12-fold improvement over P25 for 75% and 94.7% coatings, respectively. Heat treatments did not affect the activity of the Ti-PDMS coatings.

Medical x-rays caused MB clearance as a function of exposure and Ti-PDMS mixture, while polystyrene and P25 coated wells showed little activity (Fig. 5.1d,e). Highly active, 97.4% Ti-PDMS coating cleared 0.44 OD of MB after 668 mAs of radiation. A typical radiograph for this machine is 6.8 mAs at 69 kVp. In contrast, effective radiolysis by crystalline commercial TiO_2 required 300-1500 Grays (Gy) of x-rays ~30-150 times the lethal human dose[24].

Bright field microscopy showed the appearance of a micron-sized second phase within the coatings as Ti-iso concentration was increased (Fig. 5.2a). Photoactivity correlated

with the presence of this phase as seen by the comparison of non-active 46.1 % Ti-PDMS and photoactive 66.6 % Ti-PDMS coatings. Highest photoactivated MB clearance occurred when this phase formed an interconnected network throughout the coatings as seen in the images of 75% and 88.8% Ti-PDMS. Coatings with 88.8% Ti-PDMS and higher looked very similar to 100% Ti-iso coatings with dense clusters of micron sized phases.

The optical transmission spectra of the coating (290-1000 nm) showed that PDMS, Ti-iso and low photoresponsive hybrids began as opaque and became rapidly transparent in the transition from 290 nm to 390 nm, while photoactive coatings continued to absorb light up to 1000 nm (Fig. 5.2b). Similar monotonic absorption has been reported with Ti^{+} implanted single crystal SiO_2 and to a lesser extent with toluene diisocyanate modified TiO_2[25,26]. The transmission of light through the coatings as a function of Ti-iso concentration and wavelength mimicked the profile of photoactivated MB clearance (Fig. 5.2c). P25 also showed absorption extending into the visible spectrum, usually seen when TiO_2 is doped to add additional energy states into the band gap[27].

Near and mid FT-IR reflectance spectra of powdered coating samples (10,500 to 450 cm^{-1}) showed that reflectance increased with increasing Ti-iso concentration compared to PDMS (Fig. 5.3a). The peaks observed with highly photoactive coatings (75% and 94.7% Ti-PDMS) could all be attributed to those found on either the PDMS or Ti-iso.

FT-IR transmission spectra of powdered coating samples (4000 to 650 cm^{-1}) showed that the Ti-PDMS coatings had absorption peaks corresponding to the Si-O, Si-C, C-H bonding and methyl groups within PDMS and the Ti-O-Ti (650 cm^{-1}), H-O-H and O-H of

titanium oxide with absorbed water (Fig. 5.3c, Table 5.1)[28]. No peak, indicating Si-O-Ti bonding, was observed at 950 cm^{-1}.

Raman spectroscopy was used to determine if Si-Si bonding was present (Fig. 5.3c). Spectra of PDMS indicated peaks typical of Si-O, Si-C and methyl group bonding[28]. Three broad peaks were identified for Ti-iso centered at ~612, 422 and 180 cm^{-1}, which appear similar to summations of typical TiO_2 anatase peaks at 640, 515, 398, 198, 147 and 144 cm^{-1} with those at 612 and 448 for rutile[29]. Poor Raman peak development is typical of amorphous TiO_2[29]. The 94.7% plot consisted of three broad peaks similar to the Ti-iso plot, but of lower intensity, except for a small spike at 610 cm^{-1}. The 75% plot had peaks associated with typical bonding of either PDMS or Ti-iso, except for unassigned peaks at 1451, 1024, 833 and 593 cm^{-1} (Fig. 5.3c, Table 5.1). There were no peaks in the Ti-PDMS samples indicating Si-O-Ti bonding at 950 cm^{-1} or Si-Si bonding at 520 cm^{-1} (the longitudinal optical phonon)[28,29]. Since Si-Si bonding gives a strong Raman signal, small quantities should have been detected, if present.

X-ray photoelectric spectroscopy (XPS) was used to determine chemistry of coatings at the surface (~2.6-5.0 nm, the inelastic mean free path for Si 2p electrons in either TiO_2 or PDMS matrices, respectively) (Fig. 5.4a). The silicon concentration of hybrids was higher than expected, especially for Ti-oil hybrid (Fig. 5.4a, Table 5.2). The atomic ratio of Ti to Si for 94.7% Ti-PDMS was 1.57:1 and 0.016:1 for 94.7% Ti-silicone oil (measured) compared to 5.07:1 (~ theoretical bulk). This suggests that the surface of photoactive coatings consists of a titanium rich phase surrounded by a thin PDMS rich phase. The stoichiometry from P25 and Ti-iso chemistry indicate excesses of surface carbon and oxygen in the ratio of ~3:1, suggesting a composition of C_3H_NO bound or

absorbed onto the surface. P25 chemistry also showed additional nitrogen and chlorine. High resolution XPS of coatings show that the binding energies for Ti 2p3/2 (458.5-459.5 eV), C 1p (285 eV) and Si 2p (102-102.5 eV) shells are typical of TiO_2, aliphatic hydrocarbon and PDMS bonding, respectively (Fig. 5.4b). Bonding for metallic Ti is reported at 454.1 eV, TiO at 455.1 eV, Ti_2O_3 at 456.7 eV and TiO_2 (458.7 eV), while Si 2p at 99.5 eV indicates Si-Si bonding and 100.2 eV Si-C and 102.5 eV Si-O[29]. The 71.5 eV space between Ti 2p3/2 and O 1s with Ti-PDMS also indicates TiO_2 bonding[29].

Transmission electron microscopy (TEM) of coatings revealed a transformation from the simple structures of non-active coatings and pure Ti-iso to a complex mixture of micro and nano features with the most photoactive coatings (Fig. 5.5). Micron-sized precipitates seen with optical microscopy were made up of clusters of spheres 200-300 nm in diameter. Some of the spheres took on a torus shape as seen with the most active 88.8% and 94.7% Ti-PDMS samples. These also had nanometer-sized light and dark regions dispersed throughout the electron transparent microstructures. The atomic resolution TEM image of the 88% Ti-PDMS coating showed ordered, but crystallographically amorphous strands, approximately 1 nm by 0.2 nm. Electron diffraction patterns (Fig. 5.5, insets) confirmed the amorphous condition by the lack of distinct rings indicative of crystallinity.

In summation, characterization showed an amorphous network of TiO_2 rich phases dispersed within a PDMS rich matrix, each possessing additional amorphous nano-phases, without any indication of covalent bonding between phases or Si-Si formation. The large difference in dielectric properties between TiO_2 and PDMS and the fractal-like repetition of nano/microstructures strongly suggests a photonic involvement[30,31], where

intercollated nano phases capture x-rays, single spheres and clusters of ~200 nm features capture UV-visible light and the micron scale heterostructures capture the red and infrared photons. We propose that the extraordinary photoactivity observed with maximally dispersive compositions is driven by localized photon induced charging of the titanium oxide rich regions, causing rapid attraction of the positively charged MB molecules. We also suggest that the PDMS rich regions act as an insulator between the leaky capacitor-like titanium oxide rich regions resulting in the surface production of superoxide from absorbed oxygen.

5.3 Methods

5.3.1 Coating solutions. To make titanium stock solutions, 10 ml of titanium isopropoxide 99.999% (Sigma-Aldrich, St. Louis, MO) was added to 100 ml of isopropanol >=99.8% (Riedel-de Haën, Seelze, Germany) and mixed by brief shaking. A PDMS stock solution was made by adding 10 ml of Dow Corning MDX4-4159, 50% Medical Grade Dispersion into 100 ml of 70 % hexanes/30% isopropanol (vol/vol) and mixed by brief shaking at room temperature. This PDMS is supplied as a dispersion of 50% silicone in a co-solvent system of 70% Stoddard Solvent (mineral spirits) and 30% isopropanol. This amine functional polymer also incorporates reactive methoxy- groups that generally polymerizes in contact with moisture to form thin coatings. Alternately, silicone oil stock solution was made by adding 5 ml of non-active linear silicone oil (Dow Corning, 200 fluid 20cst) to 105 ml of 70 % hexanes/30% isopropanol. Stock solutions were allowed to age 15 minutes at room temperature and briefly shaken before use. These stock solutions were added together in a separate glass container using a

pipette to make hybrid stock solutions of specific compositions and briefly shaken before use. Coating compositions were identified by vol % titanium isopropoxide precursor (% Ti-iso) to volume of PDMS oligomers, excluding all volatile solvents.

To make Degussa Aerogel P25 TiO_2 solutions (Evonik Degussa Corporation, Parsippany, NJ), the powder was mixed in isopropanol with atomic Ti concentrations equal to 66.6% and 75% Ti-iso in PDMS hybrids and used for making coatings.

5.3.2 Preparation of coatings. For microplate assays, metal-organic coated polystyrene 96-well tissue culture microplates (Corning Costar, Lowell, MA) were prepared under a fume hood. Using a multi-channel pipette, 20 μl of solution was pipetted into four to eight wells of a microplate column. After each filling, the plate was inverted and briefly shaken out to remove excess solution before filling the next group of wells. Ti-iso (100%) and Degussa P25 coatings and non-coated polystyrene wells were used as controls. The microplates were air-dried, without lids, under a chemical hood for 12 to 24 hours.

5.3.3 Microplate photocatalysis assays. To measure photoactive methylene blue (MB) clearance, a high throughput assay was developed using coated 96-well microplates and an optical microplate reader. MB solution (200 μl, 0.3mg/liter in dH_2O, ~$OD664_{nm}$ of 0.5) was pipetted into each well. With microplate lid removed, the $OD664_{nm}$ of MB was pre-read (SPECTRAmax® PLUS 384 Microplate Spectrometer with SOFTmax PRO software, Molecular Devices Corporation, Sunnyvale, CA). The wells were exposed to 161 flashes of a selected wavelength (5 seconds between flashes) using the same plate

reader in dynamic mode. At the end of irradiation, $OD664_{nm}$ was measured to quantify catalytic MB clearance. Results were plotted as change in $OD664_{nm}$ as a function of irradiation wavelength and coating composition using SigmaPlot 8.0 (Systat Software Inc., San Jose, California, USA).

Alternately, to provide broad spectrum visible light irradiation, the microplates were floated in a cold water bath (< 27 °C) and irradiated with a 250 watt halogen work light (250T3Q, Philips Lighting Company, Somerset, NJ) at a distance of 18 cm, using the attached glass UV filter and 2.5 cm of water in a Pyrex breaker as an IR filter.

5.3.4 Scintillation vial photocatalysis assay. The inside of 20 ml borosilicate scintillation vials were coated with 300 µl of coating solution or an equal atomic titanium concentration of Degussa TiO_2 P25 suspended in isopropanol and allowed to air dry at room temperature overnight. To test temperature stability of coatings some vials were heat treated in air to either 250 °C for 1 hr or 400 °C for 2 hr. Vials were filled with MB solution (1.5mg/liter in dH_2O) and constantly agitated with a stir bar at 350 rpm (Dataplate, Barnstead/Thermolyte, Dubuque, IA). One vial was covered with a beaker wrapped in aluminum foil to serve as a light-free control. The second vial was irradiated with visible light (UV and 700 nm cutoff filters) using a Fostec 8375 (Schott, Inc., Auburn, NY) EKE modulamp high intensity, dual gooseneck fiber optic cool light source. The tip of each fiber optical line was placed in direct contact with opposite sides of the vial and full power applied. MB clearance was determined from triplicate 100 µl aliquots removed at various time points and $OD664_{nm}$ determined.

5.3.5 Radiolysis by medical x-rays assay. To measure radiolysis of MB, coated microplates were filled with 200 μl of MB solution (3mg/liter in dH_2O) and subjected to flashes of ionizing radiation from a medical (veterinary) x-ray unit (Bennett model RXT-150W, Copiague, NY) operating at 110kVp, 150 milliampere (mA) and 0.40 second exposures or 60.0 mAs/flash. The second experiment involved 60 flash exposures operating at 69kVp, 200 mA and 0.5 second duration. MB clearance was determined by $OD664_{nm}$ after various repeated flash exposures.

5.3.6 Optical microscopy. Bright field images of coated microplates were obtained using transmitted light and a 100X oil objective with 1.5X optivar on an Olympus IX70 inverted microscope (Olympus, Center Valley, PA) equipped with an AxioCam MRc camera (Carl Zeiss MicroImaging, Thornwood, NY).

5.3.7 UV-Visible-IR spectra. Transmission spectra on coated microplates were determined from 290 to 1000 nm in 4 nm steps using a microplate reader.

The near and mid FT-IR reflectance spectra of powder samples scraped from coatings (10500 to 450 cm^{-1}) were collected at the Keck/NASA Reflectance Experimental Laboratory (RELAB) (Brown University, Providence, RI) using a Thermo Nicolet Nexus 870 FT-IR spectrometer (Thermo Fisher Scientific, Inc., Waltham, MA) with PIKE AutoDiffuse attachment which has an off-axis biconical diffuse reflectance configuration. Spectra from 0.95 to 4.0 microns were collected using a quartz light source, Si-on-CaF_2 beam splitter and TE cooled DTGS detector, while spectra from 2.0 to 25 microns used a Glowbar light source, Ge-on-KBr beam splitter and TE cooled DTGS detector.

Standard FT-IR transmission spectra were collected from scraped samples of coatings using a Perkin Elmer (Wellesley, MA) Spectrum One B spectrophotometer with a zinc-selenide (Sn-SE) universal attenuated total reflectance attachment. Samples were analyzed between 4000 and 650 cm^{-1}.

5.3.8 Raman analysis. Spectra were collected from scraped samples of coatings using a SENTERRA Dispersive Raman Microscope (Bruker Optics, Inc., Billerica, MA) operating at 100 mW with 785 nm Laser source and 25 μm aperture, 0.5 cm^{-1} steps.

5.3.9 XPS binding energy spectra. Spectra were collected from dip coated plastic microscope slides using a PHI (Physical Electronics, Inc., Chanhassen, Minnesota) Model 5600 ESCA system with monochromatic Al kα source, concentric hemisphere analyzer and AugerScan (RBD Enterprises, Inc., Bend, Oregon) analytical software version 3.02 and 0.4 mm spot size. Surveys were taken at 0.8 eV steps from 0 to 1100 eV, 50 mSec/step, 6 sweeps, a pass energy of 187.85 eV, and 4 eV work function, while high resolution scans were taken at 0.1 eV steps, 5 sweeps, and a pass energy of 23.5 eV.

5.3.10 Transmission electron microscopy. To determine crystal structure, we collected TEM images and electron diffraction patterns of as-coated samples using a Philips EM420T operating at 120 kV, while atomic resolution TEM images were collected with a JEOL model 2010 operating at 200 kV. Samples were prepared by dipping variable mesh copper TEM grids (Electron Microscopy Science, Hatfield, PA; CAT# TMV-Cu, 3.05

diameter, 0.8 mil thickness, combined 150, 200, 300, 400 mesh) in coating solutions and allowing to air-dry overnight at room temperature.

Acknowledgements

Special thanks to Dr. Takahiro Hiroi for IR reflectance data and Anthony W. McCormick for TEM. This work was funded, in part, by VA Rehabilitation Research and Development Center for Restorative and Regenerative Medicine, Department of Veterans Affairs.

5.4 Figures

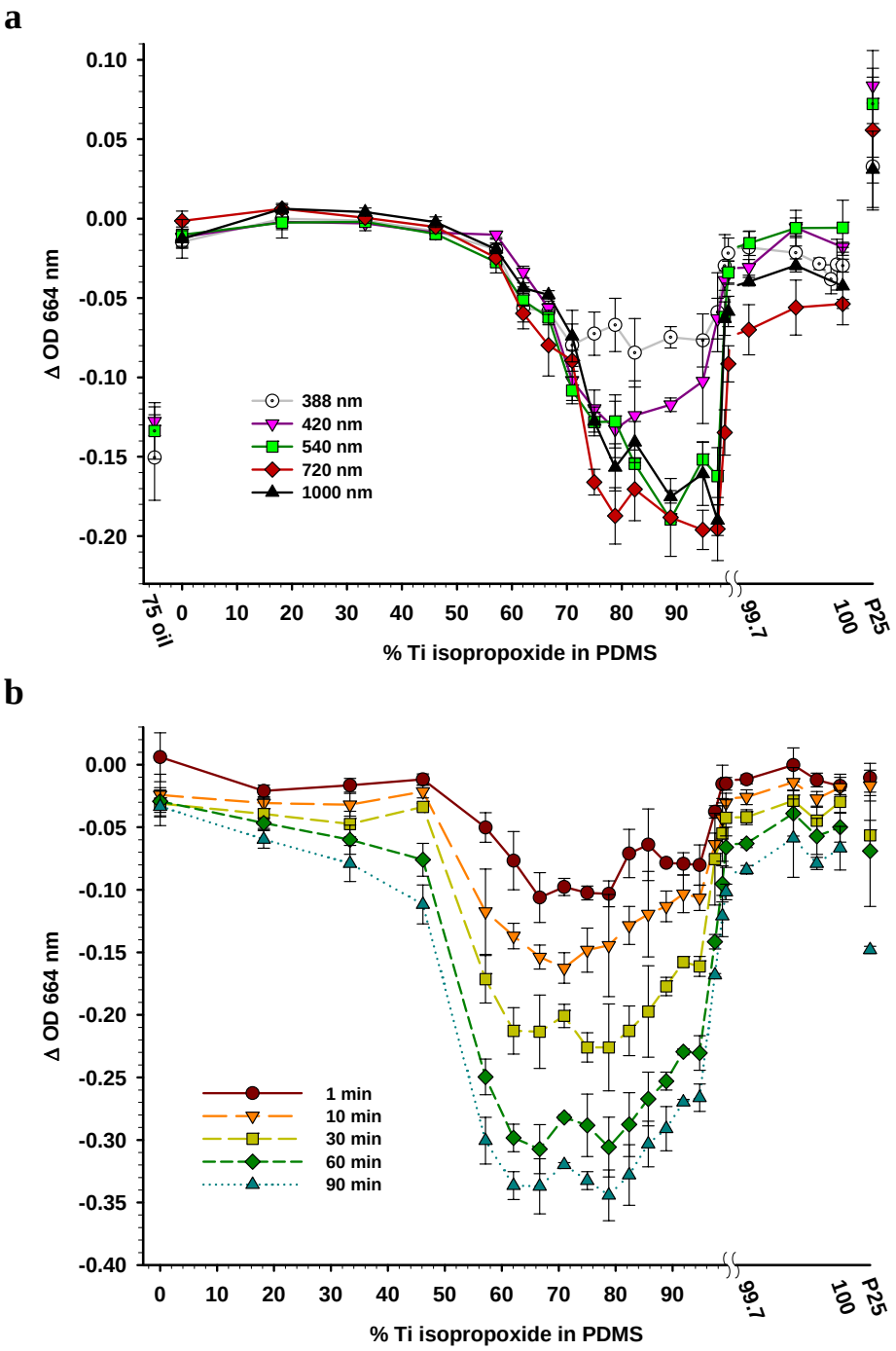

Figure 5.1a,b: Photoactive methylene blue (MB) clearance by coated microplates compared to Degussa P25 TiO_2. **a**, MB clearance as a function of Ti-iso concentration in PDMS and non-reactive silicone oil (75 oil) after monochromatic flash irradiation at one of five wavelengths between 388 and 1000 nm, 388 (white), 420 (violet), 540 (green), 720 (red) and 1000 nm (black). **b**, MB clearance on coated plates in response to 250 watt quartz halogen light source with UV and IR filters, as a function of Ti-iso concentration and exposure for 1 (red), 10 (orange), 30 (yellow), 60 (green) and 90 minutes (cyan).

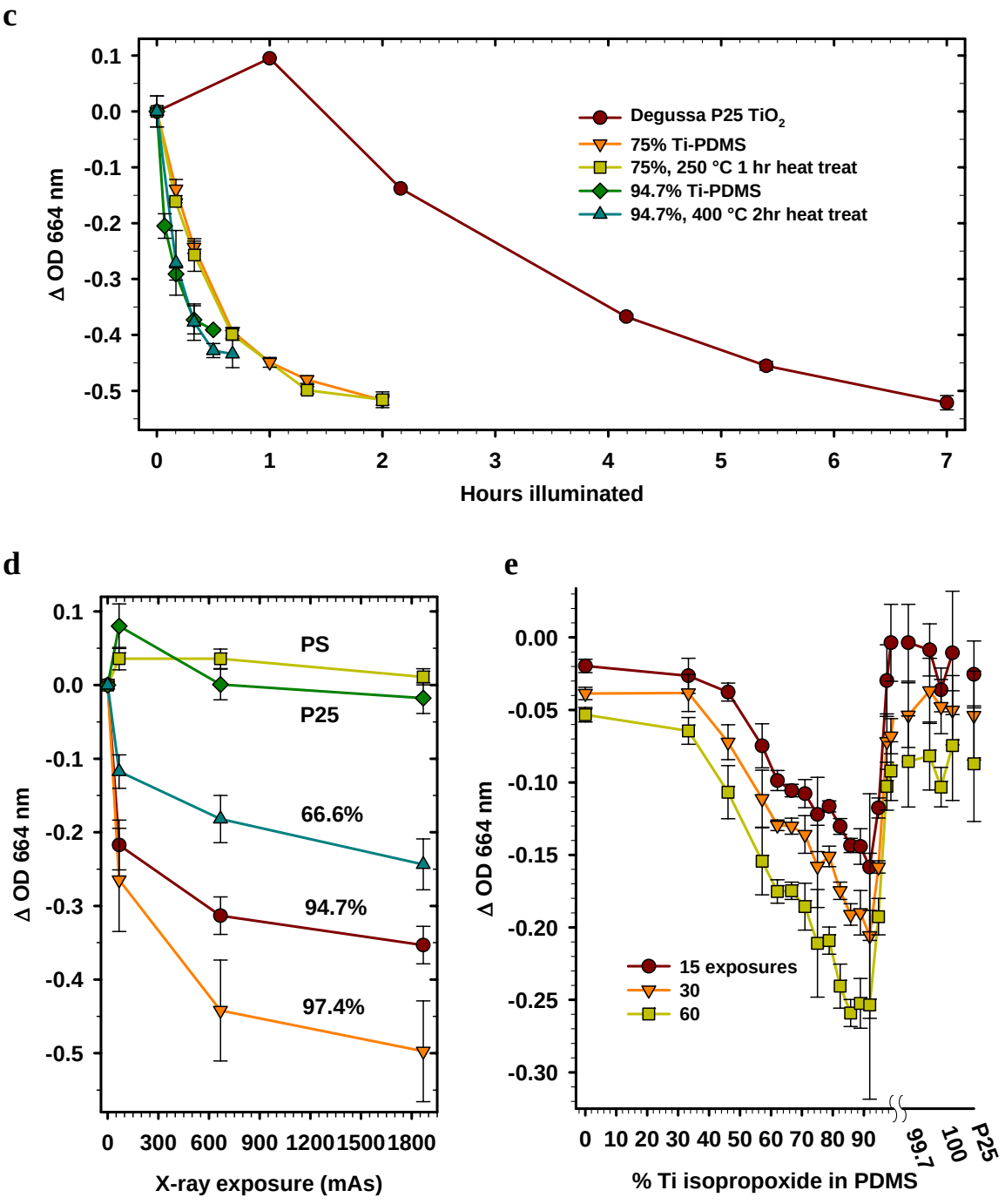

Figure 5.1c,d,e: **c**, Photoactive methylene blue (MB) clearance in Ti-PDMS coated glass vials compared to Degussa P25 TiO_2, exposed to 150 watt halogen fiber optic source with UV and 700 nm cutoff filters and stirring. P25 required 4 hr to clear 0.367 OD, while 75% and 94.7% Ti-PDMS required < 40 min and < 20 min, respectively. **d**, Medical x-ray caused MB clearance on coated microplates as a function of exposure and **e**, Ti-iso concentration in coatings, while polystyrene (PS) and P25 coated wells showed little activity.

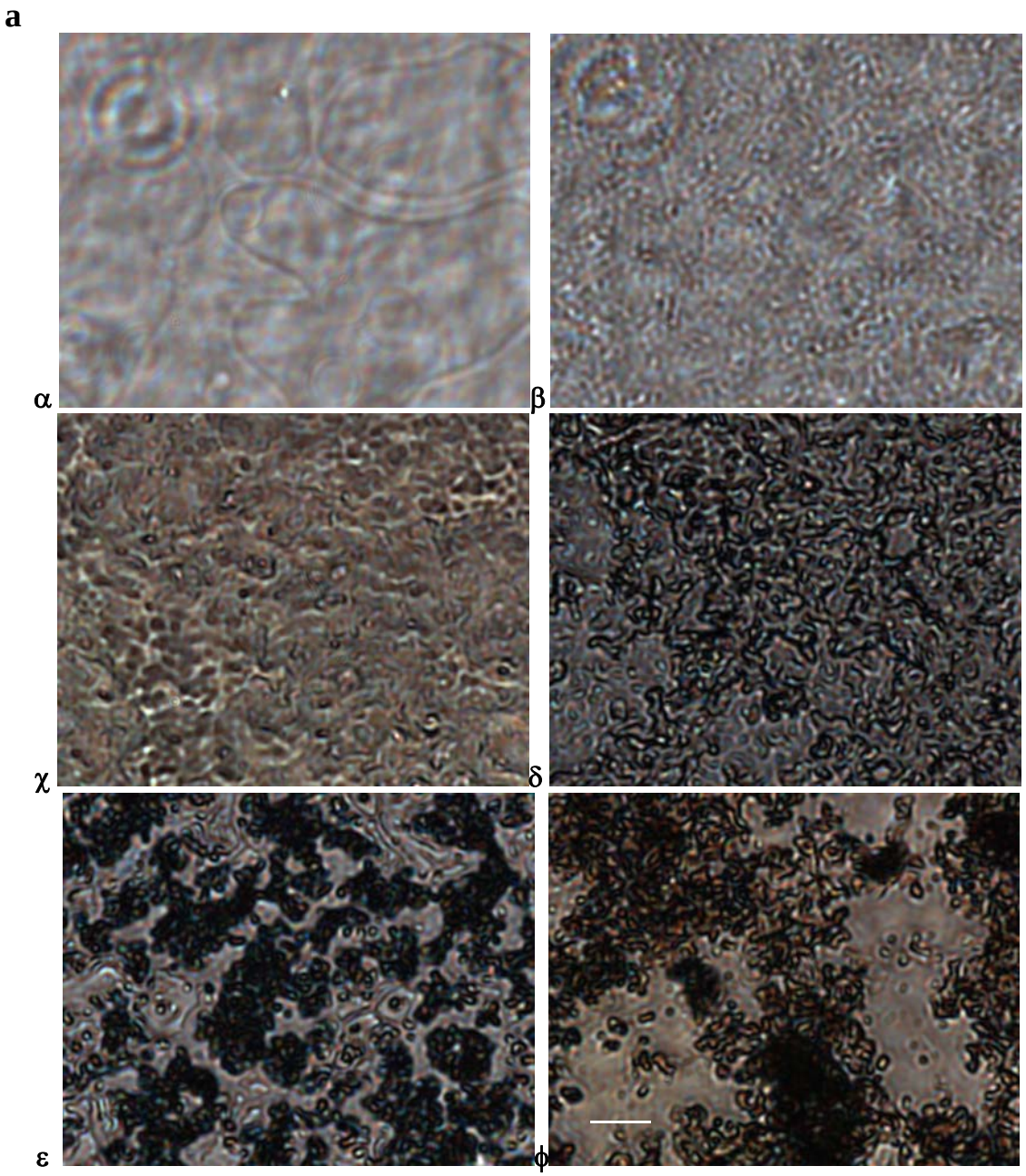

Figure 5.2a: **a**, Brightfield images show that Ti-PDMS coatings develop unique heterostructures. α, pure PDMS; β, 46.1% Ti-iso in PDMS (non-photoactive); χ, 66.6% (photoactive); δ 75% (highly photoactive); ε, 88.8% (highly photoactive); ϕ, 100 % metal-organic derived titanium oxide (non-photoactive). Scale bar is 5 μm.

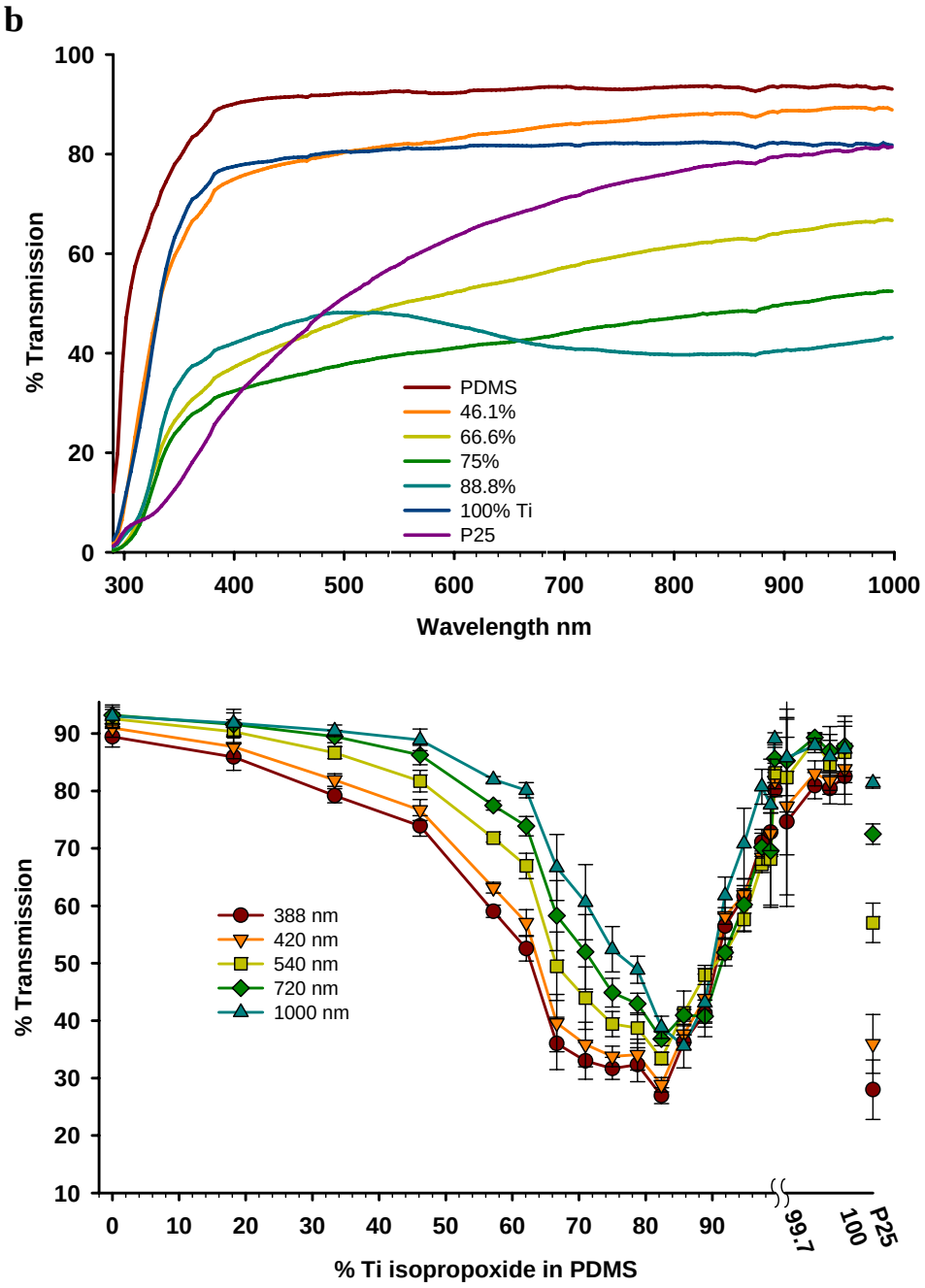

Figure 5.2b: **b**, UV-Visible-IR transmission spectra of coatings (top) for PDMS (red), 46.1% (orange), 66.6% (yellow), 75% (green), 88.8% (cyan), 100% (blue), P25 (violet) and selected wavelengths as a function of Ti-iso concentration (bottom), 388 nm (red), 420 nm (orange), 540 nm (yellow), 720 nm (green) and 1000 nm (cyan).

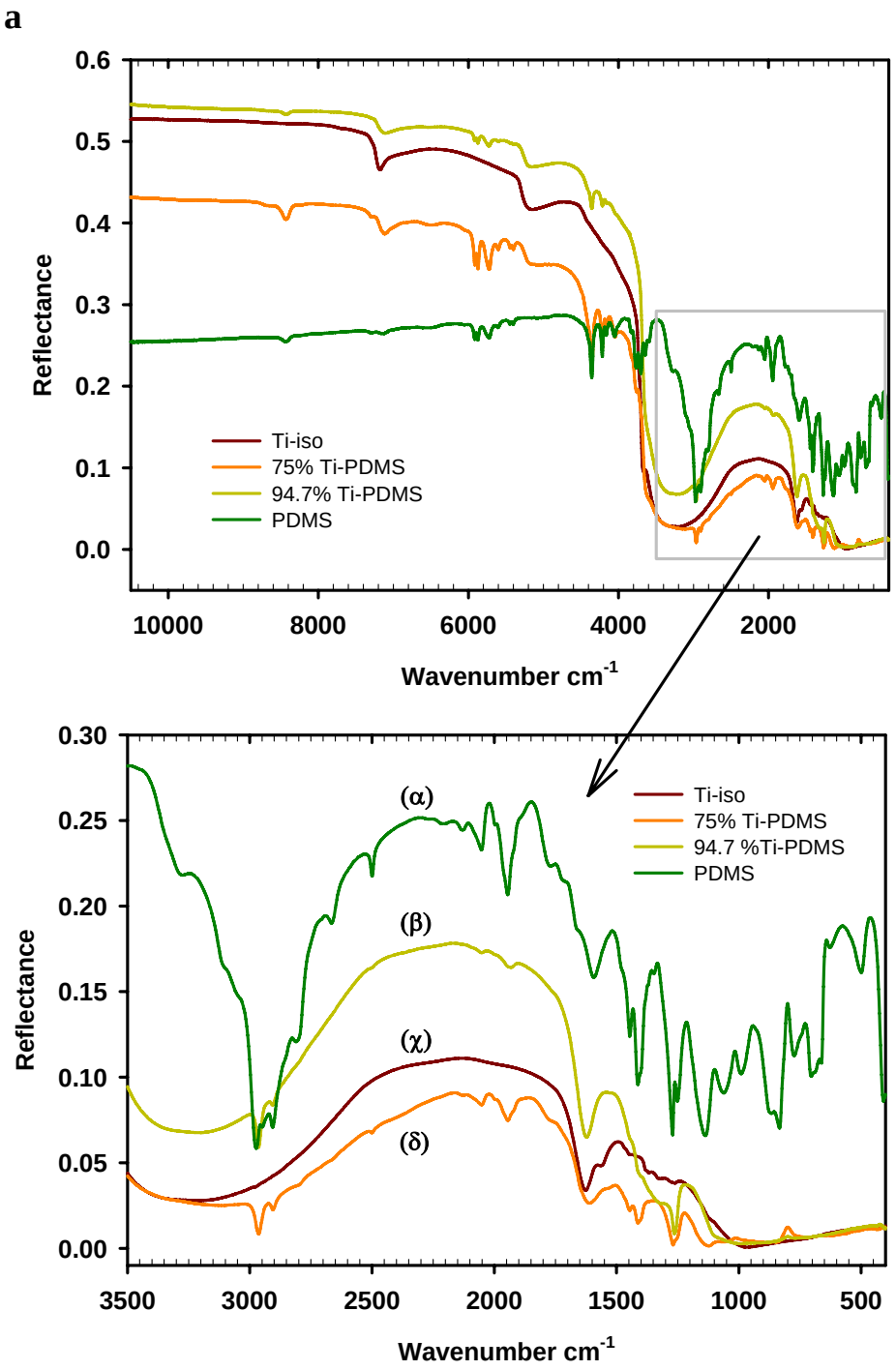

Figure 5.3a: **a**, Near and mid IR reflectance spectra of powders made from coatings; (α) PDMS, (β) 94.7% Ti-PDMS, (χ) 100% Ti-iso, (δ) 75% Ti-PDMS. All FT-IR peaks were associated with either PDMS or titanium oxide.

b

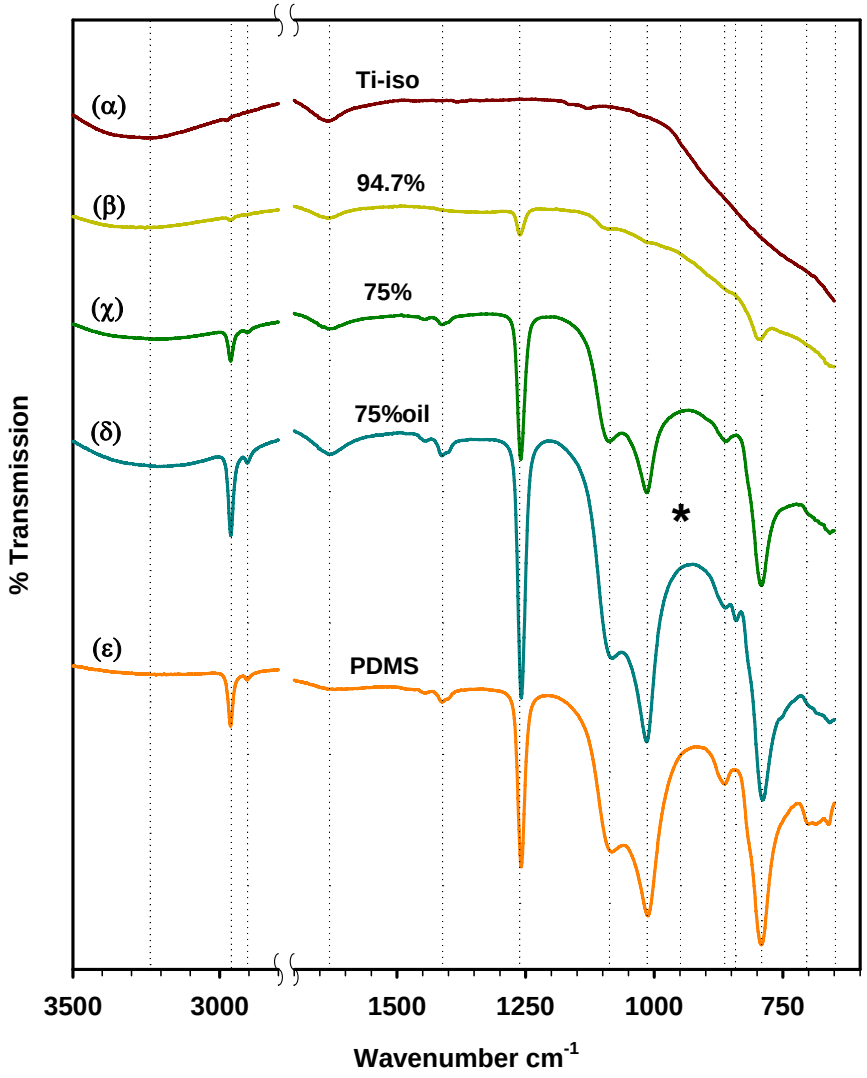

Figure 5.3b: **b**, FT-IR transmission spectra of powders made from coatings. (α)100% Ti-iso, (β) 94.7% Ti-PDMS, (χ) 75% Ti-PDMS, (δ) 75% Ti-silicone oil, (ε) PDMS.
All FT-IR peaks were associated with either PDMS or titanium oxide (Table 5.1). The spike at 950 cm^{-1}, normally associated with Si-O-Ti bonding [ν(Si-O-Ti)], was not observed on any hybrids (*).

c

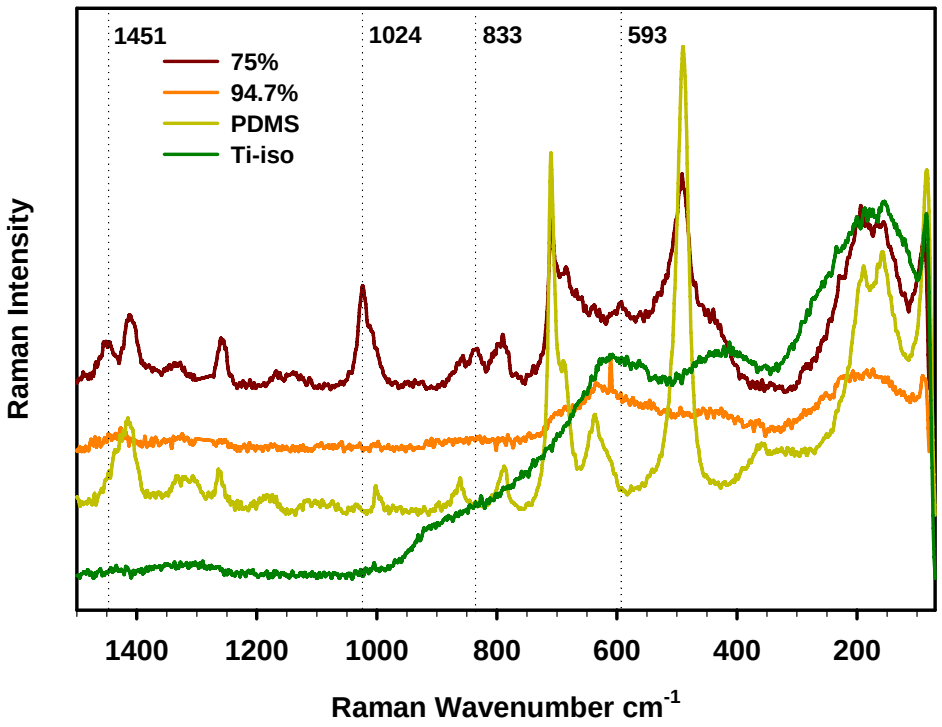

Table 5.1

IR (v/cm^{-1})	Raman	Assignment	Attributed	Source
~3232	-	ν(O-H)	water, hydroxyl	absorbed H_2O & OH
2963	-	ν_a(C-H)	methyl groups	PDMS backbone
2906	-	ν_s(C-H)	methyl groups	PDMS backbone
1635	-	δ(H-O-H)	water molecules	absorbed H_2O
1412	1414	δ_a(C-H)	methyl groups	PDMS backbone
1258vs	1265	δ_s(C-H)	methyl groups	PDMS backbone
1012, ~1083	not active	ν_a(Si-O-Si)	silicon dioxide	PDMS backbone
950	**950**	ν (Si-O-Ti)	stretching Si-O by Ti	**Not observed**
863	863	$\rho_s(CH_3)$	methyl groups	PDMS backbone
792s	788	ν_a(C-Si-C) + $\rho_a(CH_3)$	methyl groups	PDMS backbone
700m	709	ν_s(C-Si-C)	methyl groups	PDMS backbone
650	640,612	(Ti-O-Ti)	titanium oxide	TiO_2
-	637	$\rho_a[Si(CH_3)_3]$	methyl groups	PDMS backbone
not active	**520**	(Si-Si) LO-phonon	Si-Si bond formation	**Not observed**
-	490	ν_s(Si-O-Si)	silicon dioxide	PDMS backbone
vs=very strong, s= strong, m=medium, w=weak, *v*=stretching, δ=bending, ρ=rocking				

Figure 5.3c: **c**, Raman spectroscopy of scraped samples of coatings and tabulated peak assignments for FT-IR and Raman spectroscopy. All Raman peaks were associated with typical bonding of either PDMS or Ti-iso controls except for unassigned lines at 1451, 1024, 833 and 593 cm^{-1} (**Table 5.1**). No peaks, associated with Si-O-Ti bonding (950 cm^{-1}) or Si-Si bonding (520), were observed[28,29].

a

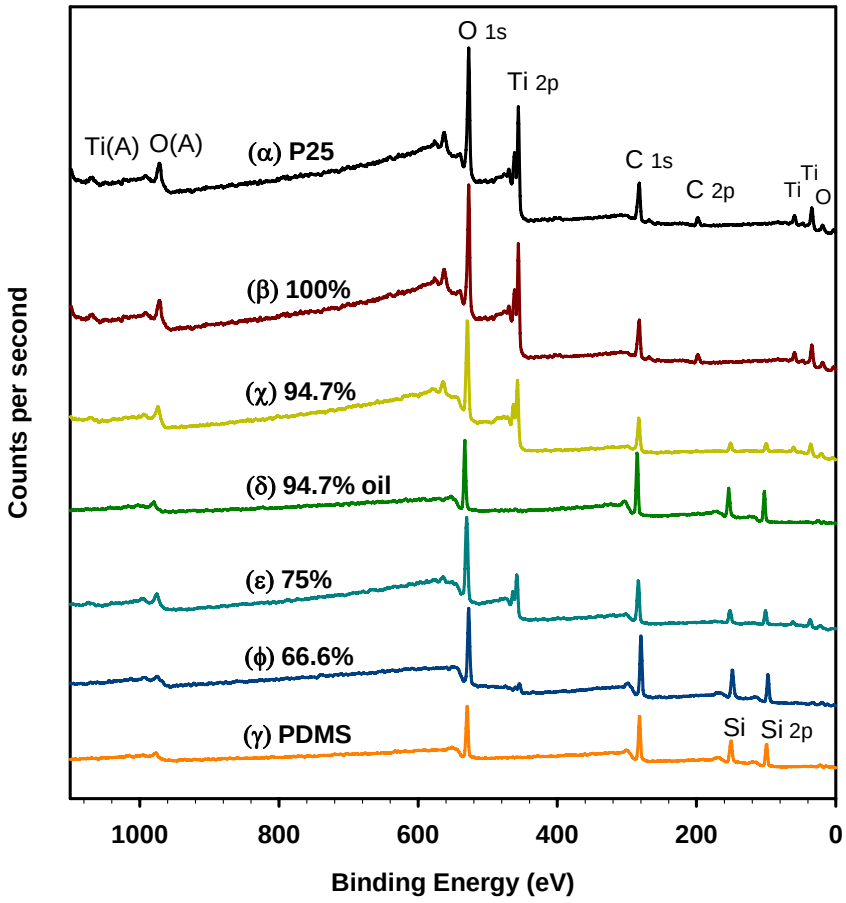

Table 5.2

Sample ID	Atomic % by XPS ~2.6-5.0 nm into surface					
	Ti	Si	O	C	Cl	N
Degussa P25 TiO_2	16.9	-	44.4	33.8	3.1	1.9
100% Ti-iso	18.4	-	47.5	32.5	-	-
94.7% Ti-PDMS	14.2	9.0	41.0	35.8	-	-
94.7% Ti-Oil	0.4	25.4	22.8	51.4	-	-
75% Ti-PDMS	8.6	13.4	36.1	41.8	-	-
66.6% Ti-PDMS	1.6	23.3	26.3	48.7	-	-
PDMS	-	24.4	24.2	51.4	-	-
PDMS (theoretical)	-	25	25	50		

Figure 5.4a: **a**, XPS spectra of coatings on plastic slides and tabulated surface chemical composition. (α) Degussa P25 TiO_2, (β) 100% Ti-iso, (χ) 94.7% Ti-PDMS, (δ) 94.7% Ti-silicone oil, (ε) 75% Ti-PDMS, (ϕ) 66.6% Ti-PDMS, (γ) PDMS. **Table 5.2**, Surface chemical analysis of coatings by XPS indicates silicon concentration is elevated at surface compared to theoretical bulk compositions, especially for silicone oil hybrid. Atomic ratio of Ti to Si for 94.7% Ti-PDMS was 1.57:1 and 0.016:1 for 94.7% Ti-silicone oil (measured at surface) compared to 5.07:1 (~ theoretical bulk).

b

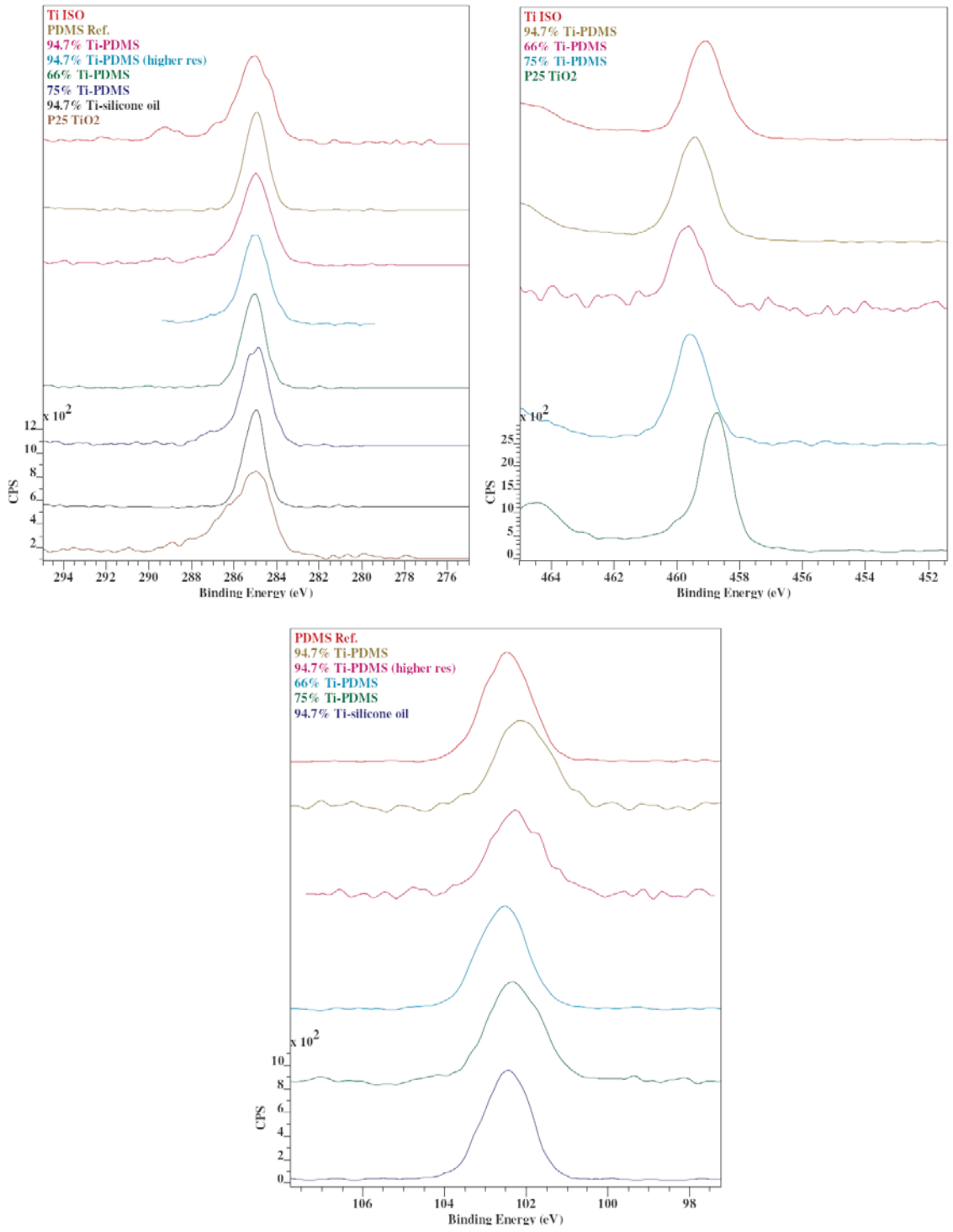

Figure 5.4b: **b**, High resolution XPS spectrum of coatings. Binding energies of Ti 2p3/2 (458.5-459.5 eV), C 1p (285 eV) and Si 2p (102-102.5 eV) shells are typical of unaltered titanium dioxide, aliphatic hydrocarbon and polydimethylsiloxane bonding, respectively.

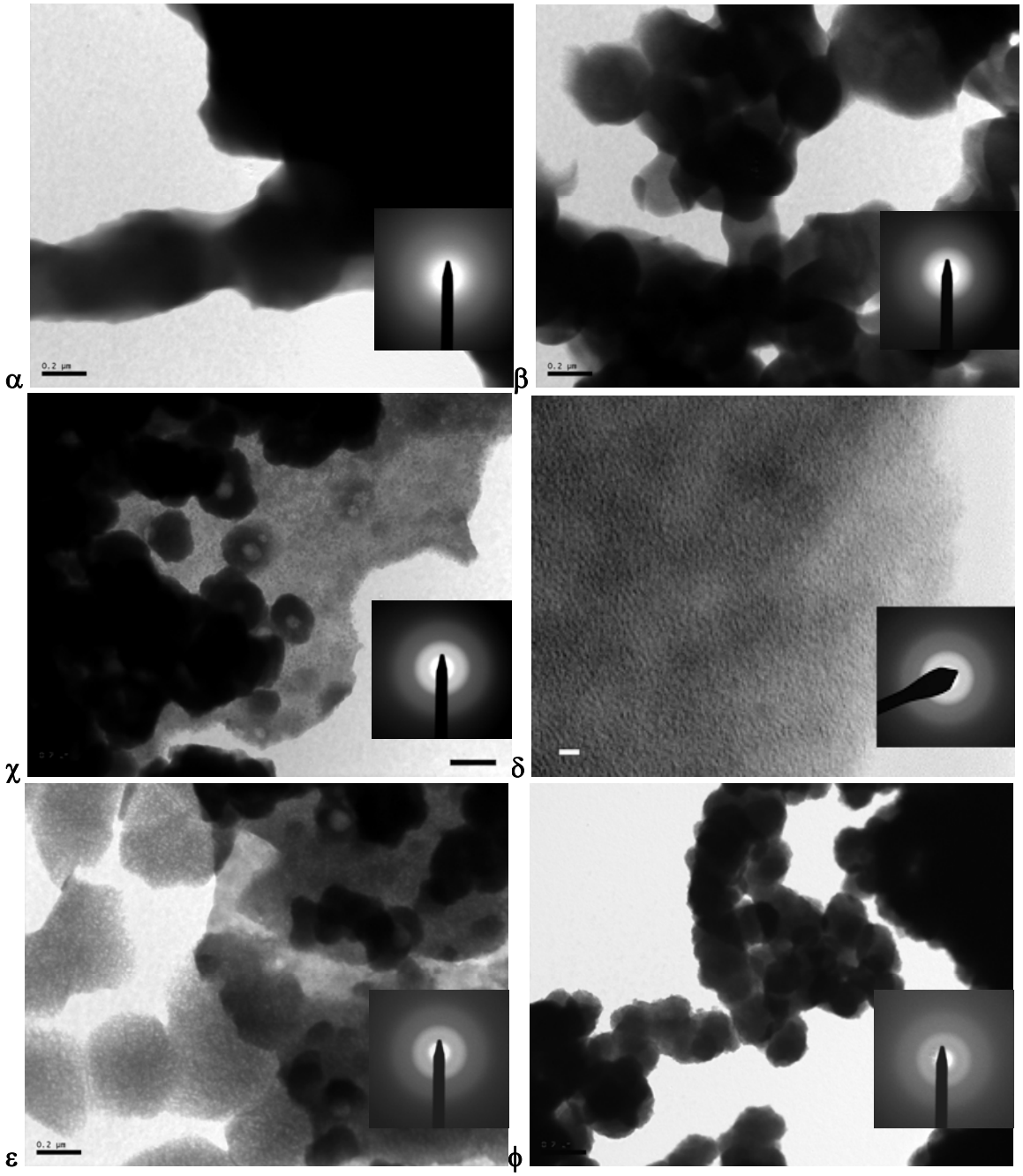

Figure 5.5: Transmission electron microscopy of amorphous Ti-PDMS hybrids indicates presence of sub micron torus structures and nano-phases within microstructure of highly photoactive coatings. α, 46.1% (scale = 200 nm, all except δ); β, 66.6%; χ, 88.8%; δ, 88.9% (atomic resolution scale = 1 nm); ε, 94.7%; ϕ, 100% Ti-iso, indicating regular, but crystallographically amorphous structures, confirmed by the accompanying electron diffraction patterns (insets), which lacks distinct rings indicative of crystallinity.

5.6 References

1. Akira Fujishima, Kenichi Honda. Electrochemical photolysis of water at a semiconductor electrode. *Nature* **238**, 37-38 (1972).

2. Anders Hagfeldt, Michael Grätzel. Molecular photovoltaics. *Acc. Chem. Res.* **33**(5) 269 -277 (2000).

3. Kazuhito Hashimoto, Hiroshi Irie, Akira Fujishima. TiO_2 photocatalysis: A historical overview and future prospects. *Japanese J. of Applied Physics*, **44**, 8269-8285 (2005).

4. Michael R. Hoffmann, Scot T. Martin, Wonyong Choi, and Detlef W. Bahnemannt. Environmental applications of semiconductor photocatalysis. *Chemical Rev*, **95**, 69-91 (1995).

5. J Blanco-Galvez, P Fernandez-Ibanez, S Malato-Rodriguez. Solar photocatalytic detoxification of water: *Recent Overview. Trans ASME* **129**:4-15 (2007).

6. S. I. Shah, W. Li, C.-P. Huang, O. Jung, and C. Ni. Study of Nd3+, Pd2+, Pt4+, and Fe3+ dopant effect on photoreactivity of TiO_2 nanoparticles. *Proc. Natl. Acad. Sci.*, **99**, suppl. 2, 6482–6486 (2002).

7. R. Asahi, T. Morikawa, T. Ohwaki, K. Aoki, Y. Taga. Visible-light photocatalysis in nitrogen-doped titanium oxides. *Science*, **293,** 269-271 (2001).

8. Hiroaki Tada, Tomohiro Mitsui, Tomokazu Kiyonaga, Tomoki Akita, Koji Tanaka. All-solid-state Z-scheme in CdS–Au–TiO_2 three-component nanojunction system. *Nature Materials* **5**, 283-286 (2006).

9. RMP Doornbos, R Lang, MC Aalders, FW Cross, HJCM Sterenborg. The determination of the in vivo human tissue optical properties and absolute chromophore concentration using spatially resolved steady-state diffuse reflectance spectroscopy. *Phy. Med. Biol.* **44**, 967-981 (1999).

10. B Chance, M Cope, E Gratton, N Ramanujam, B Troberg. Review Article: Phase measurement of light absorption and scatter in human tissue. *Rev. Sci. Instrum.* **69**, 3457-3481 (1998).

11. Pin-Chin Manes, Sharon Smolinski, Daniel M. Blake, Zheng Huang, Edward J. Wolfurm, William A. Jacoby. Bactericidal activity of photocatalytic TiO_2 reaction: toward an understanding of its killing mechanism. *Appli. Envir. Micro.* **65**, 4094–4098 (1999).

12. S. Banerjee, Judy Gopal, P. Muraleedharan, A. K. Tyagi and Baldev Raj. Physics and chemistry of photocatalytic titanium dioxide: Visualization of bactericidal activity using atomic force microscopy. *Current Science* **90**,1378-1383 (2006).

13. Wong M-S, Chu W-C, Sun D-S, Huang H-S, Chen J-H, Tsai P-T, Lin N-T, Yu M-S, Hsu S-F, Wang S-L, Chang H-H. Visible-light-induced bactericidal activity of a nitrogen-doped titanium photocatalyst against human pathogens. *Applied and Environmental Microbiology*, 6111-6116 (2006).

14. Yuki Sekiguchi, Yanyan Yao, Yoshihisa Ohko, Katsuyuki Tanaka, Tetsuro Ishido, Akira Fujishima and Yoshinobu Kubota. Self-sterilizing catheters with titanium dioxide photocatalyst thin films for clean intermittent catheterization: Basis and study of clinical use. *International Journal of Urology* **14**, 426–430 (2007).

15. Ulrike P Kappes, Dan Luo, Marisa Potter, Karl Schulmeister and Thomas M Rünger. Short- and long-wave UV light (UVB and UVA) induce similar mutations in human Skin cells. *J. of Invest. Dermatol.* **126**, 667–675 (2006).

16. Stéphane Mouret, Caroline Baudouin, Marie Charveron, Alain Favier, Jean Cadet, and Thierry Douki. Cyclobutane pyrimidine dimers are predominant DNA lesions in whole human skin exposed to UVA radiation. *Proc. Natl. Acad. Sci. U S A* **103**,13765-70 2006.

17. Iketani K, Sun R-D, Toki M, Hirota K, Yamaguchi O. Sol-gel-derived TiO_2/poly(dimethylsiloxane) hybrid films and their photocatalytic activates. *J. Physics and Chem of Solids* **64,** 507-513 (2003).

18. Andrew Mills, Jishun Wang. Photobleaching of methylene blue sensitized by TiO_2: an ambiguous system? *J. of Photochemistry and Photobiology A: Chemistry* **127,** 123–134 (1999).

19. Wang C-C, Ying JY. Sol-gel synthesis and hydrothermal processing of anatase and rutile titania nanocrystals. *Chem. Mater.* **11**, 3113-3120 (1999).

20. Branemark R, Branemark P-I, Rydevik B, Myers R. Osseointegration in skeletal reconstruction and rehabilitation: A review. *J.R.R.D.* **3**, 175-181 (2001).

21. DeNicola RR. Permanent artificial (silicone) urethra. *J. Urol.* **63**, 168-172 (1950).

22. J.D. Jarrell, T.H. Eun, M. Samale, C. Briant, B. Sheldon, J.R. Morgan, Metal oxide coated cell culture arrays for rapid biological screening. *J. Biomed. Mater. Res. A*, **83A**, 853-860 (2007).

23. JD Jarrell, EC Werlin, J.R. Morgan. Biological response to polydimethylsiloxane coatings doped with titanium and vanadium for soft tissue contact, implantation and controlled delivery. (*Biomaterials* Submitted 6 December 2007).

24. Jinho Jung, Jeong-Hyo Yoon, Hung-Ho Chung, Myun-Joo Lee. Radiation treatment of secondary effluent from a sewage treatment plant. *Radiation Physics & Chemistry* **65** 533–537 (2002).

25. JP Zhao, ZY Chen, M Lu, JW Rabalais. Linear optical properties of a Ti-SiO_2 nanoparticle composite. *J. Appl. Phy.* **93**, 566-575 (2003).

26. Dong Jiang, Yao Xu, Bo Hou, Dong Wu, Yuhan Sun. Synthesis of visible light-activated TiO_2 photocatalyst via surface organic modification. *J. of Solid State Chemistry* **180**, 1787–179 (2007).

27. Gole JL, Stout JD. Highly efficient formation of visible light tunable TiO_2-xNx photocatalysts and their transformation at the nanoscale. *J. Phys. Chem*. B **108**, 1230-1240 2004).

28. B Julián, C Gervais, E Cordoncillo, P Escribano, F Babonneau, C Sanchez. Synthesis and characterization of transparent PDMS-metal-oxo based organic-inorganic nanocomposites. *Chem. Mater.* **15**, 3026-3034 (2003).

29. Z Zhao, B Kang Tay, G Yu. Room-temperature deposition of amorphous titanium dioxide thin film with high refractive index by a filtered cathodic vacuum arc technique. *Applied Optics* **43**, 1281-1285 (2004).

30. X Wang , M Fujimaki, and K Awazu. Photonic crystal structures in titanium dioxide (TiO_2) and their optimal design. *Optics Express* **13**, 1486-1497 (2005).

31. G Subramania, K Constant, R Biswas, MM Sigalas, K-M Ho. Optical photonic crystals synthesized from colloidal systems of polystyrene spheres and nanocrystalline titania. *J Lightwave Technol*, **17**(11), 1970-1974 (1999).

Chapter 6

Cellular bioresponse, bacterial growth and photocatalytic analysis of doped titanium oxide and polymer hybrid coatings

John D. Jarrell, Evan C. Werlin, Jeffrey R. Morgan

Department of Molecular Pharmacology, Physiology, and Biotechnology, and the Center for Biomedical Engineering, Brown University, Providence, RI, USA

Abstract

In this study, we used a high throughput platform to investigate the influence of metal-organic silver, zinc, vanadium, aluminum, calcium and phosphorous doping of titanium oxide coatings on the viability, proliferation and adherence of human fibroblasts, keratinocytes and Hela cells. The influence of hydrothermal treatments, previously shown to induce crystallinity, was explored as well as the influence of Ag and Zn doping on *E. coli* proliferation. We also investigated how silver doping influenced the photocatalytic degradation of methylene blue by titanium dioxide and polydimethylsiloxane (PDMS) hybridized titanium coatings in response to monochromatic and broad spectrum irradiation with UV and visible light. We demonstrate that the bioresponse of cells to titanium oxide coatings is influenced by doping and that bacterial growth was greatly reduced or stopped by Ag, but not Zn doping. Hydrothermal heat treatments (65 °C and 121 °C) did not greatly influence cellular bioresponse to titanium coatings. We also show that silver doping improved the photocatalytic activity of titanium oxide coatings, but 6.25% silver hindered the high photoactivity of PDMS hybridized titanium coatings.

Keywords: Polydimethylsiloxane; Titanium oxide; Cell proliferation; Fibroblast; Silver

6.1 Introduction

Both titanium and polydimethylsiloxane (PDMS) have long histories of successful application to medical implants [1-7]. A bioactive surface oxide layer is primarily responsible for titanium's corrosion resistance, biocompatibility, anti-inflammatory and osseointegrative properties [8-17]. The bioinert properties of PDMS come from the strong chemical bonds between silicon, oxygen and carbon, which are stable up to 400 °C, allowing autoclave sterilization, and preventing chemical decomposition under most physiological conditions [18,19]. Wet chemistry techniques allow the application of well adherent titanium oxide-based coatings to various substrates for medical applications [20-23], which may be left amorphous or transformed to crystalline phases by high heat or hydrothermal treatments [24,25]. Silver compounds have been used on, wounds, burns, dressings and catheters to provide broad spectrum protection against bacteria, yeasts and biofilms [26-29].Vanadium oxide compounds have been found to synergistically mimic insulin, have anti-diabetic effects [30-32] and improve soft tissue healing [33-38]. Low doses of vanadium compounds can increase fibroblast proliferation, while high doses inhibit proliferation and cell spreading [39-42]. Some forms of titanium dioxide show antimicrobial photocatalytic activity in response to light [43].

In this study, we created unique binary and tertiary hybrid coatings formed from the co-hydrolysis and polycondensation (copolymerization) of various concentrations of titanium tetraisopropoxide or titanium n-butoxide with metal-organic precursors for silver, zinc [44-46], vanadium, aluminum, calcium and phosphorous and active linear PDMS or silicone oil, diluted in mixed organic solvents without the addition of water, acids or bases. High throughput methods were developed for rapidly screening the bioresponse of

mammalian cells (human fibroblasts, keratinocytes and Hela cells), the antimicrobial effect (*E. coli*) and the photoactivity using coatings applied directly to polystyrene and polypropylene microplates [47-49].

6.2 Materials and Methods

6.2.1 Materials

To make Ti-iso stock solutions 10 ml of titanium isopropoxide 99.999% (Sigma-Aldrich, St. Louis, MO) was added to 100 ml of isopropanol >=99.8% (Riedel-de Haën, Seelze, Germany) and mixed by brief shaking. To make Ti-bu stock solutions, 10 ml of titanium n-butoxide (Sigma-Aldrich) was added to 100 ml of toluene. Silver stock solutions consisted of 10 ml of 25% silver neodecanoate in xylene (Gelest, Morrisville, PA) in 100 ml of isopropanol (for hydrids) or toluene (for Ti-bu doping). Zn-neo stock solutions were make by adding 5gm of 95% zinc neodecanoate (Gelest) in 100 ml of toluene and stirring overnight. To make 10% and 20% aluminum solutions, 0.06 and 0.12 gm of aluminum isopropoxide were added to the toluene solution, while 0.07 and 0.14 gm were added to the isopropanol solution. To make 10% and 20% vanadium solutions, 0.1 and 0.2 gm of vanadium oxytripropoxide were added to the toluene solution, while 0.12 and 0.24 gm were added to the isopropanol solution. To make 10% calcium solutions, 69.4 mg of calcium nitrate hydrate was added to the toluene solution, while 83.1 mg was added to the isopropanol solution. To make 10% phosphorus solutions, 53.5 mg of triethyl phosphate was added to the toluene solution, while 64.1 mg was added to the isopropanol solution. The 10% calcium plus phosphorus solution had 10% of each precursor added.

A PDMS stock solution was made by adding 10 ml of Dow Corning MDX4-4159, 50% Medical Grade Dispersion into 100 ml of 70 % hexanes/30% isopropanol (vol/vol) and mixed by brief shaking at room temperature. This PDMS was supplied as a dispersion of 50% silicone in a co-solvent system of 70% Stoddard Solvent (mineral spirits) and 30% isopropanol. This amine functional polymer also incorporates reactive methoxy- groups that generally polymerizes in contact with moisture to form thin coatings. Stock solutions were allowed to age a minimum of one hour at room temperature and briefly shaken before use.

These stock solutions were added together in a separate glass container using a pipette to make metal-organic or hybrid stock solutions of specific compositions and briefly shaken before use. Hybrid coating compositions are identified by vol % precursor to precursor (or PDMS), excluding all volatile solvents. To make TiO_2 particle dispersion solutions, 2.632 gm of Degussa Aerogel P25 (Evonik Degussa Corporation, Parsippany, NJ) or ultrafine TTO-51 (Ishihara Sangyo Kaisha, LTD, Japan) was mixed in 100 ml isopropanol to give an atomic Ti concentrations equal to 66.6% Ti-PDMS. Tertiary coatings are reported as vol % of metal-organic silver solution per volume of titanium-PDMS hybrid solution

6.2.2 Preparation of coatings

Metal-organic coatings were applied directly to the bottom of polystyrene or polypropylene 96-well tissue culture microplates (Corning Costar, Lowell, MA) under a fume hood. Using an multi-channel pipette, 20 μl of solution was pipetted into each well of the microplate. After each filling, the plate was inverted and briefly shaken out to

remove excess solution before filling the next column of wells. Four to eight replicates of 23 to 11 different coatings plus non-alloyed titanium oxide xerogel and non-coated wells controls were used in each plate. The microplates were air-dried face up, without lids, under a chemical hood for 12 to 24 hours. Subsequently, they were heat treated in air on a hot plate (Dataplate, Barnstead/Thermolyte, Dubuque, IA) at 95 °C for one hour with the lids in place. Hydrothermal heat treatment consisted of 24 hr at 65 °C and 100 % humidity or autoclave steam sterilization for 1 hr at 121°C and 20 psi.

6.2.3 Cell viability and proliferation assays

Normal human dermal fibroblasts (NHFB) were derived from neonatal foreskins, obtained at the Women & Infants Hospital of Rhode Island, Providence, RI, USA (approved by the Institutional Review Board). Foreskins were trimmed with scissors to remove excess fatty tissue, rinsed repeatedly with sterile phosphate buffered saline (PBS) (Invitrogen Corporation, Carlsbad, CA), and diced into small fragments. The fragments were allowed to adhere to the bottom of a tissue culture plate in a humidified 10% CO_2 atmosphere, at 37 °C for 1 hour, and were covered with Dulbecco's Modified Eagle Medium (DMEM) (Invitrogen Corporation) supplemented with 20% fetal bovine serum containing 100U of penicillin and 100μg of streptomycin per ml. Over a period of 14 days, fibroblasts migrated from the tissue fragments and formed a confluent layer on the culture plate. Fibroblasts were harvested with a 0.05% trypsin/0.53 mM EDTA solution and subcultured to near confluence in Human Fibroblast Medium (HFM) consisting of DMEM containing high glucose, L-glutamine, pyruvate and pyridoxine hydrochloride (Invitrogen Corporation) with additions of 10% fetal bovine serum and 1% penicillin-

streptomycin. Alternately, Hela cells, a cervical cancer line, were grown and subcultured as above. Cells (NHFB or Hela) were detached using 0.05% trypsin/0.53 mM EDTA for 3 minutes and re-suspended in serum containing medium. The cells were seeded onto 96 well microplates at a density of 5,000 cells per well in 100 µl of HFM.

Normal human epidermal keratinocytes (NHEK) derived from a single neonatal foreskin were purchased from Cambrex (Lot# 5F1310, Cambrex Bio Science Walkersville, Inc., Walkersville, MD) and grown up according to Clonetics® Epidermal Keratinocyte Cell Systems instructions, using Cambrex keratinocyte growth medium (KGM) at 5% CO_2 atmosphere and 37 °C to near confluence before subculture. Cells were rinsed with HEPES buffered saline solution (HEPES-BSS, Cambrex) and detached using 0.025% trypsin/0.53 mM EDTA for 3-6 minutes, quenched with trypsin neutralizing solution (Cambrex), centrifuged and re-suspended in HGM. The cells were seeded onto 96 well microplates at a density of 5,000 cells per well in 100 µl of HGM.

To measure viability of cells, seeded microplates were seeded with 5,000 cells and incubated at 37 °C with 10 % (NHFB and Hela) or 5% (NHEK) CO_2 for 24 hours, rinsed with PBS with 100 mg of CaCl and 100 mg MgCl+6H_2O per liter added (complete PBS) (Invitrogen Corporation) and incubated in 100 µl of complete PBS with 2 mM dextrose and 1 µg/ml calcein-AM (Molecular Probes, Inc., Eugene, OR) for 30 minutes at 22 °C.

Plates were read using a fluorescent microplate reader (SPECTRAmax® GEMINI XS Dual-Scanning Microplate Spectrofluorometer with SOFTmax PRO software, Molecular Devices Corporation, Sunnyvale, CA) set to 485 nm excitation, 535 nm emission. Five replicates with three cell-free controls were used for each coating type and the polystyrene plate bottom. Calibration curves were previously established for cell number

versus fluorescence on polystyrene and used to select a seeding density within the linear portion of the calibration curve.

To measure cell proliferation, seeded microplates were incubated at 37 °C with 10 % (NHFB and Hela) or 5% (NHEK) CO_2 for 48 hours, after which 10 μl of WST-1 (Roche Applied Science, Indianapolis, IN) was added into each well and incubated for 3 hours at 37 °C. The microplates were quantified using a microplate reader for absorbance at 440 nm (SPECTRAmax® PLUS 384 Microplate Spectrometer with SOFTmax PRO software, Molecular Devices Corporation, Sunnyvale, CA) and plotted. Five replicates with three cell-free controls were used for each coating type and the polystyrene plate bottom. Plates were also inspected under optical microscopy for cell spreading and morphology. Calibration curves were previously established for cell number versus optical density on polystyrene. Seeding density for the cell type was chosen within the linear portion of the calibration curve.

6.2.4 Centrifugation cell adhesion assay

To characterize cell attachment and adhesion of the coatings, a modification of a previous reported method was used [50,51]. Cells were grown in 500 cm^2 triple flasks to near-confluence, rinsed with complete PBS and incubated in 45 ml of 1 μg/ml calcein-AM in complete PBS with 2 mM dextrose for 30 minutes at 22 °C. Cells were detached using 0.05% trypsin and 0.53 mM EDTA for 3 minutes and re-suspended in growth medium. Cells were centrifuged at 500 rpm for 5 minutes and re-suspended in PBS dextrose, centrifuged again and re-suspended in PBS dextrose. The cells were then seeded onto microplates at a density of 10,000 cells per well and left to attach for one hour at 22 °C.

Calibration curves were previously established for cell number versus fluorescence on polystyrene and used to select a seeding density within the linear portion of the calibration curve and to maximize the signal to noise response of the plate reader.

Each well was completely filled with PBS-dextrose and the baseline fluorescence read (485 nm excitation, 535 nm emission). The wells were emptied by inversion to remove floating cells, refilled with PBS-dextrose and read. The microplate was covered with sealing tape (Corning Costar) and centrifuged upside down in a Centra-GP8R Refrigerated Centrifuge (Thermo Electron Corporation, Waltham, MA) using microplate buckets at 500 rpm for 5 minutes. The microplates were again inverted to empty and refilled with PBS-dextrose and read again. For simplicity, we compared the first and last reading to measure the total fraction of initially seeded cell which remained attached after centrifugation. The speed of the centrifuge was selected to remove approximately 50% of the cells from the tissue culture treated polystyrene. Five replicates with three cell-free controls were used for each coating type and the polystyrene (PS) microplate bottom.

6.2.5 Bacterial growth assay

To determine the antimicrobial properties of coatings, bacterial growth rates were determined by monitoring optical density (OD 578 nm) of microplate wells filled with 100 μl of inoculated Luria-Bertani broth (LB). To prepare an inoculation solution, 2 ml of LB was inoculated with 100 μl of thawed HB101 *E. coli* solution with $>10^8$ cfu/μg (Cat. L2011, System Lot 228848, Promega Corp, Madison, WI) and agitated for 6 hr at 37 °C. Serial dilutions (log) of the inoculation solution in LB were pippetted (100 μl) into wells of a non-coated microplate (11 replicates with pure LB controls) incubated at 37 °C

for 24 hrs and growth monitored at OD 578 nm. Readings were taken every 20 minutes with 5 seconds of vibratory agitation before each reading. Growth curves were plotted and the onset of bacterial growth defined as 0.1 OD, approximately the center of the exponential growth phase. A starting dilution of e^{-3} was used on coated microplates (6 replicates and 2 pure LB controls for each coating type) and monitored and compared to control Onsets and growth curves.

6.2.6 Microplate photocatalysis assays

To measure photocatalytic methylene blue (MB) clearance, a high throughput assay was developed using coated 96-well microplates and an optical microplate reader. MB solution (200 μl, 0.3mg/liter in dH_2O, ~$OD664_{nm}$ of 0.5) was pipetted into each well. With microplate lid removed, the $OD664_{nm}$ of MB was pre-read. The wells were exposed to 161 flashes of a selected wavelength (5 seconds between flashes) using the same plate reader in dynamic mode. At the end of irradiation, $OD664_{nm}$ was measured to quantify catalytic MB clearance. Results were plotted as change in $OD664_{nm}$ as a function of irradiation wavelength and coating composition using SigmaPlot 8.0 (Systat Software Inc., San Jose, California, USA).

Alternately, to provide broad spectrum visible light irradiation, the microplates were floated in a cold water bath (< 27 °C) and irradiated with a 250 watt halogen work light (250T3Q, Philips Lighting Company, Somerset, NJ) at a distance of 18 cm, using the attached glass UV filter and 2.5 cm of water in a Pyrex breaker as an IR filter.

UV-Visible-IR transmission spectra on coated microplates were determined from 290 to 1000 nm in 4 nm steps using an optical microplate reader and averaged over 8 replicates of each coating tested.

6.3 Results and Discussion

6.3.1 Cell viability and proliferation assays

To quantify the effects of Ag, Zn, V , Ca and P doping of titanium on mammalian cell viability and proliferation (NHFBs, NHEKs and Helas), we used fluorescent calcein and WST-1 colorimetric assays. After 24 hours, Ag doping of Ti-bu coatings lowered the viability of NHFB in a dose dependant manner, while both hydrothermal and autoclave heat treatments had little influence (Fig. 6.1). Coatings of pure Ti-bu and Ag doping up to 0.4% showed viability equal to or greater than non-coated cell culture polystyrene (PS). NHFBs were more sensitive to Ag concentration on coated polypropylene (PP) microplates. Coating with <0.1% Ag showed higher viability than non-coated PP. After 48 hours, cells showed improved proliferation on Ag doped coatings compared to pure Ti-bu, PS and PP (Fig. 6.2). Hydrothermal treatment had no influence on proliferation with coatings on PS. Cell proliferation was slightly improved by autoclave treatment on coatings with high Ag doping.

Doping of Ti-bu with zinc caused an immediate, but consistent reduction in viability with additions as low as 0.2%, up to 100% zinc for both NHFB and Hela cells after 24 hours (Fig. 6.3). Hela cell proliferation showed a dose dependent response to both Ag and V doping of Ti-bu coatings (Fig. 6.4). Low doses had little influence, but concentrations greater than 0.2% Ag or 1.6% V caused a sharp decrease in proliferation. The viability of

NHEK cells was greatly enhanced on microtextured Ti-iso coatings compared to smooth Ti-bu and those doped with Al, V, Ca, P or Ag (Fig. 6.5). NHEK viability was severely depressed by 3-20% Ag doping as noticed with NHFB. To a lesser extent, reduced viability was seen with 10 and 20% V doping of Ti-iso/Ti-bu. Viability of NHFB was depressed by doping with 10-20% V, but less influenced by Al, Ca or P (Fig. 6.6). Proliferation of Hela cells was generally greater than NHFB on pure and doped Ti-bu coatings (Fig. 6.7). Both cells showed depressed proliferation with 10-20% V and NHFB with 20% Al as well. Both cells were relatively insensitive to 10% Al, C and P doping.

6.3.2 Centrifugation cell adhesion assay

To determine the influence of coatings on 1 hr cell attachment and adhesion under load, a centrifugation cell adhesion assay was used. The adherent fraction of NHEK cells remaining after washing and centrifugation was improved by titanium coatings compared to polystyrene and insensitive to Al, V, Ca, and P doping of both Ti-iso and Ti-bu coatings (Fig. 6.8). Ag doping caused nearly a total loss of adherence. NHEK cells showed similar, but lower adherence to coatings on polypropylene plates (pretreated 1hr autoclave) compared to coated polystyrene plates (Fig. 6.9). This, like the results presented in Fig. 6.1, indicate that the bioresponse of cells to the coatings is influenced somewhat by the substrate. NHFB showed a stronger 1 hr adherence after centrifugation compared to NHEK seeded on the same coatings (Fig. 6.10). The NHEKs, however, were seeded with serum-free (but supplemented) KGB, which may have negatively influenced short-term attachment. The serum used in seeding NHFB, is rich in proteins which assist initial cell attachment.

6.3.3 Bacterial growth assay

The antimicrobial properties of Ag and Zn doped coatings were evaluated from the growth of HB101 *E. coli* (monitored as increase in general turbidity) in microplate wells filled with 100 μl of inoculated Luria-Bertani broth (LB). The Onset time for 0.1 OD 578 nm for bacteria grown on non-coated PS showed a linear relationship for dilutions of e-1 to e-7, when plotted on a log scale (Fig. 6.11). This standardized plot was used to evaluate the influence of Ag and Zn doping of Ti-bu coatings on bacteria growth of an e-3 dilution (Fig. 6.12). Zinc doping from 0.2% to 100% concentration had little to no influence on bacteria proliferation. Low concentrations of Ag had no influence on Onset time, but 7.7% and 20% Ag caused a 5 and 8 log reduction in bacteria. No growth of bacteria was detected on 100% Ag coatings after 24 hrs.

6.3.4 Microplate photocatalysis assay

To measure Ag doping on the photocatalytic clearance of methylene blue (MB), high throughput assays were developed using coated 96-well microplates exposed to either broad spectrum visible light or monochromatic flash irradiation. Silver doping of Ti-bu coatings >1.6% improved photocatalytic degradation of MB, when exposed to full spectrum light from a 250 watt quartz halogen bulb with UV and IR filters (Fig. 6.13). Approximately half of the MB was cleared by coatings doped with 7.7 and 20% Ag after 2 hrs of exposure, while pure Ag and PS showed minimal activity. Some direct photo degradation of MB can occur, explaining the minor loss of OD for non-coated PS and pure Ag coatings. Pure Ti-bu coatings also showed some MB degradation after 1 and 2

hrs of exposure. Earlier studies indicated that Ti-iso showed similar activity to this light source. Pure Ag coatings had a local transmission peak at 335 nm and absorption peak at 435 (Fig. 6.14). The 7.7% Ag coating, which had the highest MB clearance, also absorbed more light than the other Ti-bu coatings.

The doping of Ti-iso with 33.3% PDMS or silicone oil produced a large improvement in photocatalytic activity to monochromatic light irradiation compared to P25 (Fig. 6.15). Under these conditions P25 showed no MB clearance. These results indicate that methoxy and amino terminal groups are not required to induce photoactivity. Ultrafine TiO_2 pigment and Ti-iso also showed no MB clearance when exposed to flash radiation between 388 and 480 nm (Fig. 6.16). TiO_2 pigment (like ultrafine TTO-51) is deactivated with a surface treated of $Al(OH)_3$ during manufacture to limit photo bleaching of paints and similar products [http://www.iskweb.co.jp/functional_e/ISKWEB1-3-PureTitop.htm, 01-21-2008]. The addition of 6.25% Ag to 66.6% Ti-iso-PDMS coatings caused a large, but uniform reduction in photocatalytic activity, in contrast to results seen with Ag doping of Ti-bu.

6.4 Conclusions

In this study, we used a high throughput platform to investigate the influence of metal-organic silver, zinc, vanadium, aluminum, calcium and phosphorous doping of titanium oxide coatings on the viability, proliferation and adherence of human fibroblasts, keratinocytes and Hela cells and influence of Ag and Zn doping on *E. coli* proliferation. We demonstrated that the bioresponse of cells to titanium oxide coatings is highly influenced by doping with Ag and V and to lesser extent by Zn. Doping titanium with 7.7

and 20% Ag resulted in a 5+ and 8 log reduction in bacterial growth, while 100% Ag coatings showed no growth after 24 hours. Zinc doping and pure Zn showed no reduction of *E. coli* growth. Hydrothermal heat treatments (65 °C and 121 °C) did not greatly influence cellular bioresponse to titanium coatings. Silver doping improved photocatalytic activity of titanium oxide coatings, but hindered the high photoactivity of PDMS hybridized titanium coatings. These finding show promise for the production of bioactive, antimicrobial coatings with improved photocatalytic properties.

Acknowledgements

This work was funded, in part, by the VA Rehabilitation Research and Development Center for Restorative and Regenerative Medicine, Department of Veterans Affairs, Providence, Rhode Island.

6.5 Figures

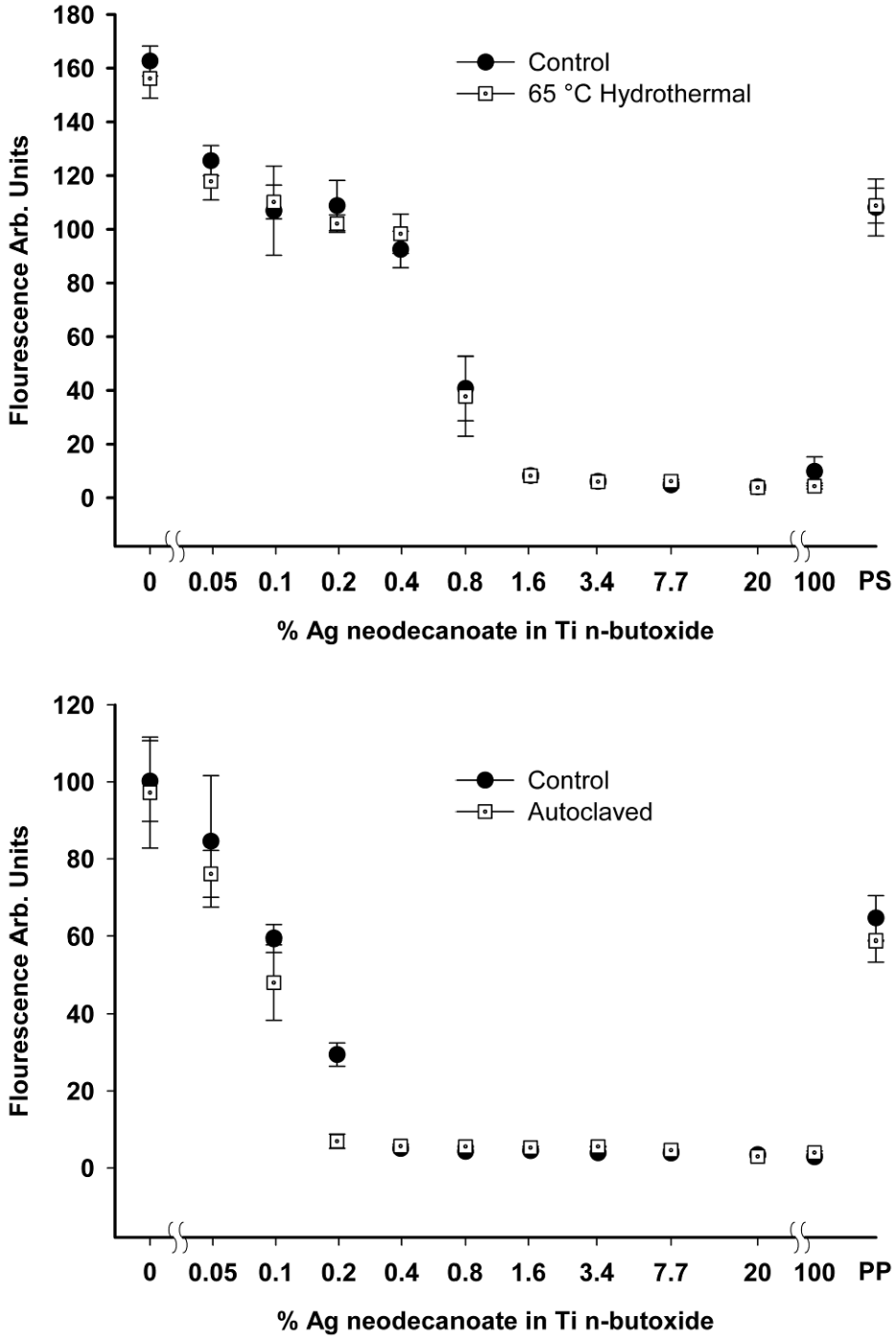

Figure 6.1: Doping titanium coatings with silver influences 24 hr fibroblast viability, but hydrothermal treatments (65 °C and 121 °C) did not. Top, fluorescence of calcein loaded cells as a function of Ag doping of titanium n-butoxide coatings (Ti-bu) and additional 65 °C, 24 hr hydrothermal treatment. Bottom, fluorescence of calcein loaded cells as a function of Ag doping of Ti-bu coatings and additional 121 °C, 1 hr autoclave treatment.

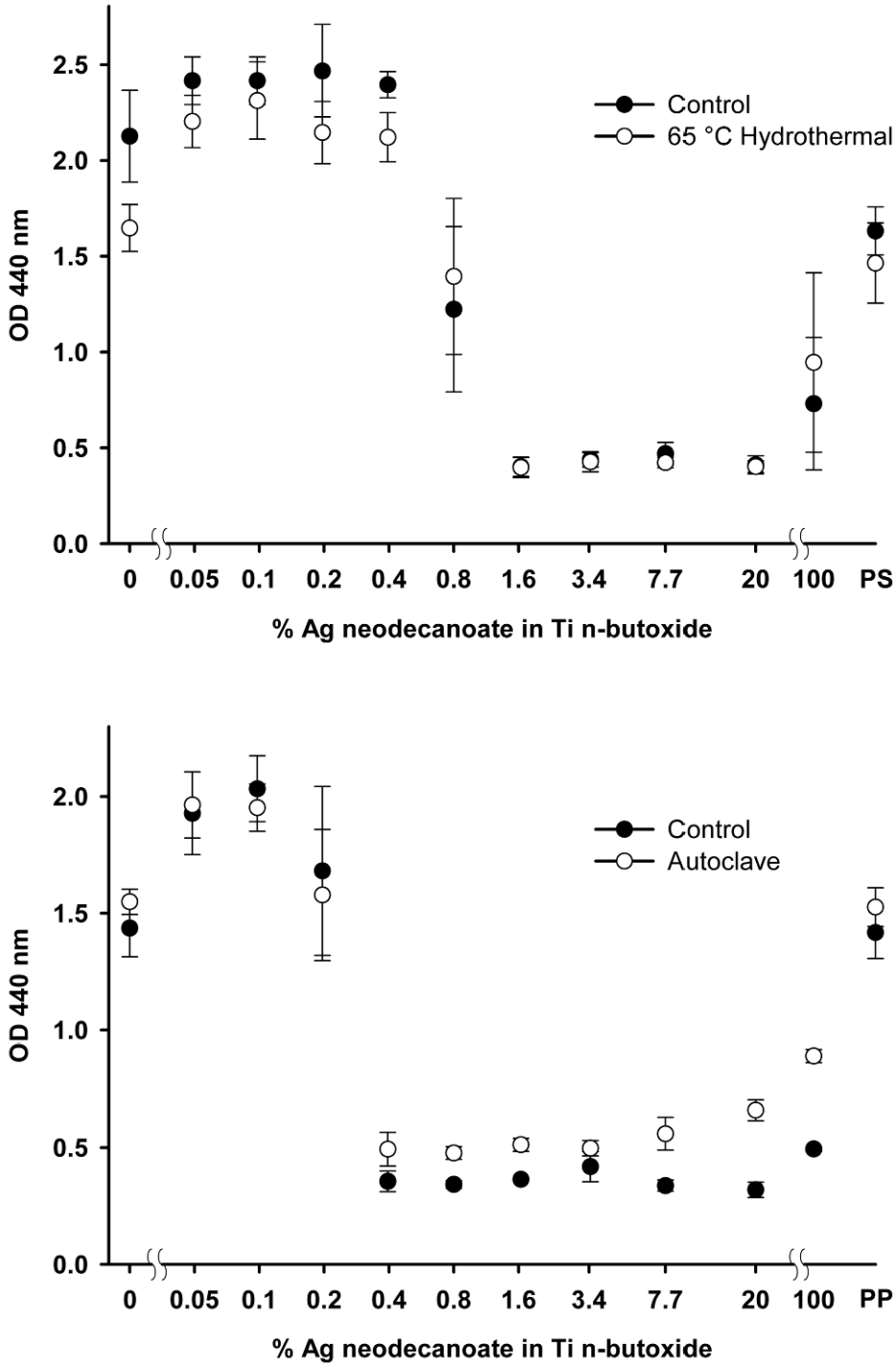

Figure 6.2: Doping titanium coatings with silver influences 48 hr fibroblast proliferation in a biphasic manner. Top, WST-1 colorimetric measurement of cell proliferation as a function of Ag doping of Ti-bu coatings and additional 65 °C, 24 hr hydrothermal treatment. Bottom, WST-1 colorimetric measurement of cell proliferation as a function of Ag doping of Ti-bu coating and additional 121 °C, 1 hr autoclave treatment.

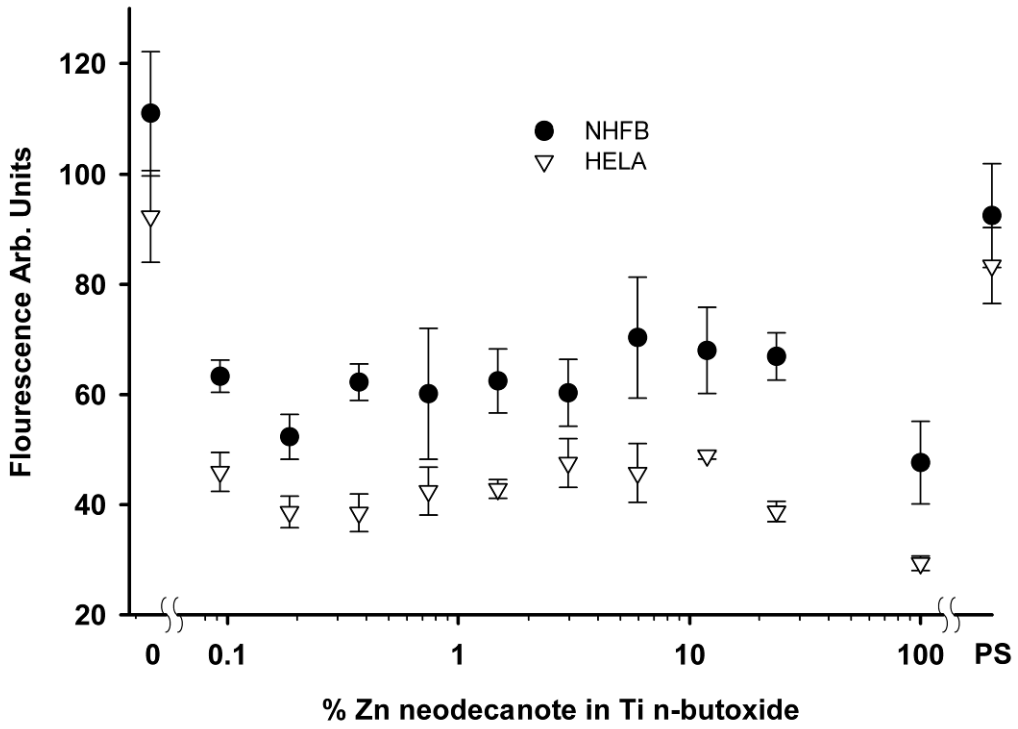

Figure 6.3: Doping of Ti-bu with zinc caused an immediate, but consistent reduction in viability with additions as low as 0.2%, up through 100% zinc for both NHFB and Hela cells after 24 hours.

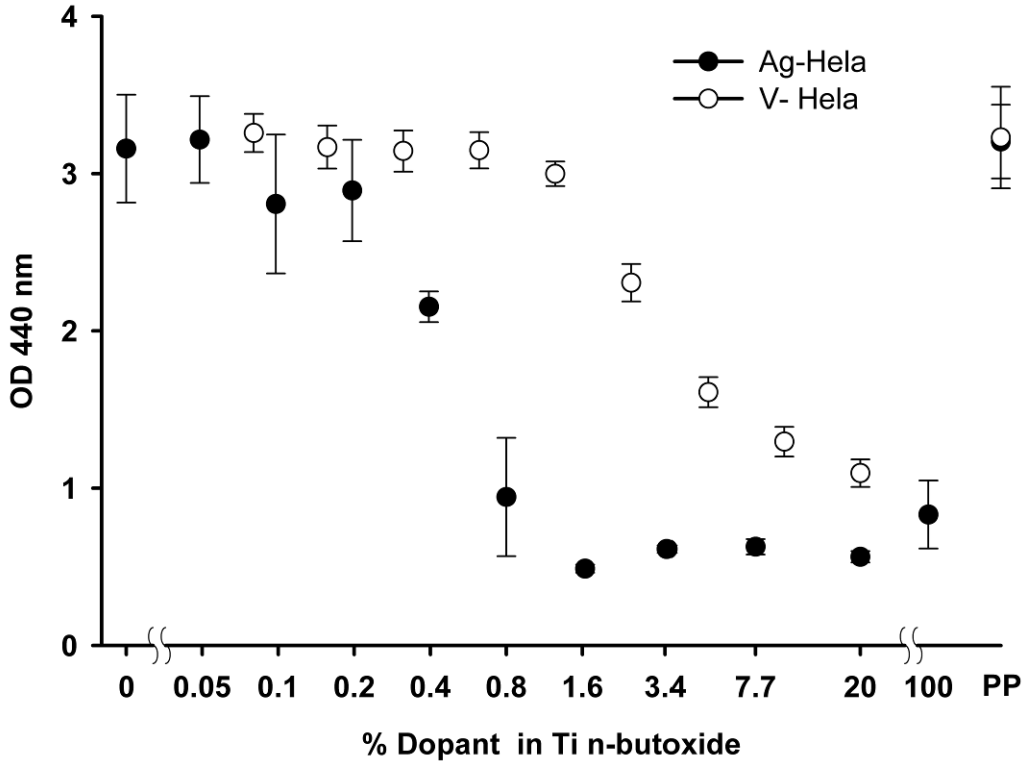

Figure 6.4: Hela cell proliferation showed a dose dependent response to both Ag and V doping of Ti-bu coatings.

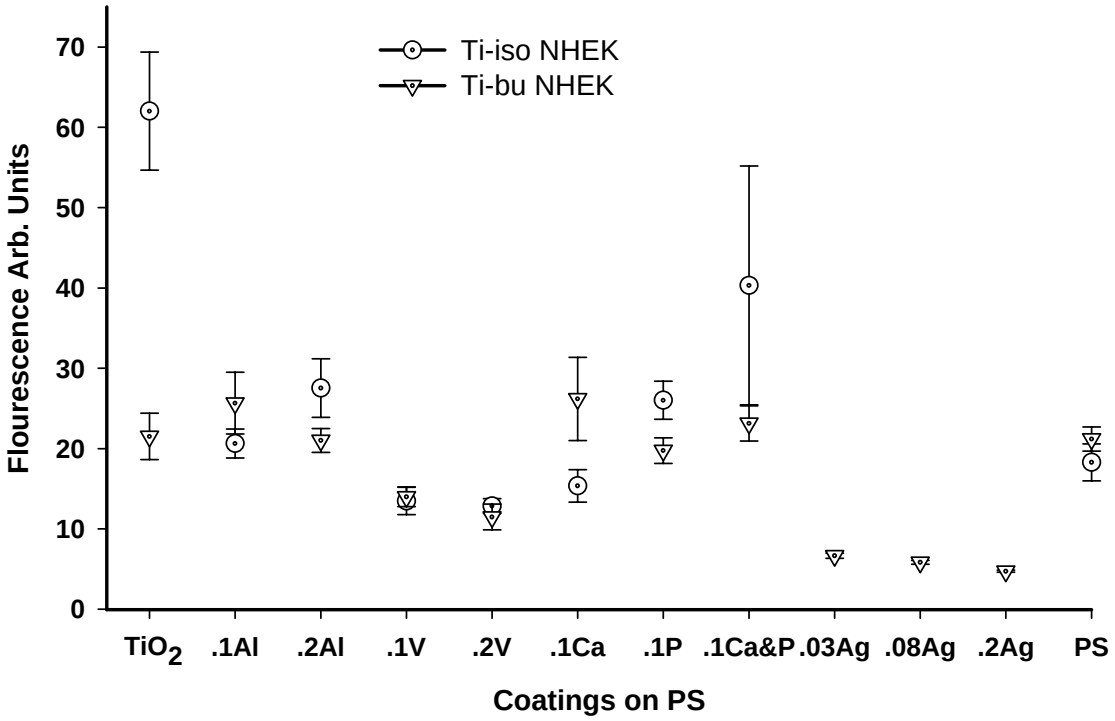

Figure 6.5: The viability of NHEK cells was greatly enhanced on microtextured Ti-iso coatings compared to smooth Ti-bu and those doped with Al, V, Ca, P or Ag. NHEK viability was severely depressed by 3-20% Ag doping as noticed with NHFB. To a lesser extent, reduced viability was seen with 10 and 20% V doping of Ti-iso/Ti-bu.

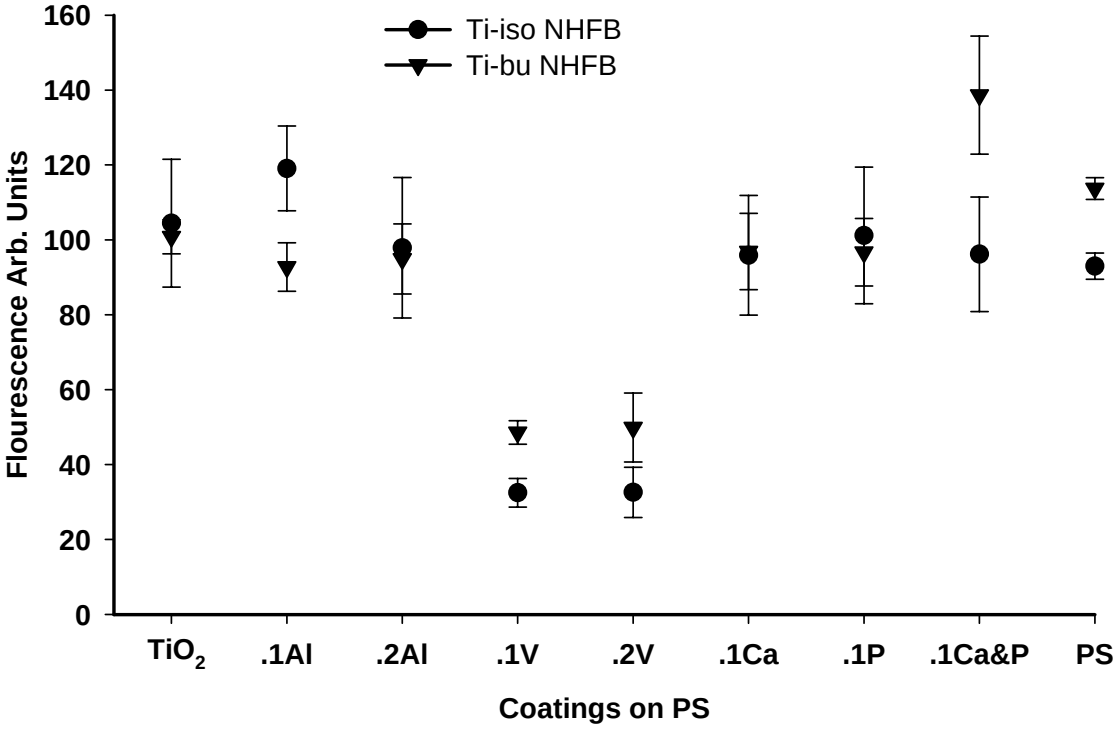

Figure 6.6: Viability of NHFB was depressed by doping with 10-20% V, but less influenced by Al, Ca or P.

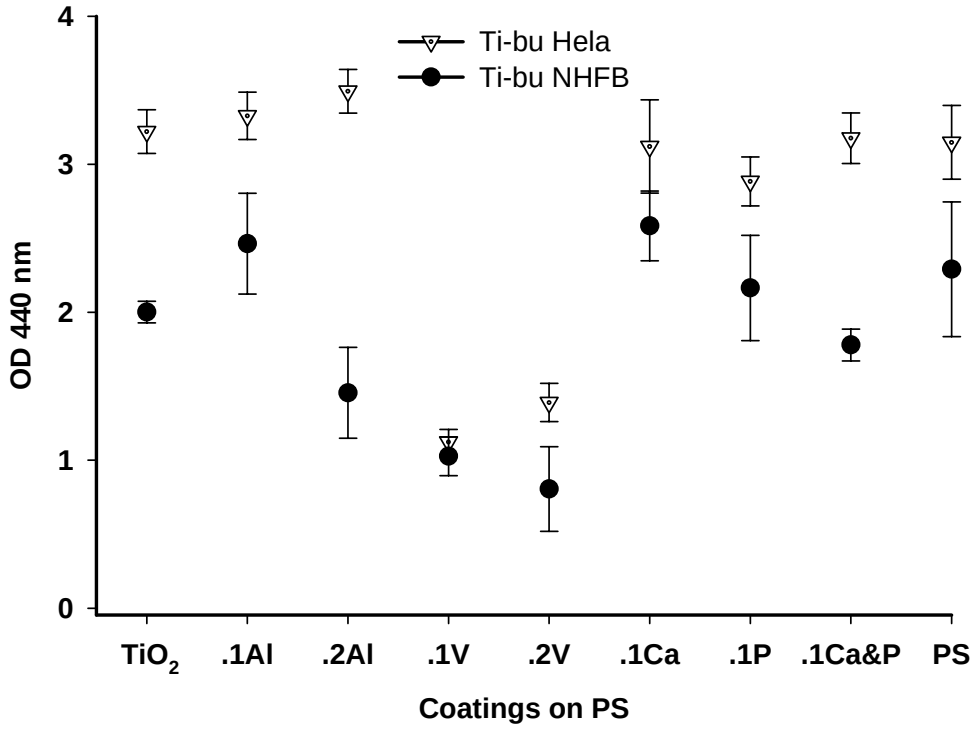

Figure 6.7: Proliferation of Hela cells was generally greater than NHFB on pure and doped Ti-bu coatings.

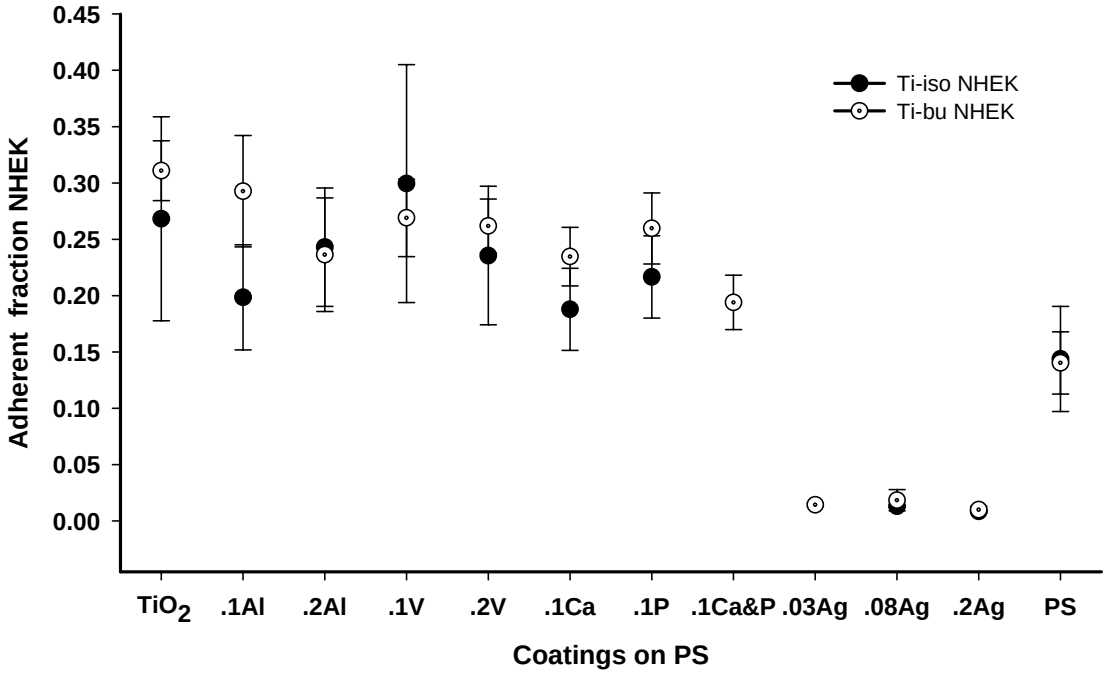

Figure 6.8: The adherent fraction of NHEK cells remaining after washing and centrifugation was improved by titanium coatings compared to polystyrene and insensitive to Al, V, Ca, and P doping of both Ti-iso and Ti-bu coatings. Ag doping caused nearly a total loss of adherence.

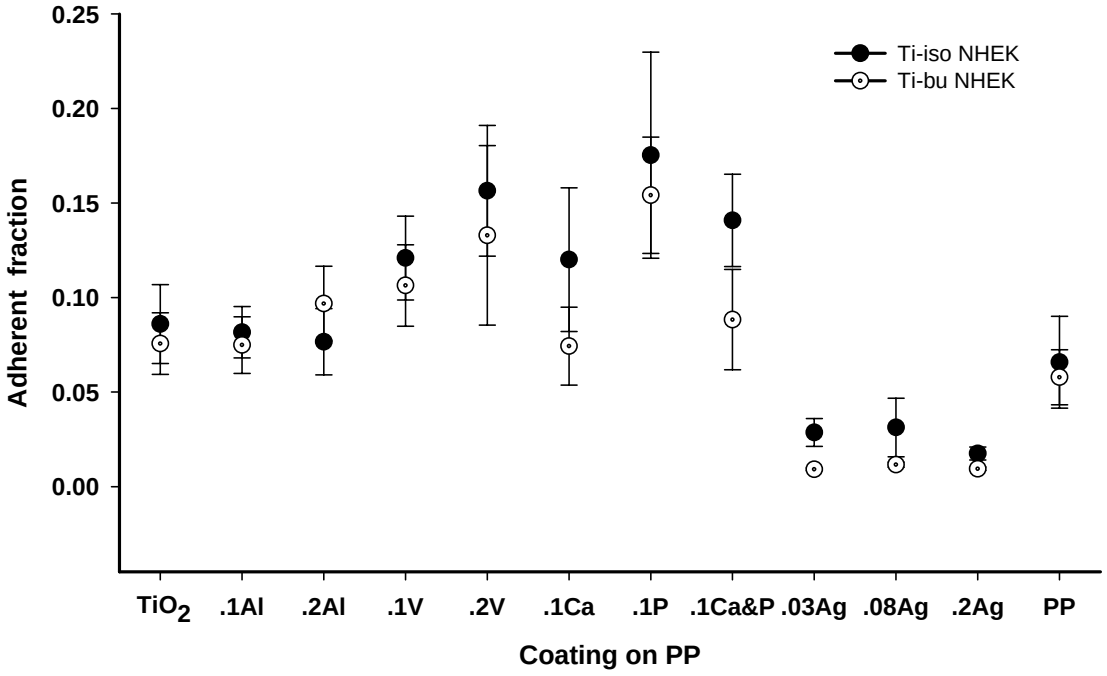

Figure 6.9: NHEK cells showed similar, but lower adherence to coatings on polypropylene plates (pretreated 1 hr autoclave) compared to coated polystyrene plates.

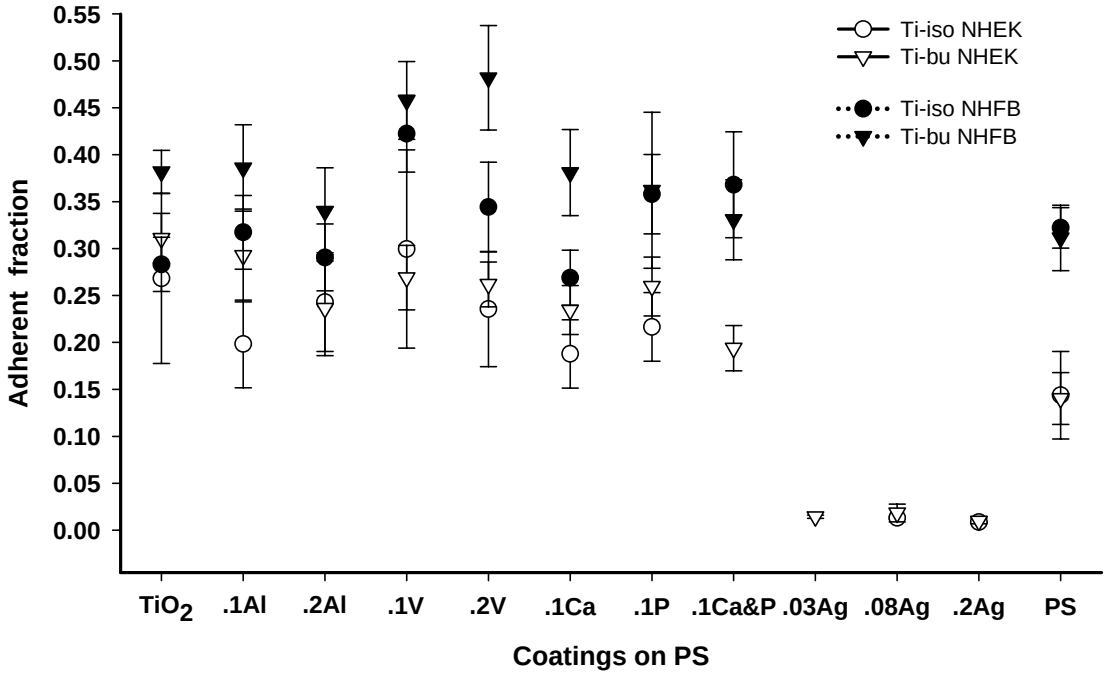

Figure 6.10: NHFB showed a stronger 1 hr adherence after centrifugation compared to NHEK seeded on the same coatings.

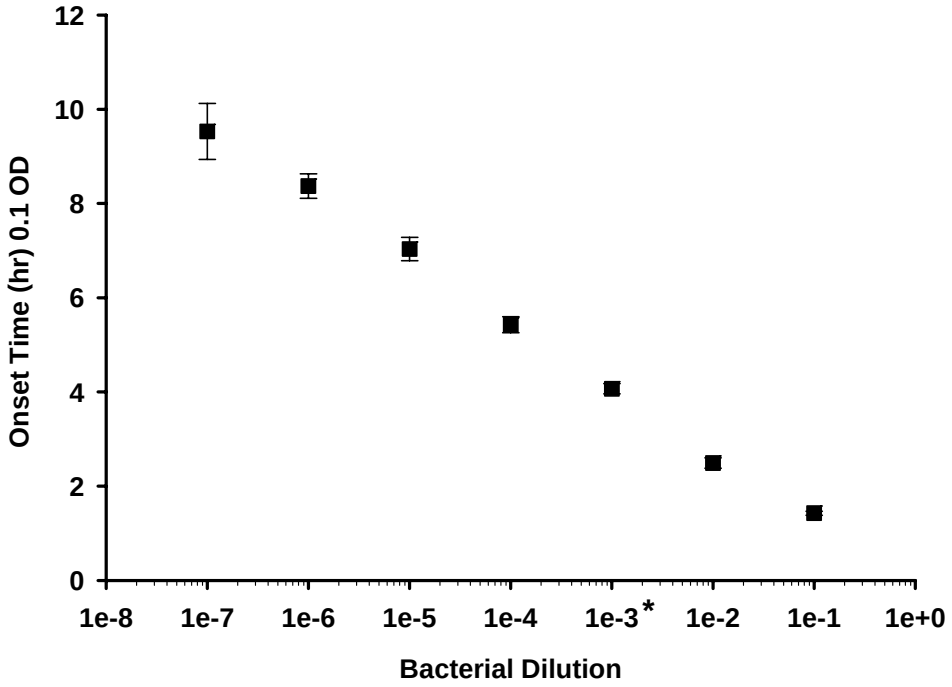

Figure 6.11: The Onset time for 0.1 OD 578 nm for bacteria grown on non-coated PS showed a linear relationship for dilutions of e-1 to e-7, when plotted on a log scale.

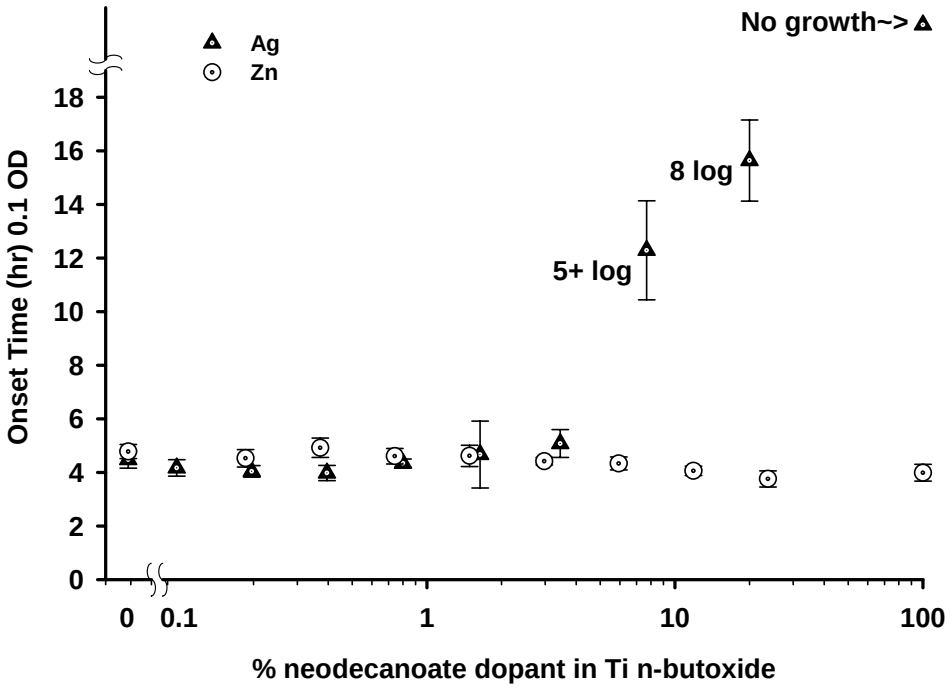

Figure 6.12: Ag doping of Ti-bu coatings slows or stops *E. coli* bacteria growth, but Zn doping did not. Starting bacteria dilution was e-3 of grow up stock.

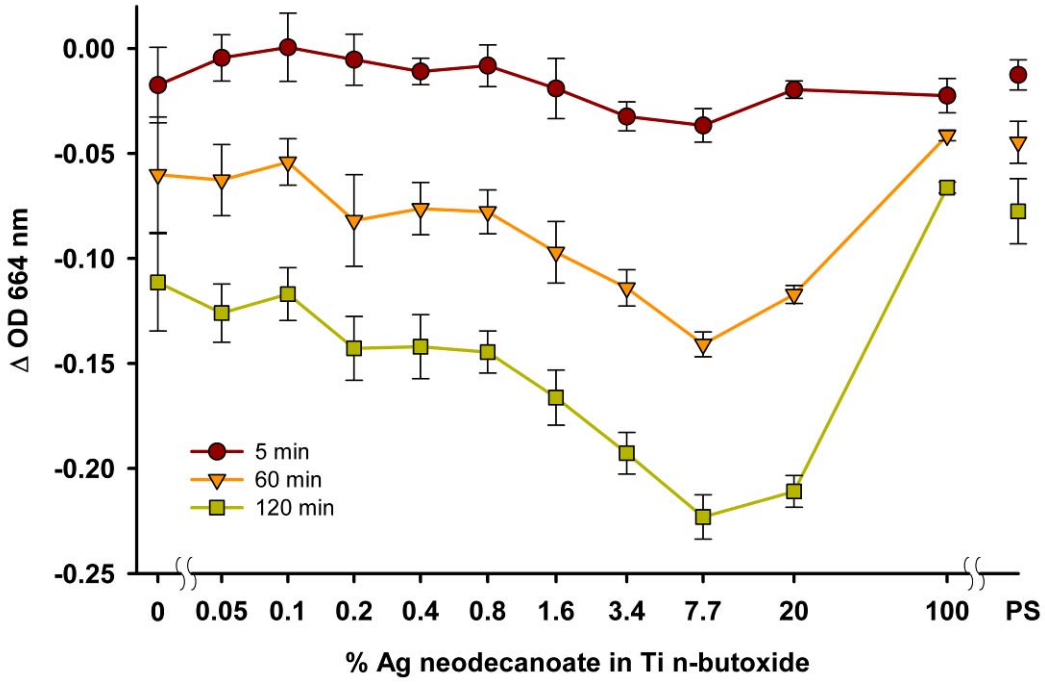

Figure 6.13: Silver doping of Ti-bu coatings >1.6% improved photocatalytic degradation of MB, when exposed to full spectrum light from a 250 watt quartz halogen bulb with UV and IR filters. Clearance of MB determined after 5 min (circles), 60 min (triangles) and 120 min (squares) of light exposure.

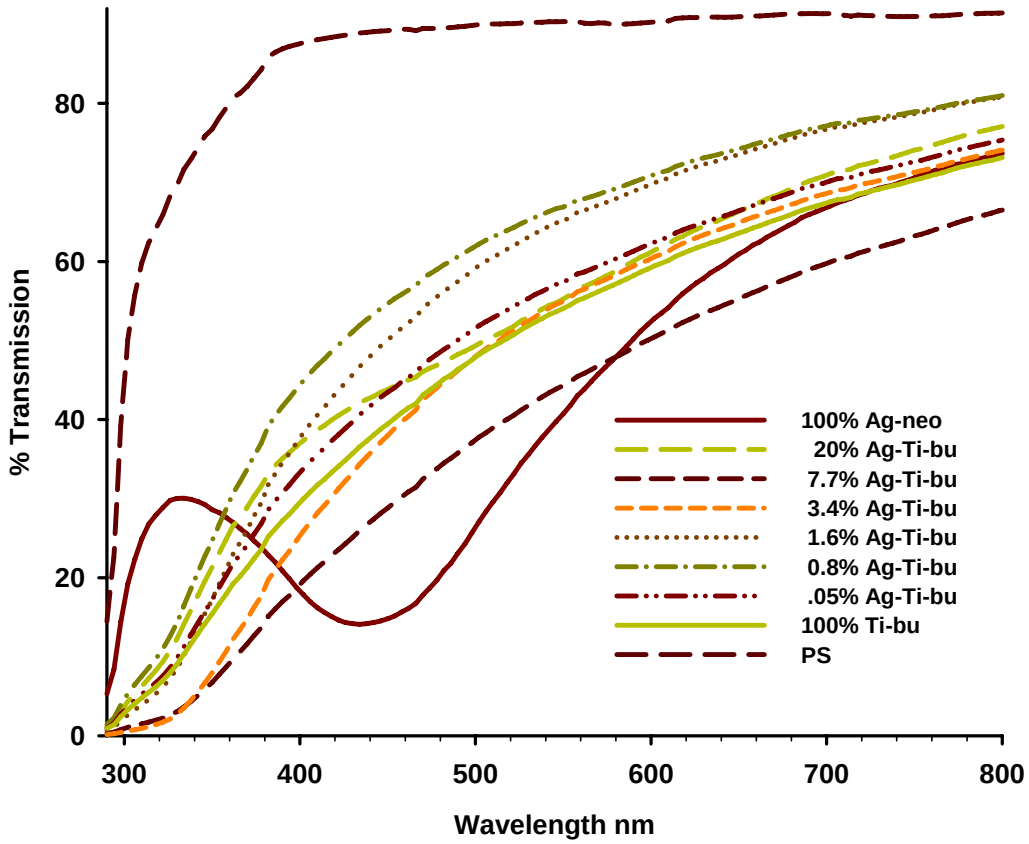

Figure 6.14: Optical transmission spectra of Ag and Ti-bu doped coatings. Pure Ag coatings had a local transmission peak at 335 nm and absorption peak at 435. The 7.7% Ag coating, which had the highest MB clearance, also absorbed more light than the other Ti-bu coatings.

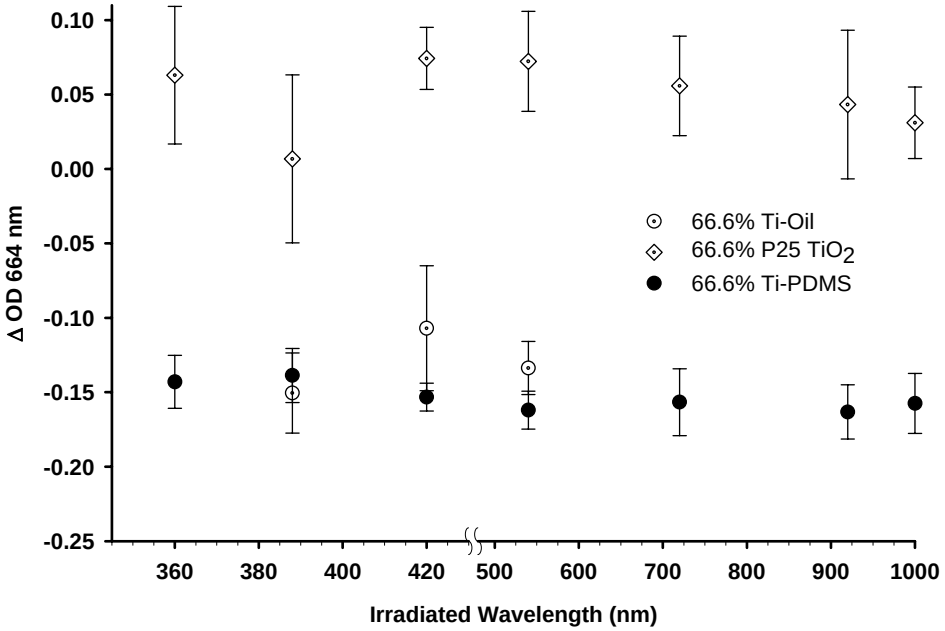

Figure 6.15: Photocatalytic clearance of methylene blue (MB) by coated microplates compared to Degussa P25 TiO_2. The doping of Ti-iso with 33.3% PDMS or silicone oil produced a large improvement in photocatalytic activity to monochromatic light irradiation compared to P25.

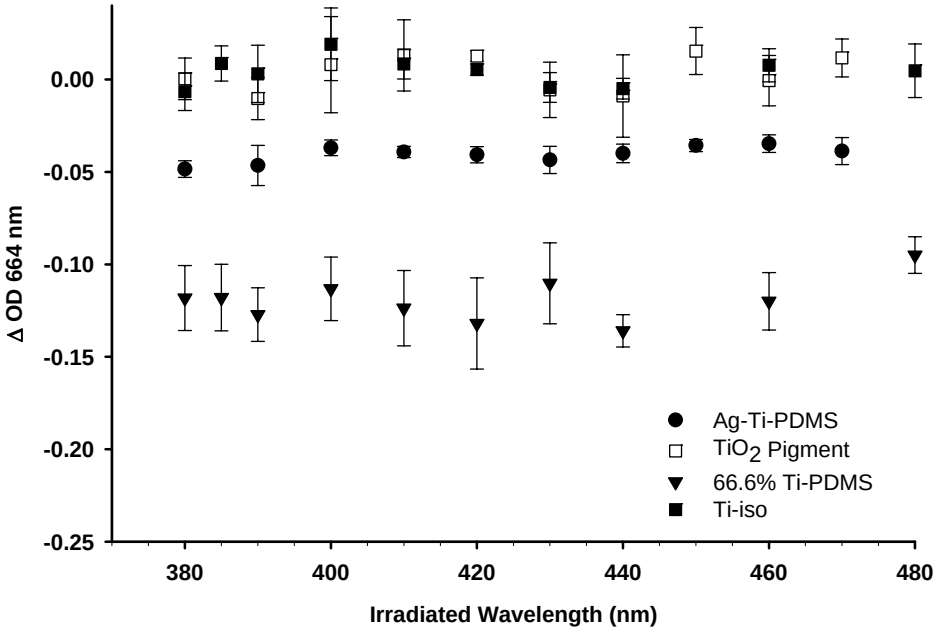

Figure 6.16: Photocatalytic clearance of methylene blue (MB) by hybrid and 6.25% Ag doped hybrid coatings compared to TiO_2 pigment and Ti-iso coatings, showed Ag doping reduced photoactivity.

6.6 References

1. Branemark R, Branemark PI, Rydevik B, Myers RR. Osseointegration in skeletal reconstruction and rehabilitation: a review. J Rehabil Res Dev 2001;38(2):175-181.

2. Lahey FH. Comments made following the speech, "Results from using Vitallium tubes in biliary surgery," read by Pearse HE before the American Surgical Association, Hot Springs, VA. Ann Surg 1946;124:1027.

3. DeNicola RR. Permanent artificial (silicone) urethra. J Urol 1950;63(1) :168-172.

4. LaFay H. A father's last-chance invention saves his son. Reader's Digest, January, 1957; 29-32.

5. Rowe VK. Spencer HC, Bass SL. Toxicological studies on certain commercial silicones and hydrolizable silane intermediates. J Indust Hyg Toxicol 1948;30:332.

6. Curtis J, Colas A. Medical applications of silicones, Biomaterials Science, 2nd Edition: An introduction to materials in medicine. Elsevier, Inc., July 29, 2004;697-706.

7. Hron P. Hydrophilisation of silicone rubber for medical applications. Polym Int 2003;52:1531–1539.

8. Jacobs JJ, Cilbert JL, Urban RM. Current concepts review. Corrosion of metal orthopaedic implants. J Bone Joint Surg Am 1998;80(10):1554.

9. Brunski JB, D.Puleo DA, Nanci A. Biomaterials and biomechanics of oral and maxillofacial implants: current status and future developments. Int J Oral Maxillofac Implants 2000;15(1):15-46.

10. Sundgren JE, Bodo P, Lundstrom I. Auger electron spectroscopic studies of the interface between human tissue and implants of titanium and stainless steel. J Colloid Interface Sci1986;110(1):9-20.

11. Effah EA, Bianco PD, Ducheyne P. Crystal structure of the surface oxide layer on titanium and its changes arising from immersion. J Biomed Mater Res 1995;29(1):73-80.

12. Overgaard L, Danielsen N, Bjursten LM. Anti-inflammatory properties of titanium in the joint environment. An experimental study in rats. J Bone Joint Surg Br1998;80(5):888-893.

13. Kraft CN, Hansis M, Aren S, Menger MD, Vollmar B. Striated muscle microvascular response to silver implants: A comparative *in vivo* study with titanium and stainless steel. J Biomed Mater Res 2000;49(2):192-199.

14. Suzuki R, Muyco J, McKittrick J, Frangos JA. Reactive oxygen species inhibited by titanium oxide coatings. J Biomed Mater Res 2003;66(2):396–402.

15. Suzuki R, Frangos JA. Inhibition of inflammatory species by titanium surfaces. Clin Orthop Relat Res 2000;372:280-289.

16. Healy KE, Ducheyne P. Hydration and preferential molecular adsorption on titanium *in vitro*. Biomaterials 1992;13(8):553-561.

17. Li P, Ducheyne P. Quasi-biological apatite film induced by titanium in simulated body fluid. J Biomed Mater Res 1998;41(3):341-348.

18. Colas A, Curtis J. Silicone Biomaterials: History and Chemistry, Biomaterials Science, 2nd Edition: An Introduction to Materials in Medicine. Elsevier, Inc., July 29, 2004;80-86.

19. Abbasi F, Mirzadeh H, Katbab A-A. Modification of polysiloxane polymers for biomedical applications: a review. Polym Int 2001;50:1279-1287.

20. Piveteau L-D, Gasser B, Shlabach L. Evaluating mechanical adhesion of sol-gel titanium dioxide coatings containing calcium phosphate for metal implant application. Biomaterials 2000;21:2193-2201.

21. Podbielska H., Ulatowska-Jarza, A. Sol-gel technology for biomedical engineering. Bull Pol Ac:Tech 2005;53(3):261-271.

22. Areva S, Paldan H, Petola T, Narhi T, Jokenen M, Linden M. Use of sol-gel-derived titania coating for direct soft tissue attachment. J Biomed Mater Res 2004;70A:169-178.

23. Nakazawa K, Lee S-W, Fukuda J, Yand D-H, Kunitake T. Hepatocyte spheroid formation on a titanium dioxide gel surface and hepatocyte long-term culture. J Mater Sci: Mater Med 2006;17:359-364

24. Wang C-C, Ying JY. Sol-gel synthesis and hydrothermal processing of anatase and rutile titania nanocrystals. Chem Mater 1999;11:3113-3120.

25. Hun TH. Microstructural evolutions and stress studies of titania films derived by “spin-deposition” methods. PhD Thesis, Brown University, Providence RI, USA 2006;70-95.

26. H.J. Klasen. Historical review of the use of silver in the treatment of burns.
I. Early uses. Burns 26 (2000) 117-130.

27. H. J. Klasen. A historical review of the use of silver in the treatment of burns. II. Renewed interest for silver. Burns 2006;26(2):131-138.

28. Joseph J Castellano, Susan M Shafii, Francis Ko, Guillermo Donate, Terry E Wright, Rudolph J Mannari, Wyatt G Payne, David J Smith, Martin C Robson. Comparative evaluation of silver-containing antimicrobial dressings and drugs. International Wound Journal 2007;4(2):114-122.

29. JR Johnson, MA Kuskowski, TJ Wilt. Systematic review: Antimicrobial urinary catheters to prevent catheter-associated urinary tract infection in hospitalized patients. Annals Internal Med 2006;144(2):116-126.

30. Garcia-Vicente S, Yraola F, Marti L, Gonzalez-Munoz E, Garcia-Barrado MJ, Canto C, Abella A, Bour S, Artuch R, Sierra C, Brandi N, Carpene C, Moratinaos J, Camps M, Palacin M, Testar X, Guma A, Albericio F, Royo M, Mian A, Zorzano A. Oral insulin-mimetic compounds that act independently of insulin. Diabetes 2007;56(2):486-493.

31. Shechter Y. Insulin-mimetic effects of vanadate. Possible implications for future treatment of diabetes. Diabetes 1999;39(1):1-5.

32. Srivastava AK. Anti-diabetic and toxic effects of vanadium compounds. Mol Cell Biochem 2006; 206(1-2):177-182.

33. Ehrlich HP, Keefer KA, Myers RL, Passaniti A. Vanadate and the absence of myofibroblasts in wound contraction. Arch Surg 1999;134(5):494-501.

34. Mackay DJD, Moyer KE, Saggers GC, Myers RL, Mackay DR, Ehrlich HP. Topical vanadate optimizes collagen organization within granulation tissue. Wound Repair Regen 2003;11(3):204-212.

35. Ehrlich HP, Keefer KA, Maish GO, Myers RL, Mackay DR. Vanadate ingestion increases the gain in wound breaking strength and leads to better organized collagen fibers in rats during healing. Plast Reconstr Surg 2001;107(2):471-477.

36. Moyer KE, Saba AA, Hauck RM, Ehrlich HP. Systemic vanadate ingestion modulates rat tendon repair. Exp Mol Pathol 2003;75(1):80-88.

37. Chen J, Iosifidis M, Zhu J, Tatarintsev I, Wang JH. Vanadate ingestion enhances the organization and collagen fibril diameter of rat healing medical collateral ligaments. Knee Surg. Sports Traumatol. Arthrosc 2006;14(8):750-755.

38. Takada Y, Hashimoto M, Kasahara J, Aihara K, Fukunaga K. Cytoprotective effect of sodium orthovanadate on ischemia/reperfusion-induced injury in the rat heart involves Akt activation and inhibition of fodrin breakdown and apoptosis. J Pharmacol Exp Ther 2004;311(3):1249-1255.

39. Yamamoto A, Honma R, Sumita M. Cytotoxicity evaluation of 43 metal salts using murine fibroblasts and osteoblastic cells. J Biomed Mater Res 1998;39(2):331-340.

40. Huang C, Zhang Z, Ding M, Li J, Ye J, Leonard SS, Shen HM, Butterworth L, Lu Y, Coasta M, Rojanasakul Y, Castranova V, Vallyathan V, Shi X. Vanadate Induces p53 transactivation through hydrogen peroxide and causes apoptosis. J Biol Chem 2000;275(42):32516-32522.

41. Cortizo AM, Salice VC, Vescina CM, Etcheverry SB. Proliferative and morphological changes induced by vanadium compounds on Swiss 3T3 fibroblasts. BioMetals 1997;10(2):127-133.

42. Jarrell JD, Eun TH, Samale M, Briant C, Sheldon B, Morgan JR. Use of specialized metal oxide films for delivery of bioactive metal compounds. Orthopaedic Research Society Annual Meeting, February 2007;32:1590.

43. G Gogniat, M Thyssen, M Denis, C Pulgarin, S Dukan. The bactericidal effect of TiO_2 photocatalysis involves absorption ont on catalyst and loss of membrane integrity. FEMS Microbol Lett 258 (2006) 18-24.

44. Jeon H-J, Yi S-C, Oh S-G. Preparation and antibacterial effects of Ag-SiO2 thin films by sol-gel. Biomaterials 2003;24:4921-4928.

45. Lee MS, Hong S-S, Mohseni M. Synthesis of photocatalytic nanosized TiO_2-Ag particles with sol-gel method using reduction agent. Journal of Molecular Catalysis A: Chemical 2005;242:135-140.

46 Grandjean-Laquerriere A, Laquerriere P, Jallot E, Nedelec J-M, Guenounou M, Laurent-Maquin D, Phillips TM. Influence of the zinc concentration of sol-gel derived zinc substituted hydroxyapatite on cytokine production by human monocytes *in vitro*. Biomaterial 2006;27:3195-3200.

47. Jarrell JD, Eun TH, Samale M, Briant C, Sheldon B, Morgan JR. Metal oxide coated cell culture arrays for rapid biological screening. J Biomed Mater Res A 2007;83A(3):853-860.

48. Bechert T, Steinrucke P, Guggenbichler J-P. A new method for screening anti-infective biomaterials. Nature Medicine 2000;6(8):1053-1056.

49. Alt V, Bechert T, Steinrucke P, Wagener M., Seidel P, Dingeldein E, Domann E, Schnettler R. *In vitro* testing of antimicrobial activity of bone cement. Antimicrobial Agents and Chemotherapy 2004;48(11):4084-4088.

50. Garcia AJ. A centrifuge cell adhesion assay for high-throughput screening of biomaterial surfaces. J Biomed Mater Res 2003;67A(1):328-333.

51. Garcia AJ, Gallant ND. Stick and grip: measurement systems and quantitative analyses of integrin-mediated cell adhesion strength. Cell Biochem and Biophys 2003;39(1):61-73.

Chapter 7

Development of coated percutaneous implants and hairless rat model to evaluate soft tissue integration of metal oxides and hybrid

John D. Jarrell *, Evan C. Werlin, Jeffrey R. Morgan

Department of Molecular Pharmacology, Physiology, and Biotechnology, and the Center for Biomedical Engineering, Brown University, Providence, RI, USA

Abstract

This study presents the development of a combined sub/percutaneous, polyurethane implant device and CD hairless rat model to explore the influence of metal oxide and photoactive hybrid coatings on soft tissue integration. Silicone rubber molds were made from CAD generated wax models, into which a dispersion of polyurethane was solvent cast, resulting in flexible implants with open-pore structure (~30 μm dia.). These were either left non-coated or dip-coated with nine compositions of titanium oxide, vanadium and PDMS. Six devices were sub/percutaneously implanted in three bilateral dorsal positions (2 pilot and 15 test animals). Visual scoring of exit site inflammation indicated good response from all implants at 3 weeks, except vanadium doped hybrids. There were no statistical differences between matched sets, except pure titanium oxide coatings outperformed those doped with 33.3% PDMS. Rat models were sensitive to implant location, with shoulder implants performing better than the lower back. Best performance was with titanium coatings doped with 20% vanadium. Collars used to prevent chewing of implants hindered self-grooming of exit sites, giving poorer outcomes than pilot animals, reinforcing the importance of clean exit sites with percutaneous devices. Optical spectra of skin, muscle and bone, indicated optimum transparency between 640-920 nm, where hybrid coatings produced high levels of photoactivity in prior *in vitro* studies. This suggests the future development of medical implants which are activated with externally applied photons to provide controlled delivery and antimicrobial disinfection.

Keywords: Metal ion release, Titanium oxide, Fibroblast, Bioactivity, Sol-gel techniques, Wound healing

7.1 Introduction

Poor integration and infection are the greatest challenges to skin penetrating devices, such as simple gastronomy and peritoneal dialysis (PD) catheters and complex bone anchored prosthetic attachments [1,2]. PD catheters are generally constructed of silicone (or occationally polyurethane) with porous Decron velour cuffs for tissue ingrowth and anchorage [3]. Silicone, however, is relatively inert and resists protein, cell and tissue attachment [4]. Histology of the Dacron cuffs after implantation show chronic inflammatory cell infiltration with macrophages, foreign body giant cells, polymorphonuclear leucocytes, with some lymphocytes and plasma cells [5]. The cellular reaction of the host tissue surrounding Dacron is primarily a foreign body response with chronic inflammation, while titanium meshes used for similar anchorage showed better biocompatibility and connective tissue ingrowth [6,7].

Bone-anchored transcutaneous prosthetic attachments consist of a threaded osseointegrated portion and a percutaneous abutment, similar in design to dental implants [8]. These devices generally consist of either separate bone and skin contacting components, after the traditional Branemark design, or a single combined implant. Pure and alloyed titanium are the materials of choice for osseointegrated percutaneous devices, because of a long history of sucessful use in bone implants and fixation devices, desirable mechanical and anti-inflammatory properties [9-17]. Clinically useful abutments generally require smooth, non-porous surfaces to prevent bacterial colonization.

Attempts have been made to improve percutaneous devices by looking to analogous structures like mammalian teeth, tusks and antlers. Feathers, hooves, finger nails and hair, while seeming to penetrate the skin, are merely keratinized appendages of the epidermal

layer [18]. Dental histology shows a perpendicular alignment of collagen fibers embedded in the surface of natural teeth running into the connective tissue underlying the gingival epithelium [19,20]. These fibers provide a barrier to junctional epithelium down growth. When dental prosthetics are implanted, these Sharpey's fibers are lost along with normal epithelial attachment and are replaced with a functional soft tissue seal. The tusks of the babyrussa pig from South-East Asia are the only natural example of a permanent percutaneous structure [5]. The tusks, actually teeth, avoid the oral cavity and grow through the dermal and epidermal layers of the face. The skin surface is covered with extensive keratin accumulation and a mycelium of fungi, which possibly has an antibacterial function. Histology indicates the direct cellular attachment of junctional epithelium to the tusks, mediated by hemidesmosomes, similar to teeth in the oral cavity [5]. The surrounding tissues display a layer with chronic inflammation (i.e. infiltration by lymphocytes, plasma cells, macrophages and a few polymorphonuclear leucocytes). Histology studies of percutaneous titanium implants show a similar stable immune surveillance where the devices penetrate the skin, without direct attachment of junctional epithelium via hemidesmosomes [21]. Recently, a characterization of deer antler histology was used to develop a titanium device that mimics its structure to provide a tight soft tissue seal, for use in amputation prosthetics [22]. The implant had a subcutaneous porous flange coated with hydroxyapatite which successfully encouraged dermal ingrowth and attachment as a barrier to epithelial downgrowth [23].

Research with vanadium compounds indicate that they mimicked insulin in a synergetic fashion, with systemic anti-diabetic effects [24-26] and increase proliferation at low doses, but inhibited cell growth and spreading at higher concentrations [27-30].

Oral ingestion of vanadium oxides dissolved in drinking water has improved wound strength [31], promoted rapid and orderly collagen deposition during skin wound healing [32], and improved tendon and ligament repair in rat models [33,34] and similar effects with local bolus injections of vanadium oxides dissolved in saline into subcutaneous sponges [35]. In contrast to these prior methods of delivery, we have developed solid state coatings for controlled local vanadium release to modulate wound healing dynamics [36].

We designed a porous solvent cast polyurethane device with a circular subcutaneous button and a cylindrical transdermal portion. Six devices were implanted into the back of each of CD hairless rats in the shoulder, midsection and lower back region to test the influence of coatings made of titanium and vanadium oxides and metal oxide-PDMS hybrids on soft tissue integration. These materials have the potential for reducing localized inflammation, providing unique antimicrobial properties and delivery of bioactive metal oxide compounds. These coatings were previously screened *in vitro* for cellular proliferation, attachment, elution of bioactive components and antimicrobial potential [36-39]. A porous disk-like cuff is used to control the stresses around the percutaneous device and provides for soft tissue anchorage. We hypothesize that the oxides will improve soft tissue integration over unalloyed medical polymers and that the cuff can be used to dissipate stresses between the implant and surrounding skin.

7.2 Materials and Methods

7.2.1 Implant mold design and fabrication

We used a multi-step process to create polymeric percutaneous implants with a porous subcutaneous flanged. Three dimensional renderings of several designs were made using computer-assisted design (CAD) (Solid Works Corporation, Concord, MA). Wax molds from the CAD files were produced with a ThermoJet® rapid prototyping machine (3D Systems Corporation, Valencia, CA). Our use of solvent-casting made it necessary to increase the thickness of the flange in the wax molds to compensate for evaporation. Several wax models were spaced out on a polystyrene petri dish, covered with uncured medical grade silicone rubber (Dow Corning) and allowed to set 48 hours. The silicone mold was removed from the petri dish and flexed to remove the wax models.

To make the polyurethane (PU) solution for solvent-casting of implants, five grams of Carbothane PC-3585A (Lubrizol Advanced Materials, Inc.) and 14 ml of dimethylformamide (DMF) were mixed together at 65 °C in a closed scintilation vial with stirring until a uniform dispersion was formed. A l000 µl micropipette was used to dispense 450 µl of PU solution into the pin and flange recess of each implant mold, while being careful to prevent the introduction of air bubbles. Because the fluid is viscous, approximately 3 mm was snipped off the end of a 1 ml micro- pippet tip to aid dispensing. Implants were air dried in a chemical hood at 22 °C for 24-48 hours to allow for solvent evaporation, before being removed from the molds. Using aseptic techniques under a HEPA filtered laminar flow hood, one hundred implants were twice rinsed with 250 ml of isopropanol with aggitation at 37 °C, to disinfect and remove residual DMF. Implants

were stored individually in sterile 12-well cell culture plates (Corning Costar) prior to being coated.

7.2.2 Coating solutions and process

To make titanium stock solutions 10 ml of titanium isopropoxide 99.999% (Sigma-Aldrich, St. Louis, MO) was added to 100 ml of isopropanol >=99.8% (Riedel-de Haën, Seelze, Germany) and mixed by brief shaking. Vanadium stock solution consisted of 10 ml of vanadium oxytripropoxide (Sigma-Aldrich) in 100 ml of isopropanol. A PDMS stock solution was made by adding 10 ml of Dow Corning MDX4-4159, 50% Medical Grade Dispersion into 100 ml of 70 % hexanes/30% isopropanol (vol/vol) and mixed by brief shaking at room temperature. This PDMS is supplied as a dispersion of 50% silicone in a co-solvent system of 70% Stoddard Solvent (mineral spirits) and 30% isopropanol. This amine functional polymer also incorporates reactive methoxy- groups that generally polymerizes in contact with moisture or added water to form thin coatings.

Stock solutions were allowed to age 15 minutes at room temperature and briefly shaken before use. These stock solutions were added together in a separate glass container using a pipette to make hybrid stock solutions of specific compositions and briefly shaken before use. Coating compositions were identified by vol % titanium isopropoxide precursor to polymer, excluding all volatile solvents. Stock solutions were mixed for 66.6% titanium-PDMS hybrids and were subsequently doped with vanadium solutions. Tertiary coatings are reported as vol % of metal-organic vanadium solution per volume of metal-organic titanium-PDMS hybrid solution.

To apply coatings to implants, 50 ml centrifuge tubes were filled with 40 ml of xerogel or hybrid solution, into which 10 implants were added using aseptic techniques and soaked for 5 minutes. Each implant was removed, shaken briefly and placed back into the bottom of a labeled and sterile 12-well cell culture plate to air dry overnight in a HEPA filtered laminar flow hood and covered with sterile lids. Implants were covered in sterile PBS at the beginning of the surgical procedure (~ 1 hr).

7.2.3 Animal implant model

Outbred male CD hairless rats (16-17 weeks old, Crl:CD(SD)-*hr*) (Charles River Laboratories, Wilmington, MA) were used, as approved by the Institutional Animal Care and Use Committee (IACUC). Six devices were sub/percutaneously implanted in three bilateral dorsal positions of CD hairless rats (2 pilot study and 15 test animals). One coating type was on one side of an animal, a second was on the other side with three replicate animals. The five compared implant combinations were:

1) non-coated PU to PDMS coating

2) Ti-iso to 66.6% Ti-PDMS

3) 1.25% V Ti-iso to 20% V Ti-iso

4) 1.25% V Ti-PDMS to 20% V Ti-PDMS

5) 97.5% Ti-PDMS to 97.7% Ti-silicone oil

Surgery involved isoflurane induction, a single longitudinal dermal section and blunt dissection of subcutaneous fascia. Percutaneous stubs were inserted through holes made

with a 3 mm biopsy punch (Sklar Instruments, West Chester, PA), beginning 5 cm down from the ears and spaced apart 3.5 cm longitudinally and 2 cm away from incision. A single stitch was used to secure the implant stub to the dermis and the incision closed with interrupted stitches ~ ½ cm apart. Test animals were fitted with Elizabethan collars (Lomir Biomedical, Malone, NY) to prevent chewing of implants, while pilot animals were not. The visual appearance of inflammation and swelling around each test implant was graded at weeks, 1, 2 and 3, based on a predetermined scale from 1-4 (with ½ steps), where 1 – no swelling, 2 – low swelling, 3 – high swelling, 4 – ulceration. Photographic examples (from pilot study) were provided to the grader prior to the experiment, who also photographed animals before grading. Euthanasia was performed with CO_2 at the end of the four week study. Cold mounted histology and paraffin sections were prepared from pilot animals at 13 days and stained with hematoxylin and eosin (H&E).

7.2.4 Optical spectroscopy of rat tissues

To aid in the development of light activated implant materials, optical density (OD) spectra were collected from rat tissue samples. A 6 mm biopsy punch was used to remove full thickness dorsal scapular skin samples (4 replicates), latissimus dorsi muscle (4 replicates). Full sidewall samples (3 replicates) of femural diaphysis bone were taken and scraped to remove periosteum and marrow, rinsed briefly in PBS. Tissue samples were placed in 96-well microplate (Corning Costar, Lowell, MA) to which 100 μl PBS was added (with empty well and PBS controls) and the optical density spectra determined from 190-1000 nm with a plate reader (SPECTRAmax® PLUS 384 Microplate Spectrometer with SOFTmax PRO software, Molecular Devices Corporation, Sunnyvale,

CA). Normal and side views of tissue samples were documented using a Digital Stereo Zoom 10-40X Microscope (LEICA**,** Bannockburn, IL**)** to measure sample thickness.

7.3 Results and Discussion

The original goal of the animal model was to mimick the rapid screening potental of the cell culture microplate. Using CAD and prototyping methods, we took conceptual sketches and rapidly produced implants to our own specifications and a working surgical model (Fig. 7.1). We wanted to determine if each animal could function as a 6 or 8 well microplate to increase the number of test samples per animal and reduce animal useage.

7.3.3 Animal implant model

Pilot animals were visually inspected and photographed to evaluate tissue reaction to implants. Photographs of pilot animal #1 at 6 weeks showed stable integration of Ti-iso coated implants, but epidermal regression and swelling on non-coated polyurethane implant (Fig. 7.2, top). After 13 weeks, the Ti-iso coated implant still showed stable integration, but the non-coated implant had already experienced complete marsupialization and rejection (Fig. 7.2, bottom). Accumulation of dry exudate appeared around the device after we began the use of a collar beginning at 2 months.

To determine the cellular interactions with the devices, the second pilot animal was sacrificed at 13 days and implants removed for histology (Fig. 7.3). Explants from the first pilot study animal showed growth of vascularized connective tissue surrounding the subcutaneous cuffs (Fig. 7.3b) and good soft tissue sealing in cross section after 13 days (Fig. 7.3c) and tapered junctional epithelium (Fig. 7.3d). The pore diameter of implants

was ~ 30 μm (Fig. 7.3e). Epithelial down growth measured 875μm below top of the epidermal layer (Fig. 7.4). Thickened, hyper proliferative epidermis was present around the exit site. Our animal pathologist characterized histology of non-coated PU implant and the surrounding tissue as showing inflammatory cells with macrophages populating nearly every pore of the material, while cellular indications of inflammation were greatly reduced in the Ti-iso coated samples.

Visual scoring of exit site inflammation indicated good compatibility over 3 weeks for all materials, except vanadium doped hybrids (Table 7.1). When using the Student paired t-test ($p < 0.05$), to compare matched sets of implants, only Ti-iso implants were statistically better than its paired sample (66.6% Ti-PDMS). Rat models were sensitive to implant location, with shoulder implants showing the least inflammation. When comparing all results from shoulder implants, Ti-iso coatings doped with 20% V had the best performance (Fig. 7.5). Collars used to prevent chewing of implants in the larger study hindered self-grooming of the exit sites by the rats. We believe this caused some of the poorer outcomes we observed compared to pilot animals. This reinforces the importance of maintaining a clean exit site with percutaneous devices.

7.3.4 Optical spectroscopy of rat tissues

To aid in the development of light activated implant materials, tissue samples were removed from rats (Fig. 7.6) and optical density spectra collected between 190 and 1000 nm (Fig. 7.7) Absorbance peaks corresponding to oxygenated and deoxygenated hemoglobin in the UV and visible range and water in the IR range were present, with optimum tissue transparency being between 640-920 nm [40,41]. The average thickness

(and standard deviation) for the tissue samples was 2.49 mm (0.29) skin, 2.18 mm (0.47) and 0.56 mm (.05) bone.

7.4 Conclusions

Visual scoring of exit site inflammation indicated good response from all implants at 3 weeks, except vanadium doped hybrids, with no statistical difference between matched sets except pure titanium oxide coatings outperformed those doped with 33.3% PDMS. The rat model was sensitive to implant location, with shoulder implants performing better than those lower on the back. The best performance of shoulder implants was with Ti-iso coatings doped with 20% V. Collars used to prevent chewing of implants (seen in pilot studies) hindered self-grooming of exit sites, giving poorer outcomes. This reinforces the importance of maintaining a clean exit site with percutaneous devices.

Optical transmission spectra collected from samples of rat skin, muscle and bone, indicated optimum transparency between 640-920 nm which induced the highest high levels of photoactivity for the 97.4% Ti-PDMS coatings during prior *in vitro* studies [42]. This suggests the future development of medical implants which are activated with externally applied photons to provide controlled delivery and antimicrobial disinfection.

Acknowledgements

We thank Roxanne Burrill for help with animal care and Paula Weston, Mary Hixon and Dr. Hideki Yamasaki for help with the histology slides. This work was funded, in part, by VA Rehabilitation Research and Development Center for Restorative and Regenerative Medicine, Providence, Rhode Island.

7.5 Figures

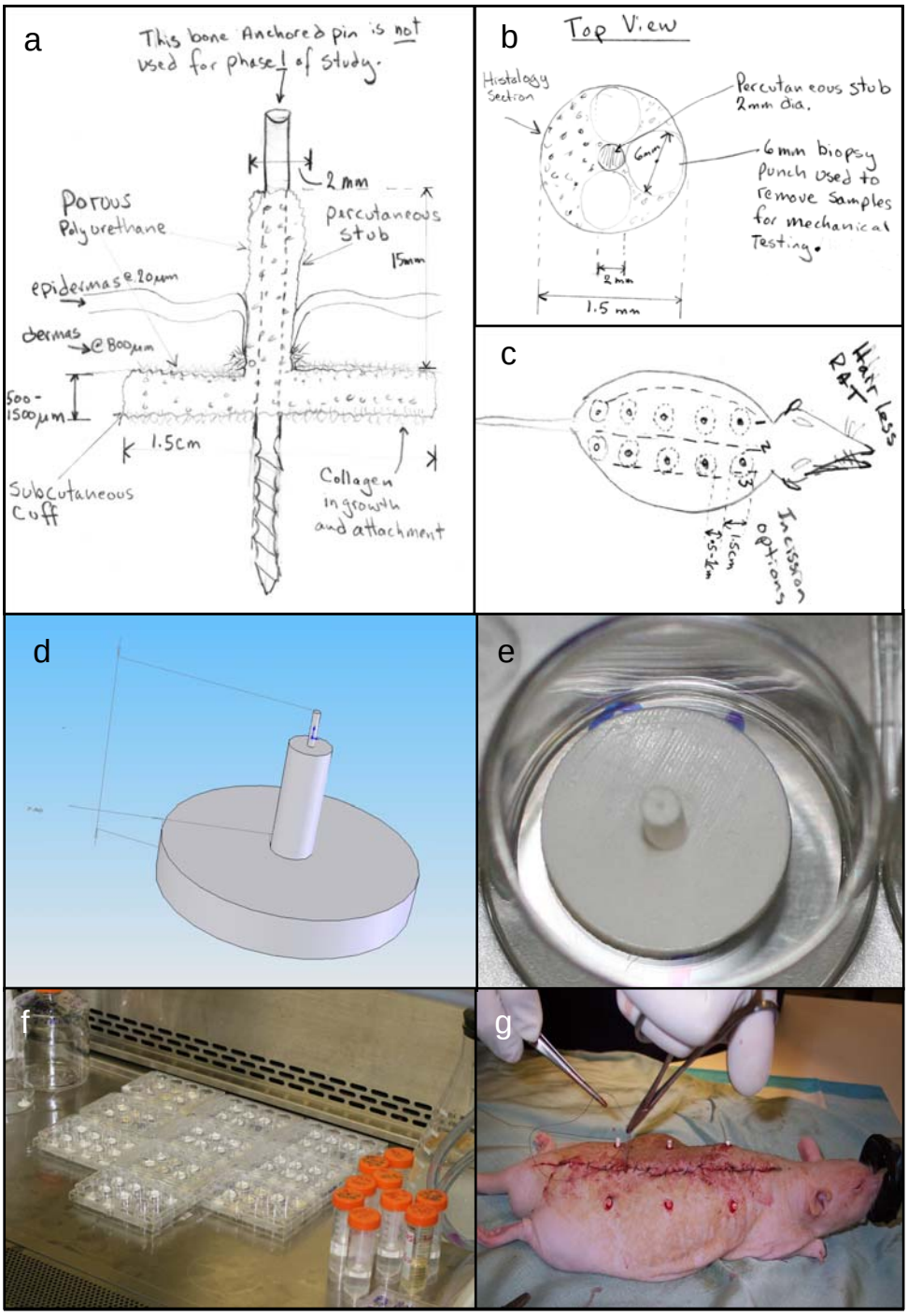

Figure 7.1: Images showing progression from conceptual drawings of implants (a,b) and animal model (c), to CAD of wax model (d) cast polyurethane implant (e), aseptic processing and coating of implants (f) and surgical implantation (g).

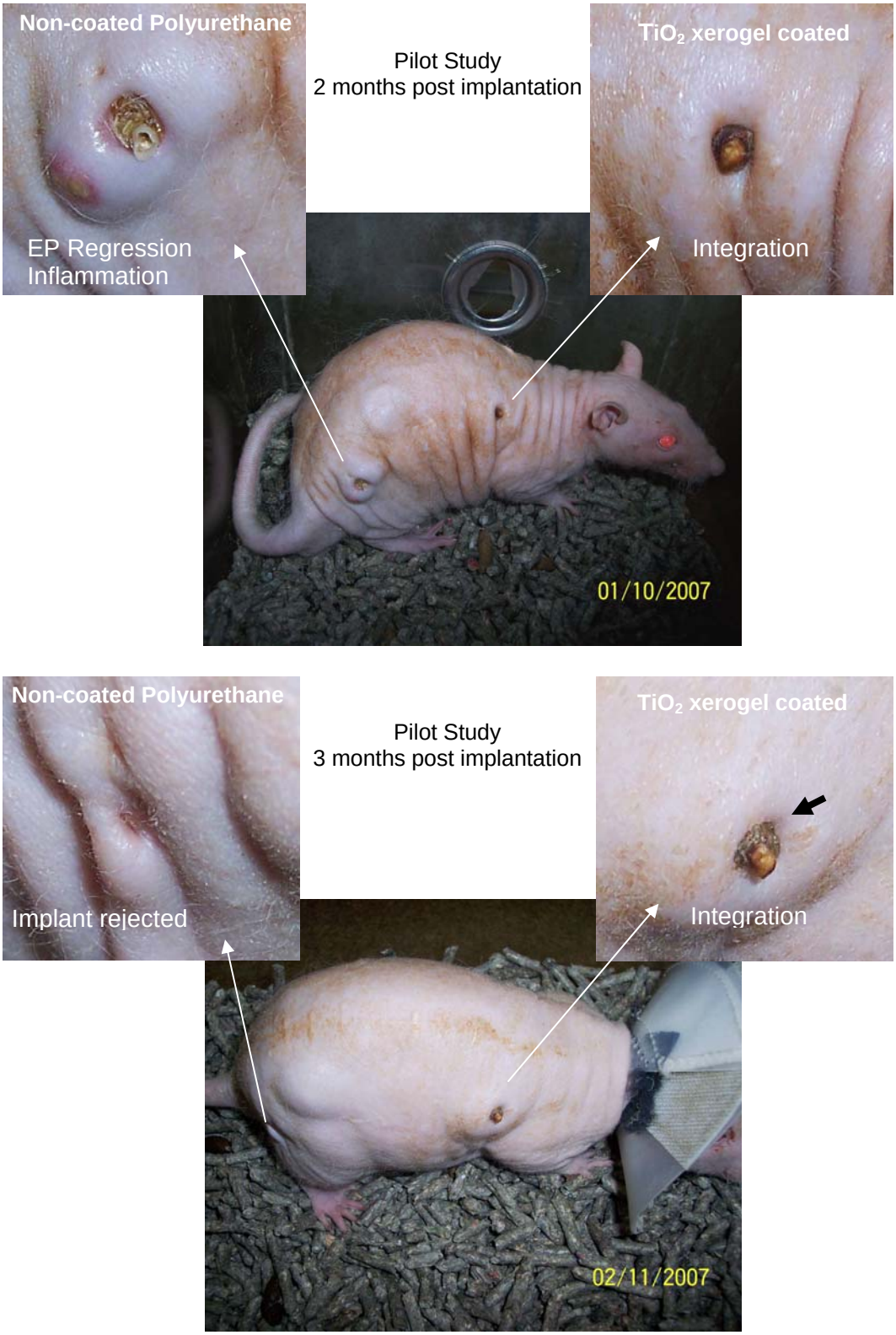

Figure 7.2: Comparison of non-coated polyurethane and Ti-iso coated implants at 2 months (top) and 3 months (bottom) in pilot animal #1. An accumulation of dry exudate (arrow) appeared around implant after 2 months, simultaneous to collar usage.

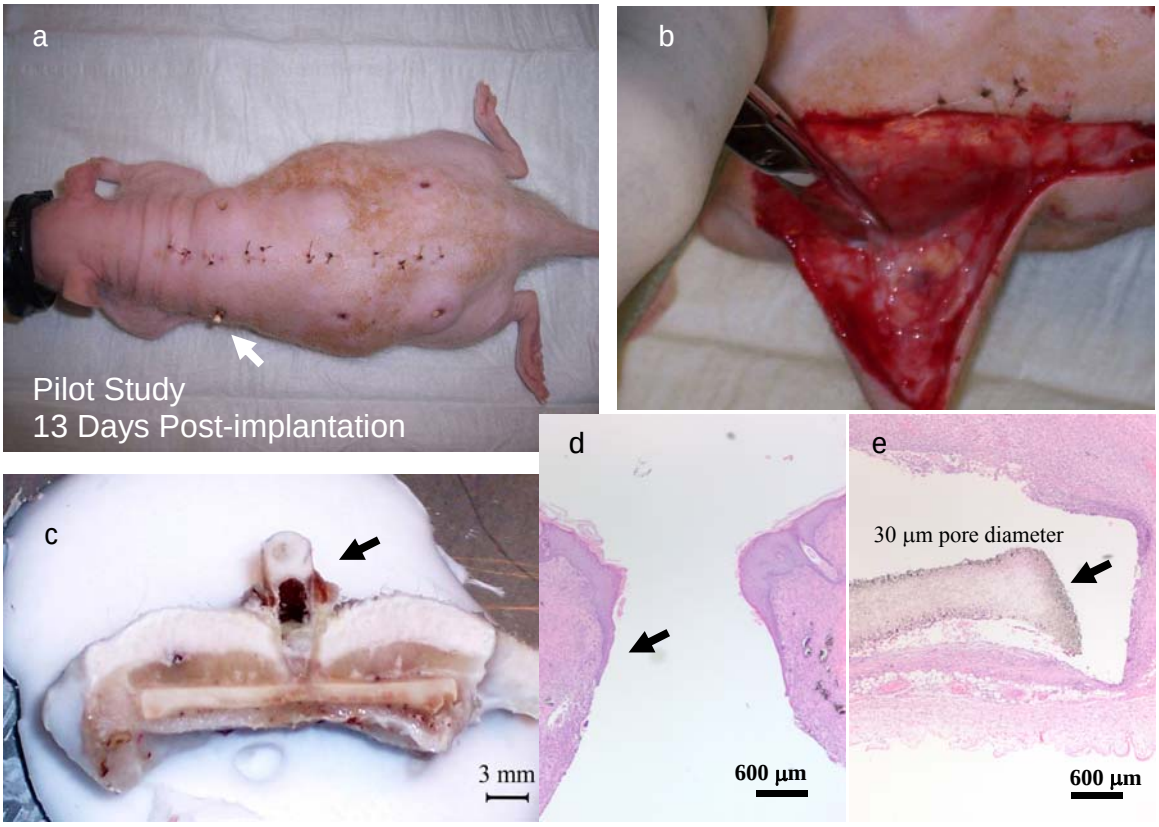

Figure 7.3: Appearance of implants at 13 days before (a) during (b) and after removal and sectioning (c) with arrows pointing to percutaneous stub. Paraffin mounted and H&E stained histology of 1.25% V Ti-iso implant at exit site (d) showing minimal epithelial down growth (arrow) and edge of cuff (e) (arrow) 13 days after surgery.

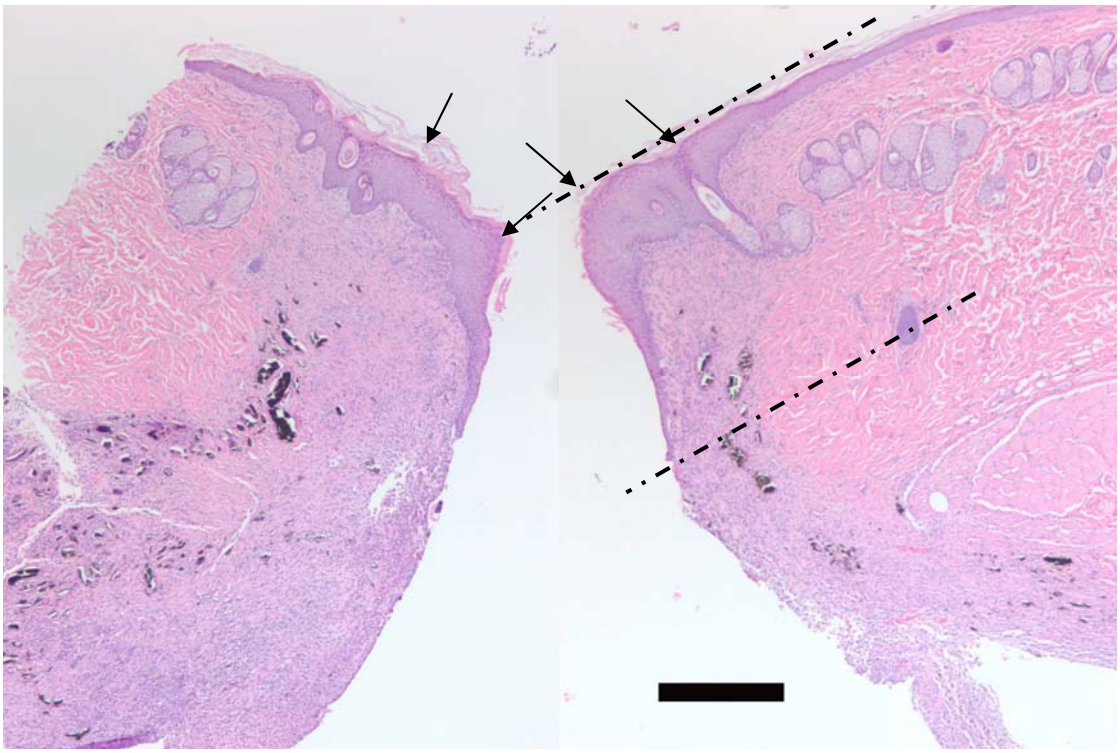

Figure 7.4: Close-up H&E histology of 1.25% V Ti-iso pilot implant, where epithelium contacted percutaneous stub. Epithelial down growth measured 875μm below top of the epidermal layer (between dotted lines). Thickened, hyper proliferative epidermis was present around the exit site (arrows). Scale bar is 500 μm.

Table 7.1

			Group 1		Group 2		Group 3		Group 4		Group 5	
	Side	Location	Avg.	SD	Avg.	SD	Avg.	SD	Avg.	SD	Avg.	SD
Wk 1	Left	Shoulder	1	0	1	0	1.17	0.29	2	0	1.33	.58
		Middle	1	0	1	0	1	0	1.17	.29	1.5	0.5
		Back	1	0	1	0	1	0	1.17	.29	1.5	.87
	Right	Shoulder	1	0	1.67	.58	1	0	1.67	.29	1	0
		Middle	1	0	1.67	.58	1.33	.58	1.33	.29	1.17	.29
		Back	1.33	.58	1.67	.58	2	0	1	0	1.33	.29
Wk 2	Left	Shoulder	1	0	1	0	1.17	.29	2	.5	1.5	.5
		Middle	1	0	1	0	1.33	.29	1.5	0	1.17	.29
		Back	1	0	1.5	.71	1.5	0	1.67	.58	1.5	0
	Right	Shoulder	1	0	1.5	.5	1	0	1.33	.29	1.33	.29
		Middle	1.25	.35	2.17	1.04	1.17	.29	1.75	.35	1	0
		Back	1	0	1.83	.29	1.5	0	1.6	.29	1.5	0
Wk 3	Left	Shoulder	1.25	.35	1.17	.29	1.17	.29	2	0	1.67	.58
		Middle	1.25	.35	1.5	.5	1.5	.5	2.17	.58	1.67	.58
		Back	1.25	.35	1.67	.29	1.17	.29	2.67	1.04	1.67	.58
	Right	Shoulder	1.25	.35	2	.5	1	0	2	0	1.5	.5
		Middle	1.25	.35	2	0	1.67	.29	1.33	.29	1.5	.5
		Back	1.5	0	2.17	.29	1.5	0	2.17	.76	1.83	.29

Key to grading (with ½ steps): 1 – no swelling, 2 – low swelling, 3 – high swelling, 4 – ulceration

Table 7.1: Visual grading of tissue surrounding implants over 3 weeks. When using the Student paired t-test ($p < 0.05$), to compare matched sets of implants, only Ti-iso was statistically better than its paired sample (66.6% Ti-PDMS). Group 1: Right (R) non-coated PU, Left (L) PDMS coating; Group 2: (R) Ti-iso, (L) 66.6% Ti-PDMS; Group 3: (R) 1.25% V Ti-iso, (L) 20% V Ti-iso; Group 4: (R) 1.25% V Ti-PDMS, (L) 20% V Ti-PDMS; Group 5: (R) 97.5% Ti-PDMS, (L) 97.7% Ti-silicone oil.

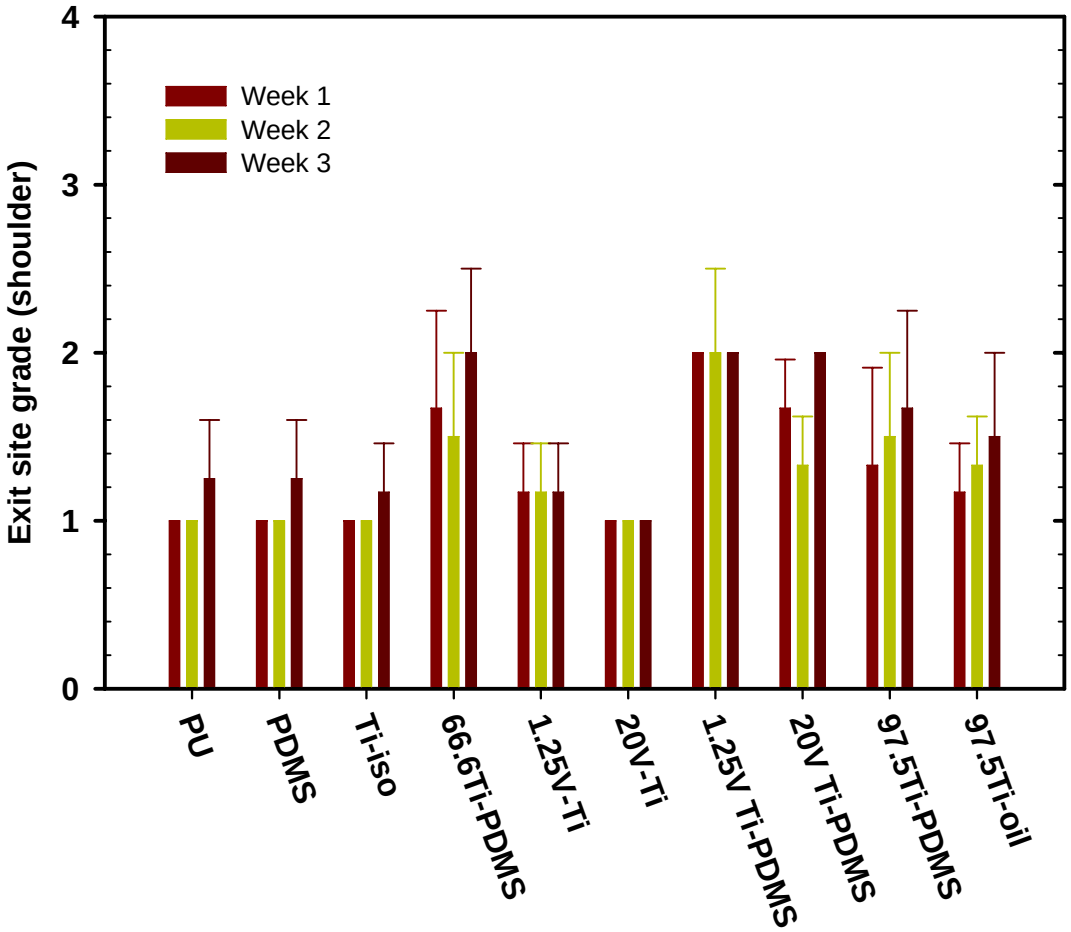

Figure 7.5: Visual grading of tissue surrounding shoulder implants over 3 weeks. When using the Student paired t-test ($p < 0.05$), to compare matched sets of implants, only Ti-iso was statistically better than its paired sample (66.6% Ti-PDMS).

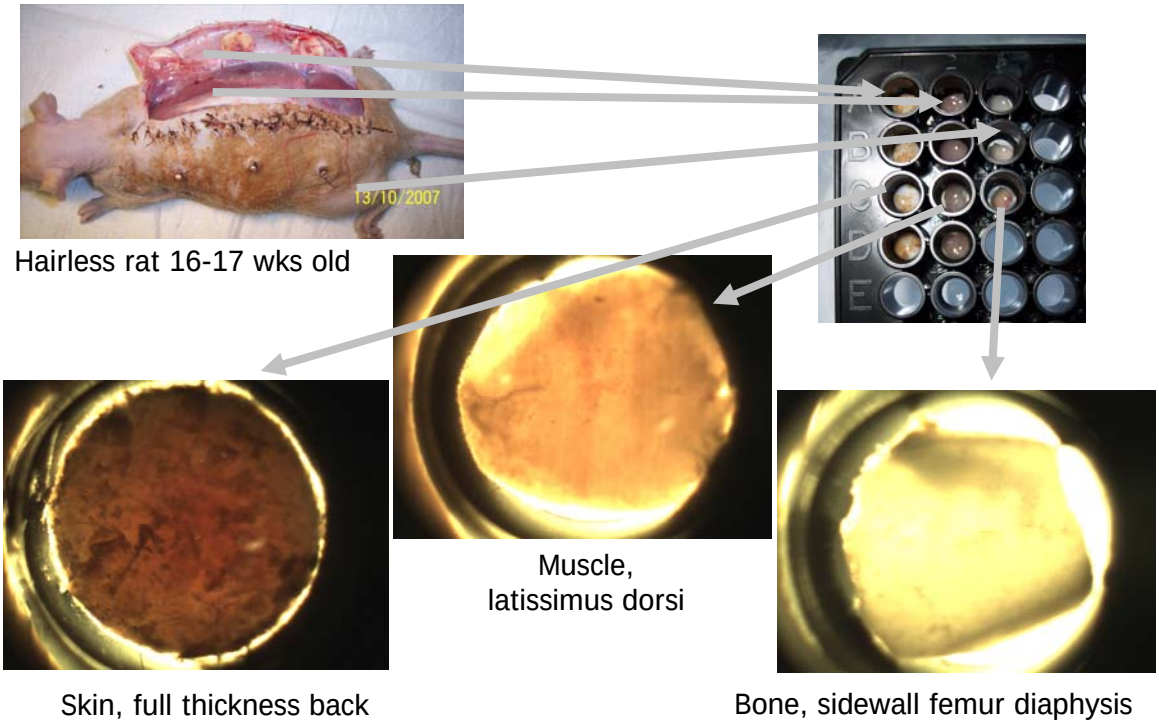

Figure 7.6: Images showing locations of tissue sample removal, microplate arrangement and macroscopic images of skin, muscle and bone samples. Diameter of wells is 6.4 mm.

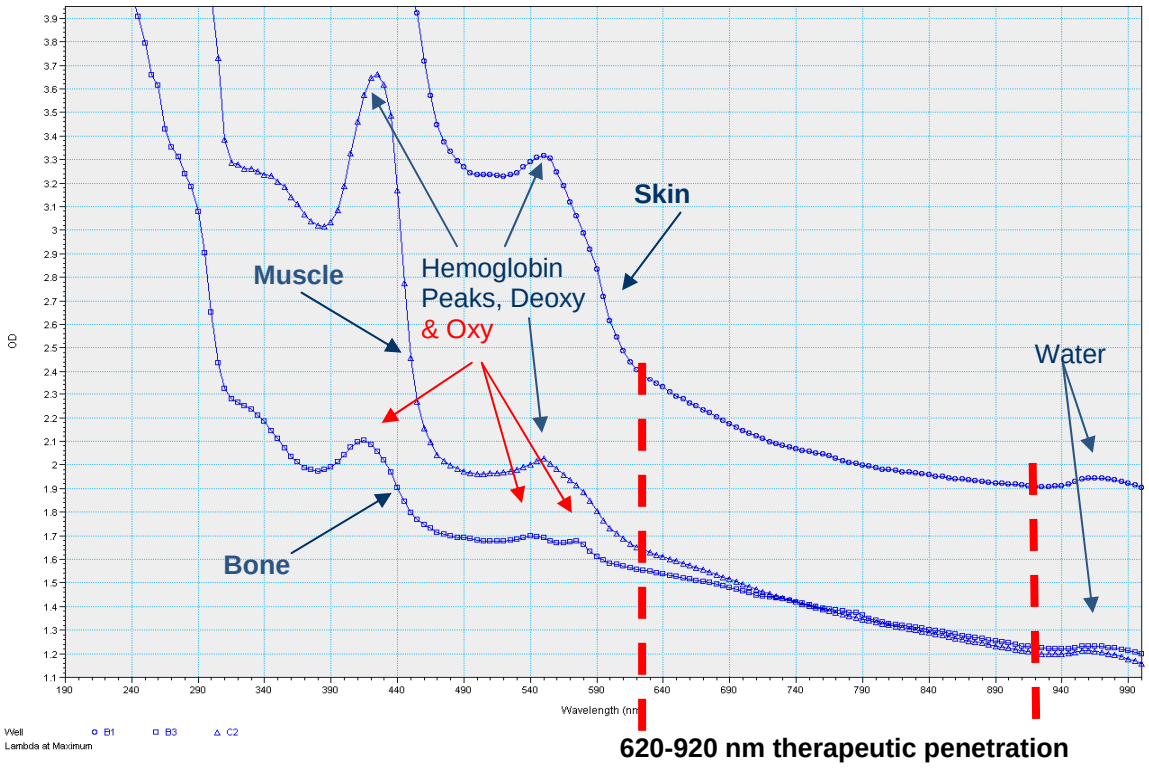

Figure 7.7: Optical density spectra (190-1000 nm) for rat skin, muscle and bone, showing peaks corresponding to oxygenated and deoxygenated hemoglobin in the UV and visible range and water in the IR range. Optimal therapeutic transparency was in 620-920 nm range.

7.6 References

1. von Recum, AF. Applications and failure modes of percutaneous devices: A review. J Biomed Mater Res 1984;18:323-336.

2. Hall CW, Cox PA, McFarland SR. Some factors that influence prolonged interfacial continuity. J Biomed Mater Res 1984;18:383-393.

3. Ash SR, Carr DJ, Diaz-Buxo JA, Crabtree JH. Peritoneal access devices: Design, function, and placement techniques, In: Allen R. Nissenson, Richard N. Fine, editors. Clinical Dialysis; 2005. p 309-323.

4. Jim Curtis, Andre Colas. Medical applications of silicones, Biomaterials Science, 2nd Edition: An introduction to materials in medicine. Elsevier, Inc., (July 29, 2004) pp. 697-706.

5. Knabe C, GroBe-Siestrup C, Gross U. Histologic evaluation of a natural permanent percutaneous structure and clinical percutaneous devices. Biomaterials 1999;20:503-510.

6. YCGJ Paquay, JE de Ruijter, JPCM. van der Waerden, JA Jansen. Tissue reaction to Dacron velour and titanium fibre mesh used for anchorage of percutaneous devices. Biomaterials 1996, Vol. 17 No. 12 1251-1256.

7. Gerritsen M, Paquay YGCJ, Jansen JA. Evaluation of the tissue reaction to a percutaneous access device using titanium mesh anchorage in goats. Journal of Materials Science: Materials in Medicine (1998) 523-528.

8 Branemark R, Branemark P-I, Rydevik B, Myers R. Osseointegration in skeletal reconstruction and rehabilitation: A review. JRRD March/April 2001;38(2):175-181.

9. L Overgaard, N Danielsen, LM Bjursten. Anti-inflammatory properties of titanium in the joint environment. An experimental study in rats. J Bone Joint Surg Br 80 (5) (1998) 888-893.

10. B Kasemo, J Lausmaa. Material-tissue interfaces: the role of surface properties and processes, Environ. Health Perspect 102 (suppl. 5) (1994) 41-45.

11. LM Bjursten. The bone-implant interface in osseointegration, in: B. Rydevik, P.I. Branemark, R. Skalak (Eds.), International Workshop on Osseointegration in skeletal reconstruction and joint replacement, The Institute for Applied Biotechnology, Goeborg, Sweden, 1991, pp. 25-31.

12. DA Puleo, A Nanci. Understanding and controlling the bone-implant interface. Biomaterials 20 (23-24) (1999) 2311-2321.

13. JB Brunski, DA Puleo, A Nanci. Biomaterials and biomechanics of oral and maxillofacial implants: current status and future developments. Int J Oral Maxillofa Implants, 15 (1) (2000) 15-46.

14. JE Sundgren, P Bodo, I Lundstrom. Auger electron spectroscopic studies of the interface between human tissue and implants of titanium and stainless steel. J Colloid Interface Sci 110 (1) (1986) 9-20.

15. EA Effah, PD Bianco, P Ducheyne. Crystal structure of the surface oxide layer on titanium and its changes arising from immersion. J. Biomed. Mater. Res. 29 (1) (1995) 73-80.

16. K.E. Healy, P. Ducheyne. Hydration and preferential molecular adsorption on titanium *in vitro*. Biomaterials 13 (8) (1992) 553-561.

17. P. Li, P. Ducheyne. Quasi-biological apatite film induced by titanium in simulated body fluid. J Biomed Mater Res 41 (3) (1998) 341-348.

18. Grosse-Siestrup C, Affeld K. Design criteria for percutaneous devices. J Biomed Mater Res 1984;18:357-382.

19. Palmer R. Teeth and implants. British Dental Journal 1999;187:183-188.

20. Sison SG, Implant maintenance and the dental hygienist. Access (supplement) 2003; May-June:1-11.

21. Holgers K.M., Thomsen P., Tjellstrom A., Ericson L.E., The soft tissue reaction around clinical long-term percutaneous titanium implants. In: Transplants and implants in otology III, p. 35-39, Proceedings of the third International symposium on transplants and implants in otology, Bordeaux, France, June 10-14, 1995, edited by M. Portmann, Kugler Publicaions, Amsterdam, The Netherlands.

22. Pendegrass CJ, Goodship AE, Price JS, Blunn GW, Nature's answer to breaching the skin barrier: an innovative development for amputees. J Anat 2006;209: pp59–67.

23. Pendegrass CJ, Goodship AE, Blunn GW. Development of a soft tissue seal around bone-anchored transcutaneous amputation prostheses. Biomaterials 27 (2006) 4183–4191.

24. S Garcia-Vicente, F Yraola, L Marti, E Gonzalez-Munoz, MJ Garcia-Barrado, C Canto, A Abella, S Bour, R Artuch, C Sierra, N Brandi, C Carpene, J Moratinaos, M Camps, M Palacin, X Testar, A Guma, F Albericio, M Royo, A Mian, A Zorzano. Oral insulin-mimetic compounds that act independently of insulin. Diabetes 56 (2) (2007) 486-493.

25. Y Shechter. Insulin-mimetic effects of vanadate. Possible implications for future treatment of diabetes. Diabetes 39 (1) (1999) 1-5.

26. AK Srivastava, MZ Mehdi. Insulino-mimetic and anti-diabetic effects of vanadium compounds. Diabet Med 2005;22:2-13.

27. A Yamamoto, R Honma, M Sumita. Cytotoxicity evaluation of 43 metal salts using murine fibroblasts and osteoblastic cells. J Biomed Mater Res 39 (2) (1998) 331-340.

28. C Huang, Z Zhang, M Ding, J Li, J Ye, SS Leonard, HM. Shen, L Butterworth, Y Lu, M Coasta, Y Rojanasakul, V Castranova, V Vallyathan, X Shi. Vanadate Induces p53 transactivation through hydrogen peroxide and causes apoptosis. J Biol Chem 275 (42) (2000) 32516-32522.

29. AM Cortizo, VC Salice, CM Vescina, SB Etcheverry. Proliferative and morphological changes induced by vanadium compounds on Swiss 3T3 fibroblasts. BioMetals 10 (2) (1997) 127-133.

30. Philippa Hulley, Allan Davison. Regulation of tyrosine phosphorylation cascades by phosphateses: What the actions of vanadium teach us. J Trace Elem Exp Med 2003;16:281-290.

31. HP Ehrlich, KA Keefer, GO Maish, RL Myers, DR Mackay. Vanadate ingestion increases the gain in wound breaking strength and leads to better organized collagen fibers in rats during healing. Plast Reconstr Surg 107 (2) (2001) 471-477.

32. HP Ehrlich, KA Keefer, RL Myers, A Passaniti. Vanadate and the absence of myofibroblasts in wound contraction. Arch Surg 134 (5) (1999) 494-501.

33. KE Moyer, AA Saba, RM Hauck, HP Ehrlich. Systemic vanadate ingestion modulates rat tendon repair. Exp Mol Pathol 75 (1) (2003) 80-88.

34. J Chen, M. Iosifidis, J Zhu, I Tatarintsev, JH Wang. Vanadate ingestion enhances the organization and collagen fibril diameter of rat healing medical collateral ligaments. Knee Surg Sports Traumatol Arthrosc 14 (8) (2006) 750-755.

35. DJD Mackay, KE Moyer, GC Saggers, RL Myers, DR Mackay, HP Ehrlich. Topical vanadate optimizes collagen organization within granulation tissue. Wound Repair Regen 11 (3) (2003) 204-212.

36 JD Jarrell, TH Eun, M Samale, C Briant, B Sheldon, JR Morgan. Use of specialized metal oxide films for delivery of bioactive metal compounds. Orthopaedic Research Society 2007 Annual Meeting, February 2007;32:1590.

37. JD Jarrell, TH. Eun, M. Samale, C Briant, B Sheldon, JR Morgan. Metal oxide coated cell culture arrays for rapid biological screening. J Biomed Mater Res 2007;83A (3):853-860.

38. JD Jarrell, B Dolly, JR Morgan, Controlled release of vanadium from titanium oxide coatings for improved integration of soft tissue implants, (accepted March 27, 2008) J. Biomed. Mater. Res. A (2008).

39. JD Jarrell, JR Morgan, Bioactive Polymers for Soft Tissue Sealing of Osseointegrated Prosthetic Attachments. 6th Combined Meeting of Orthopaedic Research Societies, Honolulu, Hawaii, October 20-24, 2007:63.

40. RMP Doornbos, R Lang, MC Aalders, FW Cross, HJCM Sterenborg. The determination of the *in vivo* human tissue optical properties and absolute chromophore concentration using spatially resolved steady-state diffuse reflectance spectroscopy. Phy Med Biol 1999;44:967-981.

41. B Chance, M Cope, E Gratton, N Ramanujam, B Troberg. Review Article: Phase measurement of light absorption and scatter in human tissue. Rev Sci Instrum 1998;69(10):3457-3481.

42. JD Jarrell, EC Werlin, JR Morgan. Novel light-activated antimicrobial controlled delivery polymer hybrids for osseointegrated transcutaneous devices. 54th Annual Meeting of the Orthopaedic Research Society, March, 2008;33:1729.

Chapter 8

Conclusions and Implications

8.1 Summary and concluding remarks

This thesis fulfilled the three Specific Aims of the research plan, which were to: #1: Create an experimental platform for rapid biological screening using sol-gel derived coatings with controlled chemistry/alloy, texture, degree of crystallinity and grain size; #2: Investigate which of the controllable material properties are most influential on the biological response of cells directly involved in soft tissue sealing (fibroblasts and epithelial keratinocytes); and #3: Develop and apply an optimized sol-gel based coating to improve soft tissue sealing in an animal model.

Chapter 1 provided an overview of the problem of percutanous devices and how they are similar to other chronic wounds. Titanium implants have provided the best long-term implant stability for both hard and soft tissues, due to the formation of a bioactive TiO_2 biointerface layer. Pure and doped titanium oxides may also be derived from metal-organic precursors and applied as thin transparent coatings, which are more suitable for use in standard biological assays than bulk metal samples. The surface morphology of

these coatings can be changed from smooth to micro or nano textured by controlling the reaction rate through solvent and precursor selection. Some titanium oxides produce efficient photocatalysts with possible application to bacterial disinfection. Much work has gone into shifting the photocatalytic activity of titanium dioxide from easily blocked UV irradiation to longer and deeper penetrating visible and infrared wavelengths, with limited success.

Chapter 2 showed the development of a novel rapid screening platform using metal oxide coated microplates[1]. These plates were well suited to use in standard high throughput biological assays for cell viability, proliferation and adhesion. The creation of thin transparent coatings overcame some of the limitations involved in using bulk metal samples, which are, opacity, difficult sample handling and low throughput. These coatings were not limited to standard alloy compositions, most of which were originally developed for industry and aerospace, like 316 stainless steel and the titanium alloy Ti6Al4V. The passive metal oxide layer, which forms the true biointerface, can now be selected based on biological criteria and without being limited by alloy availability. By selection of solvent systems, metal oxide coatings could be formed with smooth or microporous textures within the wells of cell culture microplates.

Chapter 3 explored the use of titanium oxide coatings as biocompatible, controlled delivery devices, suitable for short or permanent tissue contact and implantation[2]. Bioactive vanadium could be predictably eluted over a period of 28 days from stable, non-erodible titanium oxide matrices. Prior researchers used vanadium oxide solutions to improve wound healing and mimic insulin[3,4,5,6,7,8,9]. But, our work is the first to explore controlled delivery of vanadium from a solid state. Vanadium doped biomaterials show

promise for soft tissue applications and especially diabetic wound healing. Vanadium, however, is generally considered to have negative influences in bone contacting applications.

Chapter 4 covers the purposeful hybridization of metal oxides into a medical polymer to impart bioactivity. It is common in medical applications to avoid the use of fillers to ensure overall purity and biocompatibility. Some researchers have explored the mixing of titanium oxide particulate into biomaterials. But, our approach has been the simultaneous solidification of polymers and metal-organic derived oxides, to influence the bioactive properties of normally inert polydimethylsiloxane (PDMS) to regulate cell proliferation and adhesion. PDMS was found to increase the release rates of water soluble vanadium oxide, without release of titanium oxide particles. These materials show great potential for coating of polymeric devices where coating flexibility is important.

Chapter 5 shows that co-formation and solidification of polymers and metal oxides, created a unique class of photoactive materials responsive to a broad spectrum of x-rays, UV, visible and infrared photons. The photoactivity of these hybrid coatings was directly related to the reduction in photon transmission, during monochromatic flash irradiation. These results suggest the possibility of externally applied photons being used to activate the surface of implants below the skin and within bone. While the chemical reactions induced by irradiation of crystalline titanium dioxide photocatalysts have been well described, more research is required to understand the exact reactions produced by these hybrids during irradiation and methylene blue clearance. Currently, we hypothesize that photoactivity is from a greatly increased localized flow of conduction band electrons without the creation of electron holes in the valance band of titanium oxide. There also

appears to be a negative electrostatic charging of the coating surface during irradiation. These charges are likely localized in domains of the same size as the dispersed titanium-rich phases and separated by insulating PDMS-rich regions. We found that the hybrid coatings preferentially degraded positively charged methylene blue dye during irradiation, but was less effective degrading the neutral dye, indigo carmine (another indicator of photocatalysis, data not shown). Valence electrons are expected to cause a high production of superoxide radicals without direct production of hydroxyl radicals. If this is the case, the introduction of iron (metal-organic or nano particles) into the coatings may help to increase the production of antimicrobial hydroxyl radicals using the photo-Fenton reaction[10,11,12].

There are several questions to answer concerning the photoactivity of hybrids: the cause of photon trapping by dispersions of normally transparent phases, the mechanisms of energy transfer from photons to the coatings, conduction of energy to coating surface and exact nature of electro-chemical work being performed on methylene blue. The use of commercial microplate assays to identify specific radical production would be helpful for characterizing the mechanisms of action. One explanation for light trapping is related to photonic effects, based on the differences in dielectric properties between titanium dioxide and PDMS rich phases. Other researchers have created two phase dispersions of titanium oxide and air to make photonic materials[13,14]. A comparison of optical images of photoactive hybrid Ti-PDMS material with SEM images of two porous photonic TiO_2 materials presented as normal grayscale images and black and white threshold images, suggests a similar scale of repeating phases (Fig. 8.1). This spacing prevents transmission of certain wavelengths of light similar to the mechanism whereby crystalline structures

reflect certain wavelengths of x-rays, during x-ray diffraction. With the hybrid materials, we hypothesize that the different length-scales of repeating titanium oxide and PDMS rich phases are responsible for capturing the full spectrum of photons (Fig. 8.2). There is likely a combination of transmission, scatter and reflection as light passes through the coating and encounters multiple phases and phase boundaries. In this case, photons striking one phase would be directed to adjacent phases of various length scales and forced to interact with multiple titanium oxide and PDMS interfaces. If photoactivity is from electron flow, then the addition of crystalline semiconducting phases could possibly be used to carry irradiation induced electrons at specific quantum energies, to induce specific biological or specific electro-chemical activities. That is, these hybrid materials may provide controlled localized delivery of specific electrons, photons, electrical charges or electrical fields to cells and tissues surrounding implants, to influence bioactivity, healing and biofilm formation.

As a follow up to our earlier studies, Arto Nurmikko's Group at Brown University, Department of Engineering, spin-coated glass cover slides for optical analysis by laser light. The experimental laser setup used a 532nm, 20mW source passing through a 50% beam splitter, after being attenuated 10 times. Preliminary results from hybrids showed a large amount of scattering compared to pure titanium oxide films and PDMS coatings. The transmission and reflection spectra from the high intensity laser were very different from those seen with the flash source of the microplate reader, indicating that the hybrids were more transparent than titanium dioxide. The laser spectra seem to contradict the observed laser scattering. If this initial data is correct, it suggests the possibility of a phenomenon, where the hybrid coatings both scatter and "store" a certain amount of light

and that the “excess” photon energy is then transmitted more readily than with pure titanium dioxide. Further research is needed to find a satisfying explanation for these results.

Chapter 6 explores in more detail the influence of doping titanium oxides to influence bioactivity, antimicrobial properties and improve photocatalytic activity. Here, we demonstrated the power of the high throughput platform to screen the bioresponse of skin cells (fibroblasts and keratinocytes) and cancer cells (Hela) to serial doping of silver, vanadium and zinc and specific compositions of aluminum, calcium and phosphorous. Here, we see that in general, the most influential material property on bioresponses was the composition of the coatings. The influence of surface texture was small in comparison. Hydrothermal and autoclave heat treatments, designed to induce crystallinity, had little to no influence on the bioresponse of cells to coatings. Certain compositions of silver doped titanium oxide were found to reduce bacterial growth by 5 and 8 log (7% and 20%, respectively) within a volume of growth media, as well as, increase the photoactivity in the visible range. However, with hybrid coatings, moderate silver doping reduced photoactivity of normally active materials. Future work will require finding the precise dose response of bacteria to silver doping from more environmentally and biologically friendly titanium isopropoxide-isopropanol based solutions and hybrids as well as the influence of additional light treatments on microbe proliferation.

Our bacterial assay looked at the ability of coatings to influence planktonic growth within a volume above the coating surface. This level of antimicrobial protection is beyond that normally required by implanted biomaterials. Modifications to the assay need to be made to investigate bacterial attachment and biofilm formation, which are more

clinically relevant problems. Our coated microplate platform is well suited to screen these properties through the use of smaller inoculation volumes and bioadhesion assays similar to those developed for mammalian cells and the rapid antimicrobial screening of bulk biomaterials[15,16].

Chapter 7 presents the development of a prototype percutaneous device and an animal model to evaluate soft tissue integration. The use of computer aided design and computer aided manufacturing (CAD/CAM) was combined with rapid prototyping capabilities to create wax models, silicone rubber molds and solvent cast implants. This enabled us to turn concept drawings into devices within a week's time. Solvent casting and sol-gel techniques fit well with this rapid prototyping approach to implant development. Metal oxide coatings allowed us to impart the biointerface characteristics of metal implants to a soft implant. Polymers are more readily adapted to standard histological procedures than metal implants. Similar techniques can be applied to casting mineralized polymers, hydrogels, protein based materials and composites with metal oxides. Examples of future applications include the coating of carbon fibers, collagen or metal scaffolds and matrices, which can be mineralized or coated with metal oxides to create scaffolds and matrices for bone, cartilage and soft tissue regeneration.

The use of titanium oxide and vanadium showed promise for improving biocompatibility and reducing inflammation around polymeric implants. However, the rats tended to chew on the implants located on the lower and mid back. Collars were placed on the rats to restrict implant chewing, but added noticeably to the stress of the animals and prevented self-grooming of the exit sites. The use of a larger animal model

could overcome these problems and likely create the high throughput platform attempted with the rats.

For future experimentation, we are creating intramedullary implants, which simultaneously provide internal fixation and repair of segmental bone defects and a percutaneous bone anchored prosthetic attachment (BAPA) (Fig. 8.3). The transcutaneous titanium portion is similar to a prior model and would not be vulnerable to animal chewing like the polymer implants we used earlier[17,18]. The bone repairing and or residual limb lengthening component uses a resorbable polymeric intramedullary rod, degradable bioactive eluting bone scaffolds and a tissue engineered periosteum membrane in a rat amputation model. This model will hopefully increase our knowledge of how implant design, biomaterial selection, surface modification, coatings and bioactive delivery systems influence bone repair, soft and hard tissue integration and resistance to biofilm formation. This configuration allows for prosthetic limb attachment, unlike other studies using surface modified devices placed transversely in the cortices of rabbits[19,20] and goats[21,22]. A drawback with the amputation model is that it only allows for one device per animal and metal implants require specialized histological preparation. However, the amputation model closely matches the human situation of traumatic limb loss and provides the experience needed to improve techniques to treat bone and limb loss in larger experimental models and domestic animals[23,24], before applying them to prosthetic attachment in humans.

8.2 Figures

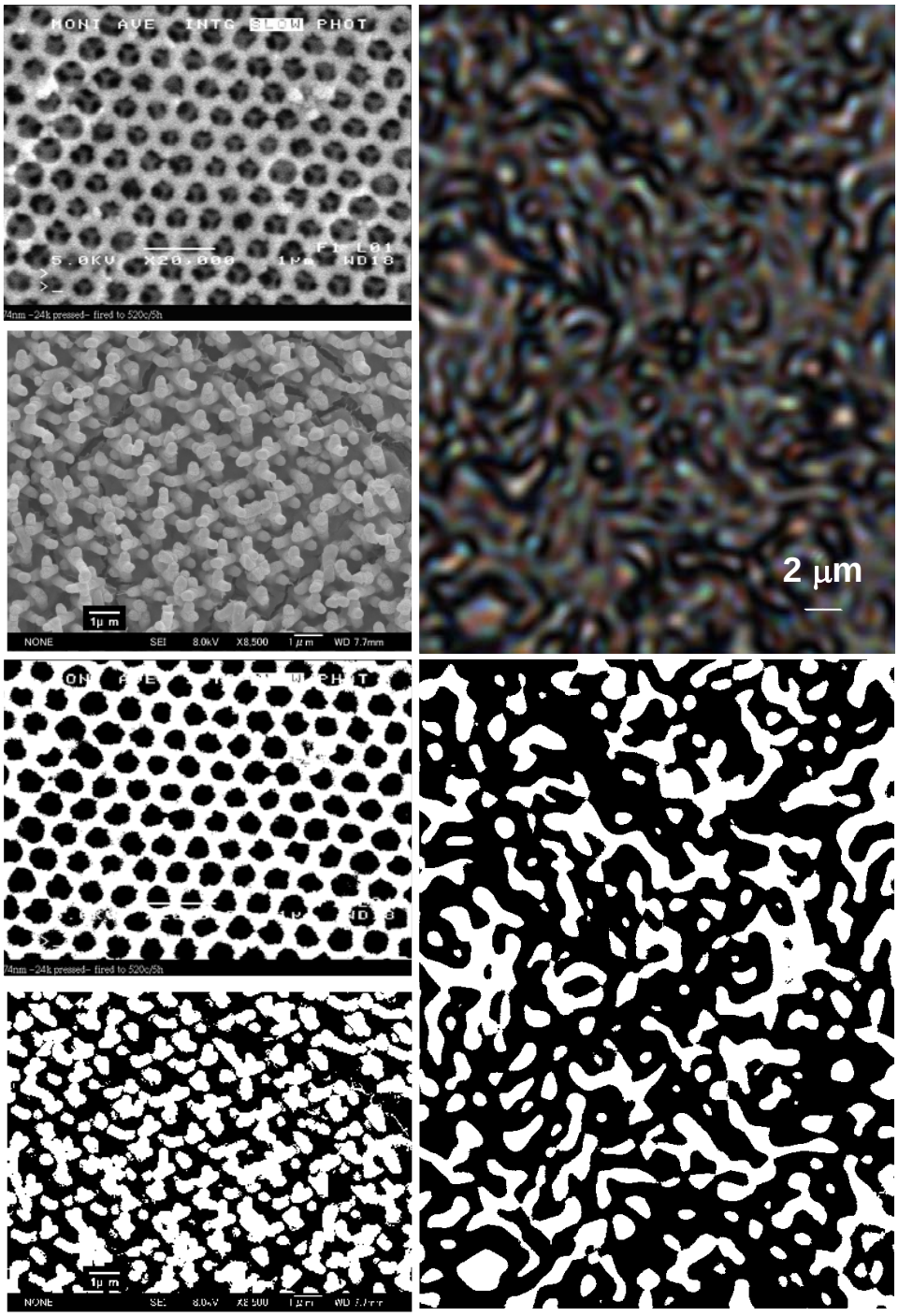

Figure 8.1: Comparison of optical images of photoactive hybrid Ti-PDMS material (large right panels, scale bar = 2 μm) with SEM images of two porous photonic TiO_2 materials (left inserts, scale bar = 1 μm) [13,14]. Normal grayscale images (top) and black and white threshold images (bottom), suggests a similar scale of repeating phases.

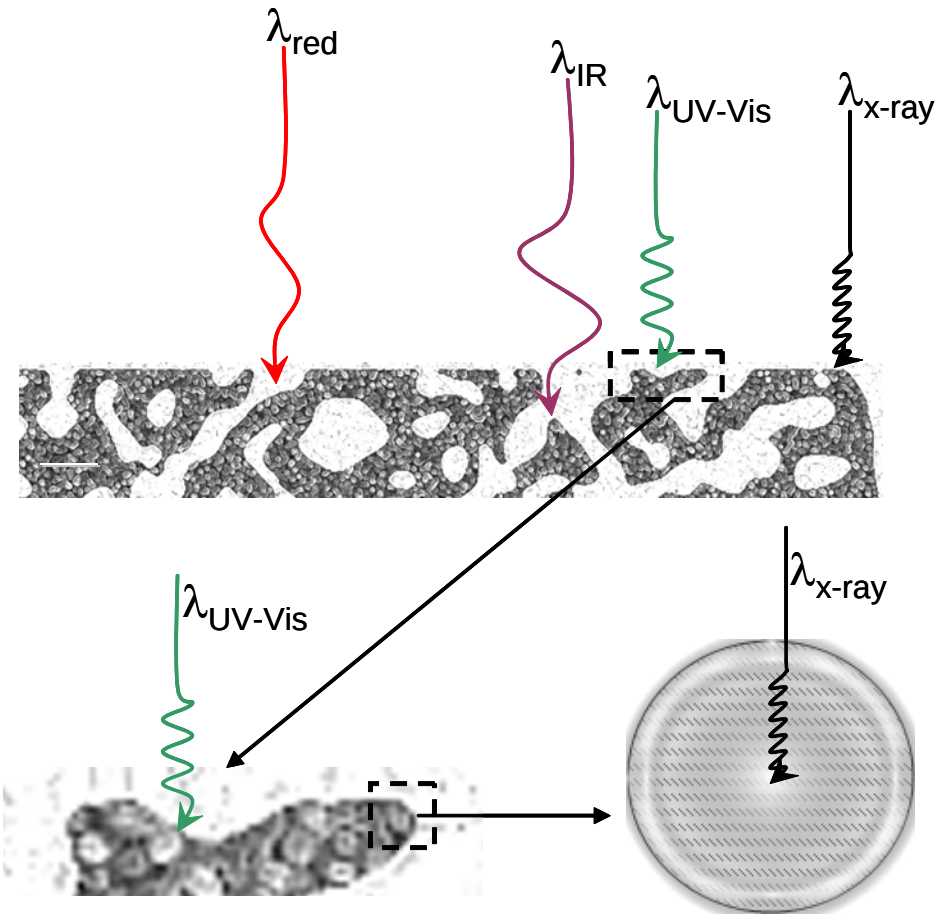

Figure 8.2: Schematic of hybrid cross section, where dark TiO_2 rich phases dispersed within PDMS rich light phases capture photons of different wavelengths (represented by colored arrows) based on spacing of fractal-like phases of different.

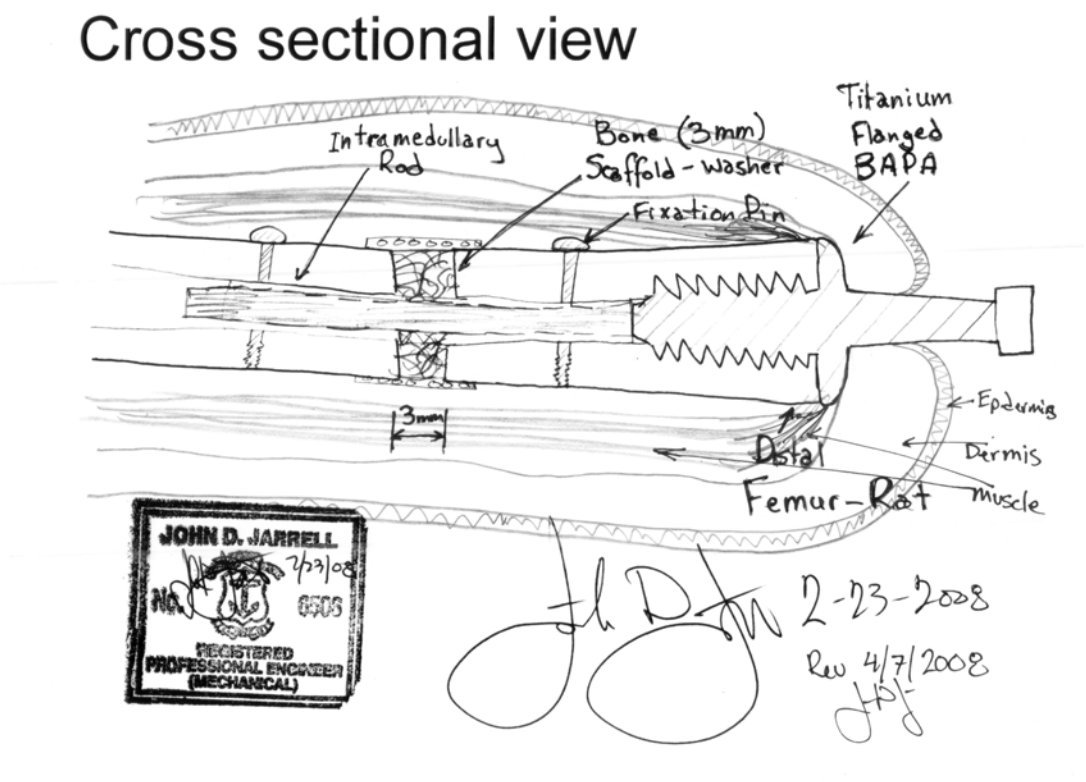

Figure 8.3: Cross sectional view of proposed custom made titanium bone anchored prosthetic attachment (BAPA) with resorbable polymeric intramedullary rod, degradable eluting bone scaffold and tissue engineered periosteum membrane for rat amputation model. BAPA device is suitable for testing influence of surface modifications and coatings on soft and hard tissue integration and resistance to biofilm formation.

8.3 References

1. JD Jarrell, TH Eun, M Samale, C Briant, B Sheldon, JR Morgan. Metal oxide coated cell culture arrays for rapid biological screening. J Biomed Mater Res 2007;83A (3):853-860.

2. JD Jarrell, B Dolly, JR Morgan. Controlled release of vanadium from titanium oxide coatings for improved integration of soft tissue implants. (accepted March 27, 2008) J Biomed Mater Res A 2008.

3. AM Cortizo, VC Salice, CM Vescina, SB Etcheverry. Proliferative and morphological changes induced by vanadium compounds on Swiss 3T3 fibroblasts, BioMetals 10 (2) (1997) 127-133.

4. HP Ehrlich, KA Keefer, GO Maish, RL Myers, DR Mackay. Vanadate ingestion increases the gain in wound breaking strength and leads to better organized collagen fibers in rats during healing. Plast. Reconstr. Surg. 107 (2) (2001) 471-477.

5. HP Ehrlich, KA Keefer, RL Myers, A Passaniti. Vanadate and the absence of myofibroblasts in wound contraction. Arch. Surg. 134 (5) (1999) 494-501.

6. KE Moyer, AA Saba, RM Hauck, HP Ehrlich. Systemic vanadate ingestion modulates rat tendon repair. Exp. Mol. Pathol. 75 (1) (2003) 80-88.

7. J Chen, M Iosifidis, J Zhu, I Tatarintsev, JH Wang. Vanadate ingestion enhances the organization and collagen fibril diameter of rat healing medical collateral ligaments. Knee Surg. Sports Traumatol. Arthrosc. 14 (8) (2006) 750-755.

8. DJ Mackay, KE Moyer, GC Saggers, RL Myers, DR Mackay, HP Ehrlich. Topical vanadate optimizes collagen organization within granulation tissue. Wound Repair Regen. 11 (3) (2003) 204-212.

9. Y Takada, M Hashimoto, J Kasahara, K Aihara, K Fukunaga. Cytoprotective effect of sodium orthovanadate on ischemia/reperfusion-induced injury in the rat heart involves Akt activation and inhibition of fodrin breakdown and apoptosis. J. Pharmacol. Exp. Ther. 311 (3) (2004) 1249-1255.

10. HJH Fenton. On a new reaction of tartaric acid. Chem. News 190 (1876).

11. R Bauer, G Waldner, H Fallmann, S Hager, M Klare, T Krutzler, S Malato, P Maletzky. The photo-fenton reaction and the TiO2/UV process for waste water treatment − novel developments. Catalysis Today 1999:53(1);131-144.

12. P Wardman, LP Candeias. Fenton Chemistry: An Introduction. Radiat. Res. 145,523-531 (1996).

13. G Subramania, K Constant, R Biswas, MM Sigalas, K-M Ho. Optical photonic crystals synthesized from colloidal systems of polystyrene spheres and nanocrystalline titania. J Lightwave Technol, **17**(11), 1970-1974 (1999).

14. X Wang , M Fujimaki, and K Awazu. Photonic crystal structures in titanium dioxide (TiO_2) and their optimal design. *Optics Express* **13**, 1486-1497 (2005).

15. T Bechert, P Steinrucke, J-P Guggenbichler. A new method for screening anti-infective biomaterials. Nature Medicine 2000;6(8):1053-1056.

16. V Alt, T Bechert, P Steinrucke, M Wagener, P Seidel, E Dingeldein, E Domann, R Schnettler. In Vitro Testing of Antimicrobial Activity of Bone Cement. Antimicrobial Agents and Chemotherapy 2004;48(11):4084-4088.

17. M Pitkin, G Raykhtsaum, OV Galibin, MV Protasov, JV Chihovskaya, IG Belyaeva. Skin and bone integrated prosthetic pylon: A pilot animal study. JRRD 43(4) (2006) 573–580.

18. OV Galibin, MV Protasov, Yu V Chikhovskaya, IG Belyaeva, MP Pitkin. Study of growth processes in bone and skin tissues in porous implants designed for fixation of external prosthesis after amputation of extremities. Cell and Tissue Biology, 2007; 1(3) 272–275.

19. Y-T Sul. The significance of the surface properties of oxidized titanium to the bone response: special emphasis on potential biochemical bonding of oxidized titanium implant. Biomaterials 24 (2003) 3893–3907.

20. Y-T Sul, C Johansson, E Byon, T Albrektsson. The bone response of oxidized bioactive and non-bioactive titanium implants. Biomaterials 26 (2005) 6720-6730.

21. CJ Pendegrass, AE Goodship, JS Price, GW Blunn. Nature's answer to breaching the skin barrier: an innovative development for amputees. J Anat 209, 59-67, 2006.

22. CJ Pendegrass, AE Goodship, GW Blunn. Development of a soft tissue seal around bone-anchored transcutaneous amputation prostheses. Biomaterials 27 (2006) 4183–4191.

23. N Ehrhart. Longitudinal Bone Transport for Treatment of Primary Bone Tumors in Dogs: Technique Description and outcome in 9 Dogs. Veterinary Surgery 2005;34:24–34.

24. World's first dog to receive prosthetic implant surgery walks, runs and plays on new legs: Alameda East Veterinary Hospital in Denver plans to provide breakthrough surgery for other amputee dogs. [http://www.marketwire.com/mw/release.do?id=715155], Market Wire, March 6, 2007.